Subthalamic deep brain stimulation for advanced Parkinson's disease

Optimizing localization and stimulation of the target area

Verhagen, R.

Publication date
2022

Document Version
Final published version

SUBTHALAMIC DEEP BRAIN STIMULATION FOR ADVANCED PARKINSON'S DISEASE

Optimizing localization
and stimulation of the target area

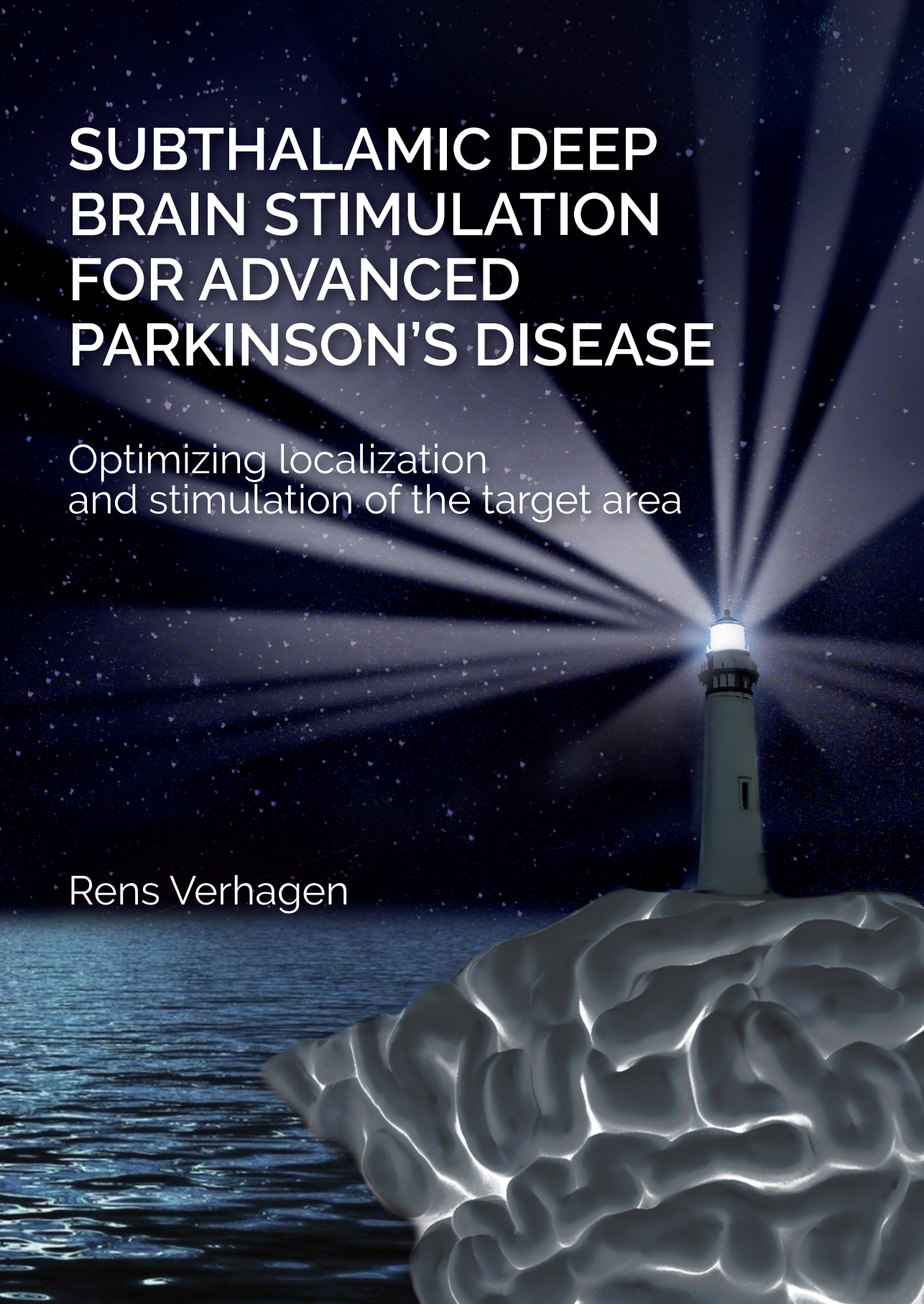

Rens Verhagen

Subthalamic deep brain stimulation for advanced Parkinson's disease

Optimizing localization and stimulation of the target area

Rens Verhagen

The research in this thesis was supported by stichting Toegepast Wetenschappelijk Instituut voor Neuromodulatie (TWIN).

The printing and distribution of this thesis was financially supported by stichting Toegepast Wetenschappelijk Instituut voor Neuromodulatie (TWIN), Stichting Klinische Neurologie, Nederlandse Vereniging voor Klinische Neurofysiologie (NVKNF), AMC Graduate School and the department of Neurosurgery of the Amsterdam University Medical Centers.

ISBN:	978-94-6458-095-2
Cover design & Lay-out:	Publiss | www.publiss.nl
Print:	Ridderprint | www.ridderprint.nl

Subthalamic deep brain stimulation for advanced Parkinson's disease

Optimizing localization and stimulation of the target area

ACADEMISCH PROEFSCHRIFT

ter verkrijging van de graad van doctor
aan de Universiteit van Amsterdam
op gezag van de Rector Magnificus
prof. dr. ir. K.I.J. Maex
ten overstaan van een door het College voor Promoties ingestelde commissie,
in het openbaar te verdedigen in de Agnietenkapel
op vrijdag 1 april 2022, te 13.00 uur

door Rens Verhagen
geboren te Geldrop

Promotiecommissie

Promotores:	prof. dr. I.N. van Schaik	AMC-UvA
	prof. dr. P.R. Schuurman	AMC-UvA
Copromotores:	dr. L.J. Bour	AMC-UvA
	dr. T. Heida	Universiteit Twente
Overige leden:	prof. dr. J.M.C. van Dijk	Rijksuniversiteit Groningen
	prof. dr. Y.B.W.E.M. Roos	AMC-UvA
	prof. dr. H.W. Berendse	Vrije Universiteit Amsterdam
	prof. dr. P.R. Roelfsema	AMC-UvA
	dr. J.H.T.M. Koelman	AMC-UvA

Faculteit der Geneeskunde

Dit proefschrift is opgedragen aan mijn oom Vincent Verhagen en alle andere mensen met de ziekte van Parkinson die, ondanks de inspanningen van hun behandelteam, nog geen optimaal profijt hebben van hun therapie.

Contents

Chapter 1	Introduction and aim of the thesis	9
Chapter 2	Comparative study of microelectrode recording-based STN location and MRI-based STN location in low to ultra-high field (7.0T) T2-weighted MRI images	17
Chapter 3	Advanced target identification in STN-DBS with beta power of combined local field potentials and spiking activity	39
Chapter 4	Electrode location in a microelectrode recording-based model of the subthalamic nucleus can predict motor improvement after deep brain stimulation for Parkinson's disease	61
Chapter 5	Directional steering: a novel approach to deep brain stimulation	75
Chapter 6	Directional recording of subthalamic spectral power densities in Parkinson's disease and the effect of steering deep brain stimulation	93
Chapter 7	A novel lead design enables selective deep brain stimulation of neural populations in the subthalamic region	117
Chapter 8	Avoiding internal capsule stimulation with a new eight-channel steering deep brain stimulation lead	135
Chapter 9	General discussion	153
	Reference list	164
	Summary	178
	Samenvatting	182
Appendices	Curriculum Vitae	188
	PhD portfolio	189
	List of publications	192
	Dankwoord	195
	Abbreviations	199


52 22.3090, 5 0.8440

CHAPTER 1

Introduction and aim of the thesis

General introduction

Parkinson's disease (PD) is a neurodegenerative movement disorder that is mainly characterized by its motor symptoms bradykinesia, rigidity, and tremor. As the disease progresses, the initial treatment with dopaminergic medication may become less effective and patients can develop medication-induced motor response fluctuations and additional dyskinesias, often referred to as on-off fluctuations. At this stage, deep brain stimulation (DBS) is a possible surgical treatment that can effectively alleviate PD motor symptoms and suppress on-off fluctuations.[1–4] For DBS therapy, electrodes are permanently implanted in the deep nuclei of the brain, the basal ganglia, using a frame-based stereotactic procedure (figure 1). After implantation, the electrodes continuously stimulate a preoperatively chosen target structure.

Although there are several target structures that can be stimulated within the basal ganglia, previous studies in our center, and in others, have shown that the subthalamic nucleus (STN) is currently the preferred target for optimal suppression of the cardinal PD motor symptoms.[5–7] On average, the improvement of motor symptoms by STN-DBS is around 50% of the off-medication symptom severity, but there are large variations in clinical outcome, both in terms of motor improvement and possible side effects.[2,6,8–12]

Several factors influence the clinical motor improvement that can be obtained by DBS. The first factor influencing the success of DBS is careful selection of DBS candidates, considering the influence of age, disease duration and the preoperative response to dopaminergic medication.[9,13–15] The second factor determining the improvement of motor symptoms is the correct location of the active contacts of the stimulating electrode relative to the target structure, the STN.[16–20] Therefore, one of the biggest challenges for the clinical team lies in the optimal identification of the STN target, preoperatively and intraoperatively. Thirdly, the outcome of DBS is determined by postoperative adaptations in the stimulation programming, optimizing the stimulation parameters to maximize symptom reduction while minimizing the stimulation of side effect inducing structures.

Preoperatively, the STN can be visualized with MRI. The contrast differences between white and gray matter seen on T2-weighted MRI images are used to identify the contours of the STN. Guided by these contours the target's cartesian coordinates are calculated and used to plan the stereotactic DBS procedure. With this stereotactic approach the neurosurgeon can place one of the contacts of the DBS electrode at the desired target coordinates with a high level of accuracy.[21] However, accurate identification of the MRI-based STN is dependent on high-quality MRI images and is further complicated by the fact that differences in MRI field strength and MRI sequencing result in varying STN shapes and sizes.

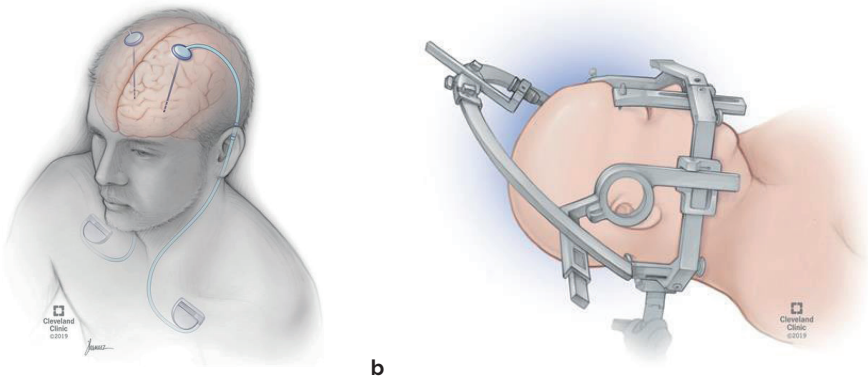

a b

Figure 1. (a) An example of DBS electrodes implanted bilaterally in the subthalamic nucleus, connected to an implantable pulse generator placed under the skin on the chest wall. **(b)** An example of the stereotactic head frame that is used during DBS surgery to ensure that the electrodes are implanted at the desired target location. *Reprinted with permission, Cleveland Clinic Center for Medical Art & Photography © 2012. All Rights Reserved.*

Therefore, in addition to the preoperative MRI-based planning, the STN can be identified intraoperatively by measuring local high frequency neuronal activity with microelectrode recordings (MER). Through interpretation of the spiking activity typical for the STN, measured with multiple MER trajectories, the functional boundaries of the STN can be delineated during the surgery. This can guide electrode placement and it allows the neurosurgeon to functionally refine the preoperative MRI-based targeting. Because MER measurements give information on the real-time functional STN activity, we consider these measurements to be the gold standard for identification of the STN.

Additionally, the measurement of low frequency local field potential (LFP) activity can give more insight into the pathological oscillations inside the STN that are typical for PD. The LFP is composed of the summation of postsynaptic potentials from local cell groups and shows a relation to the envelope of the neuronal spiking that can be measured with MER.[22,23] LFP can be measured intraoperatively, either with the microelectrode or with the contacts of the final DBS electrode. Thereby, intraoperative measurement of the LFP could be useful in identification of the STN boundaries.[24] Moreover, the oscillations in the beta (12 – 35 Hz) and gamma (35 – 80 Hz) bands of the LFP have been shown to correlate with the severity of PD symptoms.[25–27] Analysis of these oscillations can therefore give more spatial information on the theoretical target location within the STN. A possible disadvantage of using the LFP for target identification is the loss of spatial resolution due to the relatively large contacts and inter-contact spacing on the conventional cylindrical DBS electrode.

To optimize the identification of the STN as a whole and the sensorimotor target area within the STN, it is important to continuously evaluate these different imaging and measurement techniques, the way in which they relate to each other, and how this influences the identification of the target for DBS electrode implantation.

Postoperatively, the stimulation of the target can also be adapted with the final electrode in place. Apart from changing the voltage or current on the electrode, this can be done by choosing or combining different stimulation contacts. In the conventional cylindrical electrode, this is limited to selecting one of the four in-line cylindrical contacts for stimulation or combining cylindrical contacts in double monopolar and bipolar stimulation patterns. This changes the stimulation field mostly in the dorsoventral direction, along the longitudinal axis of the electrode.

Technological innovations led to the development of DBS electrodes with multiple multi-directional stimulation contacts (figure 2).[28,29] These electrodes can not only shape the stimulation field in the dorsoventral direction, but also in the anteroposterior and the mediolateral directions, providing more possibilities for postoperative adaptation of the stimulation. Moreover, because these electrodes have multiple smaller contacts, this might improve the spatial resolution for intraoperative and postoperative LFP measurements with the final DBS electrode, which as mentioned above is limited with the conventional electrode.

To optimize both the intraoperative identification and the postoperative stimulation of the STN target area, the possibilities of both measuring and stimulating multi-directionally need to be evaluated. It needs to be studied how LFP measurements with the steering electrode could aid intraoperative STN target area identification and how the steering electrode could shape the field of stimulation, steering the stimulation away from structures where side effects are induced and towards the target area where the highest amount clinical motor improvement can be achieved.

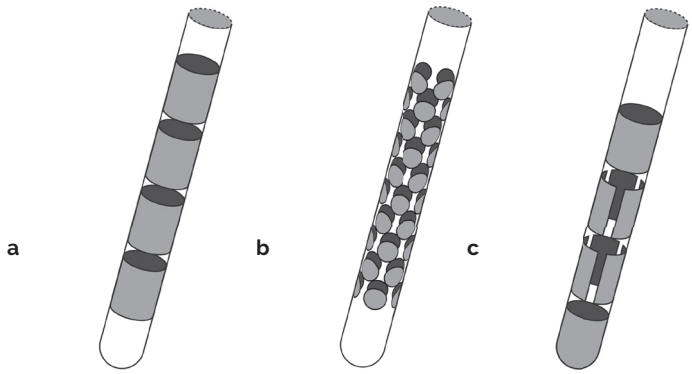

Figure 2. A comparative illustration of the conventional cylindrical DBS electrode and two steering DBS electrodes; **(a)** the conventional four-contact cylindrical electrode, **(b)** an experimental 40-contact steering electrode, and **(c)** a commercially available eight-contact steering electrode, where the middle two levels are divided into three segments.

Aim and outline of the thesis

The aim of this thesis is to evaluate the techniques used for preoperative and intraoperative identification of the STN. Also, the location of the target area within the STN itself and the relation between the location of the stimulating contact and the resulting clinical motor improvement is evaluated.

To this end we consider MER measurement of STN neuronal activity to be the gold standard for STN identification. We use a more detailed analysis of the MER data to improve our knowledge on the identification and stimulation of the target. In this more detailed analysis, we model the size and shape of each patient specific STN to which we can then relate all the locations of the recordings and stimulations that are evaluated.

Additionally, we aim to examine different types of steering DBS electrodes, both in their ability to measure and to stimulate multi-directionally. For this, we use a computational modelling approach as well as a proof-of-principle clinical study to optimize identification and stimulation of the STN target with steering DBS electrodes.

In the first part of this thesis (chapters 2 – 4), we examine the role of intraoperative measurements in target identification. We study how the MER-based STN model can lead to improved insights on the STN target, from the total STN structure, to the sensorimotor STN area, to the most effective target area within the sensorimotor STN. In chapter 2 we study how the MER-based STN relates to the STN identified on T2-weighted MRI images of different field strengths (1.5 Tesla, 3.0 Tesla and 7.0 Tesla). Using the same MER-based STN modelling approach we study in chapter 3 how the sensorimotor area of the STN can potentially be identified by combining simultaneously measured MER and LFP data. Chapter 4 describes our study into the relation between the location of the stimulating contact after one year, identified on CT, and the clinical motor improvement after one year. Hereby, we attempt to identify the most effective target area for postoperative motor improvement within the sensorimotor STN.

In the second part of this thesis (chapters 5 – 8), we evaluate the potential role of steering DBS electrodes in the identification and stimulation of the STN target. In chapter 5, we examine the working principle of steering stimulation in one of the first clinical studies with a novel multidirectional contact electrode. Using the same electrode, we study in chapter 6 the potential of multidirectional LFP recordings to identify the STN target and to measure the changes in oscillations caused by stimulating in different directions. In chapter 7 and 8 we present a computational modelling approach to evaluate how two different types of steering DBS electrodes can potentially correct for displacement of the final DBS electrode by steering stimulation away from side effect inducing structures.

Finally, a general discussion is presented in chapter 9 where the results from all these studies are combined and evaluated to provide a sense of direction towards optimizing the efficacy of STN-DBS therapy for PD in terms of identification and stimulation of the selected target.


53 21.6192, 5 12.8564

CHAPTER 2

Comparative study of microelectrode recording-based STN location and MRI-based STN location in low to ultra-high field (7.0T) T2-weighted MRI images

Rens Verhagen
P. Richard Schuurman
Pepijn van den Munckhof
M. Fiorella Contarino
Rob. M. A. de Bie
Lo J. Bour

Journal of neural engineering. 2016;13(6):066009

Objective: The correspondence between the anatomical STN and the STN observed in T2-weighted MRI images used for deep brain stimulation (DBS) targeting remains unclear. Using a new method, we compared the STN borders seen on MRI images with those estimated by intraoperative microelectrode recordings (MER).

Methods: We developed a method to automatically generate a detailed estimation of STN shape and the location of its borders, based on multiple-channel MER measurements. In 33 STN of 19 Parkinson patients, we quantitatively compared the dorsal and lateral borders of this MER-based STN model with the STN borders visualized by 1.5 T (n = 14), 3.0 T (n = 10) and 7.0 T (n = 9) T2-weighted MRI.

Results: The dorsal border was identified more dorsally on coronal T2 MRI than by the MER-based STN model, with a significant difference in the 3.0 T (range 0.97 – 1.19 mm) and 7.0 T (range 1.23 – 1.25 mm) groups. The lateral border was significantly more medial on 1.5 T (mean: 1.97 mm) and 3.0 T (mean: 2.49 mm) MRI than in the MER-based STN; a difference that was not found in the 7.0 T group.

Conclusion: The STN extends further in the dorsal direction on coronal T2 MRI images than is measured by MER. Increasing MRI field strength to 3.0 T or 7.0 T yields similar discrepancies between MER and MRI at the dorsal STN border. In contrast, increasing MRI field strength to 7.0 T may be useful for identification of the lateral STN border and thereby improve DBS targeting.

Introduction

Deep brain stimulation (DBS) of the subthalamic nucleus (STN) is an effective surgical treatment to alleviate the symptoms of severe Parkinson's disease (PD).[1,6,11,30] The surgical procedure[31], as well as the stimulation itself may lead to side effects.[32–35] These include side effects like tonic motor contractions and rhythmic myoclonus in the face[33], paresthesia, dysarthria[32], and effects on cognition and mood.[34,35] Stimulation-induced side effects are attributed to the aberrant stimulation of the limbic and associative subareas of the STN or structures outside the STN and are therefore dependent on the location of the stimulating contact.[4,36–38] Therapeutic effects of STN-DBS can be improved, and stimulation-induced side effects can be avoided by specifically targeting the dorsolateral portion of the STN[19,39–42], which is associated with sensorimotor function.[38,43,44] Therefore, it is essential that localization of the STN is performed as accurately as possible.

Targeting of the STN for the implantation of DBS electrodes has shifted from an indirect approach to direct visualization of the STN. In the indirect approach, autopsy-based atlases were used to provide the coordinates of the STN relative to landmarks that were established with imaging techniques that do not show the STN itself.[45–48] With the advances in MRI, it became possible to directly visualize (parts of) the STN on preoperative images and establish a stereotactic target for the STN directly based on the hypointense signal observed on T2-weighted MRI images.[45,48–52] This patient-specific approach is based on the contrast between white and gray matter by which the contours of the STN can be identified in the MRI images.[48,53] However, disadvantages of this direct visualization are its dependence on high-quality images and the fact that different forms of MRI sequencing result in different STN shapes and sizes.[37,48,53–55] For these reasons, the correspondence between the STN observed in T2-weighted MRI images and the exact anatomical STN still remains unclear.[56] High field strength T2 MRI can improve visualization of the STN, and it could therefore possibly improve the direct targeting approach.[57–61]

For additional verification of the STN position after imaging, microelectrode recordings (MER) are often performed during DBS surgery to delineate the boundaries of the STN.[45,54,62] The interpretation of high frequency spiking activity measured with MER thereby helps to guide electrode placement and allows the neurosurgeon to adjust MRI-based targeting.[63,64] The primary purpose of intraoperative MER measurements is to define the dorsal and ventral borders of the STN along each planned electrode path and to identify the most lateral path that passes through the STN with sufficient length.[65] Additionally, the differences between the STN dimensions based on MRI contrast and the STN dimensions based on intraoperative MER measurements could be evaluated postoperatively.[56]

The discrepancies between T2 MRI and MER in STN targeting have been the subject of several studies.[45,54,56,64,66–69] Most studies discuss the additional value of MER by reporting how frequently extra MER channels need to be added to the central one when the recordings demonstrated that MRI targeting was insufficient.[67,68] Some studies report on how the use of MER alters the predefined MRI target for DBS implantation.[45,60,64,66,69] Only a few studies actually perform a direct comparison between the STN borders estimated by preoperative T2 MRI and those found by MER.[54,56]

Hamani et al concluded that the STN was underestimated on 1.5 T T2 MRI images and mainly extended more anteriorly than was determined by T2 MRI.[54] Polanski et al reported a relatively low positive predictive value (65.5%) of 3.0 T T2 MRI for the MER-based STN and a high negative predictive value (82.5%), indicating that the STN was estimated larger on T2 MRI than it was by MER.[56] Overall, literature suggests that the borders of the STN are variable between patients and comparisons between MER and T2 MRI in literature are not always able to point out exactly where the discrepancies lie and are even sometimes contradictory.[37,54,56,66]

In the present study, a method was developed to automatically generate a detailed STN model that includes estimation of STN size, shape, and the location of its borders, based on the classifications of multiple-channel MER measurements. This estimated MER-based STN model can be easily fused with all available preoperative images and then a detailed one-on-one comparison can be performed between the STN borders seen in the MRI images and those estimated based on the MER measurements without the need for changes in standard surgical procedures. The goal of this study was to quantify the discrepancies between MRI and MER at the borders of the STN. We have compared these discrepancies between MRI images made with low (1.5 T), high (3.0 T) and ultra-high (7.0 T) magnetic field strengths.

Methods

This study consists of two separate phases. In the first phase, the model building algorithm was optimized by determining the correct boundaries for MER-based STN estimation. For this, a large dataset of preoperative images and MER measurements was used. In the second phase, the STN models created by the algorithm were used to quantitatively compare the MRI-based STN with the MER-based STN. For this second phase, a second dataset was used to prevent overfitting of the models to the initial dataset.

Surgical procedures and MER measurements

All patients presented in this study underwent DBS using either a one-stage bilateral or unilateral stereotactic approach, including MER and test stimulation. STN target

calculation and path planning was done with frame-based T2 MRI using the Leksell stereotactic frame and Surgiplan software (Elekta Instruments AB, Stockholm, Sweden). Standard STN coordinates (11 – 12 mm lateral, 2 mm posterior, and 4 mm ventral to the midcommissural point) were visually adjusted by the neurosurgeon if necessary. Cerebrospinal fluid (CSF) loss and subdural air invasion was minimized by planning the paths to enter on top of a precoronal gyrus, by operating patients while in a semi-sitting position with the head elevated at 20˚ – 30˚ and by closing the burr holes with fibrin glue after introduction of the microelectrodes.[70]

To identify the STN during surgery, MER measurements were performed with one to five steel cannulas and microelectrodes (FHC, Inc., Bowdoin, ME, USA). The MER electrodes were arranged in a cross-shaped array with an inter-electrode distance of 2 mm. MER measurements started 6 mm above the planned STN target, simultaneously advancing downward in 0.5 mm steps until substantia nigra activity was visible in at least one channel or STN activity significantly decreased in all channels.

Over time, two different systems were used for the MER measurements: first the Leadpoint system (Medtronic, Minneapolis, MN, USA) and later the ISIS MER System (Inomed, Emmendingen, Germany). Using the Leadpoint system, recordings were amplified with a gain of 10 000, analogue bandpass filtered between 500 Hz and 5000 Hz and sampled at 12 kHz. Later, using the ISIS MER System, recordings were amplified with a gain of 10 000, analogue bandpass filtered between 160 Hz and 5000 Hz and sampled at 20 kHz. Although the two recording techniques are slightly different, this should not interfere with the identification of STN activity. Both systems are well able to measure single/ multi-unit spiking within 100 – 200 µm of the electrode[71] and overall background activity. Recordings were visually assessed by an experienced physicist and a neurologist who scored them as recorded either inside or outside the STN. The scoring of MER measurements was based on the observed abrupt increase in background activity upon entry into the STN combined with the amount of single/ multi-unit spiking activity.[63,65,72]

Phase 1: optimization of the model building algorithm

In the first phase, to optimize the model building algorithm, we studied the surgical records and MRI images of 34 PD patients (63 STN) who underwent DBS surgery in the Academic Medical Center in Amsterdam between April 2004 and July 2007.

To estimate patient-specific models of STN size and position, the model building algorithm used the classifications of MER measurements, either inside or outside the STN, to fit an atlas-derived representation of the STN onto the coordinates of the MER sites. The MER coordinates were all in reference to the stereotactic frame, which is recognized in the Surgiplan software that is used for preoperative targeting. Only MER

tracks that passed through the STN were used in the model building algorithm.[73,74] Tracks that did not show STN activity in any of its recordings were excluded. This was done because high values of electrode impedance and other possible microelectrode malfunctioning could have interfered with the visual MER assessment and it could therefore not be concluded with certainty that these tracks missed the STN, which could induce large estimation errors in the model.

STN fitting was performed offline using Matlab (Mathworks, Inc., Natick, MA, USA). The original STN representation was a three-dimensional polygon surface extracted from the Cicerone software package.[75,76] First, this STN body was placed with its center on the planned stereotactic target, then both the STN body and the MER sites were rotated using the arc and ring angles of the preoperative planning, such that the MER trajectories were aligned parallel to the z-axis. This MER-based orientation, centered on the planned stereotactic target, is the starting point of the optimization procedure. This was done so to be able to estimate appropriate boundaries for the STN fitting algorithm based on the directions in which there was either a high or low density of MER measurements. From here, the size and location of the patient specific STN was estimated based on the MER classifications. Using an optimization routine, the initial 3D body was translated, rotated, and scaled in all three directions (in total nine degrees of freedom) to fit the classifications of the MER sites as good as possible. The optimization routine itself has been described in more detail by Lourens et al[73] initial boundaries for the transformations were based on the variability of STN size and location reported by Daniluk et al[37] and were ±2 mm translation in all directions, ±20˚ rotation around all axes and ±25% scaling in all directions. To obtain the best possible estimation of STN size and location, the optimization routine was performed 50 times. The best fittings were selected by excluding all STN for which the fitting value, which was minimized in the optimization routine, exceeded the median fitting value of 50 iterations. From the remaining STN, the model that had the lowest amount of total transformation was chosen as the best STN model.

The model building algorithm was further optimized by examining the size and location of MER-based STN models in relation to the preoperative 1.5 T T2 MRI images and determining the appropriate boundaries for the transformations. For this, cross-sections of the best STN model in stereotactic orientation were made at 0.5 mm slices with a pixel size of 0.5 mm × 0.5 mm. The contours of these cross-sections were then exported as a set of DICOM images. Every DICOM image included markers on the stereotactic coordinates of the Leksell frame fiducials. This created an image of the same stereotactic frame as the one used in preoperative targeting, together with a patient specific STN body which is in reference to this frame. The images were then imported into the Surgiplan software with the original frame recognition and co-registered to the preoperative images using the stereotactic frame. The overlays of MER-based STN contours and the T2 MRI images of the STN were then independently

evaluated in axial and coronal images by two experienced DBS neurosurgeons (P.R.S. and P.v.d.M.). Cases with too much rotation, translation or scaling were identified based on the discrepancies between the contours of the STN model and parts of the STN border that were well visible on 1.5 T T2 MRI. Based on these cases, realistic boundaries for all transformations were identified in relation to the information available for the optimization routine, that is, the amount of MER trajectories that measured STN activity. Visual assessment of the fused images suggested that at least three MER tracks were needed for adequate estimation of the STN; this was not the case in 8 out of 63 STN. The specific transformation boundaries for STN estimated by three or more tracks can be found in the supplementary materials (table S1). In general, the presence of more MER trajectories passing through the STN results in more freedom for the optimization routine to transform the STN. If a certain direction of the cross-shaped array only has two MER tracks instead of three, then the freedom for transformations in this direction was limited. Transformations affecting the dorsoventral dimensions of the STN had the highest degree of freedom and were independent of the number of MER tracks available. This was done because the resolution of MER classifications is highest in this direction and therefore these transformations will always be accurately limited.

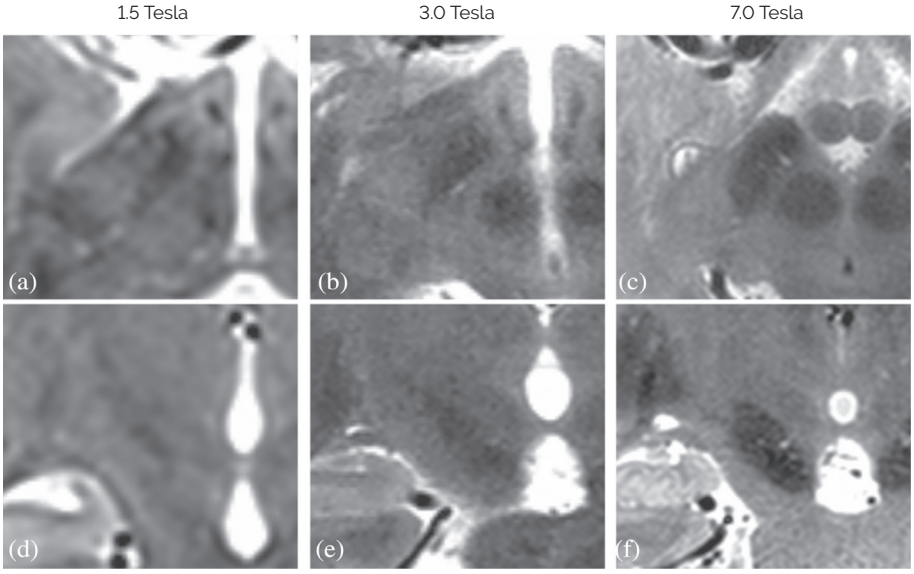

Figure 1. Examples of STN imaging using T2-weighted MRI in three different field strengths. Figures **(a) – (c)** show axial cross-sections of the STN in 1.5 T, 3.0 T and 7.0 T MRI respectively. Figures **(d) – (f)** show coronal cross-sections of the STN in 1.5 T, 3.0 T and 7.0 T MRI respectively.

Phase 2: quantified comparison between the MER-based STN model and the MRI-based STN

In the second phase of this study, after optimization of the model building algorithm, a new dataset was used to compare the STN borders in a quantitative manner. The first phase of model optimization suggested that at least three MER tracks were needed for adequate estimation of the STN, therefore in the second dataset only STN for which three or more MER tracks showed STN activity were included. Additionally, cases in which only three MER tracks showed STN activity were not included when these three tracks were in the same plane (e.g., when only the lateral, central, and medial channels in the cross-shaped array showed STN activity). This new dataset was composed out of the surgical records and T2 MRI images of PD patients who underwent DBS surgery in the Academic Medical Center in Amsterdam between November 2009 and November 2015. Surgical procedures were identical to those in the first dataset. From this period, three groups of patients were selected based on the field strengths in which T2-weighted MRI images were available: 1.5 T, 3.0 T or 7.0 T. The MRI images that were used for the quantitative comparison were the same as the images used for preoperative targeting. A strict selection of patients was performed to ensure that only MRI images of the highest possible quality were used for STN identification in all groups. Figure 1 shows examples of both axial and coronal cross-sections of the STN in T2-weighted MRI images in the three different groups.

To objectively compare the STN borders on these MRI images with the MER-based STN borders, one neurosurgeon (P.R.S.) used the coronal MRI images to identify the borders without knowledge of the MER-based STN borders. The STN identification was performed in the Surgiplan software with the original stereotactic frame recognition. The neurosurgeon that performed the anatomical STN identification had extensive experience with this software and with STN identification in 1.5 T, 3.0 T and 7.0 T MRI images. If, however, he was unable to accurately identify the STN borders in a certain patient because of low quality MRI images, this patient was excluded from further analysis. This resulted in 19 PD patients that were used for the quantitative analysis. Table 1 shows the number of patients and STN included in each group together with the MRI systems, MRI sequences and specific scanning parameters that were used to obtain images of the STN. While in the 1.5 T and 3.0 T groups we used coronal MRI images with a good in-plane resolution and a slice thickness of 2 mm, in the 7.0 T group the in-plane coronal MRI images often suffered from motion artifacts and we had to use the coronal reconstruction of the 3D T2 acquisition instead.

Table 1. Overview of the number of patients and STN included, and the scanning parameters used to obtain MRI images of the STN in the three groups of different magnetic field strengths

Field strength	MRI system	MRI sequence	TR (ms)	TE (ms)	Voxel size [x, y, z] (mm × mm × mm)	Number of patients	Number of STN [7]
1.5 T	Siemens Avanto[5]	Coronal T2-weighted TSE	5750	99	0.5 × 2.0 × 0.5	8	14
3.0 T	Philips Ingenia[6]	Coronal T2-weighted TSE	4823	80	0.4 × 2.0 × 0.4	5	10
7.0 T	Philips Achieva[6]	Three-dimensional T2-weighted TSE	3000	295	0.7 × 0.7 × 0.7	6	9

[5] Siemens Healthcare, Erlangen, Germany.
[6] Philips Healthcare, Eindhoven, The Netherlands.
[7] In the 1.5 T group, only 14 out of 16 imaged STN were used because in 2 STN less than three MER tracks were available. In the 7.0 T group, only 9 out of 12 imaged STN were used because of the same reason.
TE = echo time, TR = repetition time, TSE = turbo spin-echo.

All T2 MRI images were co-registered with the 1.5 T axial T1 images with stereotactic frame and MRI-based STN borders were identified based on the difference in contrast between the gray matter of the STN and the surrounding white matter. The initial visual comparison, performed during the optimization of the model building algorithm, showed the greatest discrepancies between MER-based and MRI-based STN at the dorsal and lateral borders. Moreover, the dorsolateral part of the STN is associated with sensorimotor function, which makes the dorsal and lateral borders the most relevant borders to identify. Therefore, the quantitative comparison focused on both these borders, but especially on the dorsal border because the accuracy of the MER-based STN estimation was highest in the dorsoventral direction.

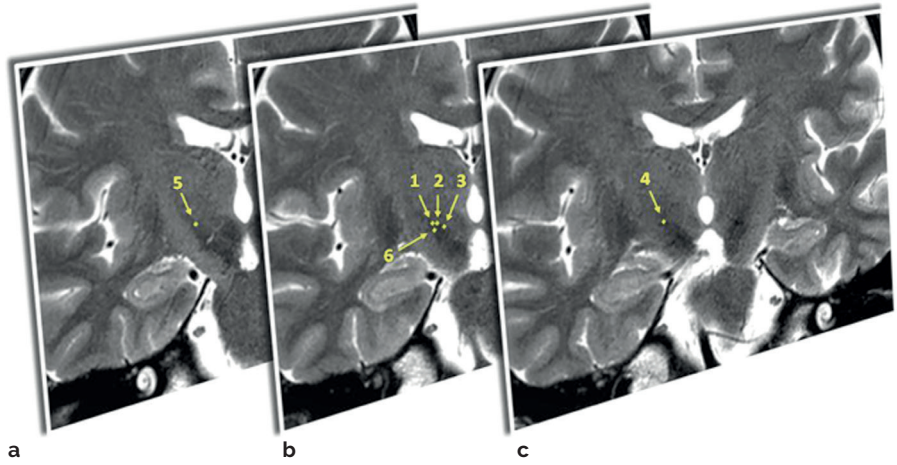

Figure 2. Example of three coronal 3.0 T T2-weighted MRI images, **(b)** the central image closest to the y-coordinate of the stereotactic target on the right side, **(a)** the image 2 mm more posterior and **(c)** 2 mm more anterior. In these images the dorsal **(1 – 5)** and lateral **(6)** border points of the right STN are identified by the neurosurgeon.

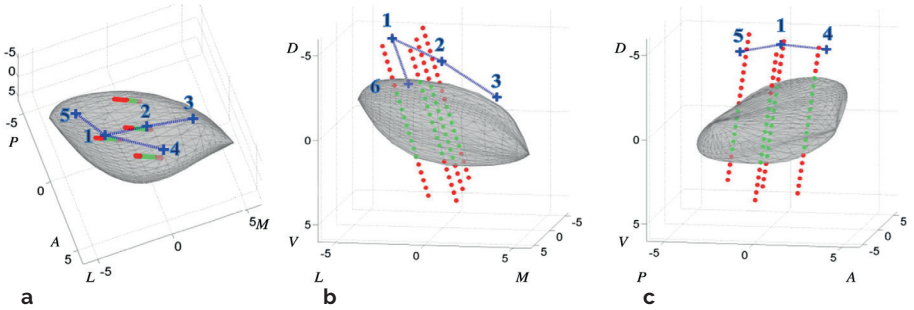

Figure 3. Example of the model STN body (gray) fitted onto the classifications of the MER sites (red dot = outside, green dot = inside) viewed from a **(a)** dorsal, **(b)** anterior and **(c)** lateral perspective. The blue crosses represent the STN dorsal and lateral border points as they are identified in coronal 1.5 T, T2-weighted MRI images. In every view, only the most relevant border points for that perspective are displayed. The numbering on the axes shows the distance to the stereotactic target in mm. P = posterior, A = anterior, L = lateral, M = medial, D = dorsal, V = ventral

Three coronal T2 MRI images were used to identify six points that represent the dorsal and lateral STN borders. MRI-based borders were identified in a coronal image based on the y-coordinate of the target. Three points were placed by the neurosurgeon representing the dorsal border in this image on (1) the most lateral part of the dorsal border visible on the MRI, (2) on the dorsal border 2 mm more medial than the first point and (3) on the dorsal border 2 mm more medial than the second point (points 1 – 3, figure 2b). Two more points were identified on the most lateral part of the dorsal border in the coronal images which were 2 mm more anterior (point 4, figure 2c) and 2 mm more posterior (point 5, figure 2a) to the central image. Finally, a 6th point was placed on the most lateral part of the STN in the central image, approximately 3 mm ventral to the dorsal border (point 6, figure 2b).

This procedure resulted in six points representing the most relevant STN borders in reference to the original stereotactic frame that was used for preoperative targeting and thus for the creation of the MER-based STN model. These six stereotactic coordinates were then exported from the Surgiplan software to Matlab. There, the MER-based STN model was combined with the points that represent the MRI-based STN borders, both in reference to the original stereotactic frame. An example of this is shown in figure 3. Both the STN model and the identified border points were rotated from the patient specific stereotactic orientation to the general AC – PC aligned orientation. In this orientation, the dorsoventral distances between the dorsal border points (points 1 – 5) and the dorsal border of the MER-based STN model directly above or beneath it were calculated. Additionally, we calculated the mediolateral distance between the lateral border point (point 6) and the lateral border of the STN model directly medial or lateral to this point.

Statistical analysis

Two-way ANOVA was used to compare mean values of size and location of the MER-based STN models between the three groups: the 1.5 T, 3.0 T and 7.0 T MRI groups. Similarly, the mean amount of transformation in all directions was compared between groups.

The quantified difference between the MRI-based STN border points and the MER-based STN borders was compared to a value of zero using two-tailed one-sample t-tests with Bonferroni correction (n = 6). This was done for all three groups of images independently.

Results

Patient data

For the comparison between the MER-based STN and the MRI-based STN, the MER records and MRI images of 33 STN in 19 patients were examined. The clinical characteristics of the patients are shown in table 2. In eight patients, 14 STN were compared using 1.5 T MRI images, in five patients, 10 STN were compared using 3.0 T MRI images and in six patients, 9 STN were compared using 7.0 T MRI images. Two-way ANOVA showed no significant differences in clinical characteristics between the 1.5 T, 3.0 T and 7.0 T groups.

Table 2. Clinical characteristics of the 19 patients at time of surgery (mean ± SD, [range])

Patient characteristics	**Values (*n* = 19)**
Male/female	10/9
Age (years)	61.1 ± 6.0, [48.6 – 70.5]
Disease duration (years)	12.6 ± 5.0, [7.4 – 29.4]
UPDRS part III motor score off medication	44.4 ± 12.3, [31 – 77]
UPDRS part III motor score on medication	20.0 ± 6.5, [8 – 34]

UPDRS = Unified Parkinson's disease rating scale.

Table 3. Characteristics (mean ± SD, [range]) describing the size and location of the 33 MER-based STN models in an AC – PC aligned orientation

STN characteristics*	**Values (*n* = 33)**
Dorsoventral dimension (mm)	5.3 ± 0.5, [4.5 – 7.3]
Anteroposterior dimension (mm)	8.2 ± 0.5, [7.2 – 9.2]
Mediolateral dimension (mm)	9.1 ± 0.9, [7.4 – 11.0]
Target x-coordinate (mm lateral to MCP)	11.0 ± 0.8, [8.4 – 12.2]
Target y-coordinate (mm posterior to MCP)	2.4 ± 0.5, [1.4 – 3.9]
Target z-coordinate (mm ventral to MCP)	4.1 ± 0.4, [3.4 – 5.4]

*All measures of size and location were assessed in an AC – PC aligned orientation. The STN dimensions were assessed by calculating the difference between two most extreme points in a certain direction. MCP = midcommissural point.

MER-based STN models

Using the optimized STN fitting routine, 33 MER-based STN models were created. Characteristics describing the size and location of these STN models are shown in table 3. Statistical testing of the variables in table 3 with two-way ANOVA showed no significant differences in MER-based STN size and location between the 1.5 T, 3.0 T and 7.0 T groups. Additionally, no significant differences between the three groups were found when comparing the amount of transformation. This was found for all transformations (translation, rotation, and scaling) in all individual directions (x, y, and z).

Quantified comparison between MER-based STN and MRI-based STN

The results of the assessment of dorsoventral distances between the five dorsal border points identified in the MRI by the neurosurgeon and the dorsal borders of the MER-based STN models are shown in figure 4. Per group, for each of the dorsal border points, the mean distance in millimeter plus and minus one standard deviation of the distribution is shown. Here, a positive distance indicates that the dorsal border of the STN was identified more dorsally on MRI than it was by MER. In figure 4a, the comparisons of points 1, 2, and 3 in the MRI are shown against a centrally located coronal cross-section of the MER-based STN model. Figure 4b shows the comparisons of points 1, 4, and 5 in the MRI against a sagittal cross-section of the MER-based STN.

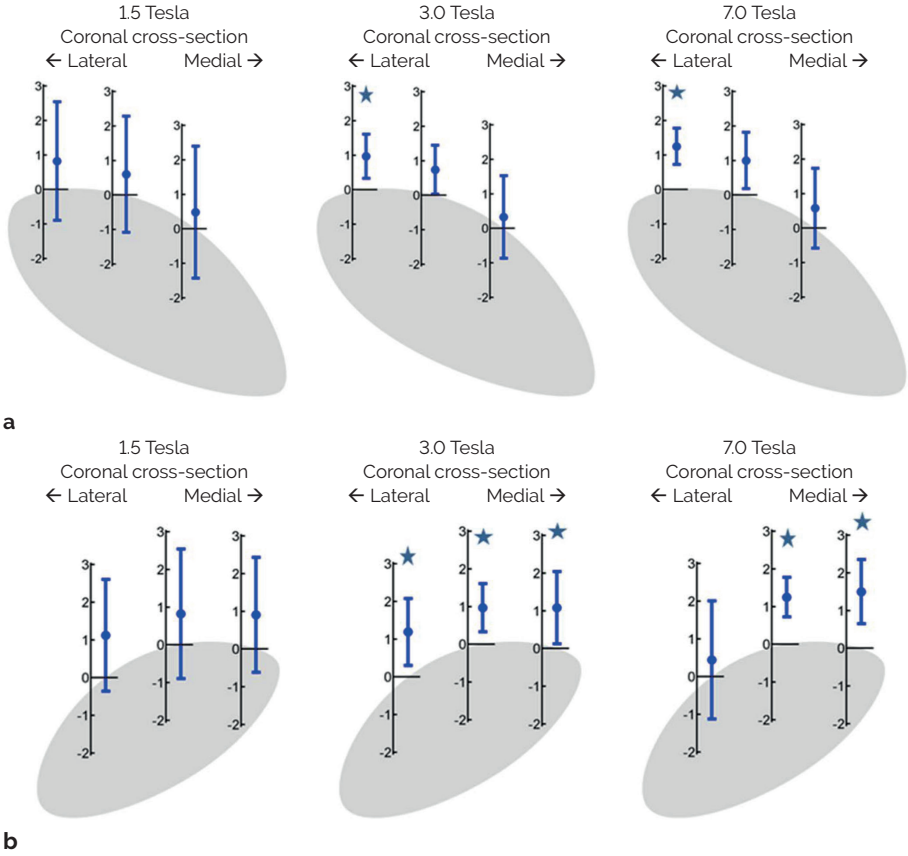

Figure 4. Overview of discrepancies between MRI-based STN and MER-based STN at the dorsal border. Shown are the mean distances in millimeters plus and minus one standard deviation, a positive distance indicates that the dorsal border of the STN is identified more dorsally by MRI than it is by MER. Results significantly different from zero are marked. **(a)** Comparisons of (from left to right) points 1, 2, and 3 identified in the MRI. For comparison with the MER-based STN, a centrally located coronal cross-section the STN model is shown. **(b)** Comparisons of (from left to right) points 5, 1, and 4 identified in the MRI. For comparison with the MER-based STN, a laterally located sagittal cross-section the STN model is shown.

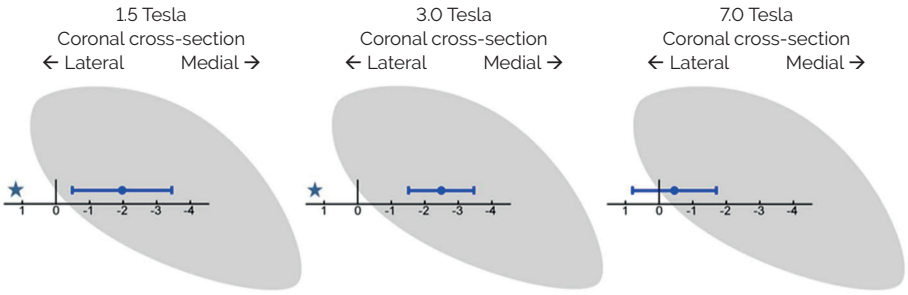

Figure 5. Overview of discrepancies between MRI-based STN and MER-based STN at the lateral border. Shown are the mean distances in millimeters plus and minus one standard deviation, a negative distance indicates that the lateral border of the STN is identified more medially by MRI than it is by MER. Results significantly different from zero are marked. For comparison with the MER-based STN, a centrally located coronal cross-section the STN model is shown.

The average identification of the dorsal border of the STN based on the MRI was located more dorsally on all points compared to the MER-based STN. Two-tailed one-sample t-tests with Bonferroni correction (n = 6) showed that, in the 3.0 T and 7.0 T groups, the lateral part of the dorsal border was identified significantly more dorsal on the MRI than by the MER-based STN model (i.e., the distance was significantly greater than zero). In the 3.0 T group, significant differences were found at the lateral part of the dorsal border at the central (point 1, M = 0.97 mm, $p < 0.001$), anterior (point 4, M = 1.05 mm, $p = 0.006$) and posterior (point 5, M = 1.19 mm, $p = 0.002$) levels. The 7.0 T group shows significant differences at the central (point 1, M = 1.23 mm, $p < 0.001$) and anterior (point 4, M = 1.25 mm, $p = 0.002$) levels of the dorsolateral border.

Figure 5 shows the results when comparing the lateral border point identified on the MRI with the lateral border of the MER-based STN model for the three groups. Here, a negative distance indicates that the lateral border was identified more medially by MRI than it was by MER. Two-tailed one-sample t-tests with Bonferroni correction (n = 6) showed that the lateral border was identified significantly more medial on the MRI (i.e., the distance was significantly smaller than zero) in both the 1.5 T (point 6, M = –1.97 mm, $p < 0.001$) and 3.0 T (point 6, M = –2.49 mm, $p < 0.001$) group.

Discussion

The results of this study suggest that there are discrepancies between the borders of the STN identified by MRI and those identified by MER, found at the dorsal border and at the lateral border. These discrepancies are different depending on the field strength of the T2 MRI used for identification of the borders.

Discrepancies at the dorsal STN border

Both the 3.0 T group and the 7.0 T group showed significant differences at the lateral part of the dorsal border. The mean difference was comparable between the two groups and indicates that the dorsal border was identified approximately 1.00 – 1.25 mm more dorsally by MRI than by MER. The mean difference in the 1.5 T group was similar, but it did not reach significance because of the larger spread of observations. This spread decreases with the increase in field strength from 1.5 to 3.0 T which can be explained by the increased signal to noise ratio and increased MRI contrast obtained with higher field strengths. Furthermore, the voxel size decreases from 0.5 × 2.0 × 0.5 mm^3 to 0.4 × 2.0 × 0.4 mm^3. This leads to an MRI image with a higher spatial resolution and better MRI contrast and should therefore lead to a more precise identification of the STN border. However, only the spread of the observations seems to decrease, while the mean difference between the MRI-based border and the MER-based border remains the same. Even when field strength increases to 7.0 T, a mean difference remains. This may indicate that the discrepancies at the dorsal border are not just the result of a random error due to low MRI contrast, but also of a systematic difference in the visualization of the STN on MRI and the localization of the STN based on MER. This systematic difference implies that either there is a systematic error in the used comparison method or the dorsal border of the STN as seen on MRI extends beyond the functional border as found by MER.

Errors in the comparison itself can be caused by inaccuracy of the co-registration of T1 and T2 images or by inaccuracies in the stereotactic frame.[77] However, these errors would be random errors and can explain some of the variance, but they cannot explain the systematic difference. A systematic difference might by caused by the comparison of the preoperative brain (on MRI) with the intraoperative brain (on MER) due to either positional differences of the brain or brain shift caused by CSF leakage. However, it is very unlikely that brain shift caused by leakage of CSF is the cause as CSF leakage is kept to an absolute minimum by the surgical procedures described in the methods[70,78] and CSF leakage would mainly lead to posterior displacement of the frontal lobe with very little effect on the basal structures like the STN.[79,80] Because of the different effect of gravity when comparing preoperative MRI taken in supine position, with intraoperative MER taken in semi-sitting position, a caudal displacement of the brain could possibly be a contributing cause of the difference found in this study. Another contributing factor to the more ventral location of the STN as determined by MER could be that the insertion of several cannulas for the MER close to the STN actually causes drag and compression, resulting in a ventral displacement of the structures during surgery. Misidentification of the STN on MER measurements is unlikely to be the cause of the systematic difference. The STN is very densely populated with neurons and, therefore, the observed increase in background activity is easy to identify and abrupt.[65] A structural border zone that does not display typical neuronal firing has

not been reported. Although the density of MER measurements around the dorsal STN border is high, the distance between two successive measurements in the same trajectory is still

0.5 mm. This will result in an imprecision in MER-based dorsal border estimation of maximally 0.5 mm. Moreover, the model building algorithm will interpolate the border somewhere between a MER site classified as inside the STN and one classified as outside the STN. This interpolation is also based on the information from surrounding MER trajectories, which will likely make the imprecision less than 0.5 mm. Again, this imprecision would lead to a random error and could explain some of the variance observed in the discrepancies at the dorsal border, but it cannot explain the systematic difference that has been observed.

A plausible explanation for the systematic difference is that the dorsal anatomical border of the STN seen on MRI extends beyond the functional border found by MER. The systematic difference we found on the anterior side of the dorsolateral border of STN might be associated with the findings of others that the anteriorly located pallidofugal fiber pathways result in extra hypointense T2 MRI signal and are therefore difficult to distinguish from the STN.[50,54] Previous reports on discrepancies between MER and T2 MRI have been contradictory.[54,56] While Hamani et al[54] showed a smaller estimation of the STN in the dorsoventral direction on T2 MRI compared to MER, Polanksi et al[56] showed a larger estimation on T2 MRI. The contradicting results at the dorsal border in previous studies could be the result of a limited analysis of the locations of MER measurements. MER trajectories are often analyzed separately or the location of the MER sites with respect to the STN is only based on the preoperative planning. The advantage of this study lies in the detailed estimation of the complete STN based by multiple channel MER measurements. Thereby, we could locate the discrepancies between MER and MRI more accurately and discriminate between discrepancies at the anterior and posterior levels of the dorsal border. This can be seen in figure 4b in the sagittal cross-section of the 7.0 T results. A significant difference of approximately 1.25 mm was found at the central and anterior level of the dorsolateral border, possibly the result of extra hypointense T2 MRI signal caused by the pallidofugal pathways, while at the posterior level of the dorsolateral border, a large variability but no mean difference was found, which may possibly be caused by the smaller iron content and consequently a less accurate delineation of the posterior STN by hypointense T2 MRI signal.[50]

Discrepancies at the lateral STN border

Figure 5 shows that in the 1.5 T and the 3.0 T groups the lateral border was identified significantly more medial on coronal T2 MRI images than by MER. The mean differences found in these groups are approximately 2.0 – 2.5 mm. Similar to the dorsal border, the spread decreases with increased field strength from 1.5 to 3.0 T. Again, this

may be caused by the increase in MRI contrast and the decrease in voxel size which should lead to a more precise identification of the lateral border. However, a significant discrepancy between MRI and MER still remains. When the field strength increases further to 7.0 T, the mean difference between the lateral border on MRI and the border estimated by MER greatly decreases and was no longer significantly different from zero. This may indicate that the observed mismatch in the 1.5 T group, and even in the 3.0 T group, might be the result of insufficient T2 MRI contrast on coronal images at the lateral border which makes it difficult to discriminate the lateral part of the STN from the adjacent internal capsule. This finding is different from the study by Hamani et al[54] in which no STN activity was found outside the lateral border of the STN identified on 1.5 T T2 MRI images. Again, the more detailed estimation of the STN in our study may explain this difference. Fitting a 3D body of the nucleus onto the MER sites, can lead to an estimation of the lateral border several millimeters past the most lateral MER trajectory. For example, the combination of a relatively short trajectory with STN activity on the central channel with a very long trajectory on the lateral channel implies that the STN will extent some more laterally where there were no MER measurements. This estimation, compared to the limited identification of the STN only at the precise MER sites used in other studies, may explain why we find a discrepancy at the lateral border in the 1.5 T and 3.0 T groups.

It is important to note that although the dorsal border of the STN may be well identified using MER, identification of the lateral border with MER is difficult. To estimate the location of the lateral border, the model partially relies on extrapolation of the lateral STN border beyond the sites of MER measurements based on an assumed shape of the STN, which might be inaccurate. Therefore, an imprecision will always remain when estimating the lateral STN with MER and this imprecision is likely the cause of the high amount of variance that is seen in the discrepancies at the lateral border. It is however unlikely to cause systematic differences unless the assumed shape of the STN is not correct. However, the correspondence between the lateral STN border estimated with this model and the lateral border identified on the highest quality (7.0 T) MRI images indicates that the assumed STN shape is likely to be correct and our model building algorithm seems to be a valid way to estimate STN size and location, even regarding its lateral border.

Limitations

This study compared the location of the STN borders based on MER with the borders based on three groups of MRI field strengths. For this, three different groups of patients were used. To accurately study the effects of MRI field strength on the locations of the STN borders, one should compare the three types of images within the same group of patients to ensure that no other factors may influence the discrepancies between MER and MRI. However, we have ensured that all surgical techniques used in the three

groups were identical. Furthermore, we have checked for differences in the created MER-based STN models and have found no differences between the three groups. Therefore, the difference in the observed discrepancies between the groups is most likely due to differences caused by the MRI images used for STN identification. This way of comparing the discrepancies in different groups also gives extra value to the discrepancies that remain consistent over the three groups, like the discrepancies at the lateral part of the dorsal border.

Both the discrepancies at the lateral and the dorsal border showed a decrease in variability when MRI field strength increased from 1.5 to 3.0 T. We expected the variability to be decreased even more in the 7.0 T group, but it remained at the same level as in the 3.0 T group. Apparently 3.0 T scanning provides a level of detail that is surpassed only marginally when further increasing the field strength to 7.0 T for the purpose of STN target determination. However, in our comparison a different type of MRI image was used in the 7.0 T group. While in the other two groups we used coronal MRI images with a good in-plane resolution and a slice thickness of 2 mm (voxel size: 0.5 × 2.0 × 0.5 mm^3 and 0.4 × 2.0 × 0.4 mm^3 for the 1.5 T and 3.0 T group respectively), in the 7.0 T group the in-plane coronal MRI images often suffered from motion artifacts and we had to use the coronal reconstruction of the 3D T2 acquisition instead. These had a higher resolution in the y-direction, but a slightly worse resolution in the coronal plane than the in-plane acquisitions in the 1.5 T and 3.0 T group (voxel size: 0.7 × 0.7 × 0.7 mm^3). We do not expect that the use of this different type of image has influenced the systematic discrepancy between MER-based STN and MRI-based STN, but it might explain why the variability did not decrease further with 7.0 T images. Another explanation might be that the variability did not decrease any further because it was overshadowed by the random errors created by the co-registration of T1 and T2 images and the inaccuracies of the stereotactic frame or the MER fitting procedure itself, since it partially relies on interpolation and extrapolation.

In this study we have compared the MER-based STN model only with the STN border seen in T2-weighted MRI images. Other groups have reported the successful use of other MRI imaging sequences like susceptibility weighted imaging (SWI) to identify the STN.[56,81–83] However, T2 MRI images are still most widely used for DBS targeting. For the future it remains interesting to study the discrepancies at the dorsolateral border between the MER-based STN model and the SWI-based STN, although a recent study by Bot et al[84] from our group showed that the correlation between STN representation on MER and on MRI was worse for SWI images than it was for T2-weighted MRI images.

Conclusions

Using a newly developed method to accurately estimate the MER-based STN, we conclude that discrepancies exist between the T2 MRI-based STN and the MER-based STN at the dorsal and lateral borders. Therefore, MER can help to refine the delineation of the dorsal and lateral borders of the STN in T2 MRI-based targeting. Increasing the field strength to 3.0 T or 7.0 T yields similar average discrepancies between MER and MRI at the dorsal border of the STN, but with significantly smaller variations. In contrast with the dorsal border, increasing the MRI field strength further from 3.0 T to 7.0 T may be useful for identification of the lateral STN border.

Independent of the precise reasons for the discrepancies between the MER-based STN and the MRI-based STN, both the remaining discrepancies at the dorsal border and the positive effects of 7.0 T MRI on identification of the lateral border are important when relying on T2-weighted MRI images for preoperative DBS targeting.

Supplementary materials

Table S1. Overview of the transformation boundaries used in the STN estimation model after visual assessment of the fusion between preoperative MRI images and MER-based STN models. The boundaries for transformations depend on which of the MER tracks arranged in a cross-shaped array can be used to estimate the STN

Transformation [direction A]	Five MER tracks	Four MER tracks, missing one in the M – L (x) direction	Four MER tracks, missing one in the A – P (y) direction	Three MER tracks, missing one in the M – L (x) and A – P (y) directions
[x]	-2 mm : +2 mm	-1 mm : +1 mm	-2 mm : +2 mm	-1 mm : +1 mm
Translation [y]	-2 mm : +2 mm	-2 mm : +2 mm	-1 mm : +1 mm	-1 mm : +1 mm
[z]	-5 mm : +5 mm	-5 mm : +5 mm	-5 mm : +5 mm	-5 mm : +5 mm
[x]	-15° : +15°	-15° : +15°	-10° : +10°	-10° : +10°
Rotation B [y]	-15° : +15°	-10° : +10°	-15° : +15°	-10° : +10°
[z]	-15° : +15°	-10° : +10°	-10° : +10°	-15° : +15°
[x]	-25% : +5%	-15% : +5%	-25% : +5%	-15% : +5%
Scaling C [y]	-25% : +5%	-25% : +5%	-15% : +5%	-15% : +5%
[z]	-25% : +25%	-25% : +25%	-25% : +25%	-25% : +25%

A The directions of the transformations were defined in relation to the MER tracks. The z-axis runs down along the central MER track, the y-axis runs perpendicular to the z-axis from the posterior track towards the anterior track and the x-axis runs perpendicular to the z-axis from the medial track towards the lateral track. This way [z] resembles the anatomical D – V direction, [y] resembles the anatomical P – A direction and [x] resembles the anatomical M – L direction.

B The rotations in [x], [y] and [z] direction were defined as rotations around the x-, y- and z-axis respectively and they therefore resemble rotations in the sagittal, coronal, and axial plane respectively.

C During optimization of the MER-based STN model, overlays with the MRI showed that in many cases the STN was too large in the M – L or P – A or direction, which was probably the result of the original STN model being too large in these directions. Moreover, upscaling in these directions will have a large effect on the STN borders due to the extrapolation of the STN border beyond the sites of MER measurements. Therefore, the boundaries in these directions (x and y) were asymmetrical and have a tendency towards downscaling. The scaling boundaries in the D – V direction (z) remain symmetrical.

A = Anterior, D = Dorsal, L = Lateral, M = Medial, P = Posterior, V = Ventral

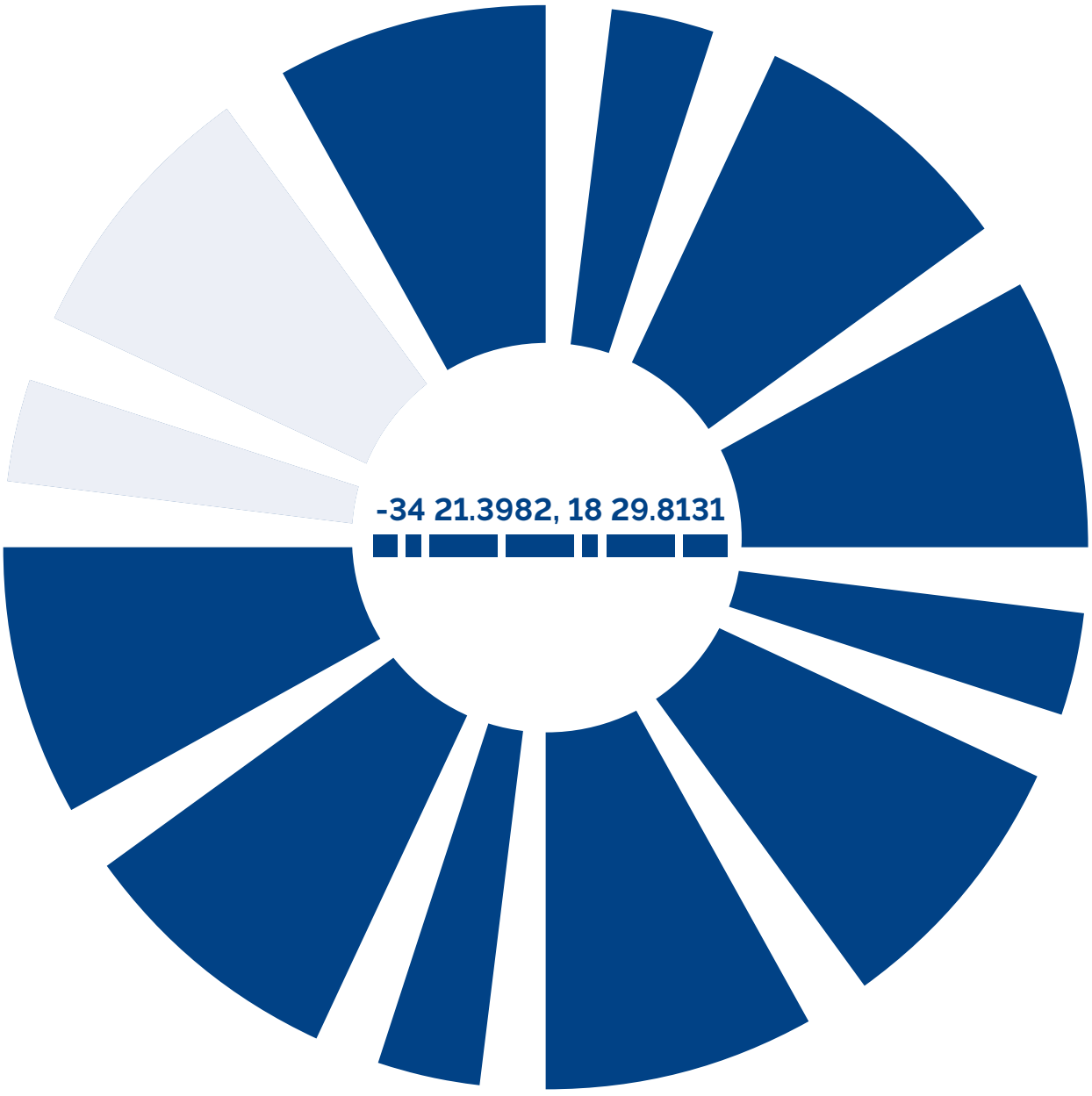
-34 21.3982, 18 29.8131

CHAPTER 3

Advanced target identification in STN-DBS with beta power of combined local field potentials and spiking activity

Rens Verhagen
Daphne G.M. Zwartjes
Ciska Heida
Evita C. Wiegers
M. Fiorella Contarino
Rob M.A. de Bie
Pepijn van den Munckhof
P. Richard Schuurman
Peter H. Veltink
Lo J. Bour

Journal of Neuroscience Methods. 2015;253:116-125

Objective: In deep brain stimulation of the subthalamic nucleus (STN-DBS) for Parkinson's Disease (PD), often microelectrode recordings (MER) are used for STN identification. However, for advanced target identification of the sensorimotor STN, it may be relevant to use local field potential (LFP) recordings. Then, it is important to assure that the measured oscillations are coming from the close proximity of the electrode.

Methods: Through multiple simultaneous recordings of LFP and neuronal spiking, we investigated the temporal relationship between local neuronal spiking and more global LFP. We analyzed the local oscillations in the LFP by calculating power only over specific frequencies that show a significant coherence between LFP and neuronal spiking. Using this 'coherence method', we investigated how well measurements in the sensorimotor STN could be discriminated from measurements elsewhere in the STN.

Results: The 'sensorimotor power index' (SMPI) of beta frequencies, representing the ability to discriminate sensorimotor STN measurements based on the beta power, was significantly larger using the 'coherence method' for LFP spectral analysis compared to other methods where either the complete LFP beta spectrum or only the prominent peaks in the LFP beta spectrum were used to calculate beta power.

Conclusion: The results suggest that due to volume conduction of beta frequency oscillations, proper localization of the sensorimotor STN with only LFP recordings is difficult. However, combining recordings of LFP and neuronal spiking and calculating beta power over the coherent parts of the LFP spectrum can be beneficial in discriminating the sensorimotor STN.

Introduction

Deep brain stimulation of the subthalamic nucleus (STN-DBS) has emerged as an effective surgical treatment for Parkinson's disease (PD)[2,6,11,85], although the underlying working mechanisms of DBS still are not fully understood. A leading hypothesis is that DBS suppresses pathological synchronized oscillations in the basal ganglia.[86,87] Besides the favorable therapeutic effects, STN-DBS may also be accompanied by side effects, including side effects on cognition, behavior, and mood.[34,35] It is thought that side effects are avoided, and therapeutic effects of DBS are improved by selectively stimulating the dorsolateral STN[19,39–42,73] which is the area of the STN predominantly associated with sensorimotor function.[38,43,44] In this regard, the challenging task in DBS surgery is to locate not only the borders of the STN, but especially its sensorimotor area.

In addition to the standard T2 MRI-based targeting, some centers are using intraoperative recordings with microelectrodes (MER) to identify STN activity. Through the interpretation of local neuronal spiking activity measured with MER, electrode placement is guided, and it allows the neurosurgeon to functionally refine targeting.[63,64,88] It may be relevant to further fine-tune targeting based on local field potential (LFP) recordings from the same electrodes or even from the contact points of the implanted DBS lead. An additional possible advantage of using LFP signals to verify electrode placement could be that they can be measured from the implanted electrode even after surgery to continuously monitor the position of the DBS lead with respect to the STN, thereby providing feedback for the configuration of the stimulation parameters.[89–92]

Disadvantages of using the LFP signal in this way are primarily the loss of spatial resolution due to the relatively large size of the electrodes and the inter-contact distance on the lead. Also, single unit or multiple unit spiking activity cannot be detected by these larger surface electrodes. When using the LFP signal one has to rely on low frequency oscillations of the background signal, for instance in the beta (12 – 35 Hz) and gamma (35 – 80 Hz) band, to localize the STN and its sensorimotor area.

Previous studies in PD have shown that neural activity in the beta frequency band, measured with LFP, has an increased power in the sensorimotor STN compared to other regions inside the STN and areas outside the STN.[23,24,93–95] Elevated synchronized beta activity is considered to be related to antikinetic motor activity and seems to be associated with bradykinesia and rigidity in PD.[87,96,97] It is suggested that beta oscillations promote tonic activity at the expense of voluntary movement and that beta oscillations are modulated by dopamine therapy[98,99], which induces a shift in the power spectrum of LFP activity, decreasing the spectral beta power and increasing the spectral power in the gamma frequency band.[100–104]

With respect to synchronized gamma oscillations of LFP in the STN, it is thought that they have a physiological rather than a pathological origin and possibly relate to specific movement parameters since elevated gamma power is found before and during the execution of movements.[96,101,102,105] In a study by Trottenberg et al.[106] in PD patients, gamma oscillatory activity measured with LFP was found to be increased in the zona incerta and the dorsal STN. Furthermore, Weinberger et al.[107], found LFP power in the gamma frequency range to be increased when comparing periods of stronger tremor with periods of weaker tremor. These sites of increased gamma oscillations were mostly located in the dorsal part of the STN.

One of the challenges in identifying these specific oscillations in the STN and its sensorimotor area is to assure that the measured LFP signal is indeed coming from the close proximity of the electrode. The electric field produced by the slow oscillations represented in the LFP is conducted through the neuronal tissue. As a result, LFP measurements can be influenced by oscillating sources up to a distance of 10 mm depending on the conductive medium, the frequency of the oscillation[108–110], the architecture of the neural tissue as well as the amount of synchronization between the neural ensembles.[111] This is in contrast to the neuronal spiking activity represented in the MER signal, which can only come from neurons within a range of 100 – 200 µm around the microelectrode.[112] Therefore, a way to verify the local nature of LFP oscillations can be by demonstrating that they correlate with local neuronal firing.[111]

The temporal relationship between LFP and neuronal spiking activity in the STN has not been widely studied. Alavi et al.[113], found that 46% of STN neurons showed beta oscillatory spiking activity coherent with LFP. Weinberger et al.[95], showed that 28% of recordings of spiking activity displayed significant oscillations in the beta frequencies of which the majority was localized in the dorsal STN. Almost all of these oscillating recordings were significantly coherent with LFP activity. In a study by Kühn et al.[23], spike triggered averages (STA) of the LFP were used to show that the beta range oscillatory activity in the LFP was time-locked to the neuronal discharge with STA amplitudes being larger in the dorsal STN than in the ventral STN. In light of these results, beta LFP activity is not thought to be caused by oscillatory firing of STN neurons, but more likely to be the result of oscillatory afferent input into the neurons from outside the STN.[23,95]

In the current study, we have investigated a method to assess the temporal relationship between strictly local neuronal spiking activity measured with MER and more global neuronal activity measured with LFP recordings inside different functional parts of the STN. By simultaneously measuring LFP and neuronal spiking activity from the microelectrodes used in standard DBS surgery, we were able to study coherence between LFP and neuronal spiking activity and spectral power of both LFP and neuronal spiking on numerous positions across the subthalamic area with only a minimal change in the standard surgical procedures.

Table 1. Clinical characteristics (mean ± SD, [rangel) of the PD patients included in this study

Number of patients	**25**
Sex (women/men)	6/19
Age (years)	60 ± 10, [38 – 76]
Disease duration (years)	13 ± 7, [6 – 32]
Total UPDRS* III off drugs score	41 ± 10, [25 – 62]
Number of sides	48
Number of microelectrodes per STN	3 ± 1, [1 – 5]

* UPDRS = Unified Parkinson's Disease Rating Scale.

The local nature of oscillations in the LFP beta and gamma band was verified by analyzing specifically those frequencies in the LFP that show a significant coherence with local neuronal firing (i.e., LFP-spiking coherence passing the 99% confidence interval). We have compared this method with other frequently used methods spectral analysis. In this way, we have explored how the temporal coupling between neuronal spiking and LFP can guide spectral analysis and how combined recordings of LFP, and neuronal spiking can be used for the localization of the sensorimotor part of the STN. Both the beta and the gamma power of the LFP and neuronal spiking signals are hypothesized to be greater inside than outside the sensorimotor STN. Furthermore, we hypothesize that the analysis of spectral power around frequencies that show significant coherence between LFP and local neuronal firing can increase this difference and thereby help to discriminate between measurements inside and outside the sensorimotor STN.

Materials and methods

Participants and surgery

The study was approved by the Medical Ethical Committee of the Academic Medical Center in Amsterdam. All the subjects received oral and written information and signed an informed consent prior to inclusion. The study was conducted conform the Declaration of Helsinki (1964 and later revisions), in accordance with the Dutch Act on Medical Research Involving Human Subjects (WMO) and with the Standard EN ISO 14155: 2011 on clinical investigation of medical devices for human subjects – Good Clinical Practice.

Twenty-five patients with idiopathic PD (age 60 ± 10 years) who underwent DBS surgery were included in this study. Twenty-three patients underwent bilateral STN-DBS and two patients had unilateral STN-surgery (table 1). The selected patients, despite optimal drug treatment, suffered from severe response fluctuations, dyskinesias,

painful dystonia and/or bradykinesia. Exclusion criteria were an age below 18 years, a Hoehn and Yahr stage of five at the best moment of the day, a Mattis dementia rating scale score of 120 or below, psychosis, and the general contra-indications for stereotactic surgery.

The procedure for DBS was a one-stage bilateral or unilateral stereotactic approach. A detailed description of the surgical procedures has been published before.[93] Standard MER was performed to determine the STN borders during DBS surgery using one to five steel cannulas and microelectrodes (FHC, Inc., Bowdoin, ME, USA) arranged in a cross shaped array with an inter-electrode distance of 2 mm.

Recording protocol

The number of microelectrodes was determined by the neurosurgeon, mainly based on the preoperative imaging. The recordings started 6 mm before the preoperatively determined MRI-based target point and was continued downward in 0.5 mm steps until substantia nigra activity was recognizable in at least one channel or STN activity significantly decreased in all channels indicating the lower border of the STN. Standard MER was performed with the Leadpoint system (Medtronic, Minneapolis, MN, USA), amplified with a gain of 10,000, analog bandpass filtered between 500 and 5000 Hz (23 dB; 12 dB/oct). The signal was sampled at 12 kHz, by use of a 16-bit AD converter and afterwards up-sampled to 24 kHz offline. Following a two second signal stabilization period after electrode movement cessation, multi-unit segments were recorded for 5 – 20 s. The MER signals were scored as recorded inside or outside the STN by an experienced physicist and a neurologist based on the observed combination of neuronal spiking activity and background noise.[63,72]

At each depth, standard MER was immediately followed by a simultaneous recording of LFP and single/multi-unit activity using a switch board to connect the same microelectrodes to a different amplifier, suited for both high and low frequency signals (REFA amplifier, TMSi, Oldenzaal, the Netherlands). The recordings from the 10 µm exposure micro-tip were referenced against the 1 mm exposed surface of the inner cannula located 10 mm above the tip of the microelectrode and were sampled at 20 kHz. For the purpose of this study, recordings of 10 s (22 sides) or 15 s (26 sides) per depth were made. This short measurement time was chosen as it was assumed that this time window provided a sufficient representation of the STN activity, while keeping the additional surgery time as short as possible. Further processing and data analysis were performed offline using Matlab (v. 7.14, R2012a, The Mathworks, Natick, MA, USA).

Mapping procedure

Multiple recordings were made inside and outside the STN. In order to discriminate between measurements in the sensorimotor area and the non-sensorimotor area of the STN, we used a novel approach to map an atlas-derived 3D body of the STN on the microelectrode recording sites.[73,114] This three-dimensional mapping method uses the classifications of the standard MER recordings with the Leadpoint system to estimate the location and orientation of the STN for each patient specifically. A 3D brain atlas was used in which the STN is represented as a three-dimensional polygon surface.[75,76] We used an optimization function to find the optimal position, rotation, and scaling of the STN atlas relative to the stereotactic locations of the MER measurements. A more extensive description of this mapping procedure and the specific settings used during the procedure has been published earlier.[73] The optimization procedure results in a spatial representation of the STN as it is defined by the observed combination of neuronal spiking activity and background noise measured by the Leadpoint microelectrode recordings. For the purpose of this study, it was assumed that at least two microelectrode tracks were required to obtain a reliable estimation of the STN location. One STN was excluded from further analysis since it was estimated by only one microelectrode track.

Based on the work of Parent and Hazrati[38], we assumed the sensorimotor area of the STN to be the lateral 2/3rd of the dorsal portion of the rostral 2/3rd of this STN body and the caudal 1/3rd of this STN body. The non-sensorimotor STN was defined to be the 1/3rd ventral part and the 1/3rd medial tip of the rostral 2/3rd of this STN body.[38,43,115] All simultaneous LFP and MER measurements done with the experimental setup were then labelled based on their stereotactic location in these different functional subthalamic areas (figure 1).

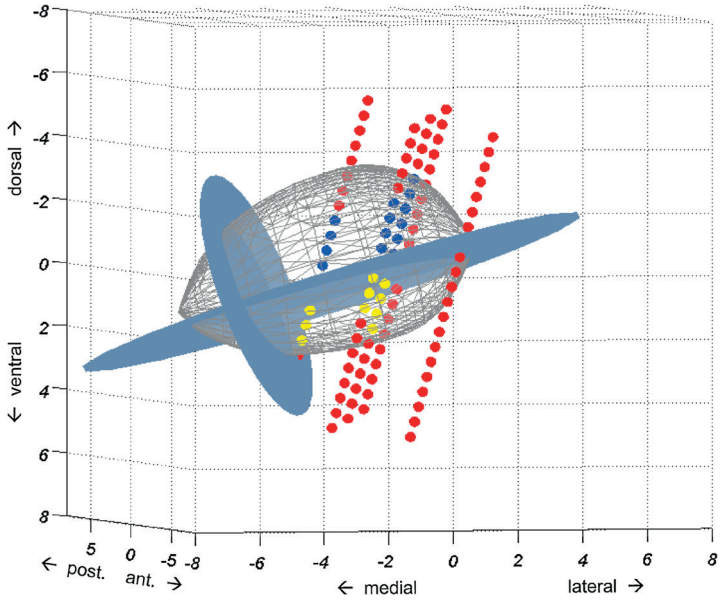

Figure 1. A 3D view of the STN showing the results of the mapping procedure. The dots represent the MER measurement sites scored as outside (red) or inside (blue and yellow) of the STN. The gray body represents the atlas STN body fitted to the MER scorings by the optimization routine. The volume dorsolateral of the two oval blue planes is assumed to be the sensorimotor part of the STN. Based on these planes, the measurement sites inside the STN are divided into measurements in the sensorimotor part of the STN (blue) and in the non-sensorimotor part of the STN (yellow).

Data analysis

Localization of the measurements

After the labeling of measurements to their corresponding locations, the measurements were divided into three areas per studied STN: (1) recorded dorsal to the STN, (2) inside the sensorimotor part of the STN and (3) inside the non-sensorimotor part of the STN (figure 1). Measurements of trajectories that missed the STN and measurements ventral to the STN were excluded from further analysis.

Artifact detection

Artifacts which interfered with the analysis, including movement of the wires, talking of the patient and other mechanical disturbances, were excluded using an extensive artifact detection procedure. First, drift was removed from the recording by subtraction of a fifth order polynomial fitted to the recorded signal. Any remaining offset was removed by high pass filtering the signal using a second order non-causal, zero-phase, Butterworth filter with a cut-off frequency of 0.5 Hz. Line noise was then removed using a second order non-causal, zero-phase, Butterworth band-stop filter between 48 Hz and 52 Hz.

To identify large amplitude artifacts and exclude them from further analysis, a visually assigned threshold was used on the instantaneous amplitude of the signal. The instantaneous amplitude was obtained by taking the real part of the Hilbert transform of the signal.[116] Subsequently, the periods in which this signal exceeded the visually assigned threshold and the 0.75 s before and after these periods were excluded from further analysis. After the identification of large amplitude artifacts, further analysis was performed on the original waveform after offset removal and line noise filtering. The remaining periods of the recordings were divided into epochs of one second duration. Welch's method was used to calculate the power spectral density (PSD) of each one second epoch. For this, four 0.4 second windows with 50% overlap were averaged, resulting in a PSD with a frequency resolution of 2.5 Hz. These PSD were further analyzed to detect artifacts in the one second epochs.

Two criteria were used for artifact detection in the one second epochs: First, the spectral power in both the 3 – 45 Hz and 55 – 95 Hz band of each epoch was not allowed to exceed four times the median spectral power in these frequency bands recorded in all epochs of a single recording. Second, to obtain a more reliable threshold in case many epochs of a single recording are influenced by artifacts, the spectral power of each epoch was also not allowed to exceed four times the median spectral power of all epochs recorded in the same neurological structure for one specific operation side (either inside or outside the STN). Epochs that did not meet both of these criteria were marked as artifacts and excluded from analysis. All remaining artifact-free segments of two or more consecutive seconds were used for further analysis.

Calculation of power spectra and coherence spectra of LFP oscillations and spike trains

Using different filters, two types of signals were obtained from the same measurement. The LFP signal was obtained by using a third order non-causal, zero-phase, Butterworth filter with bandpass frequencies between 3 Hz and 90 Hz. For analysis of the neuronal spiking activity, a spike train was retrieved from the high frequency component of the recording. For this, a third order non-causal, zero-phase, Butterworth filter with band-pass frequencies between 500 Hz and 3500 Hz was used. A spike train was created by marking local maxima of this signal as a spike event when the maxima exceeded 3.5 times the noise level estimated with the envelope method described before by Dolan et al.[116] Spikes were ignored if the spike events occurred within 1 ms of each other (overlapping spikes), if the time between the positive and negative peak of the spike waveform exceeded 0.6 ms, if the amplitude of the negative peak was smaller than 0.3 times the amplitude of the positive peak, or if the amplitude of the positive peak was larger than 10 times the estimated noise level. This procedure has been described before in more detail.[73] The resulting multiple unit spike train (MU-ST) reflects the spiking activity of multiple neurons in close proximity of the micro-tip of the electrode (between 100 µm and 200 µm).[71,112,117] For accurate analysis of the beta and gamma frequencies in the spike

trains, we assume that the MU-ST signal should contain at least one neuron spiking with a frequency of 12 Hz (start of the beta frequencies) or higher. Therefore, recordings with on average less than 12 spikes per second were excluded from further analysis. Despite the filtering of line noise, some recordings still showed a distinct 50 Hz peak in their PSD. Recordings for which the power between 48 and 52 Hz exceeded the sum of powers from 44 Hz to 48 Hz and from 52 to 56 Hz, were excluded from analysis as well.

Power spectral densities of the MU-ST and LFP signals and the spectral coherence between LFP and MU-ST were calculated using techniques described by Halliday et al.[118] PSD and coherence were calculated over the complete artifact free part of the signal by taking into account the start samples and the lengths of each of the combined artifact free epochs. The combined artifact-free signal had an average length of 10.7 s ± 3.2 s (SD). The spectral estimation uses the average of the modulus squared Fourier transformation over 0.82 s non-overlapping segments (median of 12 segments per recording) resulting in a frequency resolution of 1.22 Hz. To account for possible differences in the electrodes used in different trajectories, normalization of the PSD was performed by dividing each PSD by the maximum power between 8 and 80 Hz measured in the same electrode trajectory.

Analysis of spectral power in the PSD of LFP oscillations and spike trains

In this study we compare three different methods to analyze the spectral powers in the beta and gamma frequency bands represented in the PSD of both the LFP and the MU-ST signals. For this purpose, we analyze, using each of the three methods, the same PSD calculated out of the same artefact free parts of the same recordings. In the first method, the power of the complete beta and gamma spectrum was calculated by integration of the PSD from 12 Hz to 35 Hz and 35 Hz to 80 Hz, respectively.

In the second method, a more commonly used method of PSD analysis was used where we detected the most prominent power peak within the beta and gamma range of the PSD for every recording. We did this by identifying the highest values within the beta and the gamma frequency ranges and integrating the PSD over a narrow frequency band (4.88 Hz) surrounding these single peaks for both the beta and the gamma frequency range.

As a third, novel experimental analysis, we introduced the 'coherence method' where the PSD was only integrated over a band surrounding the frequencies that show a significant coherence between the LFP and neuronal spiking activity reflected in the MU-ST signal (i.e., the frequencies for which the coherence spectrum passes the 99% confidence interval). This was done for both the beta (12 – 35 Hz) and gamma (35 – 80 Hz) range of the PSD individually. By using this coherence condition, we make use of the correlation between the more globally measured LFP and neuronal spiking activity,

which is known to be very local. Thereby we attempted to verify the local nature of the oscillations reflected in the LFP recordings. By minimizing the influence of beta and gamma frequency oscillations from distant sites, either those measured by the reference electrode or those spreading to the microelectrode through volume conduction, we limit the analysis of the LFP spectral power as much as possible to oscillating beta and gamma sources around the location of the micro-tip. To evaluate the 'coherence method' we introduced the 'sensorimotor power index' (SMPI), a measure representing the ability to discriminate between recordings in the sensorimotor and the non-sensorimotor area based on the mean spectral power in both areas:

$$\text{Sensorimotor power index (SMPI)} = \frac{\text{mean power in sensorimotor STN}}{\text{mean power in non-sensorimotor STN}}$$

In this equation, the mean power in a specific STN area is calculated by taking the average power of all the measurements localized in that area by the mapping procedure, that remained after artefact correction and spike train creation. When using the 'coherence method', measurements that showed no significant coherence between LFP and MU-ST in a specific frequency band were treated as measurements with zero spectral power in that frequency band. The SMPI values were calculated for both the LFP and the MU-ST signal and both using the beta and the gamma range of the power spectrum.

Statistics

Paired two-tailed t-tests were used to compare the percentage of measurements that showed a significant coherence between areas, for both the beta and gamma frequency ranges. We also compared the bandwidth over which the coherence spectrum passes the 99% confidence interval between areas, using paired two-tailed t-tests.

For the statistical analysis of the SMPI values, all results were logarithmically transformed since the log of a ratio has better statistical properties than the ratio itself. One sample two-tailed t-tests, including Bonferroni correction for multiple comparisons (n = 12), were performed to test whether the log-transformed SMPI values were greater than zero, reflecting the hypothesized increased power in the sensorimotor STN. Paired two-tailed t-tests, including Bonferroni correction for multiple comparisons (n = 12), were performed to compare the log (SMPI) between the three methods used, for beta and gamma frequencies of both the LFP and the MU-ST signal.

The log (SMPI) is hypothesized to be greater than zero for both beta and gamma powers. The log (SMPI) values are hypothesized to be larger when using the 'coherence method' compared to the other two methods of spectral analysis, representing a better discrimination between the sensorimotor and the non-sensorimotor STN.

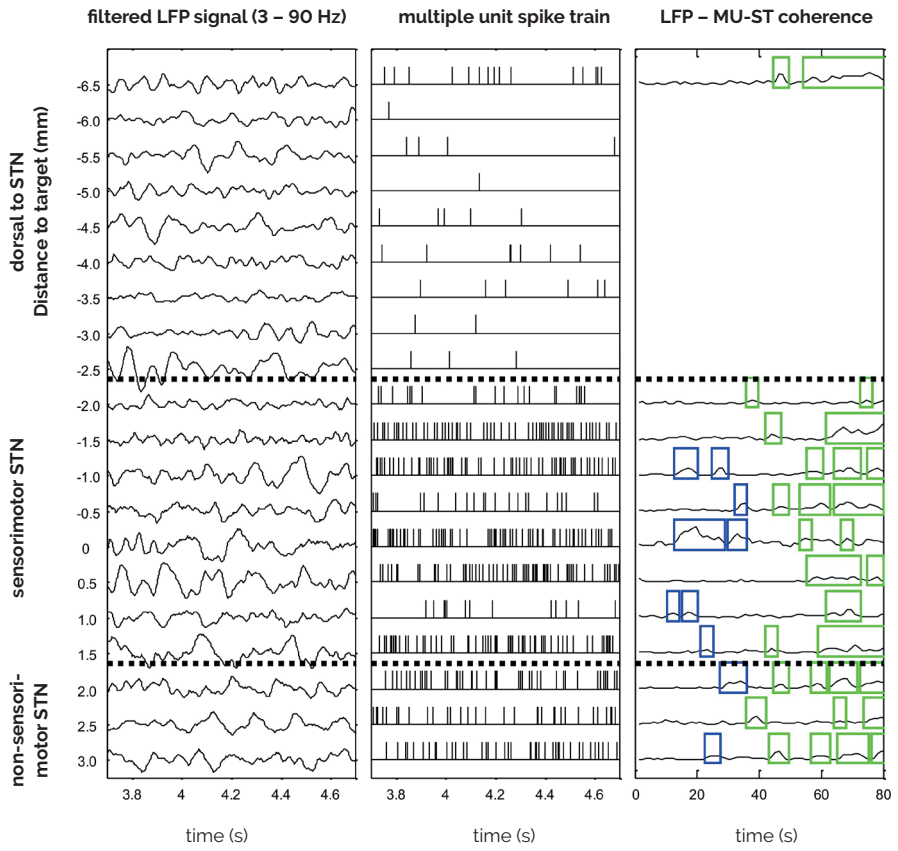

Figure 2. Example of the LFP (left) and the MU-ST (middle) signals, simultaneously recorded in one channel, passing the three area categories indicated on the far-left axis. The y-axis shows the distance in mm to the pre-defined target in the center of the STN. On the right the spectrum of the coherence between LFP and MU-ST is depicted for measurements that show enough spikes to be suited for coherence analysis. Blue and green rectangles represent frequency bands within the beta and gamma frequencies respectively for which the coherence between LFP and MU-ST passes the 99% confidence interval.

Results

After artefact correction, 44 sides (24 patients) showed enough stable recordings of adequate length to calculate reliable measures for power and coherence. Three sides had no artefact free measurements longer than two seconds in one (2 sides) of both (1 side) of the STN areas and the SMPI could therefore not be calculated. On one side, the depth of the recordings could not be confirmed with certainty and this side was also excluded.

The first two columns of figure 2 show one second examples of the LFP and the MU-ST signals that were simultaneously recorded in one channel, passing through the STN. The third column shows the coherence spectrum of the signals in the first two columns for measurements that show enough spikes to be suited for coherence analysis. The mapping procedure divided all the measurements into three area categories per STN.

Coherence between LFP and MU-ST

Table 2 shows the percentage of measurements that were used for coherence analysis after artifact correction and spike train creation. Because only a small percentage of the measurements dorsal to the STN shows spiking activity, the percentage of measurements that could be used for coherence analysis in that area was much smaller than in the sensorimotor and non-sensorimotor STN areas.

The amount of measurements outside the STN that could be used for coherence analysis proved to be too small to make any statements about the added value of coherence in the analysis of the spectral powers. Therefore, this area category was not further analyzed.

Comparing the sensorimotor and the non-sensorimotor area, paired t-tests showed no significant differences in the percentage of measurements that show a beta coherence (42.1% vs 42.0%; $p = 0.99$), nor in those that show a gamma coherence (62.8% vs 68.4%; $p = 0.10$) (table 2). However, the average bandwidth over which the beta coherence spectrum passed the 99% confidence interval was significantly larger in the sensorimotor area than in the non-sensorimotor area (4.5 Hz vs 3.6 Hz; $p = 0.005$). In the gamma coherence spectrum, no significant difference in the bandwidth of coherence was observed.

Table 2. Overview of the amount of measurements per STN remaining in the three area categories after artifact correction (column 1), the percentage of these measurements that was suited for coherence analysis (column 2) and the percentage of these measurements with a significant coherence in the beta (column 3) and gamma (column 4) frequency bands

	Average number of measurements per STN	**Average percentage of measurements suited for coherence analysis (±SD)**	**Average percentage of measurements with significant beta coherence (±SD)**	**Average percentage of measurements with significant gamma coherence (±SD)**
Dorsal to STN	18.4 (±9.9)	7.4%*		
Sensori-motor STN	20.5 (±5.3)	68.9% (±19.2)	42.1% (±13.5)	62.8% (±19.1)
Non-sensori-motor STN	8.3 (±3.2)	74.7% (±16.5)	42.0% (±17.0)	68.4% (±18.3)

* Median percentage (distribution of the percentages was skewed to the right).

Spectral power of the LFP and MU-ST

A summary of the logarithmically transformed SMPI values is shown in table 3.
Both when calculating the spectral beta power using the complete beta spectrum from 12 Hz to 35 Hz and when calculating the power around the detected peaks in the beta spectrum, we found the log (SMPI) of the LFP beta frequencies to be significantly greater than zero, with mean = 0.085, $p < 0.001$ and mean = 0.089, $p < 0.001$, respectively. Also, when using the 'coherence method', the log (SMPI) of the LFP beta frequencies was significantly greater than zero (mean = 0.262, $p < 0.001$). The average log (SMPI) of the LFP gamma frequencies was not significantly different from zero using any of the three methods of spectral analysis (table 3).

Using the same methods for SMPI calculation on the MU-ST spectral density we found that both analyzing the complete beta power spectrum and analyzing power around detected peaks in the beta spectrum did not result in log (SMPI) values different from zero (mean = 0.108 and mean = 0.119, respectively). However, when using the 'coherence method', the log (SMPI) was significantly greater than zero, with mean = 0.335, $p = 0.001$. In the gamma frequencies, none of the three methods of MU-ST spectral analysis resulted in average log (SMPI) values that were significantly different for zero (table 3).

Figure 3 shows a graphic display of the log (SMPI) values of the LFP and MU-ST beta frequencies, including the results of paired t-tests comparing the log (SMPI) values between the three methods of spectral analysis.

Comparing the log (SMPI) values of LFP signals, no significant differences were found between the analysis of the complete spectrum and the analysis of power around detected PSD peaks. However, the 'coherence method' resulted in a significantly larger log (SMPI), both compared to the analysis of the complete spectrum as well as the analysis using peak detection in the PSD ($p < 0.001$)

Table 3. Overview of the mean log (SMPI) values calculated with the three different methods for LFP and MU-ST signals, for beta and gamma frequencies; p-values are depicted for the one sample t-tests comparing the mean log (SMPI) values to a value of zero

	Complete spectrum analysis	**Peak detection method**	**Coherence method**
log (SMPI) beta LFP	0.085 **(*p* < 0.001)**	0.089 **(*p* < 0.001)**	0.262 **(*p* < 0.001)**
log (SMPI) gamma LFP	0.016 *not significant*	0.017 *not significant*	0.001 *not significant*
log (SMPI) beta MU-ST	0.108 *not significant*	0.119 *not significant*	0.335 **(*p* = 0.001)**
log (SMPI) gamma MU-ST	0.030 *not significant*	0.024 *not significant*	0.050 *not significant*

A similar trend was observed when comparing the log (SMPI) values of MU-ST signals, though less significant. Analysis of the complete MU-ST spectrum and the analysis of power around detected peaks in the spectrum did not result in significantly different log (SMPI) values. Using the 'coherence method' seems to result in higher log (SMPI) values compared to both the other two methods of spectral analysis. However, when using Bonferroni correction for multiple comparisons (n = 12), the trend does not reach significance (p = 0.016 and p = 0.025 for comparison with complete spectrum analysis and peak detection analysis, respectively).

We found no significant differences when comparing the log (SMPI) values found using the gamma frequencies between methods, neither for LFP, nor for MU-ST signals.

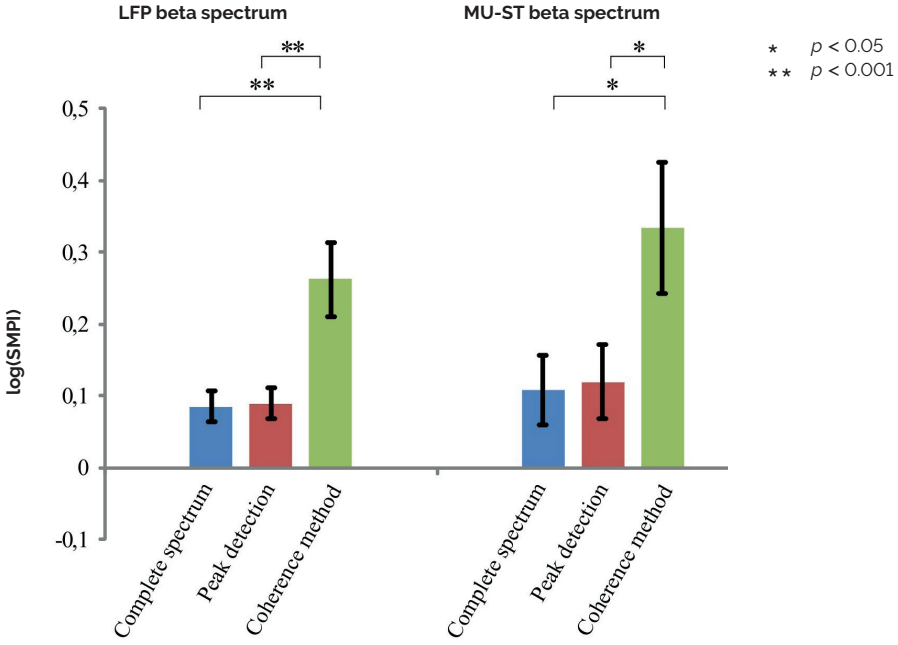

Figure 3. Overview of the mean log (SMPI) values including standard errors of the means calculated by the three different methods of spectral analysis using the beta frequencies, for both LFP and MU-ST signals; p-values are depicted for the results of paired t-tests comparing log (SMPI) values between methods.

Discussion

The results of this study suggest that, taking into account the coherence between LFP and MU-ST can help to differentiate measurements inside the sensorimotor STN from measurements elsewhere in the STN through the analysis of LFP spectral power in the beta band.

Coherence between LFP and MU-ST

The percentage of measurements that show a significant coherence between the LFP and MU-ST signals in the beta frequencies in this study is in accordance with the literature on this subject. We found significant coherence in 42.1% and 42.0% of measurements in sensorimotor and non-sensorimotor STN, respectively. Other studies report similar values of 46%[113] and 25%[95] for the whole STN. These percentages probably relate to the percentage of oscillatory spiking neurons in the STN. Weinberger et al.[95] have shown that almost all (89%) of the measurements that display oscillatory spiking activity, are coherent with simultaneously measured LFP.

Weinberger et al.[95] report that most of the oscillatory neuronal spiking activity was found in the dorsal STN while Alavi et al.[113] report no differences in localization. The latter is in accordance with our finding that the percentage of coherent measurements does not differ between sensorimotor STN and non-sensorimotor STN. In this study, the bandwidth over which the coherence between LFP and MU-ST passes the 99% confidence interval is larger inside than outside the sensorimotor STN (4.5 Hz vs 3.6 Hz; $p = 0.005$). However, the calculation of the coherence spectrum has a frequency resolution of only 1.22 Hz. Therefore, it is difficult to draw any conclusions from this minor difference in coherence bandwidth. It could potentially indicate that the MU-ST signal is a summation of multiple neurons oscillating in a broad range of beta frequencies, all coherent with similar beta frequencies in the LFP signal. This leads to a broader spectrum of coherent oscillations. This summation of multiple oscillating neurons in the MU-ST signal is more likely to occur inside the sensorimotor part of the STN, because oscillating neurons there may be more abundant.[95] We believe that more research into the bandwidth of spiking frequencies in the beta range is necessary.

Spectral power of the LFP

The results of the current study confirm our hypothesis that LFP beta power is elevated in the sensorimotor part of the STN. An average log (SMPI) value greater than zero is found using all methods of LFP spectral analysis. However, the coherence method resulted in a significantly higher beta log (SMPI) value than the other two methods.

The increased LFP beta power in the sensorimotor STN compared to the non-sensorimotor STN is in accordance with previous studies.[23,24,73,93–95] The significantly larger log (SMPI) when using the coherence method compared to the two other methods of LFP spectral analysis is probably due to the diminished influence of volume conducted oscillations in the beta frequencies.

How LFP signals are generated is rather complex.[71] It is dominated by synaptic activity, but it is also influenced by several other processes, for example Ca^{2+} spikes, membrane oscillations, action potentials and spike hyperpolarizations.[111,119–123] The dipoles and return currents created by these processes together determine the extracellular field. One of the factors influencing the conductivity of this electric field is the dendritic morphology which acts as a low pass filter.[124] Therefore, the attenuation of slow oscillations over distance is relatively small and the low frequency LFP signal measured at the microelectrode tip may even reflect sources up to a distance of 10 mm.[108–110] Volume conduction will thus play an important role in the measured LFP in the beta frequencies, especially inside a small structure like the STN.

On the contrary, spikes that are identifiable over the noise level in the high frequency signal are coming from neurons at a distance less than 150 µm around the microelectrode.[112] The distance over which spikes are measurable is limited because of the fast attenuation of these high frequency signals.[125]

By limiting our power analysis to those frequencies that show a significant coherence between the LFP and the MU-ST signals, we diminish the contribution of oscillations in the beta frequency range that are coming from sources located either in different areas of the STN or outside the STN. This confinement to local oscillating sources is in contrast to the analysis of the complete spectrum, in which distant sources can be represented. Even PSD peak detection analysis, which is used to obtain the most prominent oscillating source in the signal, does not ensure that this prominent oscillation is indeed coming from the close proximity of the electrode, making it unreliable for the identification of the sensorimotor part of the STN.

Our hypothesis that LFP spectral power around significant gamma peaks in the coherence spectrum between LFP and MU-ST will discriminate better between the sensorimotor area and the non-sensorimotor area of the STN cannot be confirmed. Gamma log (SMPI) values for all three methods of LFP spectral analysis, including the coherence method, did not significantly differ from zero. Furthermore, no significant differences were found comparing the gamma log (SMPI) values between methods.

Gamma oscillations do not spread as far through the tissue as beta oscillations and thus volume conduction has a smaller effect on the power analysis of the gamma frequencies. Also, gamma oscillations are likely to show a more out-of-phase

behavior over larger distance. This is reflected as an absence of clear peaks in the LFP power spectral density in the gamma range. Another reason for the absence of LFP gamma peaks could be that the patients in this study are measured during rest while gamma frequencies in the LFP are thought to relate more to specific movement parameters.[96,101,102,105]

Spectral power of the MU-ST

The beta log (SMPI) for MU-ST signals calculated with the coherence method is significantly greater than zero, in contrast to the other two methods in which the beta log (SMPI) does not significantly differ from zero. When comparing between methods of MU-ST spectral analysis, the difference in log (SMPI) is not significant after Bonferroni correction for multiple comparisons, but it does show a trend. Contrary to the LFP signal, the MU-ST analysis is not influenced by volume conduction in any of the methods. A way to explain the trend could be that the oscillations in the MU-ST signal that are coherent with the beta LFP can be caused by a summation of multiple oscillating neurons, leading to a larger peak in the PSD of the MU-ST signal. Because this summation of oscillating neurons in the MU-ST signal is more likely to occur in the sensorimotor STN where oscillating neurons are more abundant[95], the power of the MU-ST signal at the coherent frequencies is greater here than in the non-sensorimotor STN. This is in agreement with the finding that the beta log (SMPI) of MU-ST signals is significantly greater than zero when using the coherence methods, even though the percentage of measurements that show a significant coherence between LFP and MU-ST does not differ between sensorimotor and non-sensorimotor STN. The spectral analysis in the other two methods is probably influenced too much by other peaks in the PSD of the MU-ST signal, leading to an average log (SMPI) value which is not significantly greater than zero.

In gamma frequencies, no average log (SMPI) values significantly greater than zero were found for any of the methods and no significant differences were found between methods. Similar to the gamma LFP results, this may be explained by the fact that the measurements in this study were performed during rest. Previous research on oscillatory spiking activity has also found an equal distribution of gamma oscillations within the STN.[93]

Limitations and recommendations

In this study, we used a personalized atlas of the STN mapped on the intraoperative microelectrode recording sites to estimate the size and location of the sensorimotor and non-sensorimotor part of the STN. The subdivision of the STN in different functional areas, based on an atlas model is derived from histological studies[38], and it might not be fitting with the true subdivision for each patient. Therefore, we can only use it as an estimate. Although such an estimate will not be sufficient to correctly guide electrode

implantation, it is sufficient for this study to show the potential added value of the coherence method. We demonstrate that using this new method can be beneficial in locating the sensorimotor STN area for each patient specifically, so that electrode placement can in the future possibly be guided by beta LFP power and estimates based on atlas coordinates may no longer be necessary.

Analyzing the LFP power of only the specific coherent frequencies minimizes the influence of LFP oscillations from distant sites but it does not fully exclude it. The frequencies of distant LFP oscillations may overlap with the coherent frequencies and may therefore still add to the calculated LFP power. Often bipolar LFP recordings are used to minimize the effects of distant low frequency oscillations. However, intraoperative LFP recordings with a sufficient spatial resolution require extensive changes to the standard surgical procedures. The goal of this study was to intraoperatively localize the STN and its sensorimotor part without significant changes to the standard surgical procedures. The coherence method is used in this study as a way to do that by making the analysis of the LFP beta oscillations more local. However, many centers are no longer using microelectrodes to guide DBS implantation. We therefore recommend looking for other methods that can measure the beta oscillations in the LFP very locally without extensive changes to the surgical procedures. Recent advances in technology have led to the development of DBS leads which deliver stimulation through multiple smaller contact points, ranging from 8 to 32 individual contacts.[28,29,126] These multi-contact arrays make it possible to do bipolar LFP recordings with a much better spatial resolution. Using this type of high resolution LFP recordings might make it possible to do advanced intraoperative target identification of the sensorimotor STN.

This study demonstrates significantly elevated LFP and MU-ST beta power on a group level. Furthermore, it shows that the discriminative ratio between sensorimotor and non-sensorimotor STN based on beta frequencies can be increased by using the coherence method. However, to proof that the coherence method truly preforms better than the other two methods in identifying the sensorimotor STN, a difference between the methods should be shown at patient level. However, we found that this was not possible due to the limited number of measurement sites available per STN, especially in the non-sensorimotor STN. The median amount of measurement sites is 13 in the sensorimotor area and 6 in the non-sensorimotor area. Therefore, we chose to use the sensorimotor power index (SMPI) as a measure to express the ability to discriminate between sensorimotor and non-sensorimotor STN and compare the SMPI values between the three methods. We found that in 30 out of 44 STN the SMPI value using the coherence method was greater than the SMPI values using the other two methods.

Although the coherence method performs better at group level, the limited number of available measurement sites per patient makes a comparison between methods

at patient level unreliable. When a comparison at patient level was performed, we found that the distributions of beta powers in both the sensorimotor and the non-sensorimotor STN were skewed to the right. Therefore, we used log-transformation and independent samples t-tests to compare the beta powers in the sensorimotor STN with the beta powers in the non-sensorimotor STN, for all three methods. We found that using the coherence method, the beta power in the sensorimotor STN was significantly increased in only three out of 44 STN. In both of the other two methods, we found a significant increase in only five out of 44 STN. These numbers are too small to reliably compare the performance of the three methods at patient level.

Conclusion

In conclusion, the coherence method potentially has an added value for the discrimination of the sensorimotor STN, because of its ability to specifically analyze the power of locally measured beta oscillations. Volume conduction of beta frequency oscillations in the LFP signal interferes with the intraoperative identification of the sensorimotor STN and therefore it probably cannot be done with LFP recordings alone. However, for the use of the coherence method to discriminate the sensorimotor STN from the non-sensorimotor STN at patient level, more measurement sites per STN would be necessary. When these are available, simultaneous recordings of LFP, and neuronal spiking activity could be beneficial in intraoperative target identification of the sensorimotor STN. With only a minor modification of standard surgical procedures, it is possible to increase the discrimination between measurements inside and outside the sensorimotor STN.


39 57.6888, 3 12.7385

CHAPTER 4

Electrode location in a microelectrode recording-based model of the subthalamic nucleus can predict motor improvement after deep brain stimulation for Parkinson's disease

Rens Verhagen
Lo J. Bour
Vincent J. J. Odekerken
Pepijn van den Munckhof
P. Richard Schuurman
Rob M. A. de Bie

Brain Sciences. 2019;9(3)

Objective: Motor improvement after deep brain stimulation (DBS) in the subthalamic nucleus (STN) may vary substantially between Parkinson's disease (PD) patients. Research into the relation between improvement and active contact location requires a correction for anatomical variation.

Methods: We studied the relation between active contact location relative to the neurophysiological STN, estimated by the intraoperative microelectrode recordings (MER-based STN), and contralateral motor improvement after one year. A generic STN shape was transformed to fit onto the stereotactically defined MER sites. The location of 43 electrodes (26 patients), derived from MRI-fused CT images, was expressed relative to this patient-specific MER-based STN. Using regression analyses, the relation between contact location and motor improvement was studied.

Results: The regression model that predicts motor improvement based on levodopa effect alone was significantly improved by adding the one-year active contact coordinates (R^2 change = 0.176, p = 0.014). In the combined prediction model (adjusted R^2 = 0.389, p < 0.001), the largest contribution was made by the mediolateral location of the active contact (standardized beta = 0.490, p = 0.002).

Conclusion: With the MER-based STN as a reference, we were able to find a significant relation between active contact location and motor improvement. MER-based STN modeling can be used to complement imaging-based STN models in the application of DBS.

Introduction

Deep brain stimulation (DBS) of the subthalamic nucleus (STN) is a widely used and effective surgical treatment for advanced Parkinson's disease (PD) when treatment with dopaminergic medication is no longer satisfactory.[2,4,85] The main therapeutic effect of STN-DBS lies in the off-medication improvement of the cardinal PD motor symptoms of bradykinesia, tremor, and rigidity[11,127]; an improvement that is on average 50% of the off-medication symptom severity.[9] However, there is a large variation in outcome between patients, both in terms of motor improvement and side effects.[2,6,10–12] The postoperative motor improvement is dependent on, amongst others, age, and disease duration[13–15] as well as the preoperative response to dopaminergic medication[9,14], which makes careful selection of DBS candidates essential. However, the most important factor determining motor improvement reached through DBS is the correct positioning of the active contact in the subthalamic area.[16–20,128–132]

The relation between active contact location and motor improvement has been widely studied, but the results of these studies are not conclusive.[16] While some claim that stimulation within the borders of the STN is most effective[18,131,132], others prefer stimulation of the fiber tracts and/or the zone incerta dorsal to the STN[19,129], or specifically the border zone between the dorsal STN and the zona incerta.[17,128,130] The methodologies used to study this relation are variable.[16,133] Determining the active contact location solely in relation to the midcommissural point (MCP) as the anatomical reference ignores a large part of the anatomical variation in STN size and location. This may be the reason that a clear relation between active contact location and motor improvement was not demonstrated with these methods.[133–135] The transformation of brain atlases, based on anatomical landmarks, only partially corrects for anatomical variations.[16,128,136] Referring the active contact location to the STN visible in MRI images takes a large part of the anatomical variation into account.[20,137,138] However, this method depends on high quality MRI images, and STN size and location on MRI shows some variation depending on the field strengths and imaging sequences that are used. The dimensions of the MRI-based STN do not always match the dimensions of the neurophysiological STN as measured by intraoperative microelectrode recordings (MER).[54,56,139] Studies that use MER to define the neurophysiological STN as a reference for the active contact location have been limited in the fact that they only define dorsal and ventral STN borders. Therefore, they are unable to make any statements about the laterality of the active contact location[16,18], while MRI studies have shown that laterality can be an important factor influencing motor improvement.[20,128,138]

In this study we defined the location of the active DBS contact after one year relative to an STN model of which the size and location is automatically estimated based on multiple-channel MER measurements (MER-based STN).[139] This approach enabled us to relate the active contact location not only to the dorsoventral dimensions of the

MER-based STN, but also to its anteroposterior and mediolateral dimensions. Then we explored the predictive effect of active contact location relative to this MER-based STN on contralateral motor improvement one year after surgery.

Materials and methods

Patient selection

For this study, we selected a subset of STN implantations (n = 45) in patients enrolled in the Netherlands SubThalamic And Pallidal Stimulation (NSTAPS) trial, which compared STN-DBS with Globus Pallidus interna DBS, after receiving ethical approval (ID 07.17.0069, Medical Ethical Committee AMC, 05/17/2006). Additional selection criteria were: (1) patients received STN-DBS in the Academic Medical Center in Amsterdam, (2) three or more MER trajectories measured STN activity during DBS implantation, (3) Unified Parkinson's Disease Rating Scale (UPDRS) motor scores were available before and one year after surgery, and (4) CT images showing the implanted DBS electrode one year after surgery were available.

Surgical procedures and microelectrode recording (MER)-based subthalamic nucleus (STN) estimation

DBS surgery was performed using a one-stage unilateral or bilateral stereotactic approach. Standard stereotactic coordinates (12 mm lateral, 2 mm posterior, and 4 mm ventral to MCP) were visually adjusted based on 1.5 Tesla, T2-weighted MRI images. Neurophysiological mapping was performed with a 0.5 mm step size using three (n = 20), four (n = 19) or five (n = 6) tracks of MER to verify STN borders. After MER, macro-electrode test stimulation was performed, and all patients were then implanted with the Medtronic 3389 electrode. Detailed descriptions of the surgery and MER measurements have been published before.[93] All MER measurement sites were scored as either inside or outside the STN by a clinical physicist based on visual analysis of background activity and single/multi-unit spiking activity.[72] A previously developed method was used to automatically estimate patient-specific STN size and the location of all its borders, based on the classifications of multiple-channel MER measurements. This was done in Matlab® (Mathworks, Inc., Natick, MA, USA) by transposing and scaling an atlas-derived 3D STN shape, within previously validated boundaries[139], to optimally fit the classifications of all MER sites. The resulting MER-based STN was used as the reference for location analysis in this study. The details of this method have been published before.[73,139] This previous publication also showed that a reliable MER-based STN model could be created when STN activity was measured on three or more MER tracks, and that no big differences were found between models created from three, four, or five tracks. The higher resolution in the dorsoventral direction, compared to the anteroposterior and mediolateral directions,

is taken into account by the model. If relatively little information is available in the anteroposterior or mediolateral direction, the created model will be closer to the atlas-derived 3D STN with minimal transposing and scaling in these directions. Moreover, a previously published study has shown that the estimated lateral border of the MER-based STN corresponded to the lateral STN border identified on ultra-high field (7.0 T) T2-weighted MRI images.[139]

Postoperative electrode recognition

Using SureTune® (Medtronic Eindhoven Design Center, The Netherlands), the preoperative T1-MRI images including the stereotactic frame, which were used for preoperative target planning, were co-registered to the CT images showing the DBS electrodes one year after surgery. The software automatically projected a 3D model of the Medtronic 3389 electrode onto the electrode artifact seen on the CT. This projection was manually improved to optimally fit the artifact in three dimensions. After that, the stereotactic electrode location was exported from SureTune® to Matlab® and combined with the patient-specific MER-based STN in stereotactic space.

In this study, we calculated the position of the stimulated contact one year after surgery relative to each patient's specific MER-based STN. In order to perform a group analysis, every patient specific STN was transformed, together with the electrode location, back to the initial STN shape from which it was created. This created a generic STN shape in an anterior commissure-posterior commissure (AC – PC) -aligned orientation in reference to which all the locations were expressed, hereafter referred to as the generalized STN. By doing this, we compensated for the anatomical variation in STN size and location. The back-transformation was done using the inverse of the transposition and scaling applied to initially produce the patient-specific MER-based STN. The electrode was transformed with the same inverse transformations so that the contact locations of all patients were expressed in reference to the same generalized STN, while the position of the contact locations relative to this STN remained to be based on the patient-specific MER measurements (figure 1). For right-hemisphere implantation, all procedures were mirrored to enable a group analysis.

The contact used for stimulation was retrieved from the stimulator settings after a neurologist optimized them over the course of one year. When bipolar stimulation was used (n = 3), the negative pole was determined as the active contact. In double monopolar stimulation (n = 2), the center between the two active contacts was used as the active contact location. To verify our results, the analysis was also performed without these five electrodes.

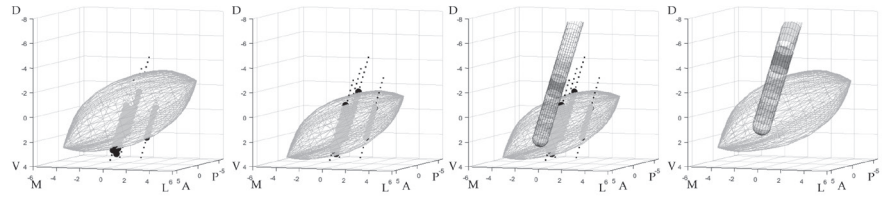

a **b** **c** **d**

Figure 1. Anterolateral view of the subthalamic nucleus (STN) in an AC – PC aligned orientation illustrating how the contact locations were expressed in reference to the generalized STN. **(a)** The atlas-derived generic 3D STN shape is placed on top of the patient-specific MER sites (• = outside STN, • = inside STN); **(b)** the STN is transformed to optimally fit the classifications of all MER sites; **(c)** the DBS electrode and its contacts, recognized in MRI-fused CT images, are combined with the MER-based STN using the patient-specific stereotactic frame (active contact after one year in darker gray); **(d)** both the MER-based STN and the recognized electrode are inversely transformed together. All the electrode contacts are now expressed in reference to the generalized STN in an AC – PC aligned orientation. A = anterior, D = dorsal, L = lateral, M = medial, P = posterior, and V = ventral. Locations displayed on the axes are in mm.

Motor improvement

In the NSTAPS trial, PD motor symptoms were assessed using the UPDRS part III after optimization of the stimulation parameters over the course of one year. Both patients and clinical raters were blinded for active contact location.[11] For this study on the contralateral motor improvement, only the purely one-sided UPDRS motor score sub-items (UPDRS-III items 20 – 26) were used.[140] Because off-medication motor improvement is typical for effective STN-DBS, the motor improvement was studied by the off-medication stimulation effect, which is defined by the change in off-medication hemibody UPDRS motor score after DBS as a percentage of the baseline off-medication hemibody UPDRS motor score determined preoperatively:

$$\text{Stimulation effect} = \frac{\text{hemibody UPDRS}_{\text{med\_off}}\,(\text{baseline}) - \text{hemibody UPDRS}_{\text{med\_off}\,|\,\text{stim\_on}}\,(1\ \text{year})}{\text{hemibody UPDRS}_{\text{med\_off}}\,(\text{baseline})}$$

Statistical analysis

The coordinates of the active contacts relative to the center of the generalized STN were statistically analyzed in an AC – PC aligned three-dimensional coordinate system with the x-axis from medial to lateral, y-axis from posterior to anterior, and the z-axis from dorsal to ventral.

Table 1. Clinical characteristics of the patients (top) and the contralateral hemibody scores per electrode (bottom)

Patient characteristics (*n* = 26)	
Male/female	20/6
Age – years (mean ± SD)	62.7 ± 7.1
Disease duration – years (mean ± SD)	12.6 ± 6.6
Contralateral hemibody scores per electrode (*n* = 43)	
Levodopa window (mean ± SD)	10.5 ± 5.5
Baseline $UPDRS_{med\_off}$ (score range = 0 – 36) (mean ± SD)	15.0 ± 5.6
One-year $UPDRS_{med\_off}$ (score range = 0 – 36) (mean ± SD)	6.6 ± 4.2
Off-medication stimulation effect – % (mean ± SD)	50.3 ± 32.5

UPDRS: Unified Parkinson's Disease Rating Scale.

To analyze the predictive power of active contact location, multiple linear regression was performed using SPSS version 23 (SPSS Inc., Chicago, IL, USA), with the off-medication stimulation effect as the dependent variable and the three coordinates (x, y, and z) of the active contact locations relative to the center of the generalized STN as independent variables. Because the preoperative response to dopaminergic medication is a known predictor for the off-medication stimulation effect, the levodopa window (*hemibody* $UPDRS_{med\_off}$ *(baseline) - hemibody* $UPDRS_{med\_on}$ *(baseline)*) was also included as an independent variable. Hierarchical multiple regression was performed to study the added predictive value of the three active contact coordinates after controlling for the influence of the levodopa window.

Results

Of the 45 implanted electrodes from the NSTAPS trial that matched our inclusion criteria, one was excluded because the MER classifications of different trajectories were conflicting, and we were unable to produce a reliable MER-based STN estimation. Furthermore, regression analysis revealed one negative outlier in the dependent variable stimulation effect (-133%). Because of the profound impact that outliers can have on linear regression fits, possibly causing overestimation or underestimation of the relation, this observation was excluded in all further regression analyses.

The relation between active contact location and contralateral off-medication stimulation effect was studied in 26 patients (43 electrodes). Clinical characteristics are summarized in table 1. The three-dimensional locations of the active contacts one year after surgery, relative to the center of the generalized STN, are summarized in table 2.

Table 2. The three-dimensional active contact locations after one year

Direction	Location to center STN mm (mean ± SD) *
Mediolateral (x)	1.0 ± 1.5
Anteroposterior (y)	1.7 ± 1.7
Dorsoventral (z)	-2.2 ± 2.1

* Distances are referenced to the center of the generalized STN. The x-coordinate is positive towards lateral, y is positive towards anterior, and z is positive towards ventral.

Hierarchical regression revealed that adding the three coordinates of the active contact to the known predictor levodopa window resulted in a significant improvement of the prediction of off-medication stimulation effect (R^2 change = 0.176, p = 0.014). The combined model, with the levodopa window and the three active contact coordinates (x, y, and z) as the independent variables, was a significant predictor of off-medication stimulation effect (adjusted R^2 = 0.389, p < 0.001). In this model, the mediolateral location (x-coordinate) of the active contact had the largest unique contribution to the prediction (standardized beta = 0.490, p = 0.002), followed by the levodopa window (standardized beta = 0.328, p = 0.022). The contributions of the anteroposterior (y-coordinate) and dorsoventral location (z-coordinate) of the active contact were not significant. Figure 2 displays the distribution of the active contact locations after one year relative to the generalized STN, which were used for the regression analysis. Figure 3 shows a scatter plot of the relation between mediolateral location (x-coordinate) relative to the center of the STN and stimulation effect.

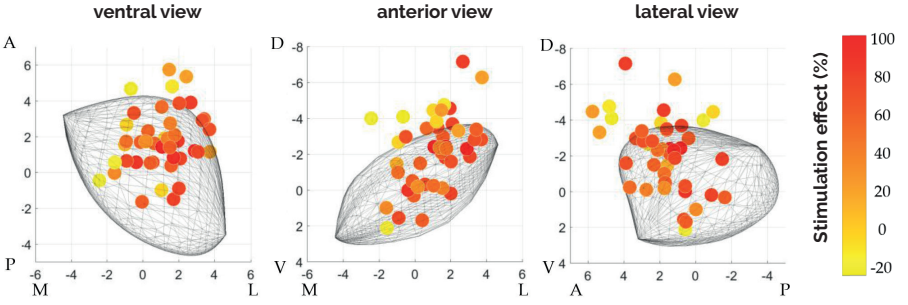

Figure 2. Distribution of the active contact locations after one year in a ventral, anterior, and lateral view. The gray shape represents the generalized STN, identical for all patients. Locations are color-coded corresponding to their contralateral off-medication stimulation effect. Overall, the distribution of the locations is centered on the anterior part of the dorsolateral STN. The relation with stimulation effect is most striking in the anterior view, where the locations at the lateral and ventral part of the distribution often correspond to good stimulation effect (red), while locations at the medial and dorsal part of the distribution are often corresponding to poor stimulation effect (yellow). A = anterior, D = dorsal, L = lateral, M = medial, P = posterior, and V = ventral. Locations displayed on the axes are in mm.

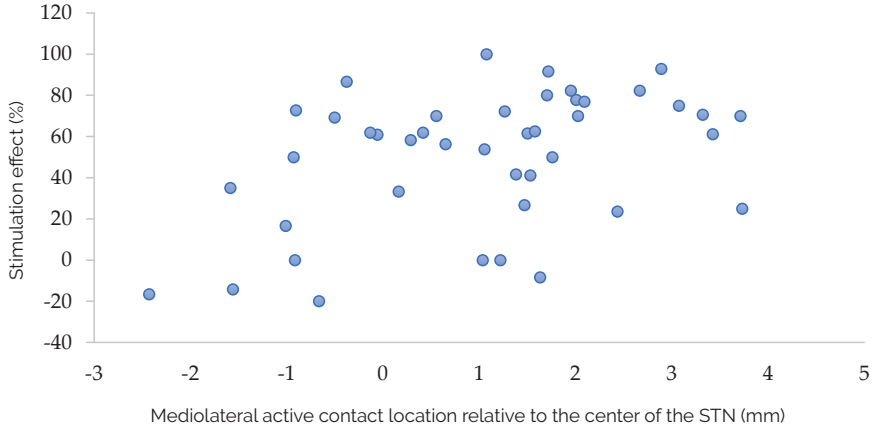

Figure 3. Scatter plot of the relation between mediolateral active contact location (x-coordinate) relative to the center of the STN, and stimulation effect.

The same analysis without exclusion of the outlier in stimulation effect resulted in the same significant relations, with even slightly higher values for R^2 change and adjusted R^2. Thereby, exclusion of this single observation was justifiable on theoretical grounds, but it had no effect on the relations found in this study.

The same analysis with exclusion of the bipolar (n = 3) and double monopolar (n = 2) stimulating electrodes led to similar main results. Namely, a significant improvement in the prediction was found by adding the coordinates (R^2 change = 0.186, p = 0.041), and this resulted in a significant combined prediction model (adjusted R^2 = 0.254, p < 0.008) in which the mediolateral location has the largest unique contribution (standardized beta = 0.388, p = 0.044). Furthermore, in this subgroup analysis, the anteroposterior location (y-coordinate) had a significant unique contribution to the prediction (standardized beta = –0.341, p = 0.048), whereas the unique contribution of the levodopa window was no longer significant.

Using the active contact locations corresponding to profound off-medication stimulation effects (≥75%, n = 10), a theoretical hotspot for DBS could be estimated at 1.9 mm lateral, 0.9 mm anterior, and 2.6 mm dorsal to the center of the generalized MER-based STN. When the same active contacts with profound effect were related to MCP, this resulted in a theoretical hotspot at 12.6 mm lateral, 2.0 mm posterior, and 2.8 mm ventral to MCP.

Discussion

Using the neurophysiological borders based on MER to create individual STN models as a reference for active contact location, we found a significant relation between active contact location and change in contralateral off-medication motor score with DBS compared to baseline. This is in contrast to earlier studies that have used active contact location relative to MCP and have reported no relation with motor improvement. Failure to find a relation in these earlier studies is likely the result of anatomical variation in STN location between patients.[133–136] This indicates that the MER-based correction of STN-modelling can result in a valid reference for active contact location. Stimulation within the lateral part of the MER-based STN resulted in more substantial motor improvement compared to stimulation more medial within the MER-based STN, confirming similar imaging-based analyses.

Our regression analysis showed that the coordinates of the active contact, relative to the MER-based STN, explained an additional 17.6% of the variance in off-medication stimulation effect after controlling for the influence of a levodopa window. Together, they explain 38.9% of the variance in off-medication stimulation effect. Of these three coordinates, the laterality (x-coordinate) has the greatest unique contribution to the regression model, greater than that of the levodopa window. This can be explained by the anatomical location of the sensorimotor area in the lateral part of the STN, while the associative and limbic areas of the STN are more medial.[38,43] The positive influence on stimulation effect of a more lateral active contact corresponds with findings that use the MRI-based STN as a reference.[20,138,141]

In the analysis where bipolar and double monopolar stimulating electrodes were excluded, the findings described above were confirmed. Furthermore, the anteroposterior location of the active contact was found to also have a significant, unique contribution to the regression model, where a more posterior active contact was related to more stimulation effects. This is in line with research showing that sensorimotor projections of the STN are more posteriorly located.[38,43] In this subgroup analysis, the levodopa window had a non-significant contribution to the regression model. This might be explained by the decreased number of analyzed electrodes compared to the full analysis. Furthermore, for both of the analyses, it should be noted that the influence of the levodopa window might be underestimated because patients were selected for DBS based on, amongst others, a large levodopa window. The location results remain valid for this group, but when considering all PD patients eligible for DBS surgery, the levodopa window is likely to remain the most important predictor for postoperative motor improvement.

The advantage of using the MER-based STN as a reference is that it derives from real-time intraoperative physiological data from the patient, confirming the location of the STN rather than relying on an indirect pre-operative dataset that can be subject to distortion (as MRI can be). Furthermore, the DBS electrode location related to the MER-based STN can easily be assessed intraoperatively, even when the MER-based STN does not correspond with the MRI-based STN. In our center, the symptomatic bleeding rate with this MER driven approach was 0.8%.

To compare implantation in our center with other centers, we also calculated the active contact locations referenced to MCP. The mean location in our patients (12.0 mm lateral; 1.0 mm posterior; 3.1 mm ventral) corresponded reasonably well with the average of eight earlier studies presented in a review by Caire et al. (12.0 mm lateral; 1.5 mm posterior; 1.9 mm ventral).[16] However, active contact locations in our group were slightly more ventral, which likely results from the fact that the targeting in our center was done with the intention to stimulate inside the STN, compared to some other centers where stimulation dorsal to the STN was intended. Thus, while our theoretical hotspot was dorsal to the center of the STN, but within its boundaries, other centers target even more dorsal (and often more posterior) to stimulate fiber tracts outside the STN boundaries. Therefore, it should be noted that the relation between active contact location and motor improvement found here is particularly valid for STN-DBS surgery using similar targeting and surgical procedures as in our center. Most importantly, these procedures include the intended stimulation within the boundaries of the STN and intraoperative refinement of STN borders by MER. Other groups might target different structures, for example more posterior or dorsal to the STN, or use different forms of intraoperative visualization of the STN. Therefore, generalization of these results to all STN-DBS should be considered with caution.

In this study, in 26 patients, the 43 electrodes and its effects on motor improvement were treated as independent. This assumes that the effect of one-sided stimulation on the purely one-sided contralateral UPDRS motor score sub-items is independent of the stimulation of the other STN in the same patient. Any dependency between these effects may have influenced the statistical significance.

Furthermore, to study solely the stimulation effect of STN-DBS, the off-medication on-stimulation motor scores after one year would have to be compared to the off-medication off-stimulation motor scores after one year. Since the latter were not available in this cohort, the off-medication scores at baseline were used. Therefore, possible effects of disease progression, microlesions, or long-term medication effects are also included in the outcome parameter called stimulation effect in this study, which may have led to both overestimation and underestimation of the pure effect of stimulation alone.

Conclusions

Our study showed that, using the neurophysiological boundaries of the STN based on MER, it is possible to create a model of the STN as a reference for active DBS contact location based on real-time, intraoperatively acquired neurophysiological data from the patient. There is a clear correlation between these locations and motor improvement after STN-DBS, whereby more lateral stimulation within the boundaries of the MER-based STN predicts more motor improvement after one year. This result is in contrast to earlier studies that have used active contact location relative to MCP and have reported no relation with motor improvement.

The neurophysiological generalized model of the STN can be used to complement imaging studies in the search for better clinical outcomes of DBS. Other neurophysiological modalities, like local field potential recordings, can be added to the model, and can become important in future stimulation paradigms of steerable or adaptive deep brain stimulation.


-34 22.5003, 115 8.1801

CHAPTER 5

Directional steering: a novel approach to deep brain stimulation

M. Fiorella Contarino
Lo J. Bour
Rens Verhagen
Marcel A.J. Lourens
Rob M.A. de Bie
Pepijn van den Munckhof
P. Richard Schuurman

Neurology. 2014;83(13):1163-1169

Objective: The aim of this study was to investigate whether directional steering through a novel 32-contact electrode is safe and can modulate the thresholds for beneficial and side effects of stimulation.

Methods: The study is a single-center, performance, and safety study. Double-blind intraoperative evaluations of the thresholds for therapeutic benefit and for side effects were performed in 8 patients with Parkinson disease while stimulating in randomized order in spherical mode and in 4 different steering modes with the 32-contact electrode, and in monopolar mode with a commercial electrode. In addition, simultaneous recordings of local field potentials through all 32 contacts were performed.

Results: There were no adverse events related to the experimental device. For 13 of 15 side effects (87%), the threshold could be increased by ≥ 1.0 mA while steering in at least one direction in comparison to conventional spherical stimulation, thereby increasing the therapeutic window by up to 1.5 mA. Recording local field potentials through all 32 electrode contacts yielded spatiotemporal information on pathologic neuronal activity.

Conclusion: Controlled steering of current through the brain may improve the effectiveness of deep brain stimulation (DBS), allow for novel applications, and provide a tool to better explore pathophysiologic activity in the brain.

Classification of evidence: This study provides Class IV evidence that for patients with Parkinson disease, steering DBS current is well tolerated, increases the threshold for side effects, and may improve the therapeutic window of subthalamic nucleus DBS as compared with current standard spherical stimulation

Introduction

Deep brain stimulation (DBS) is an effective treatment for movement disorders, including Parkinson disease, tremors, and dystonia, and is being increasingly used as investigational treatment for psychiatric disorders including obsessive-compulsive, mood, and tic disorders.[142] The efficacy of DBS may be limited by current spread into adjacent structures, inducing side effects such as muscle contractions, dysarthria, and cognitive or behavioral disturbances.[33,143]

The DBS electrodes have not changed in the past decennia,[144] and harbor four cylindrical contacts, with a surface of 6.0 mm^2 and a spherical stimulation volume with a radius of 0.5 to 4.0 mm (figure 1). To shift the horizon on potential applications of DBS and explore brain areas hitherto unreachable, electrodes are needed that have small contacts in close relation to local brain pathologic activity, can steer stimulation selectively into any direction to optimize beneficial effects and minimize side effects,[28,145–147] and are able to measure local field potentials to provide feedback for adaptive DBS.[90]

A new type of DBS electrode was developed (Sapiens Steering Brain Stimulation BV, Eindhoven, the Netherlands), with 32 small electrode contacts that can be independently activated in clusters, allowing for directional steering of the stimulation field and directional recording of local field potentials.

We describe the application of steering DBS in awake patients undergoing DBS surgery in the subthalamic nucleus (STN) for Parkinson disease.

As proof of principle, we tested the hypothesis that directional steering of DBS in the STN can modulate thresholds for both beneficial effects and side effects, widening the therapeutic window of stimulation in parkinsonism.

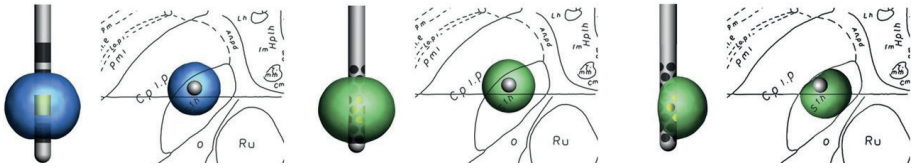

a b c

Figure 1. Schematic representation of stimulation fields superimposed on the atlas image of a target area for deep brain stimulation. **(a)** Conventional deep brain stimulation electrode with 4 cylindrical contacts. Activation of one contact (yellow) yields a spherical stimulation field (blue), influencing both the target (Stn, subthalamic nucleus) as the adjacent internal capsule (C.p.i.p.). **(b)** The 32-contacts experimental electrode. Activation of a circular array of 12 contact points in 3 rows (yellow) produces a spherical stimulation field (green) equivalent to conventional stimulation. **(c)** Activation of an array of 4 electrodes (yellow) yields a field of stimulation (green), which can be modulated to avoid stimulation of adjacent structures, only stimulating the target area. Atlas image from Schaltenbrand G, Wahren W. Atlas for Stereotaxy of the Human Brain. Stuttgart: Georg Thieme Verlag KG; 1977. Courtesy of Georg Thieme Verlag KG.

Methods

Investigational devices

The 32-contact electrode has the same diameter as the commercial Medtronic model 3389 electrode (1.27 mm) and carries 32 oval disc-shaped electrode contacts arranged on 8 rows of 4 contacts, covering a total length of 6.0 mm (figure 1).

Each contact point is 0.80 mm × 0.66 mm, with a surface area of 0.42 mm^2. The distance between the rows is 0.75 mm, while the center-to-center distance between adjacent electrodes in the same row is 1.00 mm.

Activating 12 contacts in 3 rows in circular fashion activates an area of 5.0 mm^2, equivalent to the currently used technique of spherical stimulation (figure 1b), while activating a cluster of 4 contacts in a rhomboidal pattern produces an active area of 1.7 mm^2, steering stimulation toward one quadrant (figure 1c).

The 32-contact electrode was connected to an external pulse generator system for brain stimulation (Next Wave; TMSi, Enschede, the Netherlands) and local field potential recording (Porti32; TMSi). Dedicated software (AiM system; Sapiens Steering Brain Stimulation BV, Eindhoven, the Netherlands) provided the user interface for controlling the stimulation and storing data. Stimulation was current-controlled, and current was distributed across the activated electrodes.

Patients

Patients with idiopathic Parkinson disease were included in the study between October 2012 and April 2013.

Inclusion criteria were a diagnosis of idiopathic Parkinson disease with the clinical indication for DBS of the STN, age older than 18 years, ability to comply with the study assignments, and ability to give informed consent. Exclusion criteria were disease severity according to Hoehn-Yahr stage 5, Mattis Dementia Rating Scale score < 120, psychiatric contraindications for STN-DBS, general contraindications for stereotactic surgery and general anesthesia, additional risk factors for intraoperative or postoperative bleeding, diagnosis of acute myocardial infarction or cardiac arrest up to 6 months before the screening, history of seizure, and general health issues that would preclude extended surgery time.

Standard protocol approvals, registrations, and patient consents

The study was approved by the Medical Ethical Committee of the Academic Medical Center of Amsterdam and the subjects signed an informed consent before inclusion. The study was conducted in accordance with the Declaration of Helsinki (1964 and later revisions), the Dutch Act on Medical Research Involving Human Subjects (WMO), and the Standard EN ISO 14155:2011 on clinical investigation of medical devices for human subjects-Good Clinical Practice. The trial is registered with Dutch Trial Register (NTR3655).

Standard surgical procedure

Surgery was performed with standard technique, as previously reported.[70,93,148] Briefly, frame-based, three-dimensional MRI and Leksell Surgiplan software and stereotactic frame (Elekta Instrument AB, Stockholm, Sweden) were used for targeting. Starting point for calculations of the STN coordinates were 11 to 12 mm lateral, 2 mm posterior, and 4 mm inferior to the midcommissural point. Visual adjustments were made based on T2-weighted MRI. Paths were planned with 70˚ to 75˚ anterior angulation to the intercommissural line and 20˚ to 30˚ lateral angulation from the midsagittal plane, avoiding sulci, vascular structures, lateral ventricles, and the caudate nuclei. Electrode implantation was performed with patients awake and without sedatives. Dopamine agonists, when used, were gradually reduced, and then stopped three days before surgery, while levodopa was stopped at least 12 hours before surgery. Microelectrode recordings were obtained using three electrodes, placed in an array with central, lateral, and anterior cannulas, with a center-to-center distance of 2 mm between the cannulas. After delineation of the boundaries of the STN by microelectrode recordings, clinical test stimulation was performed at several sites using the electrode's macrostimulation tip. Based on the observed therapeutic window in the tested locations, the channel and

depth for implantation of the DBS electrode were determined. Then the experimental procedure was performed, followed by implantation of the permanent electrode (model 3389; Medtronic, Minneapolis, MN). After electrode implantation, the neurostimulator was implanted under general anesthesia.

Study design

The study is a single-center, single-group, performance and safety study, conducted acutely during regular DBS surgery with an observational period of two months after surgery.

Study protocol

The rigid 32-contact electrode was inserted along the channel chosen for chronic stimulation, on the first operated side. The depth of stimulation was chosen based on the effects observed with test stimulation. Radiologic confirmation of the position of the electrode was performed with intraoperative fluoroscopy. Test stimulation with the 32-contact electrode was performed in spherical mode, followed by four directional modes with current steered in anterior, posterior, lateral, and medial direction in randomized order, obtained as described above. Finally, a second spherical mode test was repeated. Each different stimulation mode was used for up to 5 minutes. Between the different stimulation modes, an interval of on average about 2 minutes was allowed for reappearance of clinical symptoms. The total duration of the stimulation procedure with the experimental electrode was on average 31 minutes (range 25 – 40 minutes).

The patient, the evaluating neurologist, and the neurosurgeon were blind to the direction of the steering modes. Stimulation was performed with 130 Hz and 60 μs, by progressively increasing current intensity at fixed steps of 0.5 mA, until side effects induced discomfort to the patient and up to a maximum of 8 mA. In addition, local field potentials were simultaneously recorded through the 32 contacts.

A standardized clinical test protocol to establish therapeutic effects and side effects was followed, including standard scoring of parkinsonian symptoms according to the Unified Parkinson's Disease Rating Scale, Part III, and a predefined list of questions covering the potential and most frequently observed side effects.

After the second spherical mode test, the 32-contact electrode was extracted and the commercial DBS electrode (model 3389; Medtronic) was implanted for chronic stimulation, with radiologic confirmation using intraoperative fluoroscopy. Test stimulation was then performed via the commercial electrode with the contact point situated at the chosen stimulation site. Standardized neurologic examination of the patient was conducted repeatedly to assess safety.

Evaluation of outcome

The current intensity threshold (mA) for inducing side effects or motor benefit on rigidity with the commercial electrode in monopole mode and with the 32-contact electrode in spherical mode was compared for evaluation of equivalence. Only effects with reproducible and consistent thresholds were considered. The difference in stimulation threshold was considered significant when it was ≥ 1 mA. The overall effect of the 32-contact electrode in spherical mode was considered equivalent to the commercial electrode when at least 65% of the effects occurred at comparable thresholds with a lower limit of the 90% confidence interval (CI) ≥ 1 mA.

The therapeutic window was defined as the difference in mA between the threshold for obtaining clinical benefit on rigidity and the threshold for eliciting any side effect.

All patients underwent a postoperative CT scan within one to two days after surgery. Information on side effects and complications was collected during routine follow-up visits one week and two months after surgery.

Statistical analysis

This is a pilot study on a new investigational device: no previous clinical data are available on the clinical effects of steering stimulation in patients. Statistical analyses were performed using SAS version 9.3 software (SAS Institute, Cary, NC). Non-parametric methods were used as the Wilcoxon signed rank test for location testing and the binomial test for proportion testing. The one-sided exact Clapper-Pearson 95% CI was used to demonstrate equivalence.

Classification of evidence

This study provides Class IV evidence that for patients with Parkinson disease, steering DBS current is well tolerated, increases the threshold for side effects, and may improve the therapeutic window of STN-DBS as compared with current standard spherical stimulation.

Results

Demographic and clinical data of the eight patients included in the study, and details concerning the experimental procedure are reported in table 1.

Safety

No unexpected adverse events were observed during the experimental procedure. There were no serious adverse events. A total of 20 adverse events were reported in

seven patients (table S1 in supplementary materials). None of them were severe or related to the experimental device. All of the adverse events except for one (restless legs) resolved within the time window of the study.

Clinical effects of stimulation

Eighteen reproducible clinical effects were induced during the experiments, comprised of those effects often seen in DBS implantations for Parkinson disease. Thresholds for improvement of rigidity could be tested in three patients. In the remaining patients, all Parkinson symptoms disappeared after introduction of electrodes into the brain, which is a well-known transient effect and a predictor for good outcome of surgery, but it made rigidity tests unfeasible in these patients. In one patient, dyskinesias occurred during stimulation, which are involuntary movements that can be induced by dopaminergic medication, and if occurring during surgery, are also predictors of good clinical outcome. The other 14 observations concerned side effects: dysarthria (*n* = 3), gaze paresis (*n* = 6), muscle contractions (*n* = 4), and paresthesia (*n* = 1).

Thresholds observed with the first and the second spherical mode were equal in 11 of 13 tested effects, showing that fatigue and stunning effect did not vary in the time of testing.

Table 1. Demographic and clinical details of the patients included in the study

Patient	Sex	Age (y)	Disease duration (y)	UPDRS III, off/on	Duration total experimental procedure (min)	Test side	Stereotactic coordinates of test point, mm		
							X	Y	Z
1	M	47.4	8	38/10	50	L	11.7	1.6	4.2
2	M	53.4	12	45/13	33	R	11.0	2.3	3.4
3	M	54.5	5	26/12	38	R	11.2	1.7	3.9
4	M	61.9	8	43/13	40	R	11.6	0.0	1.3
5	M	43.5	7	26/12	49	R	13.9	0.7	2.6
6	F	63.0	13	41/11	32	L	12.8	2.0	2.9
7	F	60.8	17	32/20	38	L	10.4	5.1	5.6
8	F	65.1	16	31/7	28	L	11.2	2.1	2.5
Average, mean ± SD	5 M / 3 F	56.2 ± 7.8	10.8 ± 4.4	35.3 ± 7.5 / 12.3 ± 3.7	38.5 ± 7.8	4 L / 4 R	11.7 ± 1.1	1.9 ± 1.5	3.3 ± 1.3

UPDRS III = Unified Parkinson's Disease Rating Scale, Part III. Stereotactic coordinates are given with respect to the midcommissural point.

Equivalence

The thresholds of the effects of spherical stimulation, with 12 of the 32 contacts on the new electrode activated, were comparable to the thresholds of monopolar stimulation through the conventional electrode at the same location in 16 of 18 cases (difference < 1.0 mA in 88.9%; table 2), demonstrating equivalence between the two electrodes (Clapper-Pearson CI within the equivalence margin, $p < 0.0001$).

Steering DBS

In 13 of 15 side effects (86.7%), thresholds obtained with spherical mode stimulation were different (≥ 1 mA) than those obtained in at least one steering direction, showing that steering was effective in modifying the threshold for side effects by selectively targeting different areas (figure 2, table 2). In 8 of 15 side effects, there was at least one steering direction that allowed increasing the threshold for side effects of ≥ 1.0 mA (steering away from the side effect). Increase in threshold could mainly be observed when shaping in the anterior direction (6 times, 4 times ≥ 1 mA) or medial direction (6 times, 5 times ≥ 1 mA), while decrease in threshold (steering toward the side effect) was most frequently seen in the lateral direction (8 times, 4 times ≥ 1 mA).

In all of the side effects induced with the steering modes, the lowest thresholds obtained with one steering direction varied ≥ 1.0 mA with the threshold of at least one other steering direction.

Effects known to be caused by stimulation of the capsule (gaze paresis, muscle contraction, dysarthria) were observed with a lower threshold when steering the stimulation to the lateral direction as opposed to the medial direction in 9 of 13 cases (in 7 cases ≥ 1.0 mA difference). Paresthesia was observed at a lower threshold on the posterior channel with respect to the anterior, as expected based on the location of the medial lemniscus.

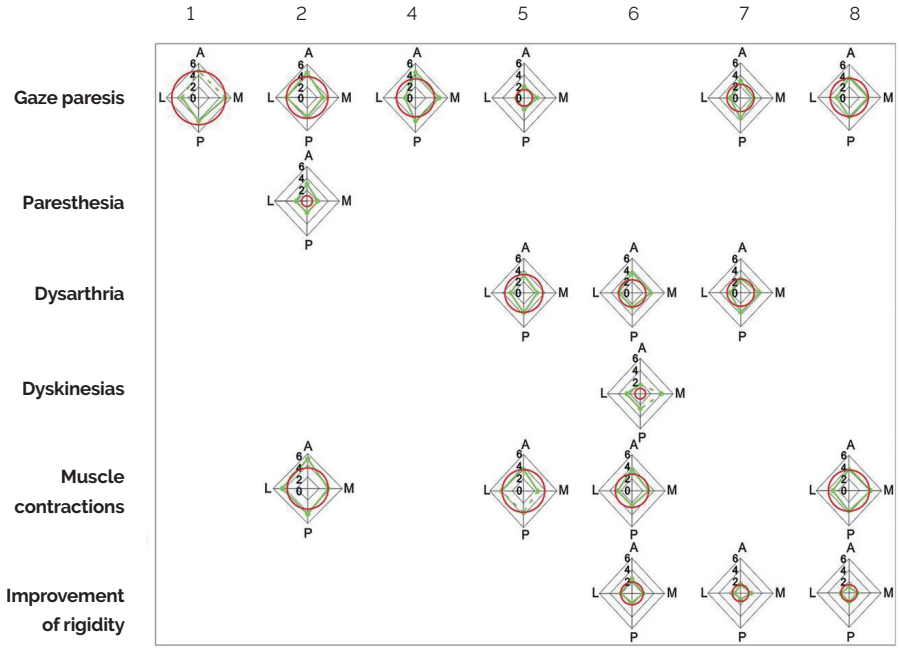

Figure 2. Spider plot representing the thresholds of all observed clinical effects per patient. Green markers indicate thresholds in the steering directions. Red circles indicate the thresholds obtained by stimulation in spherical mode. A = anterior; L = lateral; M = medial; P = posterior.

In all of the three cases in which improvement of rigidity was evaluated, there was no difference in threshold between the spherical mode and each of the four steering directions (in all three cases, the maximum reduction of threshold by steering was 0.5 mA; table 2). There was also no difference between the monopolar stimulation through the conventional electrode and the steering directions (table S2 in supplementary material). These findings suggest that the electrode was centered on the target structure. Threshold for improvement of rigidity obtained with one steering direction differed regarding the opposite steering direction of maximum 1.0 mA (table S2, figure 3).

Therapeutic window

The difference between the threshold to obtain clinical improvements and the threshold at which side effects occur (therapeutic window) could be increased in patient 6 from 0.5 to 1.0 mA by steering stimulation in the posterior direction, in patient 7 from 1.0 to 2.5 mA by steering in the posterior direction, and in patient 8 from 2.0 to 2.5 mA by stimulating in the anterior direction (figure 3).

Table 2. Thresholds of effects (mA) obtained with stimulation through the 32-contact electrode in "spherical mode" and the commercial electrode in "monopolar mode"

Patient	Effect	32-contact electrode spherical mode (mA)	3389 electrode monopolar (mA)	Difference 32-contact /3389 (mA)	Max delta steering away (threshold steering>threshold spherical mode, mA)		Max delta steering toward (threshold steering<threshold spherical mode, mA)	
5	Dysarthria	3.5	3.5	0	0	—	1.0	Medial/ lateral
6	Dysarthria	2.5	2.5	0	1.0	Anterior/ medial	0	—
7	Dysarthria	2.5	2.5	0	1.0	Posterior/ medial	0.5	Lateral
6	Dyskinesia	1.0	1.0	0	2.5	Medial	0	—
1	Gaze paresis	5.0	3.0	2.0	0	—	2.0	Lateral
2	Gaze paresis	4.0	3.5	0.5	0.5	Anterior	1.0	Medial
4	Gaze paresis	3.5	4.0	-0.5	1.0	Anterior/ medial	1.5	Lateral
5	Gaze paresis	1.5	1.5	0	1.0	Medial	0	—
7	Gaze paresis	2.5	3.0	-0.5	1.0	Posterior	0.5	Lateral
8	Gaze paresis	3.5	3.0	0.5	0	—	1.0	Lateral
2	Muscle contraction	3.5	4.0	-0.5	1.5	Anterior	0	—
5	Muscle contraction	3.5	3.5	0	0.5	Lateral	1.0	Medial
6	Muscle contraction	3.0	3.0	0	0.5	Anterior	0.5	Posterior/ lateral
8	Muscle contraction	3.5	3.0	0.5	0.5	Medial	0.5	Lateral
2	Paresthesia	1.0	1.0	0	2.0	Anterior	0	—
6	Improvement of rigidity	2.0	2.0	0	0.5	Anterior	0.5	Posterior
7	Improvement of rigidity	1.5	4.0 *	2.5	0.5	Medial	0.5	Posterior/ lateral
8	Improvement of rigidity	1.5	1.0	0.5	0	—	0.5	Anterior

* When an effect was not observed, the last tested amplitude is reported.

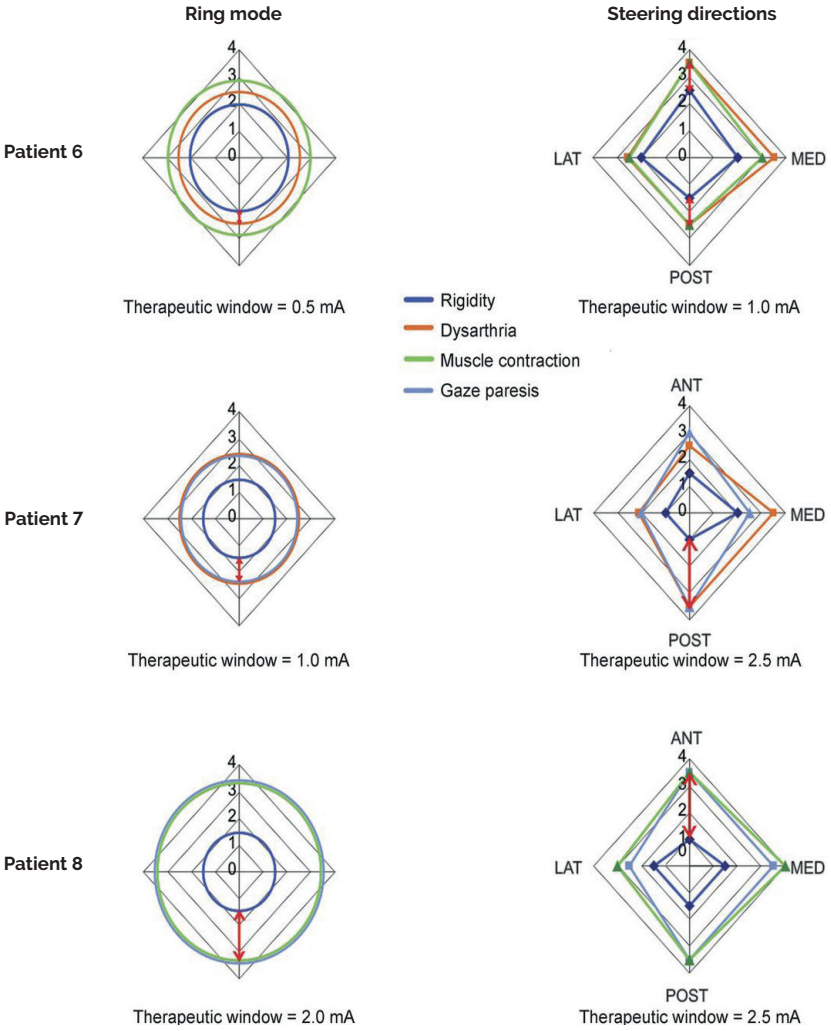

Figure 3. Difference in therapeutic window between stimulation in spherical mode and steering stimulation. Spider plots representing the difference in therapeutic window between stimulation in spherical mode (left) and stimulation in the 4 steering directions (right). Red arrows indicate the steering direction with the largest therapeutic window. ANT = anterior; LAT = lateral; MED = medial; POST = posterior.

Local field potentials

Simultaneous recordings of local field potentials from the 32 contacts when stimulation was turned off yielded the boundaries of the STN by showing increased spectral power particularly in the β band (13 – 40 Hz). In addition, recordings across the four directions showed distinct spatial patterns of neuronal activity, identifying areas with increased pathologic activity within the nucleus (figure S1 in supplementary material).

Discussion

This study showed that stimulation with the novel 32-contact electrode is safe, is capable of reproducing effects equivalent to the currently used electrodes, and can selectively influence the threshold for beneficial clinical effects and for side effects, thereby increasing the therapeutic window of DBS. No adverse events were observed during the intraoperative stimulation protocol.

In this study, we have shown that directional steering offers the opportunity of increasing the thresholds for the appearance of side effects, by redirecting the field of stimulation away from the anatomical structures responsible for the side effects and leaving the threshold for beneficial effects unaltered or even reduced. The possibility of directional steering can greatly improve effectiveness of current applications of DBS in movement disorders and psychiatric illness. Improvement of the therapeutic window was sizable in at least one of the patients (patient 7), while it was not striking in the other two. This was likely attributable to the fact that the threshold for inducing benefit was already low with the stimulation in spherical mode, suggesting a satisfying location of the electrode in the target structure.

Because of time constraints, the test stimulation was limited to four standard steering directions: it is reasonable to think that results could be further improved by more flexible fine-tuning of the stimulation fields.

It is known that intraoperative effects are predictive of long-term performance[143], thus results obtained in this study could be suggestive for similar results with chronic stimulation: this would need to be verified in an appropriately designed long-term study with the implantable system, once available.

In a chronic setting, steering could also be used to reduce the incidence of other side effects, such as cognitive deterioration or psychiatric and behavioral disturbances, which cannot be tested intraoperatively. The implications of this new technique are manifold. The possibility of directional steering can greatly improve effectiveness of current applications of DBS in movement disorders and psychiatric illness. The improved efficacy of stimulation would also allow a reduction of the energy needed, improving battery life.

New treatments can be designed by stimulation applied locally in small brain areas that are currently inaccessible because of possible induction of side effects, such as small subnuclei in the hypothalamus, in the fornix, the upper brainstem, or even the medulla oblongata and spinal cord. Vulnerable areas such as the limbic system can be stimulated with more precision and less risk, while the options for activation of these areas in behavioral and cognitive disturbances at present are limited.

Developments in structural and functional brain imaging, coupled with neuroanatomical studies, are rapidly increasing our understanding of connections and network activity throughout the brain in both normal and pathologic brain states[149,150], opening up the possibility of influencing the brain's pathologic function in many other diseases.

Directional steering of stimulation also allows exploration of the anatomical origin of the observed clinical effects, providing more insights in the pathophysiology of movement and cognition. Measuring simultaneously multichannel local field potentials allows three-dimensional pattern recognition, which can be used to improve the intraoperative localization of the target structures and will provide a completely new tool for functional analysis of network activity in the brain.

Small-scale variation in (pathologic) brain activity calls not only for high-resolution DBS, but also for new adaptive stimulation paradigms based on these individual regional differences.[151] Sensing mechanisms of local neuronal field potentials can provide the feedback of brain function on which small, steered, and adaptive stimulation can be optimized,[90] so that DBS will become a two-way phenomenon with enhanced specificity.

Supplementary materials

Table S1. Adverse events reported during the study

Patient	Side effect	Resolved	Severity	Related to the experimental procedure	Related to standard surgery	Related to standard chronic stimulation
During surgery *						
2,4	Warmth	Yes	1	Not related	Possibly related	Not related
1	Nausea	Yes	1	Not related	Not related	Not related
2	Stiff neck	Yes	1	Not related	Possibly related	Not related
4	Sweating	Yes	1	Not related	Possibly related	Not related
3	Dyskinesias	Yes	1	Not related	Not related	Not related
3	Headache	Yes	1	Not related	Possibly related	Not related
Early postoperative period (< 2 weeks postoperatively)						
2,4,5,6	Headache	Yes	1	Unlikely related/Not related	Unlikely related/Possibly related	Not related
1	Confusion	Yes	1	Possibly related	Possibly related	Not related
3	Heartburn	Yes	1	Not related	Unlikely related	Not related
1	High blood pressure	Yes	2	Not related	Not related	Not related
3	Subcutaneous bleeding around the IPG	Yes	2	Not related	Possibly related	Not related
5	Swelling nose	Yes	1	Not related	Not related	Not related
5	Attention problems	Yes	1	Not related	Unlikely related	Not related
4	Vomiting	Yes	1	Not related	Possibly related	Not related
Up to 2 months postoperatively						
4	Disinhibition	Yes	1	Not related	Not related	Possibly related
8	Restless legs	Ongoing	2	Not related	Not related	Not related

*All adverse events reported during surgery were observed before the insertion of the experimental electrode.

Table S2. Thresholds of effects (mA) obtained with stimulation through the 32-contact electrode in the four steering conditions.

Patient	Observed effect	Anterior	Posterior	Medial	Lateral	Max delta between two steering modes
5	Dysarthria	3.0	3.5	2.5	2.5	1.0
6	Dysarthria	3.5	2.5	3.5	2.5	2.0
7	Dysarthria	2.5	3.5	3.5	2.0	1.5
6	Dyskinesia	1.5	1.0	3.5 *	1.0	1.0
1	Gaze paresis	5.0 *	4.0	5.0	3.0	2.0
2	Gaze paresis	4.5	3.5	3.0	4.0	1.5
4	Gaze paresis	4.5	4.0	4.5	2.0	2.5
5	Gaze paresis	2.0	2.0	2.5	1.5	1.5
7	Gaze paresis	3.0	3.5	2.5	2.0	1.0
8	Gaze paresis	3.5	3.5	3.5	2.5	1.0
2	Muscle contraction	5.0	4.0	3.5	4.5	1.5
5	Muscle contraction	3.5	3.5	2.5	4.0	1.0
6	Muscle contraction	3.5	2.5	3.0	2.5	1.5
8	Muscle contraction	3.5	3.5	4.0	3.0	1.0
2	Paresthesia	3.0	2.0	2.0	2.0	1.0
6	Improvement of rigidity	2.5	1.5	2.0	2.0	1.0
7	Improvement of rigidity	1.5	1.0	2.0	1.0	1.0
8	Improvement of rigidity	1.0	1.5	1.5	1.5	0.5

* When an effect was not observed, the last tested amplitude is reported

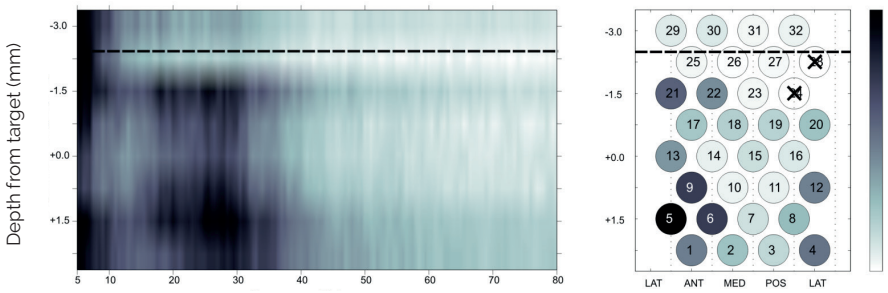

Figure e-1. Spectral representation of local field potentials simultaneously recorded from the 32-contact electrode in one patient. The dashed bar represents the extrapolated dorsal border of the STN as defined by microelectrode recordings in the same subject. **(a)** Representation of spectral powers of all simultaneous LFP recordings averaged per depth across all directions. A clear increase in power in the beta frequency range (13 – 40 Hz) marks the dorsal border of the STN. **(b)** Spectral representation of individual LFP recordings for each contact. Color range represents power intensity in the beta frequency band (13 – 40 Hz), normalized to the maximal beta power in the whole array. The laterally/anteriorly located contacts show higher power in the beta band than the medial/posterior contacts, showing regional differences in pathological activity within the target nucleus.


35 31.1714, 24 1.0044

CHAPTER 6

Directional recording of subthalamic spectral power densities in Parkinson's disease and the effect of steering deep brain stimulation

Lo J. Bour
Marcel A.J. Lourens
Rens Verhagen
Rob M.A. de Bie
Pepijn van den Munckhof
P. Richard Schuurman
M. Fiorella Contarino

Brain Stimulation. 2015;8(4):730-741

Objective: A new 32-contact deep brain stimulation (DBS) lead, capable of directionally steering stimulation, was tested intraoperatively. The aim of this pilot study was to perform recordings from the multidirectional contacts and to investigate the effect of directional current steering on the local field potentials (LFP).

Methods: In eight patients with Parkinson's disease, after standard microelectrode recording and clinical testing, the new lead was temporarily implanted. The 32-channel LFP recordings were measured simultaneously at different depths and directions before and after directional stimulation.

Results: The spatial distribution of LFP power spectral densities across the contact array at baseline marked the borders of the subthalamic nucleus (STN) with a significant increase in beta power and with a mean accuracy of approximately 0.6 mm in four patients. The power in the 18.5 – 30 Hz frequency band varied across different directions in all patients. In the three cases that showed improvement of rigidity, this was higher when current was steered toward the direction with the highest LFP power in the beta band. Subthalamic LFP in six patients showed a differential frequency-dependent suppression/enhancement of the oscillatory activity in the 10 – 45 Hz frequency band after four different 'steering' modes as compared to ring mode, suggesting a higher specificity.

Conclusion: Through a new 32-contact DBS lead it is possible to record simultaneous subthalamic LFP at different depths and directions, providing confirmation of adequate lead placement and multidirectional spatial-temporal information potentially related to pathological subthalamic electrical activity and to the effect of stimulation. Although further research is needed, this may improve the efficiency of steering stimulation

Introduction

The subthalamic nucleus (STN) is the predominantly chosen target for deep brain stimulation (DBS) in patients with Parkinson's disease.[11,152–158] Abnormal oscillatory electrical activity of ensembles of neurons in the STN, observable in the amplitude modulation of the firing patterns of these neurons in a frequency range from approximately 10 – 35 Hz, is related to the severity of the parkinsonian state.[96,102,105,159] The amount of spectral power is related to the clinical status of the patient and the level of anti-parkinsonian medication.[25,93,99,100,106,152,159–164] Furthermore, STN-DBS is capable of modulating this oscillatory activity.[25,140,165,166]

Oscillatory amplitude modulation is not only observed in the spiking patterns of STN neurons, but can also be recorded from the local field potentials (LFP), which are the low frequency (< 500 Hz) fluctuations of electrical activity. LFP reflect the linearly summed postsynaptic potential from local cell groups.[22,106,163,167,168] As such, LFP show a relationship with the envelope of the neural spiking pattern[23,71,106] and consequently are related to the on or off state of the patient or to motor tasks. Interaction between different frequency bands has been described.[25,163,169–174]

Therefore, for intraoperative fine tuning of STN localization, LFP could be used instead of the microelectrode recording (MER).[24,26,175] This could give the advantage that electrophysiological localization of the STN is derived directly from the same DBS lead that is used for chronic stimulation. In addition, knowledge about the relationship between the frequency characteristics of LFP and clinical status could be used to optimally adapt chronic DBS.[90,91,174,176]

The current pilot study describes LFP derived from a new 32-contact DBS lead. As compared with the currently available leads, in a first observation this new lead not only seems to provide higher resolution depth localization of neuronal activity, but also directional information which could be used to improve targeting and to support adaptive DBS.

Materials and methods

Participants and surgery

The study was approved by the Medical Ethical Committee of the Academic Medical Center of Amsterdam. All the subjects received oral and written information and signed an informed consent. The study was conducted in conformity to the Declaration of Helsinki, the Dutch Act on Medical Research Involving Human Subjects (WMO) and the Standard EN ISO 14155: 2011 on clinical investigation of medical devices for human subjects e-Good Clinical Practice.

Eight patients with a diagnosis of idiopathic Parkinson's disease who were candidate for STN-DBS were included in the study. Details of the surgical procedure have been described in detail elsewhere.[126] Lead implantation was performed with patients being awake, without sedatives, and in the practically defined off medication condition. MER were obtained from three needles (FHC, micro/macro electrode model 291), placed in an array with central, lateral, and anterior cannulas, with 2 mm distance. Clinical test stimulation was performed at several sites.

Investigational devices

The new 32-contact lead has the same diameter as the commercial Medtronic 3389 and 3397 leads (1.27 mm).[126] The 32 contacts, each with small dimensions (0.66 × 0.80 mm) and surface (0.42 mm^2), are equally distributed on the circular surface of the lead with a center-to-center distance of 0.75 mm. The array is arranged in eight rows covering a total length of 6.0 mm, with on each row four contact points. The return current electrode consisted of a patch attached to the shoulder. An external pulse generator system for brain stimulation (Next Wave, TMS International BV) was connected to the contacts by means of a manually operated switch box. The stimulus profile consisted of a short duration (width 60 µs) high voltage negative pulse, a short period (100 µs) of zero voltage and a longer duration (width 600 µs) low voltage positive pulse, such that the negative and positive pulse were charge balanced. Repetition rate of the paired pulses was 130 Hz. Stimulation was current-driven, in multi-electrode monopolar fashion and the applied currents varied between 0.5 mA and 5 mA, whereas the current was increased or decreased with steps of 0.5 mA. Dedicated software (AiM system, Sapiens Steering Brain Stimulation BV) provided the user-interface for continuously controlling the stimulation and storing the data. Maximum voltage was limited by the power supply to 15 V. By all these arrangements charge densities were within safe limits. Monitoring of the impedance of the prototype lead, including wiring and contacts, during the stimulation procedure yielded in a total of approximately 2.0 kΩ and 3.5 kΩ for ring and steering mode, respectively. The impedance of a single contact of the standard Medtronic lead was 1.5 kΩ.

Experimental test procedure

After completion of the routine MER and test stimulation on the first side, the rigid 32-contact lead (Sapiens Steering Brain Stimulation BV, Eindhoven) was inserted temporarily along the channel chosen for chronic stimulation. The Z-level for the experimental protocol was chosen according to clinical data obtained during test stimulation with the microelectrodes before the experimental protocol. Lead position was confirmed by intraoperative fluoroscopy. A test stimulation protocol with the 32-contact lead was then performed in ring mode, and four steering modes (anterior, posterior, lateral, medial) in blinded randomized order, as previously described.[126]

A standardized clinical test protocol to establish therapeutic effects and side effects was followed, including standard scoring of parkinsonian symptoms according to the UPDRS III, and a predefined list of questions covering the potential and most frequently observed side effects. The four steering directions were tested in a randomized order and the evaluating neurologist, the neurosurgeon and the patient were blind to the direction of steering. A ring mode is achieved by using a selection of 12 electrodes on three adjacent rows, such that a spherical field of stimulation can be created, which is similar to that produced by the existing DBS systems in monopolar mode. By using a small cluster of four adjacent electrodes, arranged in a diamond shape, directional stimulation was created (steering). Each different stimulation period lasted 3 – 5 min, followed by an interval of on average about 2 min for reappearance of clinical symptoms. LFP recordings with a 32-channel DC amplifier[126] with a low-pass frequency of 500 Hz (12 dB/oct) and within the used frequency band having a noise level of < 1 μV-RMS and a common mode rejection ratio (CMRR) > 90 dB, were performed before and after stimulation and stored for offline analysis, which was performed after the completion of the study in all patients. The high input impedance (> 1 TΩ) of the amplifiers makes them rather insensitive to impedance variations of the source (Porti7-32et, TMS International BV).

The 32-contact lead was then extracted, and the Medtronic 3389 DBS lead was implanted for chronic stimulation. All patients underwent a post-operative CT scan.

Signal analysis

LFP signals were recorded against a common reference, i.e., the average potential of all active contact points with a sample frequency of 2048 Hz. Analog data were filtered from DC to 500 Hz. For initial inspection of the data, they were digitally band-pass filtered between 3 Hz and 80 Hz with a non-causal 4th order zero phase Butterworth filter (forward and reverse IIR filtering) and segments of interest were selected. To avoid circular convolution artefacts, at the start and the end of the recording an extra second of data was added (data padding), which afterward was removed. For subsequent detailed analysis of the spatiotemporal distribution of the LFP inside the STN and the effect of DBS on the LFP, segments of interest were selected from the original data and were band-pass filtered between 8 and 80 Hz with the same filter as described above. In the LFP signals sometimes artefacts were observed in the forms of short 'jumps' in the data, which are probably hardware related. To account for artefacts, an automatic artefact detection algorithm was applied[177] and visually inspected afterward. In short, after data padding and subtraction of the mean the segments were band-pass filtered and the amplitude envelop of the filtered segments were calculated using the Hilbert transformation. If the average of the z-score of the amplitude envelope of all channels exceeded a predefined value, it was supposed there was a common artefact present in all channels. The artefact detection procedure results in the start and end indices

of epochs, which can be used to extract artefact-free data epochs from the original data. Only artefact-free data epochs longer than 2 s were selected for further analysis. Subsequently, the selected artefact-free data epochs were filtered in the same way as the segments in the artefact detection method, however, now after filtering the epoch means were subtracted, i.e., ignoring data padding. Furthermore, a 50 Hz discrete Fourier transform filter was applied to remove powerline artefacts[177] and the added data parts again were removed. Finally, data were downsampled to 256 Hz.

The Welch method with 50% overlap and a spectral resolution of 0.5 Hz was used for the estimation of the power spectral densities. If there was more data than one epoch (length of at least 2 s), power spectra of all epochs were averaged. Calculations of the power spectra were performed on monopolar derivations where each contact was referenced to the average of all active contacts (common reference). Based on the PSD measured in the patients of this study, which partially reflected also subdivisions used in the literature[163], the spectrum between 3 and 45 Hz was subdivided into four bands: 1) from 3 to 9.5 Hz, 2) from 10 to 18 Hz, 3) from 18.5 to 30 Hz, 4) from 30.5 to 45 Hz. To evaluate the effect of stimulation, power spectral densities were calculated across the electrode array just prior to (at least 15 s) and immediately 15 s after each stimulation mode. It is supposed that the spectral distribution immediately after high frequency stimulation reflects most of the effect on the LFP power. Suppression or enhancement of power after stimulation was calculated as the percentage of the power just prior to stimulation in three frequency bands, i.e., 10 – 18 Hz, 18.5 – 30 Hz and 30.5 – 45 Hz.

For the spectrogram the Welch method with 1-second, 75% overlapping windows was used, and the windows were multiplied with a Hanning window. The spectrogram was computed on a frequency grid of 8 – 50 Hz with step size 0.5 Hz using the Goertzel algorithm. Only LFP recordings with the patient at rest were analyzed.

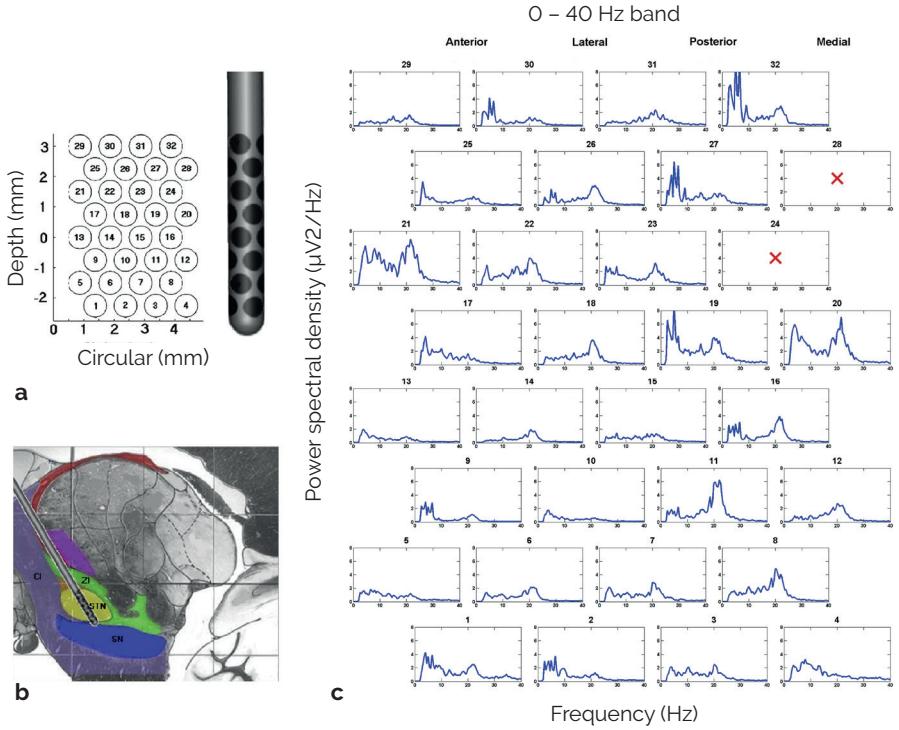

Figure 1. (a) shows a schematic two-dimensional display of the multi array lead. **(b)** shows schematically the position of the lead inside the STN (yellow) in a stereotactic atlas in a sagittal view at 12 mm from AC – PC. **(c)** shows for each contact point the power spectral density of the LFP between 0 and 40 Hz at baseline in the unfolded 2D array display in patient 6. Based on the MER recordings in this case all 32 contacts were completely inside the STN. On top of the array, the direction towards which each contact is heading is indicated (for instance, contact 1, 9, 17, and 25 are heading in the anterior direction). The contact points 24 and 28 boxes are filled with a red cross because here pre-amplifiers went into saturation due to a too high DC offset, and therefore LFP recordings were not possible.

Statistical analysis

A balanced one-way ANOVA test was performed to identify significant variations in power in the different frequency bands across depths at baseline. The average depth power of n 2-second epochs for two frequency bands, i.e., 3 – 10 Hz and 11 – 40 Hz, was calculated as a function of depth. For each epoch, the depth power for a frequency band was obtained by averaging the power spectral density (PSD) of all contacts at the same depth followed by integrating the logarithmic averaged PSD over the frequency band range and dividing by its range. A multi-comparisons Tukey Kramer method was used to assess variability across depths (significant level $\alpha = 0.001$) and a post-hoc contrast test was performed to compare the total power at the locations outside the STN with those inside the STN as defined by MER.

A one-way ANOVA was performed to assess significant variability in power variation after different stimulation modes in the three frequency bands for each patient. When the results of ANOVA were significant, a multi-comparisons Dunnet post-hoc test having ring stimulation as control group was performed to test the hypothesis that the steering directions produced different results than the conventional ring stimulation.

Results

Clinical features

Eight patients (5 males, average age 56.2 ± 7.8 years) were included in the study. The average disease duration was 10.8 ± 4.4 years (range 5 – 17 years) and the average UPDRS III score was 35.3 ± 7.5 off medication and 12.3 ± 3.7 on medication.[126]

Spectral distribution across contact array

The 32-contact DBS lead (figure 1a) implanted inside the STN (figure 1b) allowed discrete high-density 3D LFP recordings at baseline. Across the contacts that were localized inside the STN, a rather large variability of the LFP power spectral density (PSD) in direction, depth and distribution has been observed in all the patients. An example is provided in figure 1c. PSD at baseline show a multimodal distribution with peaks in the 3 – 9.5 Hz, 10 – 18 Hz and 18.5 – 30 Hz frequency bands.

In patients 1, 2, 3, and 4 the contacts of the experimental lead were lying partly outside the STN, while in patients 5, 6, 7 and 8, MER recordings indicated that all contact points of the experimental lead were completely inside the STN and therefore, it was not possible to identify the dorsal border by LFP in these patients. The average power spectral density at each depth for patients 1 and 2 is shown in figure 2. In these two patients it is observed that along the length of the electrode the distribution of power is different across the different frequencies.

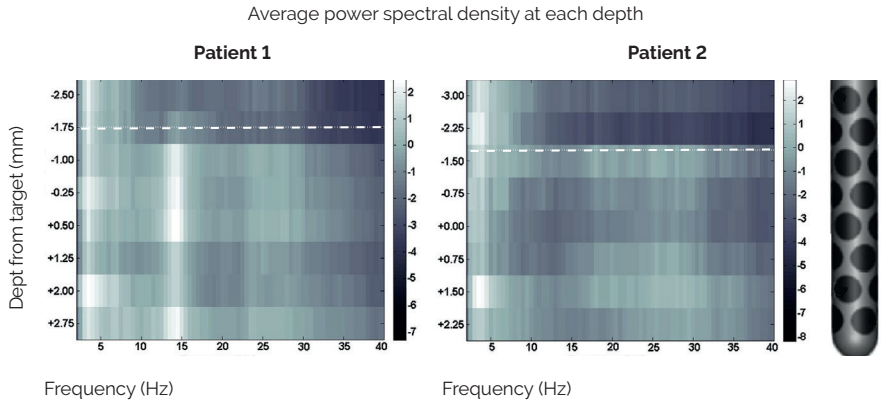

Figure 2. The left and right panels show for patients 1 and 2, respectively, the average logarithmic LFP power spectral density across the 3 – 40 Hz frequency band of all contact points at each depth (eight rows). For clarity the distal end of the new 32-contact DBS lead is shown at the right. The white dotted line indicates the start of the STN as extrapolated by MER. The vertical bar at the right of each panel indicates logarithmically the relationship between power and saturation of the color; white is highest power.

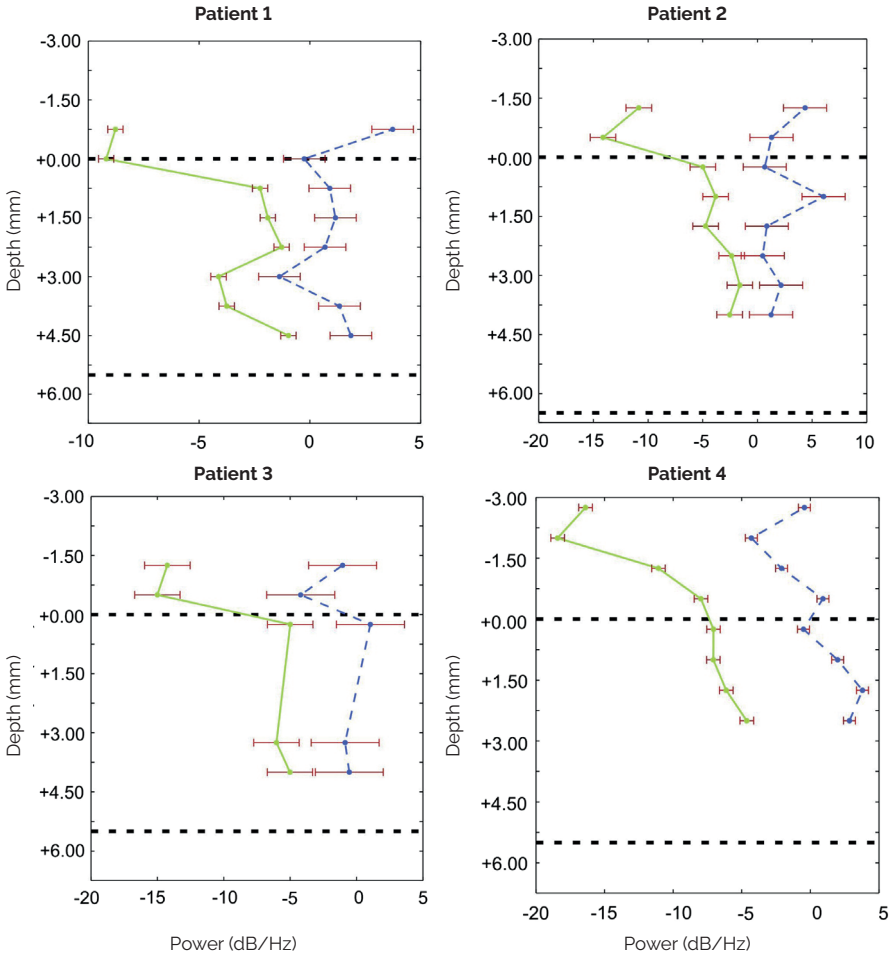

Figure 3. In four patients the average depth power of n 2-s epochs for two frequency bands, i.e., 3 – 10 Hz (blue dashed line) and 11 – 40 Hz (green line), is illustrated as a function of depth. The number of epochs was 77, 9, 7, and 50 for patients 1, 2, 3, and 4 respectively. For convenience the dorsal border of the STN, as detected by MER, is positioned at +0.00 mm. The upper and lower black dashed lines indicate the dorsal and ventral border of the STN as determined by MER, respectively. The red error bars around each mean are the comparison intervals determined by the multi-comparisons Tukey Kramer method (significant level is $\alpha = 0.001$). For balanced one-way ANOVA, significant difference between two mean values means no overlap of their comparison interval. For all patients, ANOVA showed a significant variability across depth ($p < 0.005$ for both frequency bands). Post-hoc contrast showed a significantly higher power in the 11 – 40 Hz measured inside than outside the STN for all patients ($p < 0.0001$). For the 3 – 10 Hz band power was significantly higher inside than outside only in patients 3 and 4 ($p < 0.001$).

In figure 3 it is shown that in patients 1, 2, 3, for the detection of the borders of the STN with a 32-contact DBS lead, the LFP power within the frequency band of 11 – 40 Hz could be used, while in patient 4 no step change but a gradual tailing off was observed. Balanced one-way ANOVA showed a significant variability across depth in all four patients ($p < 0.001$ for the 11 – 40 Hz band and $p < 0.005$ for the 3 – 10 Hz band). Post-hoc contrast showed a significantly higher power in the 11 – 40 Hz measured inside with respect to outside the STN for all patients ($p < 0.0001$). For the 3 – 10 Hz band this was significantly higher inside than outside only for patient 3 and 4 ($p < 0.001$). An abrupt power increase within the 11 – 40 Hz frequency band was observed at a mean distance of 0.6 mm (range 0.25 – 1.15) from the dorsal border of the STN as determined by MER. The difference in logarithmic power spectral density between the last point located outside the STN and the first point located inside the STN was -6.9, -9.1, and -10.0 for patients 1, 2, and 3 respectively. For patient 4, as noted above, this difference was -0.9, while a turning point with -7.3 difference was seen about 1.5 mm above the MER-defined STN border.

In most patients, the spatial distribution of power in the low frequencies (< 10 Hz) was different from the higher (10 – 40 Hz) frequencies, which indicates a different neurophysiological meaning of the lowest versus the higher frequencies. Figure 4a demonstrates that power distribution in the low frequency band is highest both in the anterior direction along the whole STN and in the medial-posterior direction, more dorsally (patient 6). Local peaks lie between 4 and 8 Hz. Comparison of figure 4a with the higher frequency range (figure 4b) shows a different power distribution inside the STN for the 10 – 40 Hz compared to the 0 – 10 Hz: here highest power is found in the medial-posterior direction, more ventrally. All contacts show a peak at about 21 Hz, however, contacts 7, 19, 22, 21, 27, and 29 also show a local peak in the 10 – 18 Hz band.

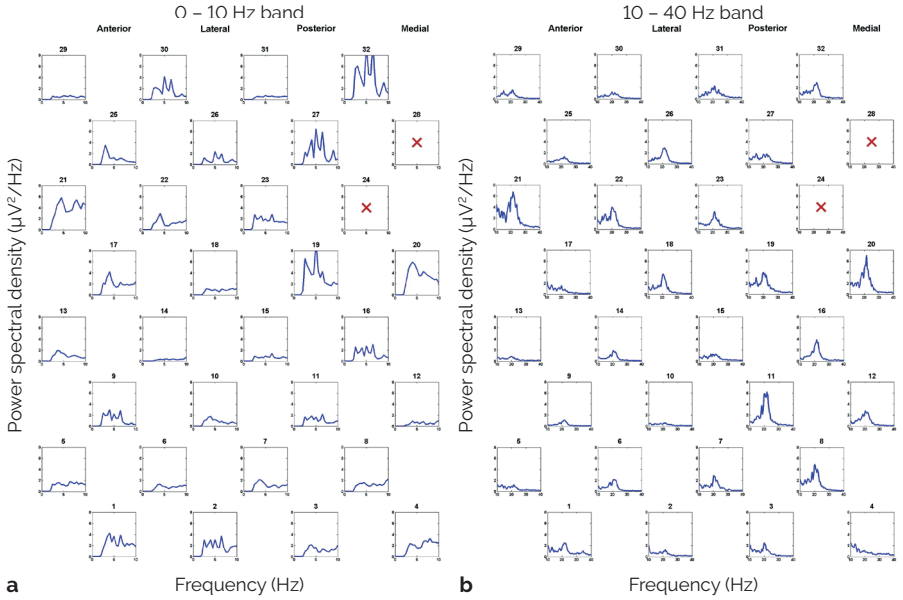

Figure 4. For each contact point, the power spectral density of the LFP at baseline in the unfolded two-dimensional array display in patient 6 is shown. Here, the power spectral density between 0 and 40 Hz inside the STN has been split up into **(a)** a low frequency part (< 10 Hz) and **(b)** a higher frequency part (10 – 40 Hz) to emphasize the different spatial distribution between these two frequency bands. On top of the array, the direction toward which each contact is heading is indicated. For instance, contact 1, 9, 17, and 25 are heading in the anterior direction. The figure shows that the power distribution in the low frequency band, **(a)**, is highest both in the anterior direction along the whole STN and in the medial – posterior direction, more dorsally while the higher frequency range, **(b)**, shows a completely different power distribution: highest power is found in the medial – posterior direction, more ventrally. Local peaks lie between 4 and 8 Hz. All contacts show a peak at about 21 Hz, however, contacts 7, 19, 22, 21, 27, and 29 also show a local peak in the 10 – 18 Hz band.

Power spectral densities recorded across all contact points inside the STN show for all patients a peak between 18.5 and 30 Hz with an average peak frequency of 24 Hz (figure 5a and b). In patients 1, 3, 4, and 7 a peak also is present in the 10 – 18 Hz range with an average peak frequency of 13 Hz. The superimposed spectral distributions (figure 5b) suggest a subdivision into two different frequency bands between 10 and 30 Hz with a bimodal spectral distribution. Based on these distributions further analysis of the spectrum between 10 and 45 Hz was performed in three separate frequency bands 1) from 10 to 18 Hz 2) from 18.5 to 30 Hz 3) from 30.5 to 45 Hz.

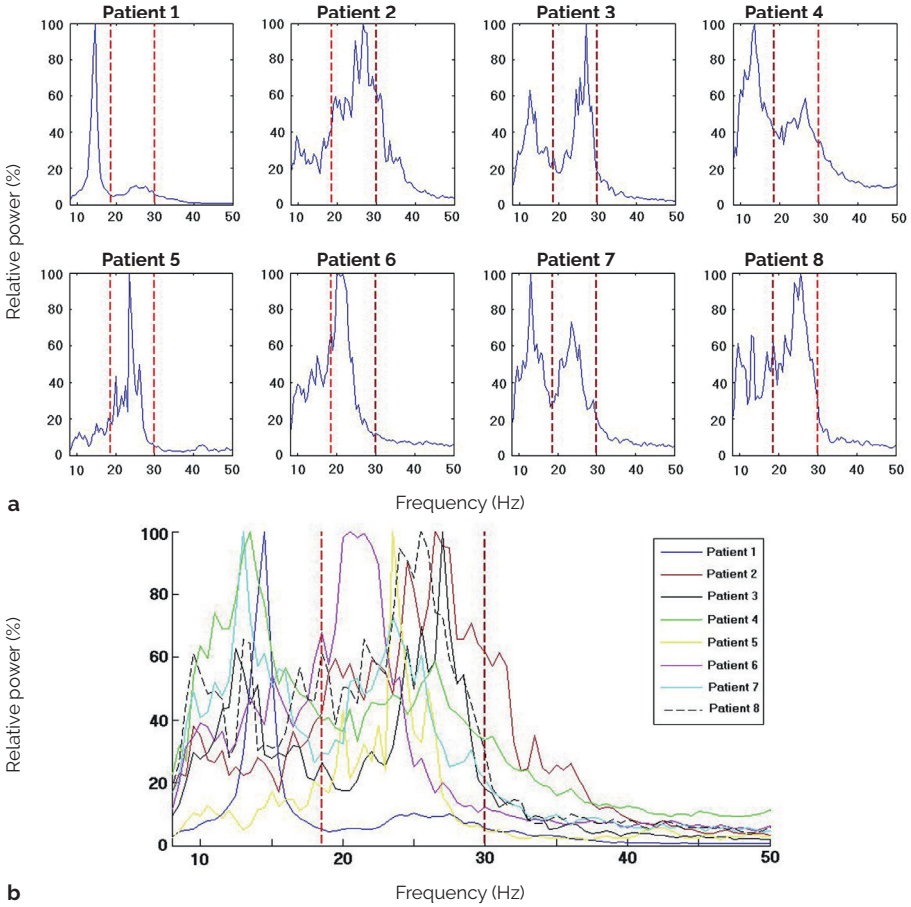

Figure 5. (a) depicts for each patient the relative power spectral densities between 10 and 50 Hz averaged across all contact points located inside the STN at baseline. **(b)** shows the same spectra as shown in **(a)** but now superimposed. The two red vertical dashed lines in each panel indicate the frequencies 18 and 30 Hz.

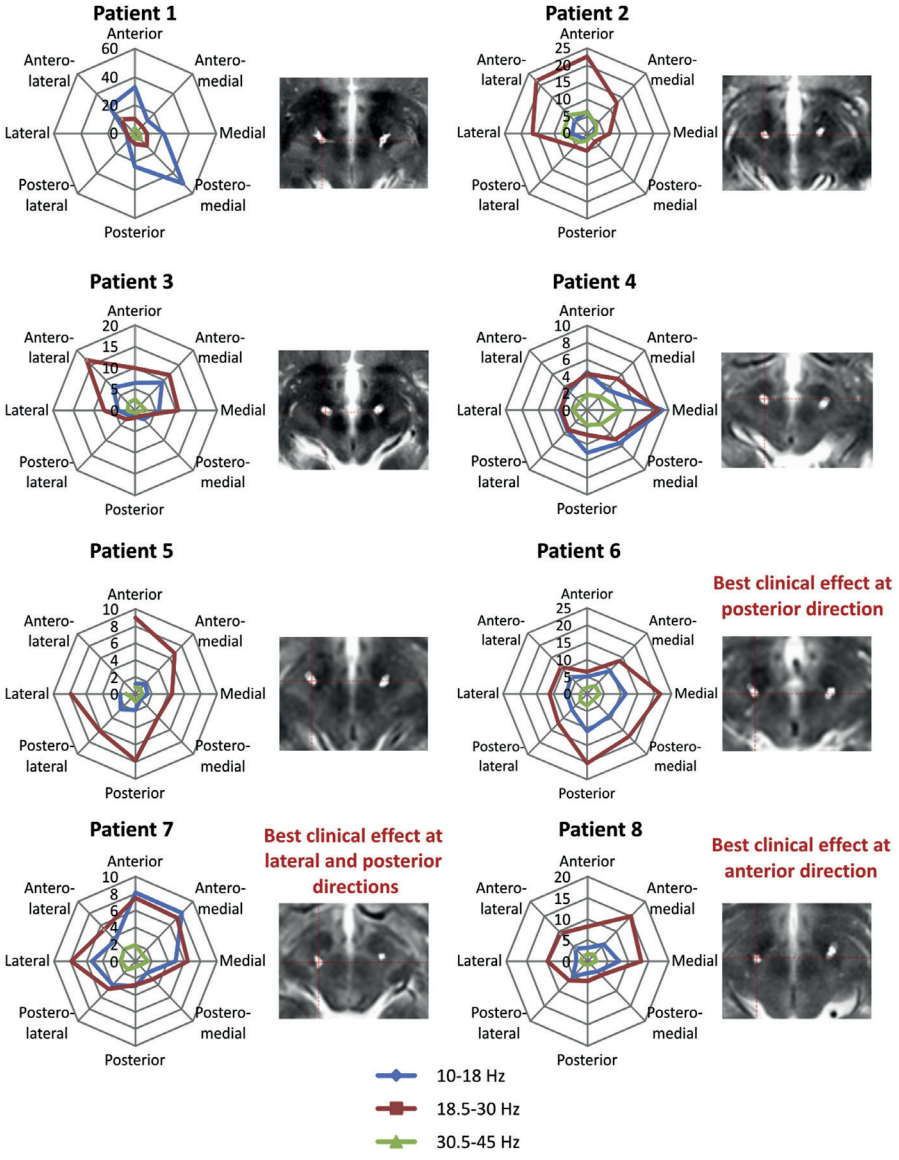

Figure 6. For all eight patients the absolute power distribution into each direction at baseline is shown. Power has been averaged along the contact points lying inside the STN for eight columns. Indicated in the figure are the three chosen frequency bands with different colors. Next to these 'spiderplots' the final DBS electrode position is shown in an axial display on the early postoperative CT fused to the preoperative MRI at the best level of the STN. In some patients the images are left/right flipped, so that all electrodes are shown on the right side. Recordings at the electrodes into the anterolateral direction for patient 5 were saturated and therefore missing. In patients 6, 7, and 8 it was possible to test for improvement of rigidity. The stimulation direction which produced improvement of rigidity at the lowest threshold corresponded with the location of the highest LFP power in the 18.5 – 30 Hz band in all three cases.

Figure 6 demonstrates the spatial distribution of the power spectral densities in different directions around the lead for the contacts that were located inside the STN. Patients 1 and 6 show a preponderance of maximal power into the posteromedial direction. Patients 2 and 3 show a preponderance of maximal power into the anterolateral direction and patients 7 and 8 more into the anteromedial direction. For patient 4 this is more into the medial direction. The difference in direction of the maximal power across the patients likely reflects a slightly different location of the lead with respect to the active spots within the STN, or inter-patient anatomophysiological variability. In the three patients in whom no stun effect was observed after insertion of the lead (patients 6, 7, and 8), clinical effect on rigidity could be tested.[126] The stimulation direction which produced improvement of rigidity at the lowest threshold corresponded with the location of the highest LFP power in the 18.5 – 30 Hz band in all three cases.

Effect of stimulation

The analysis shows that stimulation produces either LFP power suppression or enhancement. LFP power variation is not equivalent across patients and, even in the same patient, it is different across recording directions and across frequency bands (figures 7 – 9). Moreover, different stimulation modalities (ring mode or different steering modes) produced different patterns of suppression (figures 7 – 9). In general, in the frequency band from 18.5 to 30 Hz suppression was always observed, irrespective of stimulation pattern, whereas enhancement of LFP power during anterior, posterior, lateral or medial steering has been observed in the 10 – 18 Hz and the 30.5 – 45 Hz frequency bands. These variations did not always reach significance in the individual patients (figure 9). If one-way ANOVA showed significant variation ($p < 0.05$), post-hoc analysis was performed. One consistent result in all patients was a significant increase in power in the 30.5 – 45 Hz band in at least one steering direction with respect to the ring mode. Enhancement after ring mode stimulation has never been observed (figure 9). Interestingly, considering each frequency band separately, ring mode not necessarily gives the highest suppression (figure 9). Comparing the directional spatial distribution of the power spectral density in the 10 – 18 Hz and 18.5 – 30 Hz ranges (figure 6) with the amount of suppression for different steering modes (figure 9), it appeared that the percentage of power suppression was higher in the direction where the highest baseline power was measured. Patients 2 and 3, having higher power at the anterolateral side, show highest suppression with anterior mode compared to the other steering modes; patient 6, having higher power at the posteromedial side, shows highest suppression with posterior mode compared to the other steering modes.

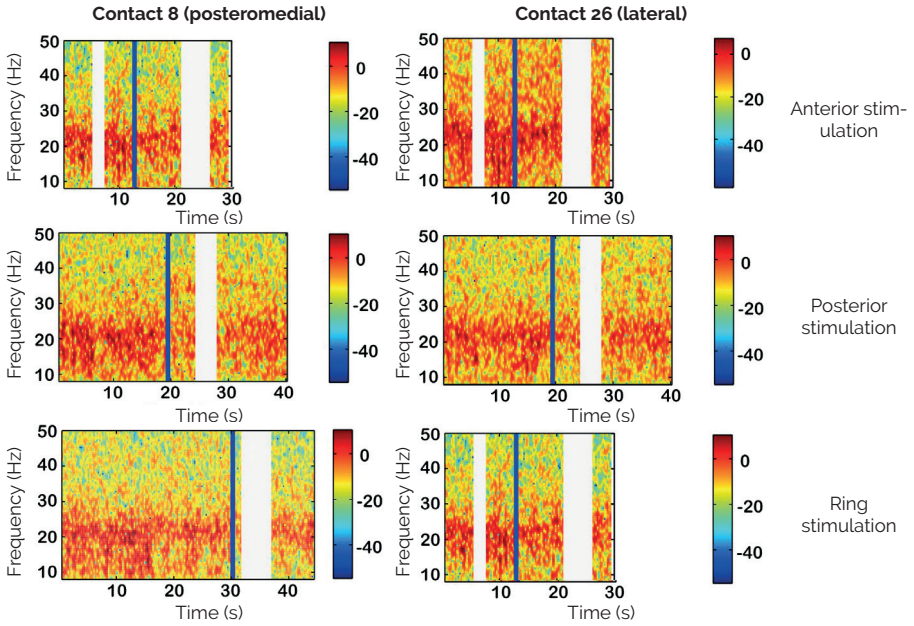

Figure 7. Spectrograms at two contact points are shown for three different modes of current steering, i.e., anterior, posterior, and ring mode in patient 6. The blue vertical bar indicates the division between pre- and post-stimulation period. Light grey bars indicate periods with artefacts. Dark red indicates high power, yellow indicates intermediate power and dark blue indicates low power. Anterior steering does not lead to so much suppression of power (less reddish) than posterior and ring mode steering. Note that after stimulation with posterior steering there is an enhancement in the 30.5 – 45 Hz frequency band, whereas in the other parts of the spectrum there is suppression. Also, it can be seen that 10 – 20 s after stimulation has been stopped, suppression of power in the 10 – 18 Hz band as well as the 18.5 – 30 Hz band diminishes.

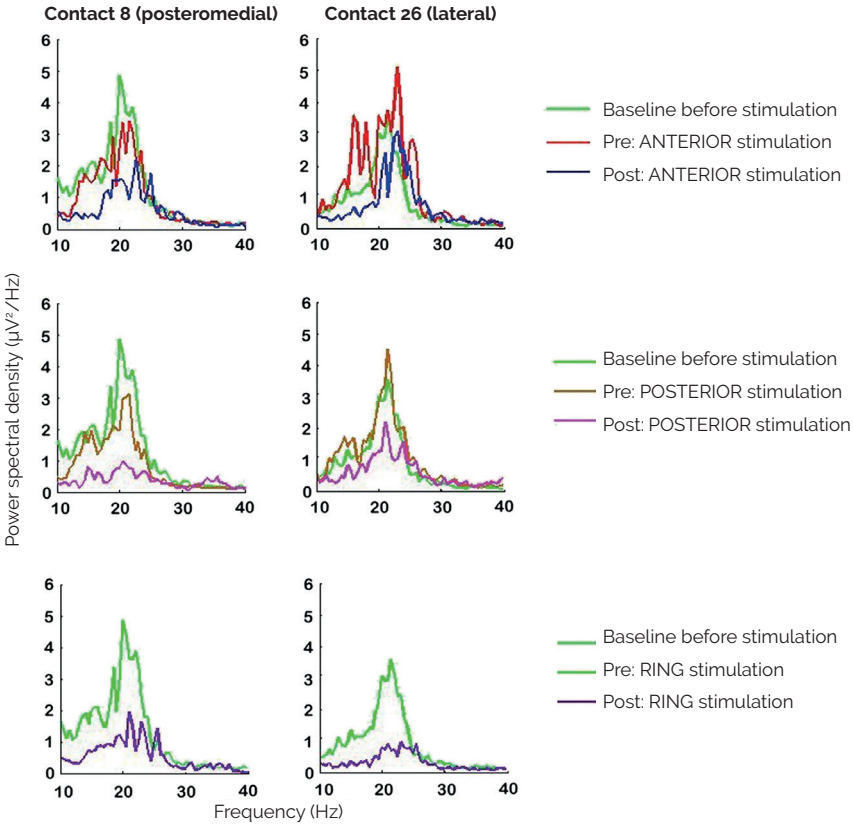

Figure 8. Variation of power spectral density in the different frequency ranges following different patterns of stimulation in patient 6. In the left column for contact 8 and in the right column for contact 26, power spectral densities are shown at baseline (green) and at a 15 s period just prior to anterior, posterior and ring stimulation and 15 s immediately after anterior, posterior and ring stimulation. It can be seen that in this patient with the highest power in the posterior direction (figure 6) for both contacts 8 and 26 posterior steering leads to a stronger suppression in the 10 – 30 Hz frequency range than anterior steering. Note the enhancement in the 30 – 40 Hz frequency range especially at contact 8 during posterior steering (purple curve).

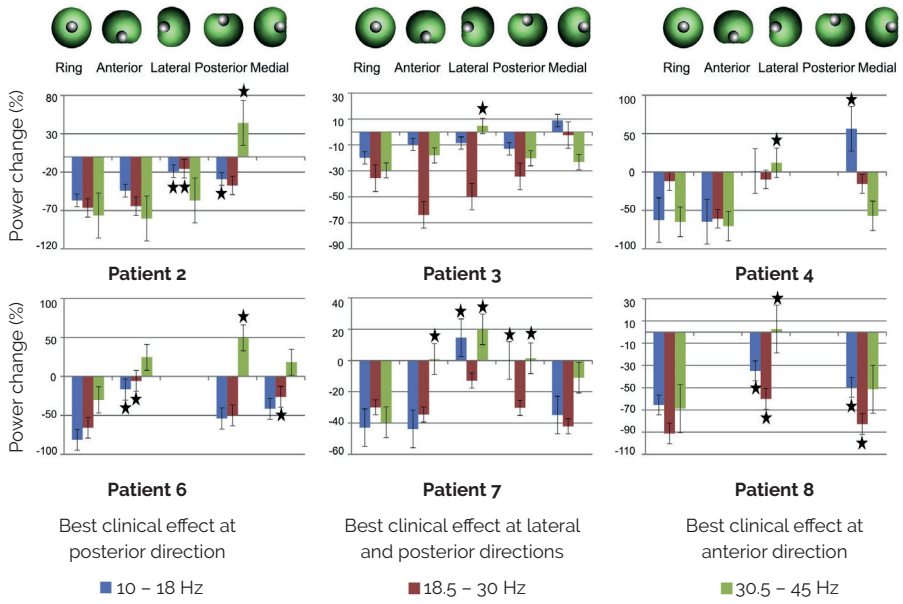

Figure 9. For six patients at each of the three frequency bands between 10 and 45 Hz the amount of suppression and/or enhancement, averaged across all electrodes inside the STN, after ring mode stimulation and anterior, lateral, posterior, and medial steering. The different colors of the bars indicate different frequency bands. The images on top indicate the spatial distribution of the electrical field in the different steering modes. Error bars indicate the standard error of mean and the black star indicates variation after steering mode stimulation that are significantly different from ring mode. For patient 6, 7 and 8 is indicated in which direction the best clinical effect on rigidity was observed. In both patients 6 and 7 suppression of the 18.5 – 30 Hz band and enhancement of the 30.5 – 45 band is seen at the best stimulation direction. Data of power change in the anterior direction for patient 8 is missing.

Patient 7 and 8 having higher power at the anteromedial side show highest suppression with anterior and medial mode (patient 7) and with the medial mode (patient 8) compared to the other steering modes. The relation between the steering direction that produced the best clinical effect on rigidity and the change in power observed after stimulation can be only analyzed for two of the three patients (due to missing post-stimulation recordings at the anterior direction for patient 8). In patients 6 and 7 suppression of the 18.5 – 30 Hz band and a significant enhancement of the 30.5 – 45 band is observed at the stimulation direction with the best clinical effect.

Discussion

First, in agreement with previous studies[23,24,178], in four patients simultaneous LFP recordings from a 32-contact DBS lead showed enhanced power spectral densities in the 11 – 40 Hz frequency band inside the STN compared to just outside, but with the advantage of a high spatial resolution (on average 0.6 mm). On the other hand, below 10 Hz with the higher resolution it has been shown for two of these four patients that power spectral densities were not significantly different just above or inside the STN. This also has been demonstrated previously by Kuhn et al.[23], where the topography of the 4 – 11 Hz band LFP activity was more distributed and variable than that of the activity in the 13 – 35 Hz band.

Secondly, inside the STN, the LFP power in the 10 – 40 Hz frequency range depended on the recording direction and depth. This may point to the presence of small cell clusters within the STN that have specific pathophysiological activity. Focality of physiological sources has been suggested in studies which used multiple passes of microelectrodes[23,24], however, their data were limited by the non-simultaneous nature of their recordings at different locations. Such a precise and directional activity localization is not possible with the conventional electrodes, which can only record LFP from a large spherical area. In addition, we have shown that directing stimulation toward the location of the highest LFP power in the 18.5 – 30 Hz band produced the best clinical effect on rigidity in all three patients in whom this could be tested.

Thirdly, immediately after stimulation, only suppression of power is found in the 18.5 – 30 Hz frequency range, whereas enhancement can be found in the 10 – 18 Hz and 30.5 – 45 Hz frequency bands after steering. Enhancement was never seen after ring mode stimulation, which suggests that it could not be detected by using stimulation through the conventional electrode. In addition, suppression after one steering mode was often stronger than after ring mode, although this did not reach significance, suggesting that in some cases steering is more specific than the conventional ring mode.

Relationship between LFP power spectral density and STN neural activity

In this study, the subdivision in bands was based on an analysis of the effective power spectral distribution. The idea of using a frequency band that is not predefined arises from the consideration that currently used frequency bands are originally based on scalp EEG recordings, whereas the STN is a different neural structure than the cerebral cortex with, therefore, also different electrophysiological properties.

Analysis of the current LFP signals at the level of the STN has shown that significant peaks are either below 10 Hz, in the conventionally used delta and theta range,

or above 10 Hz, in the conventionally used low and high beta range. This also has been demonstrated previously by Kuhn et al.[23], where first it is shown in the spectral densities that there are no peaks at 10 Hz and secondly that at the level of the STN the topography of the 4 – 11 Hz LFP activity is more distributed and variable than the topography of the activity in the 13 – 35 Hz band.

Of the four frequency bands used, i.e., 3 – 9.5 Hz, 10 – 18 Hz, 18.5 – 30 Hz and 30.5 – 45 Hz, the second and the third bands roughly correspond to the conventionally used low beta (13 – 20 Hz) and high beta (20 – 30 Hz) bands.[23–25,163,170,171,179–181] We did not split theta band (3 – 7 Hz) from alpha band (7 – 13 Hz) because the current data show, in our patients, a turning-over point around 10 Hz, in the middle of the conventional alpha band.

The smaller size of the contacts used in this study and the smaller center-to-center distance (0.75 mm) compared to the conventional DBS lead (2 mm) allowed a refined detection of the power distribution of the 3 – 10 Hz frequency band in the areas just above the STN showing in two patients no significant difference with inside the STN. The conventional DBS electrode probably cannot discriminate whether LFP power is coming from the STN or neighboring structures dorsal of the STN, including the thalamus and the zona incerta.

In previous studies, a distinction in two frequency bands within the conventional 13 – 30 Hz band showed that the lower frequencies (low beta) are more reduced with drug therapy, whereas higher frequencies (high beta) are more strongly coupled to motor and premotor cortical activity and are modulated by movement.[25,104,163,168,179,180,182–184] In the current study, four PD patients showed an extra peak in the 10 – 18 Hz band at a frequency between 13 and 14 Hz at baseline, which is not surprising since our patients were off medication. In one patient (patient 1, figure 5a) power at 14 Hz was three times higher than at 25 Hz, at which still a local maximum was evident and comparable to the other patients. All eight PD patients showed synchronization in the 18.5 – 30 Hz range with a well-defined peak between 22 and 26 Hz at baseline. Synchronization in the 30 – 45 Hz range was observed only immediately after high frequency stimulation.

Due to the high-density DBS lead, our study suggests for the first time that LFP specifically in the 10 – 45 Hz frequency range at baseline are confined to the physiologically defined subthalamic area as defined by MER. This may not necessarily correspond to the anatomically defined STN. We showed also that the lowest and highest frequency parts of the 10 – 45 Hz range react to stimulation differently than the middle frequency part. The latter always shows suppression, whereas the two former ones, varying among patients, may be enhanced or suppressed by DBS depending on the direction of steering.

Relationship between extracellular potentials and micro electrode recordings

A relationship exists between LFP oscillations and oscillatory behavior of spiking patterns particularly in the beta range[23,94], although the factors that determine this relationship remain rather complex.[22] For instance, the lower frequencies (3 – 10 Hz) of the amplitude modulation of the MER, which is derived from only a few neurons, are not comparable with the lower frequency components of the LFP, which are picked up from a much larger area and a large number of neurons.[22,167,185]

The amplitude distribution of the power spectral densities in the 10 – 40 Hz range inside the STN at baseline varies both in direction and depth across patients. Differences with respect to direction are not remarkable between the 10 – 18 Hz and the 18.5 – 30 Hz bands (figure 6). Previous MER studies found that the 13 – 30 Hz oscillatory activity was bounded more to the dorsolateral region of the STN.[73,181] However, with high density LFP recording in the 10 – 30 Hz frequency range, the subthalamic dorsal to ventral power distribution, although varying among patients, did not show systematically higher LFP power in the more proximal contacts.

Effect of DBS on the subthalamic LFP

To avoid possible effects of stimulation artefact removal on the LFP signals, only the data immediately after stimulation was considered. When DBS is switched off, a neurophysiological carry-over effect persists at least for 20 – 60 s, reflected by the ongoing suppression of parkinsonian symptoms. Indeed, continuous recordings have shown that the time needed to get the power spectral densities of LFP back to baseline was comparable to the time needed to have a complete recovery of the clinical symptoms.[165] In three out of six patients (3, 4 and 7), there was at least one steering condition that produced a stronger power suppression in the 18.5 – 30 Hz than conventional ring stimulation, although this did not reach significance (figure 9). In addition, power enhancement was never seen after ring mode stimulation while it was seen after several directional modes for selected recordings. This could point to the fact that the higher specificity of directional stimulation in modulating specific cell clusters could result in a higher effectiveness as compared to ring stimulation, which is the resultant of modulation of different cell clusters.

Possibility for STN localization

The use of a high-density array of contacts also offers the possibility to simultaneously record LFP from smaller areas inside and outside the STN. This could be used to detect the dorsal border of the STN more accurately by means of simultaneous recordings directly from the same DBS lead that would be used for chronic stimulation.

The use of LFP for determination of the borders of the STN has not been routinely introduced in the clinical practice so far. A reason for this is that the current DBS leads have a coarse spatial resolution with a relatively large contact (length of 1.5 mm; surface of 6.0 mm^2) and with a rather large inter-contact distance (2 mm) compared to the size of the STN (mean diameter of 4 – 6 mm). Moreover, due to volume conduction properties of the brain tissue, these rather large contacts may pick up also electrical activity of areas more remotely located, which may introduce an extra inaccuracy in localization.[22,186,187]

Possibility for adaptive DBS

The high-resolution electrode array may open the possibility to identify cell clusters that are closely located but may have different physiological functions. In this way, stimulation could eventually be focused on those areas in which pathological activity is maximal and spare the non-affected cells, thus improving the efficacy of stimulation.

An early hypothesis proposes that DBS creates a functional lesion by suppression of excessive STN firing, particularly in the 10 – 35 Hz frequency range.[188] However, several studies now demonstrate that DBS leads to increased action potentials along STN axons which in turn would elicit a form of short-term depression from a combination of axonal and synaptic failure.[166,189–191]

The observation that DBS suppression in the 10 – 18 Hz and 18.5 – 30 Hz frequency bands may become stronger when the current stimulation is steered into the direction where the highest power has been detected (figures 6 and 9), together with the observation that a greater clinical benefit is obtained by steering in the direction of the highest power is rather interesting. This may suggest that if LFP data should be used for adaptive DBS[90,91] one could rely on the spatially distributed power in the above-mentioned frequency bands to steer the current. Continuous recording from the implanted lead could then allow a time-locked stimulation based on the spatial-temporal pattern of the LFP activity recorded. This procedure might lead to both minimization of side effects and saving of battery power.

Further studies are needed to clarify how parts of the LFP frequency spectrum are related to different PD symptoms, including tremor, rigidity, and bradykinesia[25,90,140,175] and whether power suppression or power enhancement in the different frequency ranges and different directions should be sought and used for feedback.[166,179,190,192] A strong limitation of the current pilot study is the limited number of patients in whom the clinical effect could be tested. A chronic analysis of LFP temporal pattern and the correlation with symptoms manifestation were not addressed in this pilot study and therefore the results presented here need to be confirmed and complemented by future studies before firm conclusions can be drawn. Nevertheless, the present data

show that high-density leads and directional steering technology have the potential to contribute to an improvement of STN-DBS therapy for PD and potentially also for other targets and diseases.

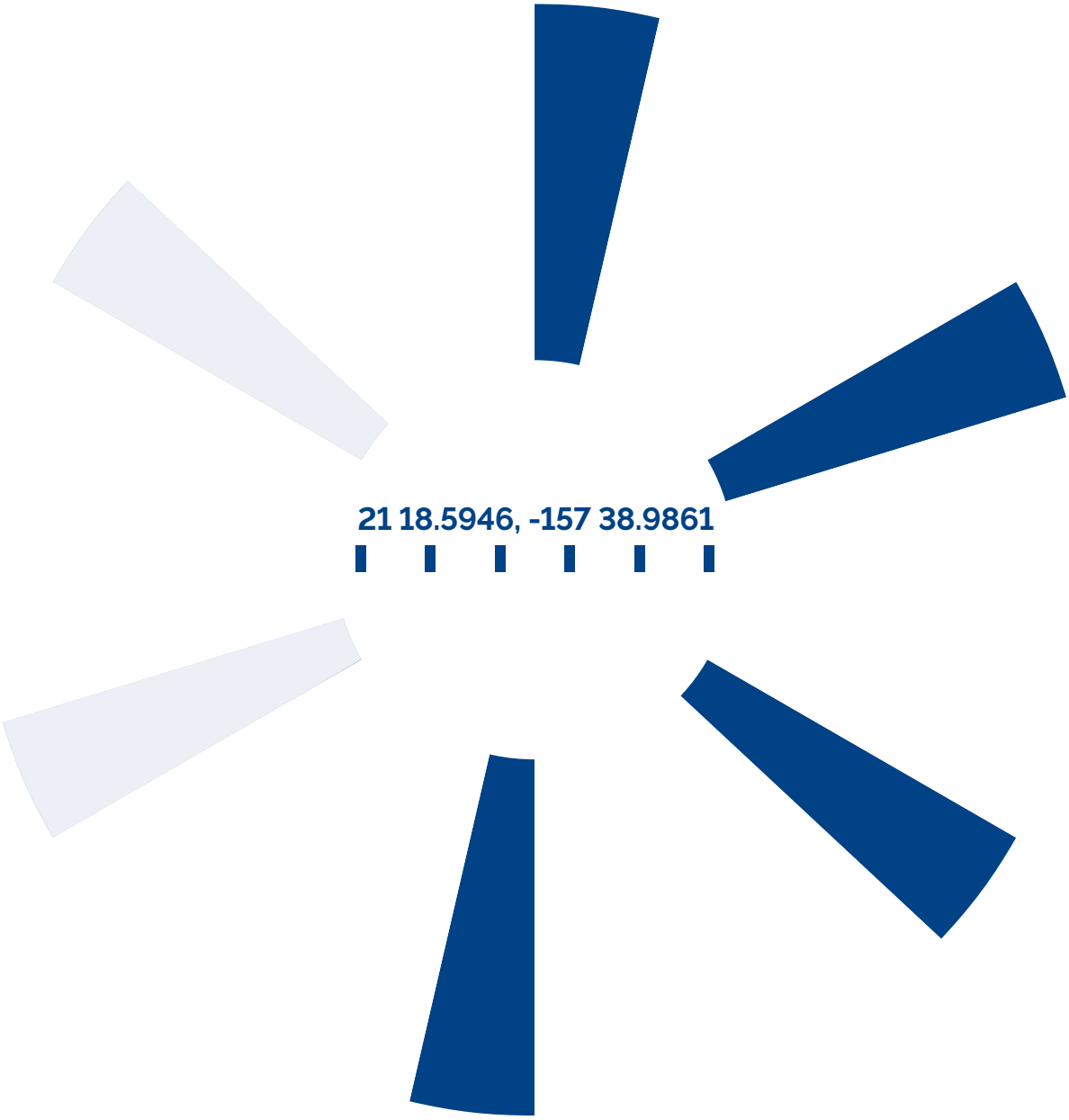
21 18.5946, -157 38.9861

CHAPTER 7

A novel lead design enables selective deep brain stimulation of neural populations in the subthalamic region

Kees J. van Dijk
Rens Verhagen
Ashutosh Chaturvedi
Cameron C. McIntyre
Lo J. Bour
Ciska Heida
Peter H. Veltink

Journal of Neural Engineering. 2015;12(4):46003

Objective: The clinical effects of deep brain stimulation (DBS) of the subthalamic nucleus (STN-DBS) as a treatment for Parkinson's disease are sensitive to the location of the DBS lead within the STN. New high density (HD) lead designs have been created which are hypothesized to provide additional degrees of freedom in shaping the stimulating electric field. The objective of this study is to compare the performances of a new HD lead with a conventional cylindrical contact (CC) lead.

Methods: A computational model, consisting of a finite element electric field model combined with multi-compartment neuron and axon models representing different neural populations in the subthalamic region, was used to evaluate the two leads. We compared ring mode and steering mode stimulation with the HD lead to single contact stimulation with the CC lead. These stimulation modes were tested for the lead: (1) positioned in the centroid of the STN, (2) shifted 1 mm towards the internal capsule (IC), and (3) shifted 2 mm towards the IC. Under these conditions, we quantified the number of STN neurons that were activated without activating IC fibers, which are known to cause side effects.

Results: The modeling results show that the HD lead is able to mimic the stimulation effect of the CC lead. Additionally, in steering mode stimulation there was a significant increase of activated STN neurons compared to the CC mode.

Conclusion: From the model simulations we conclude that the HD lead in steering mode with optimized stimulation parameter selection can stimulate more STN cells. Next, the clinical impact of the increased number of activated STN cells should be tested and balanced across the increased complexity of identifying the optimized stimulation parameter settings for the HD lead.

Introduction

Deep brain stimulation (DBS) for Parkinson's disease (PD) patients may reduce considerably their symptoms including tremor, rigidity, and akinesia.[193,194] The clinical procedure involves the implantation of a DBS lead, consisting of multiple electrode contacts, through which continuous high frequency electric pulses (typically with a frequency of 130 Hz and pulse duration of 60 – 90 μs) are delivered in a specific brain area.[195] In the case of PD, the preferred targeted brain area is the subthalamic nucleus (STN).[11,196,197] This nucleus is a small biconvex shaped structure located deep in the brain and is surrounded by several bundles of myelinated fibers such as the lenticular fasciculus, and internal capsule (IC).[43] The clinical outcome of the therapy is rather sensitive to the precise location of the DBS lead within the STN.[17,198] Unfortunately, despite careful stereotactic planning with high-tech 3D MRI imaging techniques, placement errors within a range from 1 to 3 mm still may occur.[199,200] Also, a DBS lead which initially was placed correctly post-surgery may become displaced over time due to several reasons.[70,80] In case of a displaced lead, the injected stimulation current will spread out to unwanted brain regions and, for instance, may evoke activation in the easily excitable myelinated fibers passing nearby.[201] Activation of some of these myelinated fiber tracts may have a positive clinical effect, as is the case for the efferent globus pallidus internus (GPi) fibers in the lenticular fasciculus[202], or the motor cortex axons of the hyperdirect pathway.[203] However, both activation of fibers in the IC as well as neurons in the non-sensorimotor part of the STN may cause undesirable side effects including ocular deviation, speech difficulties, facial contractions, a decline in cognitive functioning, and mood changes.[44,198,204–207] Given these side effects, it is crucial to prevent unwanted current spread and ultimately to be able to compensate for a displacement without the need to reposition the DBS lead.

To compensate for positioning errors, the stimulating electric field can be adjusted by selecting the appropriate electrode contact(s) on the lead. In this manner, the conventional lead, consisting of four cylindrical contacts (CC), is able to compensate for a displacement primarily in the dorsoventral direction. New lead designs are currently in development, which additionally enable steering of the stimulating field in the lateromedial and anteroposterior directions through a high-density (HD) array of contacts.[28,208] An example of this type is the HD lead in development at Sapiens Steering Brain Stimulation BV (Eindhoven, NL), which is currently in a clinical test phase.[126] The latest design of this HD lead, will consist of ten rows along the lead and each row containing four individual oval shaped electrode contacts, facing different directions (figure 2). With this design, the spatial steering of the stimulation field is achieved by activation of an appropriate combination of the 40 available contacts. Unfortunately, the high amount of possible combinations of contacts will increasingly complicate selecting optimal stimulation parameters. Therefore, more insight is needed into the spatial steering modes of HD leads and new tools need to be developed to find these optimal steering parameters.

Computational models can be used to evaluate and visualize steering modes DBS effects in the brain.[28,29,209] For example, Martens et al[28] evaluated a prototype design of a HD lead using a computational model. In their model, they showed that the HD lead is able to spatially steer the electric field in a homogeneous isotropic volume conductor and shift the center of the volume of activated tissue. This result suggests that indeed it is possible to compensate for lead displacement using an HD lead. However, as they also noted in their discussion, calculations were performed under the assumption that the brain acts as a homogenous isotropic volume conductor. In general, the state-of-the-art electric field models with heterogeneous anisotropic volume conduction show significant differences in the shape of their reconstructed electric fields compared to the homogeneous isotropic models.[201,210–212] To evaluate the possibility to compensate for a lead displacement, the effect of the steered field on the various neural populations in the subthalamic region needs to be estimated. The activation effect is often estimated by the volume of tissue activated, i.e., the tissue enclosed within an iso-surface of the activation function.[75,213] However, a more realistic approach, with respect to the surrounding axon fiber bundles, is to evaluate the stimulation effect in more detailed multi-compartment neuron models of different neural populations in the subthalamic region.[211]

In this study, we used computational models to investigate the stimulation effect of a HD lead and its ability to compensate for a lead displacement. The model system, based on a previous study by Chaturvedi et al[214], included a heterogeneous anisotropic volume conductor with multi-compartment neuron and axon models of three important neural populations in the subthalamic region.[214] Two populations, i.e., the STN projections cells and the efferent GPi fibers in lenticular fasciculus, represent therapeutic DBS targets while a third population, i.e., the IC fibers, represents a neural population that will cause side effects when stimulated. In the current model we have compared the stimulation effect of the conventional CC lead with that of a HD lead, which has 40 contacts. The aim of the computer simulation was to initiate an action potential in a maximum percentage of STN cells without activating IC fibers. Simulations were performed with the DBS leads positioned at three different locations within the STN, using multiple stimulation modes.

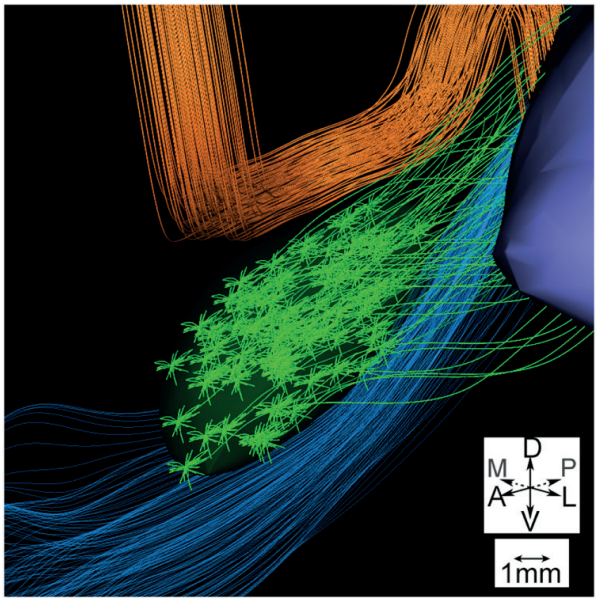

Figure 1. The anatomical model of the subthalamic region viewed from anterolateral direction. Two relevant nuclei are shown: the STN (green volume), and the globus pallidus (purple volume). The three neural populations are shown: the efferent GPi fibers (orange), the IC fibers (blue) and the STN projection neurons (green).

Materials and methods

The subthalamic region

In the current study, the computational model of the subthalamic region was based on previous work of Chaturvedi et al.[214] In summary, their model system consists of two parts: the electric field model, and the neuron model. The electric field model is a finite element method (FEM) model with the geometry and volume conduction properties of the subthalamic region based on a human brain atlas, which consists of a T1 MRI and a diffusion tensor imaging (DTI) dataset.[214,215] The DTI dataset was used to estimate the anisotropy and heterogeneity of the tissue conductivity in the brain.[216] The model incorporated a 0.5 mm tissue encapsulation layer around the electrode to account for the chronic electrode impedance of around 1 kΩ for the CC lead. A multiresolution finite element mesh was used with over 4.2 million nodes. In this FEM model the Poisson equation was solved in three-dimensions to determine the potential field generated by current stimulation and was carried out in SCIRun v3.0.2 (University of Utah, Salt Lake City, US). The computed potential field formed the input into the neuron model, which is a multi-compartment neuron model programmed in NEURON 6.2 (Yale university, New Haven, US).[217] The model consists of three neural populations in the

subthalamic region, which are most likely activated by DBS. These neural populations are the STN projections cells, the efferent GPi fibers in the lenticular fasciculus, and the IC fibers. The STN and GPi axon trajectories were based on non-human primate cell tracings[218,219], and the IC fiber trajectories were based on streamline tractography using the DTI dataset accompanying the brain atlas. Because of limited morphologic data of the axons of the neural populations, the variability between different axon models, and to enable consistent comparison between stimulation induced activation of the different neural populations, every axon was implemented with the same model parameters (5.7 µm axon diameter model).[220] Finally, SCIRun v3.0.2 was used for visualization of the complete model (figure 1).

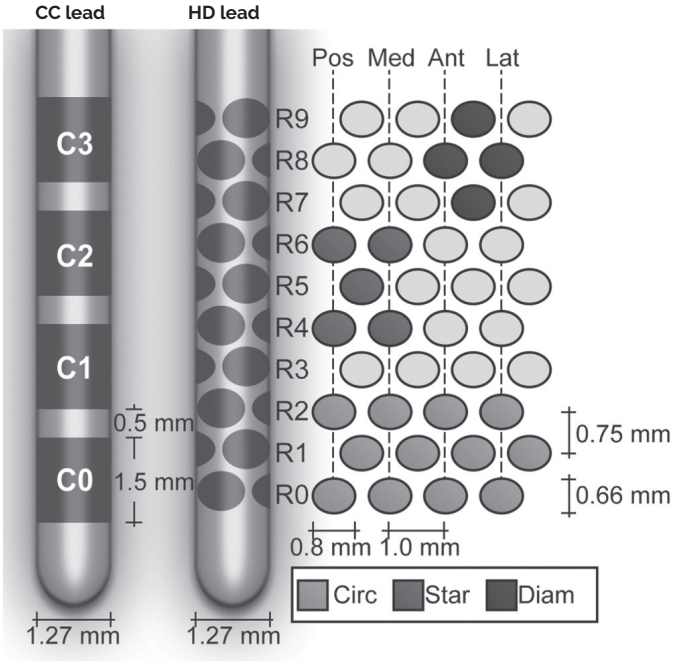

Figure 2. Representation of CC lead (left) and the HD lead with its schematic overview of the 40 contacts (right). Examples of the diam(ond) configuration in anterolateral direction, star configuration in posteromedial direction, and circ(ular)-mode (R0 – R2) of the HD lead are indicated in different gray scales.

DBS lead geometry

Either a CC lead or an HD lead (figure 2) was incorporated within the FEM model. The CC lead was based on the Medtronic 3389 electrode (Medtronic Inc., Minneapolis, US), which has a body diameter of 1.27 mm and carries four CC (C0 – C3). These contacts each have a length of 1.5 mm, a 6.0 mm^2 contact surface area, and an inter-electrode spacing of 0.5 mm. The HD lead was based on the Sapiens Steering Brain Stimulation lead design, which also has a diameter of 1.27 mm and carries 40 oval shaped electrode contacts. The 40 contacts are divided into ten rows (R0 – R9) of four contacts, and each row is rotated by 45˚ from each other. Each oval shaped contact has a 0.42 mm^2 contact surface area, and contact center-to-center distances of 1 and 0.75 mm in the horizontal and vertical directions, respectively.

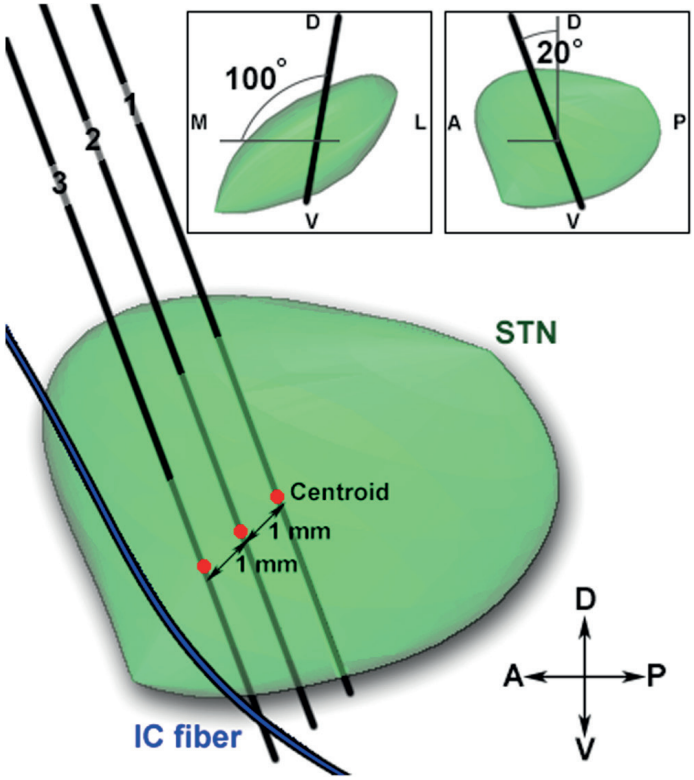

Figure 3. Representation of the DBS lead locations. The STN volume is shown in green, one IC fiber is shown in blue, and the three lead trajectories are shown by black lines. Trajectory 1 is the center location, trajectory 2 is the 1 mm off-center location, and trajectory 3 is the 2 mm off-center location. The top two views (left coronal, right sagittal) of the STN show the trajectory arc and collar angles of 20˚ and 100˚, respectively, in an AC – PC based coordinate system. The main (sagittal) view of the STN shows the shifts of the lead trajectory in the direction of the IC.

DBS lead location

For each simulation only one of the DBS leads was positioned in the STN. This DBS lead was positioned either at the center location, at a 1 mm off-center location, or at a 2 mm off-center location (figure 3). For the center location, the lead targeted the centroid of the STN: the second electrode contact from the tip (C1) of the CC lead was positioned in the center, the fourth row of electrode contacts from the tip (R3) of the HD lead was positioned in the center. At the off-center locations, the lead was linearly shifted 1 or 2 mm towards the IC, on the line between the centroid of the STN and the point given by the average location of the nearest axon segments of each IC fiber in the model. This resulted in a shift 0.46 mm posteriorly, 0.59 mm medially, and 0.66 mm ventrally with respect to the center location, per 1 mm displacement. For all three locations, the lead approached the target in an AC – PC based coordinate system with a typical lead arc and collar angles of 20˚ and 100˚, respectively (figure 3).

Stimulation protocols

Monopolar stimulation protocols were tested for different contact configurations and stimulation amplitudes. The stimulation signal was a biphasic charge-balanced stimulation pulse, i.e., a 100 µs rectangular waveform, with amplitudes ranging from –1 to –5 mA with a 0.5 mA step size, followed by a 5 ms period of low amplitude anodic stimulation. The outer boundary of the FEM model was used as reference for the return current. The stimulation signal was used for single source stimulation by evenly spreading the injected current over the selected electrode contact(s). The possible contact configurations varied per lead. For the CC lead, one of the four electrode contacts, C0 – C3 (6.0 mm^2 activated electrode surface), was selected to simulate circular mode stimulation (figure 2). For the HD lead, we distinguish two types of circular mode stimulation and two types of steering mode stimulations, i.e., HD circular 'mimic', HD circular 'free', HD star, and HD diamond (figure 2). For both HD circular modes, three adjacent rows, each with four electrode contacts, (5.0 mm^2 activated electrode surface) were selected for stimulation. In HD circular 'mimic' mode, we used the same stimulation pulse amplitude and similar vertical contacts height as the optimal CC configuration, i.e., R0 – R2 for C0, R2 – R4 for C1, R5 – R7 for C2 and R7 – R9 for C3. In HD circular 'free' mode, there were no constraints in the stimulation pulse amplitude and selection of the vertical contact height. In HD steering mode, the electrode contacts were selected in either a star or diamond configuration. In the star configuration, five adjacent electrode contacts were selected in either medial, lateral, posterior, anterior, or any of the intermediate directions (2.1 mm^2 activated electrode surface). In the diamond configuration, four adjacent electrode contacts were selected in the medial, lateral, posterior, anterior, or any of the intermediate directions (1.7 mm^2 activated electrode surface). Stimulation in diamond configuration with –5 mA stimulation amplitude results in the maximum charge density of 29 µC cm^{-2}, which is below the often-recommended charge density limit of 30 µC cm^{-2}. For each

stimulation mode, all possible directions and vertical positions of the configurations were simulated to find the optimal settings.

Activation of neural populations

The effect of the evoked potential field by each stimulation protocol (each amplitude and each contact configuration) was evaluated in the neuron part of the computational model. To quantify the differences between stimulation protocols we aimed to maximize the amount of activated STN cells without activating the IC fibers, but with allowing activation of efferent GPi fibers. A cell or axon is counted as activated when the stimulation pulse evoked at least one action potential that propagated to the end segment of the axon. The optimal stimulation protocol was defined as the configuration that activated the highest percentage of STN cells, without activating any IC fiber.

Statistical analysis

Fifteen datasets were created to compare the different stimulation configurations statistically. Five datasets were created with the leads at the center location and five datasets for each of the two off-center locations. For each dataset, the STN cell bodies were randomly distributed inside the STN, the GPi fibers were randomly distributed within a given boundary box dorsal to the STN, and the IC fibers were kept constant.[214] Differences were analyzed statistically, using a repeated measures ANOVA test with significance level of 0.05. When necessary, six Bonferroni corrected paired sample t-tests were performed, i.e., the CC configuration with each of the four HD configurations, the two HD circular modes (free and mimic) with each other, and the two HD steering modes (star and diamond) with each other.

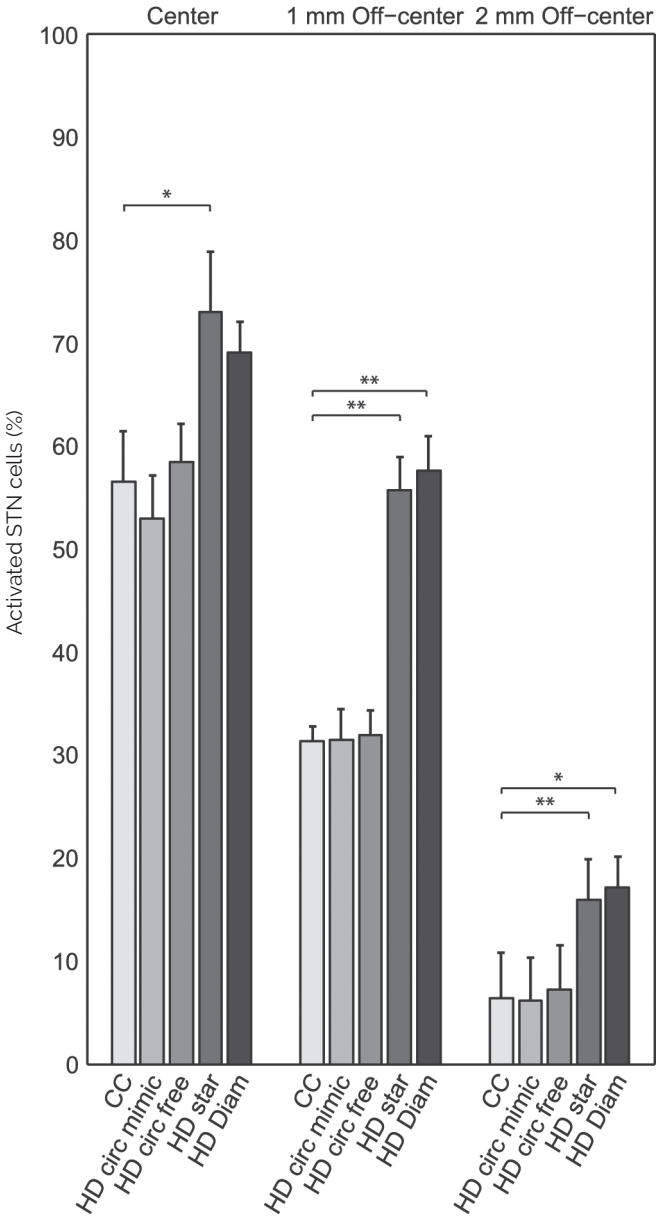

Figure 4. The performance of the five stimulation modes, i.e., the CC, HD circ(ular) mimic, HD circ(ular) free, HD star and HD diam(ond). Bars denote mean values with standard deviations of the percentage of activated STN cells after stimulation for the 5 datasets per lead location each with random distributions of the cells/fibers in the neural populations. Significant differences after Bonferroni correction for multiple comparisons (n = 6) are indicated with one asterisk ($p < 0.05$) or two asterisks ($p < 0.01$).

Results

In the model system, a population of 99 STN cells, a bundle of 99 GPi fibers, and a bundle of 199 IC fibers were placed in the subthalamic region. Each neuron with a cell segment located at the position of the DBS lead was removed from the model. For the 15 datasets, this resulted in neuron models including 182.3 ± 13.1 IC fibers, 99 GPi fibers, and 79.8 ± 4.3 STN cells.

Comparison of the CC and HD leads in circular modes

We compared the circular mode stimulation of the CC lead with the circular mode stimulations of the HD lead, both with and without the mimicking constraints ('mimic' and 'free', respectively) (figure 4). The CC lead, with its optimal stimulation settings, was able to activate 56.6 ± 4.8% STN cells at center location, 31.4 ± 1.4% of STN cells at the 1 mm off-center location, and 6.4 ± 4.4% of STN cells at the 2 mm off-center location. The HD lead in circular 'mimic' mode was able to activate 53.0 ± 4.2% of STN cells at center location, 31.5 ± 3.0% cells at the 1 mm off-center location, and 6.2 ± 4.2% cells at the 2 mm off-center location. For all locations, there were no significant differences between the percentage of activation with the CC lead and with the HD lead in circular 'mimic' mode.

Ignoring the mimicking constraints, i.e., the circular 'free' model, resulted in a maximum activation of 58.5 ± 3.7% STN cells at center location, 31.9 ± 2.4% cells at the 1 mm off-center location, and 7.2 ± 4.3% cells at the 2 mm off-center location. In all cases, there were no significant differences between the CC lead and the HD lead, with regard to the number/percentage of activated STN cells and the overall currents that were used. The corresponding optimal stimulation pulse amplitudes for each lead location are presented in table 1.

Table 1. Stimulation effect of the CC lead and HD lead

	Center		1 mm off-center		2 mm off-center	
	STN (%)	**Amp (mA)**	**STN (%)**	**Amp (mA)**	**STN (%)**	**Amp (mA)**
CC	56.6 ± 4.8	4.5 ± 0	31.4 ± 1.4	2.3 ± 0.45	6.4 ± 4.4	0.4 ± 0.22
HD circular 'mimic'	53.0 ± 4.2	4.5 ± 0	31.5 ± 3.0	2.3 ± 0.45	6.2 ± 4.2	0.4 ± 0.22
HD circular 'free'	58.5 ± 3.7	3.9 ± 0.9	31.9 ± 2.4	2.4 ± 0.22	7.2 ± 4.3	0.5 ± 0
HD star	73.0 ± 5.9	4.5 ± 0	55.7 ± 3.2	3.6 ± 0.82	16.0 ± 3.9	1.0 ± 0
HD diamond	69.1 ± 2.9	5.0 ± 0	57.7 ± 3.3	3.9 ± 0.22	17.1 ± 3.1	1.5 ± 0

Mean ± standard deviation of the percentage of activated STN cells with the corresponding stimulation amplitudes.

Comparison of the CC and HD leads in steering modes

Next, we compared the circular mode stimulation of the CC lead with the HD lead in steering mode (star and diamond configurations) (figure 4). The star configuration was able to activate 73.0 ± 5.9% of STN cells at the center location, 55.7 ± 3.2% cells at the 1 mm off-center location, and 16.0 ± 3.9% cells at the 2 off-center location. The percentage of activated STN cells by the HD lead in star steering mode was significantly larger at the center location ($p < 0.05/6$) as well as at the off-center locations ($p < 0.01/6$). The diamond configuration was able to activate 69.1 ± 2.9% of STN cells at the center location, 57.7 ± 3.3% cells at the 1 mm off-center location, and 17.1 ± 3.1% cells at the 2 mm off-center location. The percentage of activated STN cells by the HD lead in diamond steering mode was significantly larger at both off-center locations ($p < 0.01/6$ (1 mm) and $p < 0.05/6$ (2 mm)). There was no significant difference between the percentages of activated STN cells between the two types of steering configurations. The corresponding stimulation pulse amplitudes for each lead location are also included in table 1.

Finally, each stimulation mode individually activated significantly fewer STN cells at the 1 mm off-center location compared to the activation at center location ($p < 0.05$). However, there was no significant difference between the stimulation of the CC lead at center location and the HD lead stimulation in steering mode at the 1 mm off-center location. In other words, while the displacement significantly decreased the percentage of STN cell activation of both leads according to our predefined criterion, the HD lead with the 1 mm displacement error was still able to activate a similar amount of STN cells as the CC lead located in the center of the STN (figure 5).

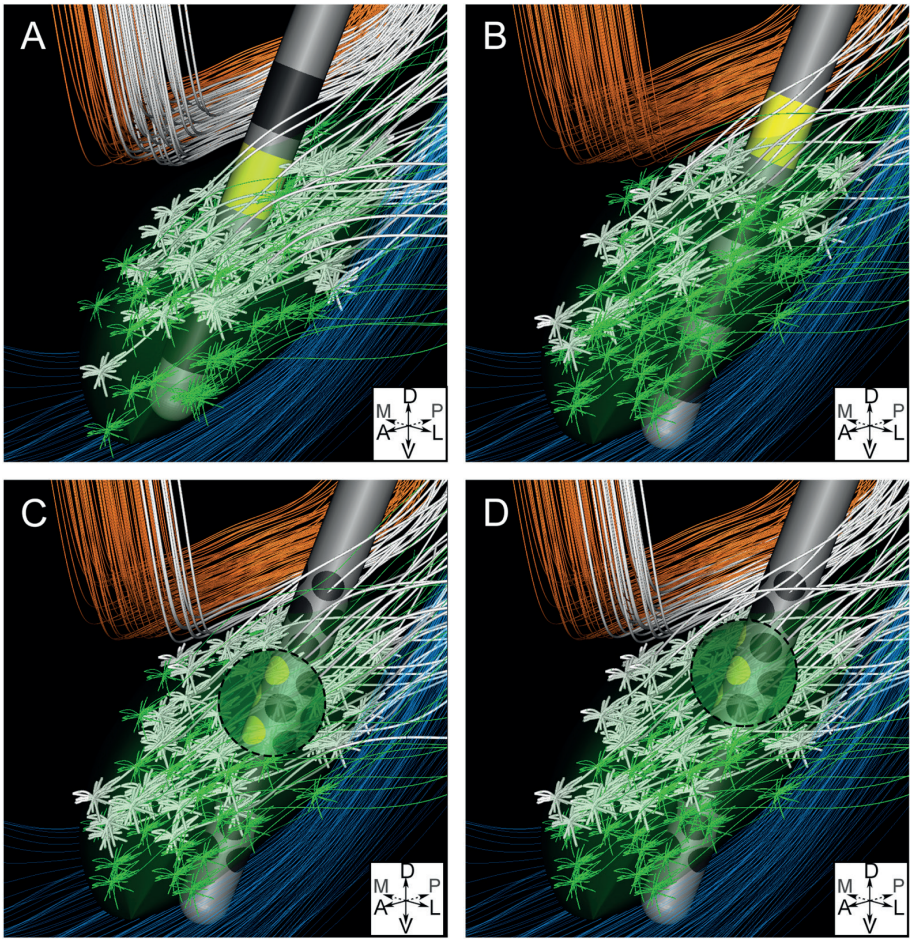

Figure 5. An example of the activation of STN cells illustrating the ability to compensate for a lead displacement error using the HD lead. The panels show the GPi efferent fibers in orange, STN cells in green, IC fibers in blue, and the STN cells in green. Cells and fibers that were activated by the stimulation pulse are displayed in white. **(A)** The optimal configuration of the CC lead at center location (4.5 mA, 53% stimulated STN cells). **(B)** The optimal configuration for the CC lead at the 1 mm off-center location (2.5 mA, 31% stimulated STN cells). **(C)** The optimal star steering configuration for the HD lead at the 1 mm off-center location (3 mA, 57% stimulated STN cells). **(D)** The optimal diamond steering configuration for the HD lead at off-center location (3,5 mA, 56% stimulated STN cells).

Discussion

In the current study, we used a computational model approach to investigate the stimulation effects of a new HD DBS lead design. The primary advantage of this HD lead is the ability to steer the stimulation field towards target areas and/or away from areas that cause side effects. However, the HD lead should also be able to mimic the conventional circular mode stimulation. This requirement is important to ensure backwards compatibility with the currently used systems.[28] By stimulating with the HD lead at the same location and amplitude as the CC lead, the HD lead is able to activate a similar percentage of STN cells. Furthermore, the HD lead has more optional configurations than the CC lead. We studied all possible 'monopolar' circular mode stimulation configurations with twelve electrode contacts in three adjacent rows. This resulted in eight different vertical positions with 0.75 mm resolution for the HD lead, against four heights with 1.5 mm resolution for the CC lead. Interestingly, the increased resolution in vertical position did not result in a significantly better performance of the HD lead in circular 'free' mode. A potential reason for this might be due to the use of three rows of smaller contacts in HD circular mode, when added together, this covers a slightly larger volume along the vertical direction as compared to a single CC contact. This reduces some specificity of the HD lead. Additionally, the stimulating field in dorsoventral direction was only bound by the IC ventrally to the STN. Therefore, by adopting the criterion that IC fibers were not allowed to be activated, the shape of the electric field dorsal of the STN was less critical, and therefore the increased vertical spatial resolution of the HD lead had a minor influence.

When looking at the steering mode stimulation, the results from the model clearly showed an increased activation by the HD lead compared to the stimulation with the CC lead. The most notable improvement was in the case where the lead was displaced 1 mm towards the IC. While the CC lead was on average only able to activate 31% of the STN cells, the HD lead activated on average 57% STN cells. This amount of activation for the HD lead was similar to the activation with the CC lead at center location. This suggests that the HD lead in steering mode, when displaced 1 mm towards the IC, is still able to generate the same neuron activation effect as the CC lead that is placed at the center of the STN. For the larger displacement of 2 mm, the HD lead in steering mode stimulation was still able to activate significantly more STN cells than the CC lead. However, the percentages of activated STN cells were very low for all of the stimulation configurations at this location. By having the lead this close to the IC field steering cannot fully compensate for the lead displacement compared to the stimulation effects of the lead at center location.

We should note, however, that we only studied two types of steering mode stimulation: star and diamond configuration. Other types of contact configurations as well as multipolar stimulation may further increase the performance of the HD lead

in specific scenarios. Of course, the same applies for the CC lead. Chaturvedi et al[214] showed in a similar computational model that the CC lead in bipolar configuration with two independent sources performs significantly better than the lead in monopolar stimulation. However, allowing additional types of configurations for the HD lead will make it extremely complicated to manually find the optimal DBS settings. Therefore, we limited the configurations to two simple types of steering modes. Both types used adjacent electrode contacts centered on certain heights and directions of the lead. The results showed no significant differences between the two configuration types. However, at center location there was no significant difference between the diamond configuration and the CC lead, while there was a significantly larger percentage of STN cells stimulated with the star steering configuration. Therefore, we prefer the star configuration for steering mode stimulation. Also, the star configuration uses five instead of four electrode contacts, which results in a larger contact surface area, and therefore a lower current density per contact.[146]

To quantify the stimulation effect, we adopted the criterion that a maximum amount of activated STN cells is desired with DBS. Therefore, we searched, for each stimulation mode, for the highest percentage of activated STN cells and allowed activation of the GPi efferent fibers. Several studies show that patients with the best clinical outcome tend to have direct activation of axonal tissue dorsal to the STN compared to those who have stimulation confined within the STN.[18,42,128,202] It has been suggested that adverse DBS effects are caused by the fact that the STN contains three functional modalities: motor, limbic and associative functions. Consequently, stimulation of the areas that are not concerned with motor function may result in adverse effects.[44,221] Additionally, instead of maximizing the activation of motor STN cells it actually might be better to focus on the activation of passing GPi fibers[128], subpopulations of fibers within the IC[222], passing fibers of the substantia nigra[18], or cortical afferents to the STN.[203] Given all these uncertainties, we decided only to focus on maximization of the amount of the activated STN cells, which is conventionally considered as the main target for STN-DBS. In principle it can be regarded as an example to show the steering effect of the HD lead on a plausible target.

We decided to focus on maximizing the activation effect, and not on minimizing energy consumption. The DBS battery is implanted under the skin below the clavicle and surgery is needed to replace it once it is depleted. Therefore, battery life is an important aspect in DBS therapy. Shaping the stimulation field to compensate for a lead displacement did demand higher stimulation amplitudes in our model simulations. However, because of the uncertainties with regard to the selection of target areas for optimal clinical effects, and inaccurate or lack of data on the resistivity of the contacts of the HD lead, a comparison of stimulation power for the different leads and configurations is at this point beyond the scope of our study.

Our model representation of the HD lead was included in a state-of-the-art computational model of the subthalamic region that included many important and realistic details. The technical limitations of this computational model are well described in previous studies.[75,202,211] The limitations will have effect on the quantified percentage of activated STN cells. For example, all axons in this model have the same diameter of 5.7 µm and therefore the same dynamic properties and excitability.[220] In the human nervous system, long-distance connections typically tend to have larger axon diameters. Given this, the IC fibers probably have relatively large axon diameters, while the STN axon diameters are known to be smaller than 5.7 µm.[223] In this study, the size of the IC fibers was more important for the results, because the selection of the steering mode stimulation parameters was based on avoiding activation of these IC fibers. In general, larger diameter axons are more easily excitable than smaller diameter ones. Therefore, when using IC pathway activation as a proxy to avoid side effects, it seemed logical to describe the IC axons more accurately with a larger diameter model. Finally, since our results focus on a comparison between the CC and HD leads in the same model, the limitations will influence both leads and therefore will have little impact on the comparison. The model already proved to be an adequate tool to study new stimulation paradigms for the CC lead.[214] In this study, we also showed that the model enables to explore new lead designs and prove the concepts of steering mode stimulation.

In conclusion, we found that the concepts of steering the stimulation field with a HD lead design used in this study may be beneficial, and it allows to correct for lead displacement errors. We have demonstrated that even a simple steering mode outperforms current state of the art systems. However, more research is needed on the stimulation of other therapeutic targets and side effect regions. In the future this information can be incorporated into a patient specific model, based on the one used in this study, to help select the contact configuration with the best therapeutic window for each patient individually.


43 37.3869, -70 12.4722

CHAPTER 8

Avoiding internal capsule stimulation with a new eight-channel steering deep brain stimulation lead

Kees J. van Dijk
Rens Verhagen
Lo J. Bour
Ciska Heida
Peter H. Veltink

Neuromodulation: Technology at the Neural Interface. 2018;21(6):553-561

Objective: Novel deep brain stimulation (DBS) lead designs are currently entering the market, which are hypothesized to provide a way to steer the stimulation field away from neural populations responsible for side effects and towards populations responsible for beneficial effects. The objective of this study is to assess the performances of a new eight channel steering DBS lead and compare this with a conventional cylindrical contact (CC) lead.

Methods: The two leads were evaluated in a finite element electric field model combined with multicompartment neuron and axon models, representing the internal capsule (IC) fibers and subthalamic nucleus (STN) cells. We defined the optimal stimulation setting as the configuration that activated the highest percentage of STN cells, without activating any IC fibers. With this criterion, we compared monopolar stimulation using a single contact of the steering DBS lead and CC lead, on three locations and four orientations of the lead. In addition, we performed a current steering test case by dividing the current over two contacts with the steering DBS lead in its worst-case orientation.

Results: In most cases, the steering DBS lead is able to stimulate a significantly higher percentage of STN cells compared to the CC lead using single contact stimulation or using a two-contact current steering protocol when there is approximately a 1 mm displacement of the CC lead. The results also show that correct placement and orientation of the lead in the target remains an important aspect in achieving the optimal stimulation outcome.

Conclusion: Currently, clinical trials are set up in Europe with a similar design as the steering DBS lead. Our results illustrate the importance of the orientation of the new steering DBS lead in avoiding side effects induced by stimulation of IC fibers. Therefore, in clinical trials sufficient attention should be paid to implanting the steering DBS lead in the most effective orientation.

Introduction

With FDA approval for almost 15 years, deep brain stimulation (DBS) of the subthalamic nucleus (STN) has become an established treatment for patients with Parkinson's disease (PD).[2,193] PD is a neurological movement disorder, and the symptoms of the disease are closely related to pathological neural activity within the basal ganglia network.[96] Because the STN is part of the basal ganglia network, STN-DBS directly modulates the pathological neural activity in the network by use of electric stimulation. Conventionally, this electric stimulation, a continuous train of electric pulses (typically with frequencies between 120 and 180 Hz, 1 – 5 mA amplitude, and 60 – 200 µs pulse width)[193], is delivered in the STN through a lead containing four cylindrical contacts (CC) and is powered by a single source from a surgical implanted pulse generator. Until now the technology for DBS has not changed tremendously over the years.[144,224] Lately however, technological developments have been reported in terms of new stimulation paradigms[151,225], closed loop DBS[90,226], independent current source stimulators[227], and directional steering DBS with high density and eight channel lead designs.[28,29,228] Most of the new technologies are still in an early development phase, although some of the technologies are already used in clinic.

Steering DBS is a method to overcome a big hurdle in DBS, that is, the stimulation of structures of fibers that cause side effects due to a small misplacement and/or displacement of the lead. The clinical outcome of the therapy is rather sensitive to the precise location of the lead with respect to the target.[17,198] Unfortunately, displacement of 1 – 3 mm can occur during surgery or post-surgery due to several reasons, such as a post-surgery brain shift and inaccuracy of the stereotactic frame and limitations of imaging methods.[70,80,199,200] In case of displacement of the lead, the stimulating electric field will influence the neurons and axons outside the intended target region. The target, the STN, is a small biconvex shaped structure surrounded by several bundles of myelinated axons such as the internal capsule (IC).[43] The large diameter, myelinated axons of the IC are easily stimulated which will induce unwanted side effects, such as dysarthria, muscle contractions, and gaze paresis.[206]

To compensate for lead displacement, the stimulating electric field can be adjusted by selecting the appropriate electrode contact(s) on the lead. In this manner, with the conventional CC lead it is possible to compensate for a displacement along the direction of the lead. Eight channel lead designs, which started with a lead specifically designed for a study by Pollo et al. by Aleva Neurotherapeutics SA (Lausanne, CH)[29], followed by Boston Scientific (Marlborough, MA, USA) and St. Jude Medical (St. Paul, MN, USA), are also able to steer the electric field in the direction perpendicular to the lead. These leads have eight electrode contacts divided over four heights along the lead. For example, the lead by Boston Scientific contains a cylindrical shaped contact including the tip of the lead as the bottom electrode contact, followed by two cylinders

which are split into three individual electrode contacts for directional steering DBS, and the top electrode is a cylindrical shaped contact (figure 1). In addition, this eight-electrode contact lead design can be connected to a matching pulse generator with eight independent current courses. To assess the benefits of this particular steering DBS system, clinical trials are currently set up in a number of clinics.[229]

To aid clinicians in clinical trials, computational models can be used to give more insight in how steering DBS is able to shape the electric field and affect the surrounding axons and neurons. Patient specific models which are used to visualize the potential field[230] and the volume of tissue activated (VTA), which is based on the spatial second order derivative of the potential field[76], can be a helpful tool for customized DBS programming in patients. Multiple modeling studies have been performed to get a more accurate representation/estimation of the potential field and VTA by adding biological details in the model such as heterogeneous tissue conductivity, anisotropic conductivity, encapsulation layers, and tissue capacitive behavior.[201,210–212] Next to the visualization, these more realistic models can also be used to automatically select stimulation parameters[204], to study new lead designs[28,29,231,232], and new stimulation paradigms such as coordinated reset.[233] Previous studies on directional DBS electrodes have emphasized the potential improvement of the clinical effect by avoiding anatomical structures responsible for side effects.[28,29] In a previous study by the authors, a high density (HD) directional DBS lead containing 40 contacts, developed at Sapiens Steering Brain Stimulation BV, currently Medtronic Eindhoven Design center (Eindhoven, NL), was assessed in a computational model.[234] Instead of looking at the potential field and VTA volume to avoid certain anatomical structures, this model included multicompartment neuron and axon models of two important neural populations in the subthalamic region, that is, the STN neurons, which represent the cells for positive clinical effect, and the IC fibers that will cause side effects when stimulated. Having the two neural populations in the model enabled adjustment of the contact configurations and stimulation amplitudes until the maximum number of activated STN cells was found without stimulating any of the axon fibers of the IC.

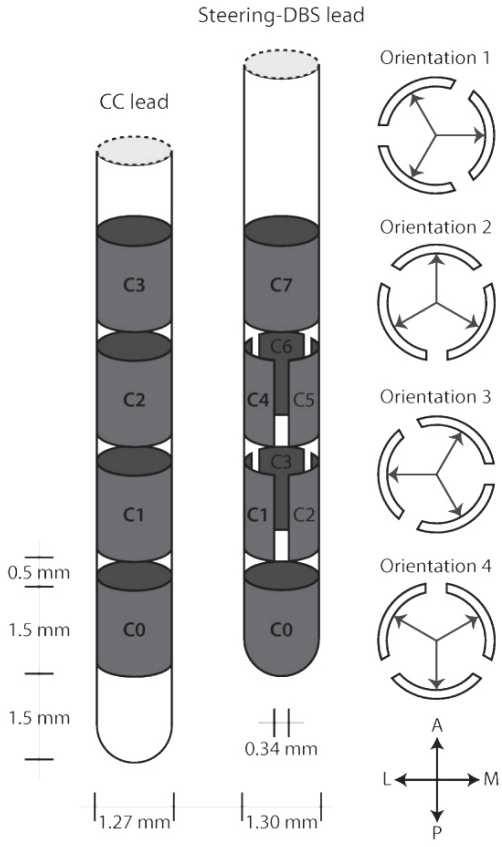

Figure 1. Representation of the CC lead (left) and the steering-DBS lead with a schematic overview of the four orientations (right). Contact C1/C4 is pointing to medial (orientation 1), anterior (orientation 2), lateral (orientation 3), or posterior (orientation 4) direction.

In this current study, we will use computational modelling procedures to assess the performance of a steering DBS lead based on the eight-electrode contacts lead design. The model includes a heterogeneous anisotropic volume conductor model to compute the evoked potential field in the subthalamic region and uses multicompartment neuron and axon models to investigate the stimulation effect of STN cells and the ability to avoid activation of IC fibers. We will compare this stimulation effect of the steering DBS lead with the CC lead. The effect of one millimeter and 2 mm displacement is investigated, and as the new steering DBS lead is not cylindrical symmetric, we will also study the effect of four different orientations of the lead. Finally, we will test for this steering DBS lead on each location and orientation the performance of monopolar stimulation vs. a current steering stimulation paradigm using two adjacent electrode contacts.

Materials and methods

The computational model

The model system of the DBS target region, the implanted DBS lead, and the stimulation effect on nearby neurons and axons, is based on previous work by Chaturvedi et al.[211,214] The model system consists of two consecutive parts. In the first part, the static electric field generated by current controlled stimulation[235], was computed in a finite element method (FEM) model of an adult brain. The geometry and conductivity of the brain is based on a human brain atlas consisting of a T1 MRI and a diffusion tensor imaging (DTI) dataset, with dimensions of 178 mm by 159 mm by 120 mm.[215] The DTI dataset was used to estimate the anisotropy and heterogeneity of the tissue conductivity. A linear transformation (0.8 S/mm^2 scaling factor) was used to convert the diffusions tensors into conductivity tensors.[216] The FEM model contains the DBS lead with a 0.5 mm tissue encapsulation layer (0.18 S/m) around the lead to account for the chronic electrode impedance of around 1 kΩ for the CC lead (mean impedance of 1005 Ω ± 6.8 Ω standard deviation for the CC lead contacts in the model). The complete geometry was divided into 4.1 million tetrahedral elements. The outer boundary was set to 0 V and Dirichlet boundary conditions were used. With this FEM model, the potential field generated by the stimulation was calculated by solving the Poisson equation in three dimensions in SCIRun v3.0.2 (University of Utah, Salt Lake City, USA).

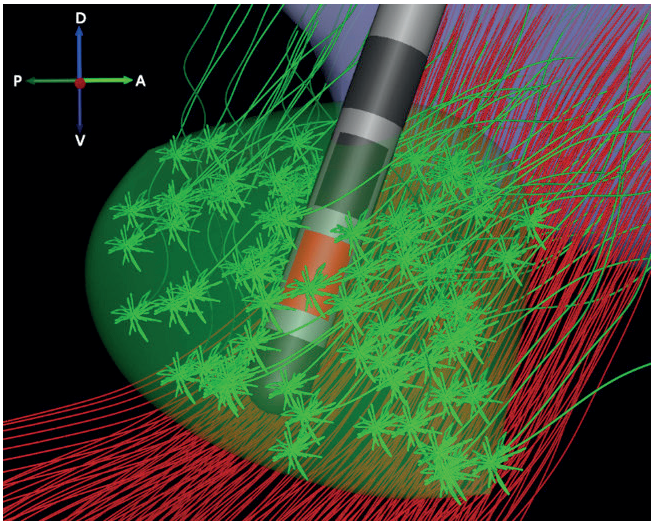

Figure 2. The visualization of the anatomical model of the subthalamic region with the steering-DBS lead at the center of the STN. Two relevant nuclei are shown: the STN (green volume in center), and the globus pallidus (purple volume in the background). The green STN cells originate from the STN volume and project to the globus pallidus. The red IC fibers are passing by underneath the STN. D = dorsal; V = ventral; P = posterior; A = anterior.

In the second part, the effect of the electric field on nearby cells was computed in a multicompartment neuron model programmed in NEURON 6.2 (Yale university, New Haven, USA).[217] Two neural populations are included in the model, that is, the STN projection cells and the IC fibers. The anatomical geometry of the IC fibers was defined through streamline tractography within SCIRun using the DTI dataset. With this, 200 fibers were tract from a seed box (5 by 1 by 2 mm) located ventrolateral to the STN. Three types of STN cells were placed in the model, each type projecting to the globus pallidus with a slightly different axon trajectory.[214,218] The somas of the STN cells were placed randomly within the atlas-defined border of the STN volume. Every axon is implemented with the same model parameters (5.7 µm axon diameter model)[220]. This cable model includes detailed representations of the nodes of Ranvier, paranodal, and intermodal sections of the axons. For visualization purposes, the output from the second part of the model system was again imported in SCIRun v3.0.2 (figure 2).

DBS lead geometry

Either a CC lead or a steering DBS lead (figure 1) was incorporated within the FEM model. The CC lead was based on the Medtronic 3389 electrode (Medtronic Inc., Minneapolis, US), which has a body diameter of 1.27 mm and carries four cylindrical contacts (C0 – C3). These contacts each have a length of 1.5 mm, a 6.0 mm^2 contact surface area, and an interelectrode spacing of 0.5 mm. The steering DBS lead was based on the design now commercially available by Boston Scientific (Marlborough, MA, USA), which has a body diameter of 1.3 mm and carries eight contacts (C0 – C7). C0 is the contact at the tip of the lead with a length of 1.5 mm and 6 mm^2 contact surface area. Contacts C1 – C6 form two rings, each of three steering DBS contacts with a length of 1.5 mm and 1.6 mm^2 contact surface area. Contact C7 has the same shape as a standard CC lead contact. The interelectrode spacing along the lead is 0.5 mm and the interelectrode circumferential spacing between the steering DBS electrode contacts (C1 – C6) is 0.34 mm.

DBS lead location and orientation

Three locations of the lead were assessed in the model, that is, the center location, a 1 mm off-center location, and a 2 mm off-center location. For the center location, The CC lead lies inside the STN with the center of contact C1 at the centroid of the STN. In case of the steering DBS lead the combined center of C1 – C3 was located at the centroid of the STN. For the 1 mm and 2 mm off-center location the lead was shifted on a line between the centroid of the STN and the middle position of the nearest axon segments for each IC fiber in the model. This resulted in our datasets in a shift of 0.46, 0.59, and 0.66 mm in posterior, medial, and ventral directionally shift per 1 mm displacement. Unlike the CC lead, the steering DBS lead is not fully symmetric with respect to the axis of the lead. Therefore, we included four different orientations of the six steering electrode contacts (figure 1). The trajectory of the lead was kept constant

in all cases, whereas the lead approached the target in an AC – PC based coordinate system with a typical lead arc and collar angle of 20˚ and 100˚, respectively.

Stimulation protocols

For the CC lead, each of the four electrode contacts were selected consecutively for stimulation with increasing stimulation amplitude up to a value at which IC fibers were activated. For the steering DBS lead, we tested two types of stimulation protocols. First, a single contact stimulation protocol was used, where stimulation on each of the individual single contacts was simulated (figure 3) with increasing stimulation amplitudes up to a value at which IC fibers were activated. Second, a current steering stimulation protocol was used, where the current was simultaneously injected through two adjacent contacts with specified percentages (20/80%, 40/60%, 60/40%, 80/20%) of the total current divided over both contacts, again with increasing stimulation amplitudes up to a value at which IC fibers were activated.

The stimulation signal was a monopolar biphasic charge-balanced current pulse, that is, a 100 µs rectangular waveform, with the total injected current ranging from -1 to -5 mA with a 0.5 mA step size, followed by a 5 ms period of low amplitude charge balanced anodic stimulation.

Activation of neural populations

The effect of the deep brain stimulation was evaluated in the neuron part of the computational model system: 15 datasets were created, five for each location of the lead. The STN cell bodies were randomly distributed inside the STN and the location of IC fibers was fixed. Each neuron or axon with a segment located at the position of the DBS lead was removed from the model. For the 15 datasets, this resulted in neuron models including 182.3 ± 13.1 IC fibers and 79.8 ± 4.3 STN cells. A cell or axon is counted as activated when the stimulation pulse evoked at least one action potential that propagated to the end segment of the axon.

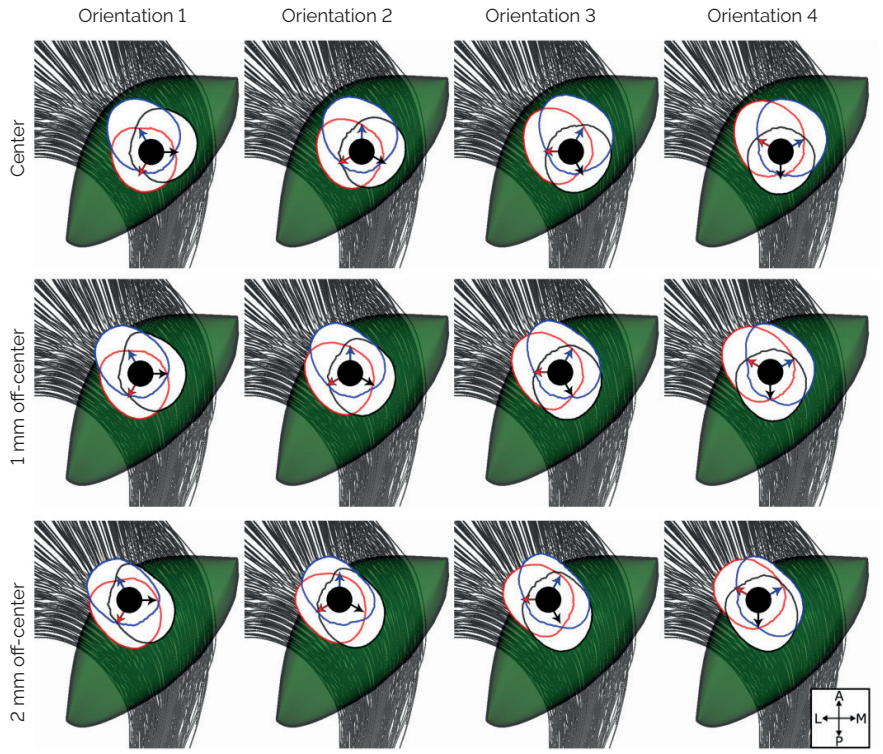

Figure 3. Top view of the STN (green volume) with the IC fibers running underneath the STN looking along the axis of the DBS-lead (black circle). On each of the lead locations and orientations, three iso-contours (0.1 V) of the potential field are shown in red, blue, and black, corresponding to monopolar stimulation (1 mA) through contact C4-C5-C6 heading in the direction of the color matched arrow. L = lateral; M = medial; P = posterior; A = anterior.

Statistical analysis

To quantify the differences between stimulation protocols, we defined the optimal stimulation protocol as the configuration that activated the highest percentage of STN cells, without activating any of the IC fibers. A repeated measure ANOVA with significance level of 0.05 was performed, followed by a Bonferroni corrected multiple comparison procedure to statistically test the individual optimal stimulation effect in each situation. In each of the three lead locations, we compared each of the four lead orientations: optimal single contact stimulation vs. optimal current steering stimulation; optimal single contact stimulation vs. the optimal stimulation effect of the CC lead; finally, optimal current steering stimulation vs. the optimal stimulation effect of the CC lead.

Results

We found for each lead location, orientation, and stimulation protocol the optimal stimulation settings. Figure 4 shows the percentage of STN cells which were activated, and which denotes all significant differences between the different orientations (see figure 1 for the orientations) and the two stimulation protocols.

Single contact stimulation protocol

At center location, the steering DBS lead using single contact stimulation was able to activate 60.3 ± 4.8% STN cells in the first orientation, 75.1 ± 5.9% STN cells in the second orientation, 72.3 ± 3.9% STN cells in the third orientation, and 53.7 ± 2.5% STN cells in the fourth orientation. In the first orientation, the optimal stimulation was applied through the bottom medial contact (3 of 5 datasets) or the top posterolateral contact (2 of 5 datasets) with an amplitude of 4.1 ± 0.82 mA. In the fourth orientation, the optimal stimulation was through the bottom or top posterior contact with an amplitude of 4.3 ± 0.76 mA. In both the second and third orientation, the optimal stimulation was through the bottom posteromedial contact with an amplitude of 5.0 ± 0.0 mA or 4.5 ± 0.0 mA, respectively.

At 1 mm off-center location, the steering DBS lead was able to activate 35.8 ± 3.5% STN cells in the first orientation, 56.3 ± 5.4% STN cells in the second orientation, 59.8 ± 3.6% STN cells in the third orientation, and 44.3 ± 2.9% STN cells in the fourth orientation. The optimal stimulation settings used the top medial contact (2.0 ± 0.0 mA) and the top posterior contact (2.5 ± 0.0 mA) for the first and fourth orientation. In the second and third orientation, the optimal stimulation settings used the top posteromedial contact (3.5 ± 0.0 mA and 4.0 ± 0.0 mA, respectively). Figure 5 shows the activated STN cells for the optimal stimulation setting in each of the four orientations.

At 2 mm off-center location, in each orientation, the steering DBS lead was able to activate 6.4 ± 4.4% STN cells, while stimulating through the cylindrical contact C7 with an amplitude of 0.4 ± 0.22 mA.

Current steering stimulation protocol

For most of the orientations and datasets, our current steering protocol prefers to steer the current into the posteromedial quadrant, only at the center location in the second orientation four datasets had the optimal stimulation toward the posterolateral direction, applying most of the total stimulation current in posterior direction.

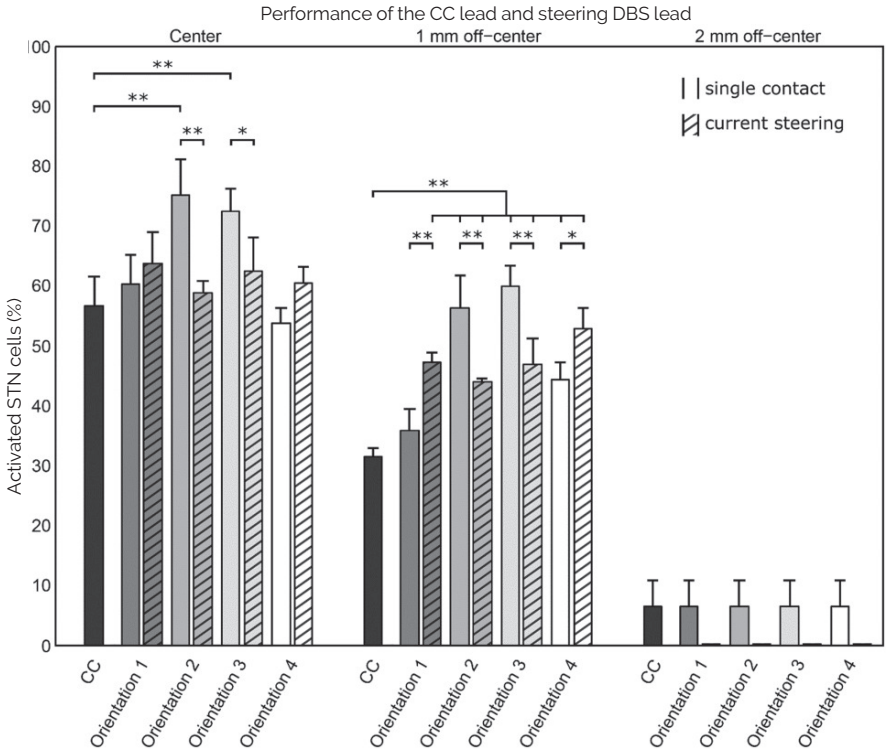

Figure 4. The performance of the five stimulation modes, that is, the CC and the four orientations of the steering-DBS lead. Bars denote mean values with standard deviations of the percentage of activated STN cells after stimulation for the 5 datasets per lead location each with random distributions of the STN cells. The non-hatched bars represent the results for single contact stimulation and the hatched bars represent the results for current steering stimulation. Significant differences are indicated with one asterisk ($p < 0.05$) or two asterisks ($p < 0.01$).

At center location with the steering DBS lead in its first orientation, it was able to activate 63.7 ± 5.2% STN cells by dividing the total current (3.8 ± 0.7 mA) over the medial contact and posterolateral contact (80/20% in four datasets and 60/40% in 1 dataset). In the second orientation, 58.7 ± 2.0% STN cells were activated by dividing the total current (4.4 ± 0.8 mA) over the posteromedial and posterolateral contact (80/20% in 1 dataset, 20/80% in 2 datasets, 40/60% in two datasets). In the third orientation, 62.5 ± 5.6% STN cells were activated by dividing the total current (3.80 ± 0.7 mA) over the posteromedial and anteromedial contact (80/20% in 5 datasets). In the fourth orientation, 60.4%±2.9% STN cells were activated by dividing the total current (4.1 ± 1.0 mA) over the posterior and anteromedial contact (80/20% in 2 datasets and 60/40% in 3 datasets). Comparing the stimulation effect of our current steering stimulation protocol to single contact stimulation, we found a significant decrease of activated STN cells in the second orientation ($p < 0.01$) and in the third orientation ($p < 0.05$).

At 1 mm off-center location, the steering DBS lead was able to activate 47.2 ± 1.5% STN cells in the first orientation by dividing the total current (2.5 ± 0.0 mA) over the medial contact and posterolateral contact (80/20% in 2 datasets and 60%/40% in 3 dataset). In the second orientation, 43.9 ± 0.7% STN cells were activated by dividing the total current (2.5 ± 0.0 mA) over the posteromedial and posterolateral contact (80/20% in 5 dataset). In the third orientation, 46.8 ± 4.4% STN cells were activated by dividing the total current (2.5 ± 0.0 mA) over the posteromedial and anteromedial contact (80/20% in 5 datasets). In the fourth orientation, 52.9 ± 3.4% STN cells were activated by dividing the total current (3.0 ± 0.0 mA) over the posterior and anteromedial contact (80/20% in 5 datasets). Comparing the stimulation effect of our current steering stimulation protocol to single contact stimulation, we found a significant decrease of activated STN cells in the second ($p < 0.01$) and third orientation ($p < 0.01$) and a significant increase in the first ($p < 0.01$) and fourth orientation ($p < 0.05$).

At 2 mm off-center location, the steering DBS lead using the current steering protocol was not able to activate any STN cells without activating one or more IC fibers.

Comparison of the CC lead and the steering DBS lead

Finally, we statically compared the stimulation effect of the steering DBS lead with the stimulation effect of the CC lead (figure 4). The CC lead, with its optimal stimulation settings, was able to activate 56.6 ± 4.8% STN cells at center location, 31.4 ± 1.4% of STN cells at 1 mm off-center location, and 6.4 ± 4.4% of STN cells at 2 mm off-center location.[234] At center location, the steering DBS lead using single contact stimulation was able to activate significantly more STN cells in the second and third orientation ($p < 0.01$). Interestingly, in none of the four orientations the steering DBS lead using current steering stimulation was able to activate significantly more STN cells than the CC lead.

At 1 mm off-center location, a significant increase was found for all the orientations when using the current steering stimulation ($p < 0.01$), while using single contact stimulation a significant increase was found at the second, third, and fourth orientation ($p < 0.01$). At 2 mm off-center location there were no significant differences found.

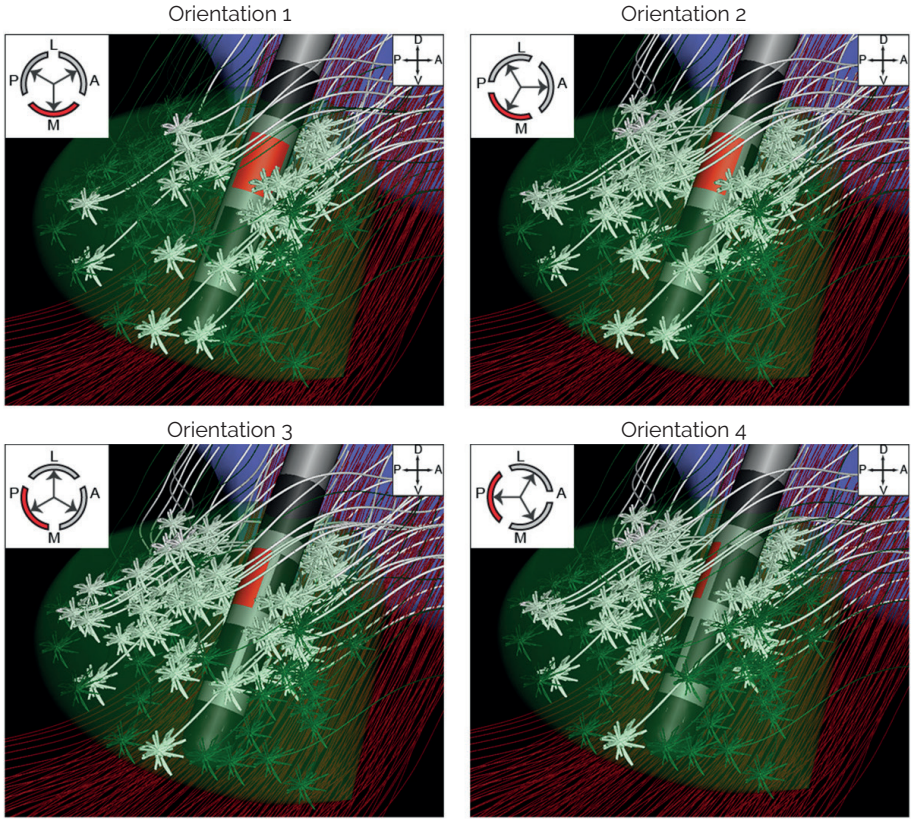

Figure 5. An example of the activation of STN cells illustrating the variability in the four orientations while using a monopolar stimulation protocol. The panels show a medial perspective of the STN (green volume), the globus pallidus (purple volume), IC fibers in red, and the STN cells in green and white. STN cells that were activated by the stimulation pulse are displayed in white. The stimulation pulse activated 35%, 55%, 61%, and 49% of the STN cells in orientation 1 – 4, respectively.

Discussion

In this computational modeling study, we investigated a new steering DBS lead design. The steering DBS lead is able to shape the stimulation field by selecting appropriate electrode contacts for stimulation. In this manner, it is possible to stimulate target areas while not stimulating areas that cause side effects. Our results show that under the right circumstances, even using only single contact stimulation, the steering DBS lead is indeed able to stimulate a significantly higher percentage of STN cells without activating any of the IC fibers compared to the CC lead. Especially in the case of a 1 mm displacement and the lead in optimal orientation, the steering DBS lead

outperforms the conventional lead. The current steering stimulation protocol shows that in case of a 1 mm displacement of the lead, where the single contact stimulation is performing weakly, dividing the stimulation current over two contacts opposing the IC can increase the percentage of activated STN cells. However, the results also show that correct placement and orientation of the lead within the target remains an important aspect for optimal stimulation outcome.

Using single contact stimulation at center and 1 mm off-center location, we found significantly different results in STN activation for the four orientations. The steering DBS lead in its second and third orientation, which had an electrode contact in the opposite direction of the IC, the posteromedial direction, was able to activate a significantly higher percentage of STN cells compared to the CC lead. The two other orientations did not have a steering electrode contact in opposite direction of the IC, which resulted in a less effective performance. Nevertheless, even in these two orientations the performances of the steering DBS lead were never significantly worse than the CC lead and even at 1 mm off-center location the steering DBS performed significantly better than the CC lead while stimulating through the posterior contact (orientation 4).

The varied results that were obtained for the different orientations, illustrates a new challenge in correctly implanting the lead in the target. The lead contains a marker to verify the orientation of the lead by x-ray imaging. However, in order to make use of the full potential of the steering DBS lead, the clinical effect of different orientations should be tested first during clinical trials. For this, computational models such as described in this study, can be a useful tool to gain more insight in the effect of the different orientations and finding the correct orientation. Finally, future studies should assess besides lead displacements also the rotation of the lead over time and find ways to guarantee a fixed orientation of the lead.

One way to compensate for the orientation dependency of the steering DBS lead is current steering stimulation. We showed that by balancing current across the medial and posterolateral contact it is possible to increase the percentage of activated STN cells. This suggests that current steering enables stimulation in intermediate direction to a certain level. Unfortunately, stimulation through two contacts increases the active contact surface surrounding the lead, with which the selectivity of directional steering is reduced. This might explain why the current steering protocol is not performing better than stimulation through a cylindrical contact placed in the center of the STN. It should be noted that we presented the current steering separately from the single contact stimulation. In the clinic, the current steering protocol will be an addition to the single contact stimulation protocol. This means a clinician will not use the current steering protocol in case single contact stimulation is already the optimal stimulation protocol, such as in second and third orientation. Second, only current steering through

the two adjacent contacts on the same row was tested to show the potential of an easy to interpret current steering protocol. More advanced current steering patterns with multiple contacts might enable more selective stimulation, such that similar percentages of STN cells are activated as those achieved by using a single contact in posteromedial direction. Third, it should be noted, more advantaged current steering patterns can also be performed with the CC lead. A previous modeling study, using similar methods, showed that the CC lead at the center of STN was able to activate 8% more STN cells using current steering with two independent sources than with monopolar stimulation.[214] This will level out the performances of the leads, especially at center location. However, with a 1 mm displacement the decrease in performance of the CC lead is considerably larger than the decrease in performance of the directional lead. This indicates that the directional lead, within the 1 mm window, is less sensitive to the displacement away from the optimal center location.

At the 2 mm off-center location, we found no difference between de CC lead and the steering DBS lead. This was due to the fact that the optimal electrode contact for both leads were the same top cylindrical contact, C3 and C7. The steering DBS lead has only two rows of electrode contacts along the lead which can be used for steered stimulation (C1 – C6). In the 2 mm displacement scenario, the two rows of steering electrode contacts were shifted 1.32 mm ventrally and ended up too close to the ventrally located axon segments of the IC fibers. This scenario illustrates that with the limited amount of rows of steering electrode contacts it remains important to position the lead at the correct depth. In addition, the possible advantage of this steering DBS lead is vulnerable to a displacement along the trajectory of the lead.

We decided to include the model representation of the steering DBS lead in a well-described model of the subthalamic region that included many important and realistic details. The technical limitations of this computational model are comprehensively described in previous studies, such as the large voxel size of the DTI dataset, and ignoring the capacitive behavior at the electrode-tissue interface.[75,202,211] In this specific study, the large voxel size of the DTI dataset had an effect on two aspects of the model. First, the conductivity of the tissue in model was based on the DTI and this resulted in a low spatial resolution. Therefore, the anisotropy of small fiber bundles in the brain were not included in the model. Second, because of the low spatial resolution of the DTI dataset we were only able to trace the IC fibers and not the STN axons projecting to the pallidum. With respect to the capacitive behavior, in case of voltage-controlled stimulation, the capacitive behavior of the electrode-tissue interface is important, especially for small contact surfaces area, because of its reduced electrode capacitance. However, while using current-controlled stimulation, similar to the one used in our current study, the electrode capacitance had negligible effects on the corresponding tissue voltage.[212] A previous study on a segmented lead with similar contact surface areas as the one in our model also showed that including

this capacitive behavior in their model did not significantly change their results.[231] Finally, since our results focus on a comparison between the CC and HD leads in the same model, the limitations will influence both leads and therefore will have little impact on the comparison.

We should note that, in order to quantify the stimulation effect, we adopted the criterion that with DBS a maximum percentage of activated STN cells is needed while not stimulating the IC. Clinical research is needed to find more realistic and more detailed criterions. Therefore, our criterion should only be regarded as an example to show the steering effect on a plausible target while steering away from a region causing side effects. Using this criterion also meant we did not pay attention to power consumption. We believed maximizing the effect of DBS is of greater importance than battery lifetime, especially now that rechargeable implantable pulse generators have become available.[236,237]

Because we used the same modelling procedure, we are able to compare the current results of the steering DBS lead with a previously described 40-contact lead.[234] This shows that at center and 1 mm off-center location the steering DBS lead with the option to steer the stimulation field in posteromedial direction performed very similar as the 40-contact lead. However, at 2 mm off-center location the HD lead was able to perform significantly better (10 – 11% more STN cells activated) than the CC lead, which was due to the fact that the dorsally located electrode contact of the 40-contact lead also can be used for steering. The previous study did not investigate different orientations of the 40-contact lead; however, this lead is always able to stimulate in posteromedial direction, and is, therefore, probably less sensitive to rotations of the lead.

Having only eight electrode contacts is a great advantage in programming the stimulation settings when monopolar stimulation is used. For a HD lead with a large number of electrode contacts programming the stimulation settings with a trial-and-error approach will not suffice in clinical practice.[228] For a 32-contact HD lead, which was used in a proof-of-concept study the test stimulation was limited to four standard steering directions, because of time constraints.[126] The eight-channel lead has the advantage that it can be combined with a novel internal pulse generator, which includes eight independent current sources.[227] We used just a simple current steering stimulation protocol with two contacts, which already showed an improvement of the stimulation effect in certain cases. By selecting the appropriate current strength on each contact, the steering properties of DBS can be improved even more[214], however, finding the correct current for each of the eight contacts will highly increase the complexity of programming the stimulation parameters. Thus, unless new technological tools will be developed to aid clinicians in selecting the optimal stimulation settings, the theoretical advantage of having many contacts or

many current sources might not be fully utilized in practice. Creating patient specific models, by using the patients MRI/DTI dataset and using the same methodology as the current study, can be one of these tools. Patient specific models effectively have been used before to select stimulation settings, which maximize neural activation in a certain area.[204] Additionally, using the patient specific IC in the model can be used to warn the clinician to avoid certain settings.

Besides running through all possible settings in an electric field model, more advanced techniques based on machine learning[231] and particles swarm optimization[238] can be the next step in finding the optimal settings in a time efficient way.

Conclusion

In conclusion, we found that the concepts of steering the stimulation field with a steering DBS lead with only eight channels may be beneficial compared to the conventional lead, and it allows to correct for lead displacement errors of approximately 1 mm when it has the correct orientation or using current steering. While using single contact stimulation, which has the advantage of being easy to use in the clinic, our results illustrate the importance of the orientation of this lead. Therefore, sufficient attention should be paid to implanting the steering DBS lead in the most effective orientation, and to keep this orientation of the lead over time.

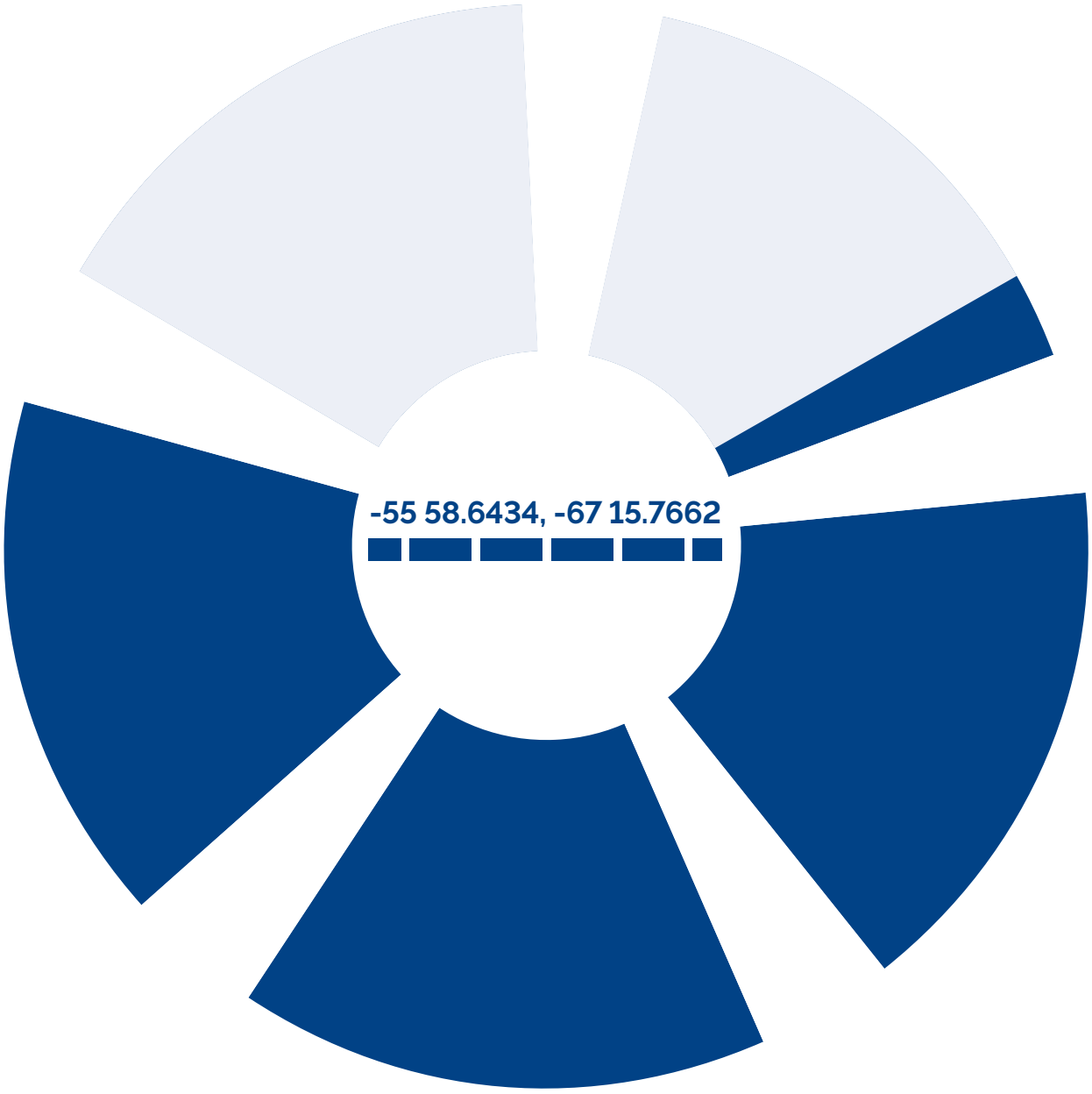
-55 58.6434, -67 15.7662

CHAPTER 9

General discussion

Deep brain stimulation (DBS) is an effective surgical treatment for advanced Parkinson's Disease (PD). Continuous electrical stimulation within the subthalamic nucleus (STN), one of the basal ganglia, can successfully alleviate PD motor symptoms. However, the success of STN-DBS can be limited by side effects which can occur when unwanted neuronal areas or connections are stimulated. Therefore, it is important that the stimulation is targeted at the right location as specifically as possible.

In this thesis we have studied several aspects of STN-DBS and how they contribute to optimal localization and stimulation of the preferred target area. We have used conventional imaging and electrode technology to study how the target area can be optimally located. Additionally, we have studied developments in imaging techniques and electrode design to investigate how future technology can be used to further optimize both localization and stimulation of the most effective target area.

Active contact location

In chapter 4 we showed that, together with the preoperative response to levodopa, the location of the active contact of the DBS electrode was the main predictor for postoperative motor improvement. A more lateral active contact location was a large positive predictor for motor improvement. In a sub-analysis, a more anterior location was a negative predictor for improvement. This result was also found in other studies using MRI, and can be explained by the anatomical location of the sensorimotor projections in the dorsolateral STN. Using the data from chapter 4, and the STN model based on microelectrode recordings (MER), a theoretical hotspot for the active contact location could be defined at 1.9 mm lateral, 0.9 mm anterior, and 2.6 mm dorsal to the geometric center of the MER-based STN, within its boundaries. It should be noted here that there are DBS groups that target more dorsal and more posterior, to deliberately stimulate fiber tracts outside of STN boundaries. However, this thesis focusses on stimulation inside the boundaries of the STN as this is the aim of our group and most DBS groups worldwide.

Intraoperative and postoperative adjustments of location

Even though the (dorso)lateral STN is targeted preoperatively, we showed that several electrodes still end up in the central, or even the medial parts of the STN. This can be caused by inaccuracies of the DBS procedure, for example the small remaining inaccuracy of the stereotactic frame.[21] Intraoperative test stimulation might also play a role in the final position of the electrode.[239] During test stimulation, the therapeutic window of different stimulation sites is compared. The therapeutic window compares the amplitude thresholds for therapeutic benefit and side effects of stimulation. The preferred stimulation site would have a large therapeutic window. However, the introduction of the electrode in the subthalamic area can induce a 'stunning effect' where the motor

symptoms of PD are alleviated for longer time, possibly because of microlesions. Because of this stunning effect, the thresholds for therapeutic benefit become difficult to verify during surgery. This can lead to a situation where the final position of the electrode is mainly guided by side effects and less by the therapeutic benefit. The most prominent side effects result from stimulation of the internal capsule which runs anterolateral and ventral to the STN and contains the corticospinal motor tract. Therefore, searching high thresholds for side effects can lead the final electrode position away from the lateral part of the STN and into the central or even the medial STN.

After surgery, the stimulation with sub-optimally placed electrodes is mostly finetuned by choosing an alternative contact on the electrode. In conventional DBS electrodes with four or more in-line cylindrical contacts, clinicians only have the possibility to choose another cylindrical contact on the electrode, or to combine cylindrical contacts in double monopolar and bipolar stimulation patterns. When the final electrode ends up too medial, an alternative contact is chosen to obtain a better therapeutic effect, and possibly to move away from side effects of the associative and limbic projections in the medial STN. When the final electrode ends up too lateral, an alternative contact is chosen to move away from side effects caused by stimulation of the internal capsule. In both cases, often a more dorsal contact on the electrode is selected. However, because of the oblique orientation of the electrode, a more dorsal contact does not only move the stimulation more dorsal, but also more lateral, and largely more anterior.

In conclusion, when intraoperative placement is sub-optimal, a conventional cylindrical electrode has limited options for successful postoperative finetuning of the stimulation. Therefore, although chapter 4 suggests that more lateral targeting might be beneficial, it should be approached with caution when using conventional cylindrical electrodes. Targeting more lateral, closer to the theoretical hotspot, but also closer to the internal capsule, will lead to lower thresholds for side effects. With conventional cylindrical electrodes, these thresholds can be difficult to increase postoperatively without also increasing the thresholds for therapeutic effect, thus resulting in an insufficient therapeutic window. However, a new design of DBS electrode can make more postoperative adjustments possible.

Steering DBS electrodes

In chapters 5 to 8, two different designs of steering DBS electrodes were studied. Both electrodes offer more freedom in finetuning the stimulation postoperatively with the final electrode in place. Besides changing the stimulation field along the trajectory of the electrode, mostly in the dorsoventral direction, they can effectively shape the field in the anteroposterior and the mediolateral directions as well. In chapter 5 we showed how a 32-contact type of steering electrode could increase the thresholds for side

effects and thereby increase the therapeutic window. The thresholds for side effects of the internal capsule were elevated in 9 out of 13 cases by redirecting the field of stimulation medial, away for the responsible anatomical structure. The thresholds for therapeutic effect remained unaltered and were sometimes even reduced. This indicates that patients with sub-optimally placed electrodes, suffering from a low threshold for side effects, might benefit from steering technology.

Because the treatment with steering DBS electrodes is likely to be more complex, its benefit must be evaluated carefully. A survey amongst specialists from five different DBS centers, evaluating 293 electrodes implanted in the STN, reports that steering technology was considered useful in 8.5% of STN electrodes (12.8% of patients).[240] This number seems relatively low, but this survey focused only on lowering the thresholds for side effects, not on lowering the thresholds for therapeutic effect. Thresholds for therapeutic effect could be lowered by steering current towards the preferred target cells. However, another perhaps more effective way to lower the thresholds for therapeutic effect is to actively aim for a final position of the electrode that is closer to the most effective target area, i.e., more lateral within the sensorimotor STN. Of course, this cannot be done postoperatively, but it should already be considered in the preoperative planning of the target. In other words, this survey studied the potential benefit of steering electrodes, that would be placed like conventional electrodes, or that would be placed too lateral by accident. However, it does not account for the potential benefit that can be achieved when DBS targeting would be optimized with specifically the steering DBS electrode in mind.

In chapters 7 and 8 we studied the stimulation of the subthalamic area in a computational model and showed how two different types of steering electrodes could potentially provide a benefit over the conventional cylindrical electrode. In this model, different final positions of the electrode were studied, i.e., a central position in the STN, a position 1 mm lateral from central and 2 mm lateral from central. In chapter 7 we modelled the stimulation with a 40-contact multidirectional steering electrode, similar to the electrode from chapter 5, but with two additional dorsal rows of four contacts each. In all three positions, this electrode was able to activate more of the STN than the cylindrical electrode, without activating internal capsule fibers (table 1).

It is challenging to appreciate the differences in the percentages in table 1. A limitation of this study is that it optimized STN cell activation over the complete nucleus, not just the target area in the dorsolateral sensorimotor STN. It was designed in this way to theoretically support how a steering electrode could compensate accidental lateral displacement, towards to the internal capsule. With respect to the goal of this modelling study, we have showed that this steering electrode can compensate for an accidental displacement of 1 mm lateral. The steering electrode in the 1 mm lateral position reaches the same percentage of STN cell activation as the conventional

electrode in the central position (57.7% and 56.6% respectively). The same is true for the 8-contact steering electrode studied in chapter 8 which has two segmented levels consisting of three separate multidirectional steering contacts, enclosed by a cylindrical dorsal and ventral contact (59.8 % of STN cell activation).

However, because of the displacement towards lateral, it is very likely that the activated STN cells are located more lateral in the STN, closer to the hotspot for therapeutic effect described in chapter 4. These findings lead to the suggestion that a steering electrode can not only compensate for accidental displacement towards lateral but, when it is placed more lateral, it can actually be more effective than a centrally placed conventional electrode. In other words, when steering electrodes are used, it could be beneficial to deliberately target more lateral compared to the targeting for conventional cylindrical electrodes.

Moreover, to achieve this percentage of activation, both steering electrodes use smaller stimulation amplitudes (3.9 mA and 4.0 mA) than the conventional electrode (4.5 mA). This may not only improve battery life of the DBS implanted pulse generator (IPG) lowering the need for surgical replacement, but it also has implications for the effectiveness of current steering. Other modelling studies have shown that the shaping of the field of neuronal cell activation, which a steering electrode tries to achieve, is more effective with lower stimulation amplitudes.[28] With high amplitudes, the field of activation becomes more spherical again, even in current steering configurations. This is an additional reason to deliberately target more lateral when using steering electrodes. In the central STN, further from the hotspot for therapeutic effect, the stimulation amplitudes will likely be higher and current steering will therefore be less effective compared to stimulation with lower amplitudes in the lateral STN. Stimulation here might be closer to the internal capsule, but also closer to the hotspot for therapeutic effect. In other words, for steering DBS electrodes a therapeutic window in the low amplitudes is preferred over an equally large therapeutic window in the high amplitudes.

Table 1. Modelled stimulation effect of three different DBS electrode designs

Final electrode position	**Mean percentage of activated STN cells without internal capsule activation (and mean amplitude used), after optimization of all tested possibilities**		
	Conventional cylindrical electrode	40-contact steering electrode (chapter 7)	8-contact steering electrode (chapter 8)
Central in the STN	56.6 % (4.5 mA)	73.0 % (5.9 mA)	75.1 % (5.0 mA)
1 mm lateral to center STN	31.4 % (2.3 mA)	57.7 % (3.9 mA)	59.8 % (4.0 mA)
2 mm lateral to center STN	6.4 % (0.4 mA)	17.1 % (1.5 mA)	6.4 % (0.4 mA)

The percentages of STN cell activation in table 1 could even suggest that the 2 mm more lateral position also has a certain benefit. Here, the 40-contact steering electrode can activate almost three times the amount of STN cells (17.1 %) compared to the conventional cylindrical electrode (6.4 %). Although the percentage of activated cells seems low, in this position, the largest part of activated cells is likely to be in the dorsolateral sensorimotor STN, thus close to the hotspot for therapeutic effect. Since these modelling studies were not designed to answer this question, no clear conclusions can be formulated. It does however suggest an interesting topic for future studies.

In future studies, new designs for steering electrodes should also be taken into consideration as both electrodes studied here have their own limitations. The 40-contact electrode from chapter 7 offers a high degree of freedom in steering the current at all dorsoventral levels. However, its complicated design makes it very costly to produce and it is currently not commercially available. Moreover, the design has a single current source which makes the actual current distribution over different contacts, and thus the efficacy of steering, very dependent on the individual impedances of these contacts. The 8-contact electrode from chapter 8 does not have this limitation because all contacts are stimulated with independent current sources, and it is commercially available. However, it offers a lower degree of freedom for effective current steering, because of the limited number of contacts but especially because the most ventral and dorsal contacts remain cylindrical. This is especially reflected in the STN activation percentage at the 2 mm lateral position in table 1. Here, the 40-contact steering electrode can still activate substantially more STN cells than the conventional cylindrical electrode, but the 8-contact steering electrode cannot. This is because in this position the optimal stimulation configuration uses the most dorsal contacts on all three types of electrodes. In the 8-contact steering electrode, the most dorsal contact is not segmented and identical to the most dorsal contact on the conventional cylindrical electrode. Therefore, the results are also identical. These results indicate that if more lateral targeting would be pursued to optimize the performance of steering DBS electrodes, an electrode with steering possibilities at more dorsoventral levels would leave more room for placement inaccuracies or would potentially be more effective.

Future perspectives on DBS targeting

Together, the results from chapters 4, 5, 7, and 8 indicate that steering DBS electrodes can compensate for accidental misplacement where conventional cylindrical electrodes might not. The current clinical need for this solution seems limited in STN-DBS for PD, which could be the result of how the STN is currently targeted. Our results suggest that the full potential of the steering DBS electrode might be unleashed when it is combined with more lateral targeting, closer to the hot spot in the sensorimotor STN from chapter 4, and closer to the internal capsule.

Chapter 5 already suggests that steering electrodes might enable the formation of new treatments by stimulating small neuronal areas that are currently inaccessible because of induction of side effects. Areas suggested in this chapter are for example small subnuclei in the hypothalamus, the fornix, the upper brainstem, or even the medulla oblongata and spinal cord. Perhaps the hot spot for STN-DBS within the dorsolateral STN could also be counted among these small inaccessible areas. To reach this hot spot, more lateral targeting might be required. This is supported by studies that have found most of the connections between the STN and cortical motor areas to lie in the dorsolateral STN.[241,242] In recent work from our group we were able to show that these connections lie indeed more lateral than our current target (unpublished data). With conventional electrodes, this area might be inaccessible because of the induction of side effects, but with steering electrodes it might be possible to specifically target this more lateral part of the STN.

In conclusion, adapting the targeting specifically to steering DBS electrodes, could result in a higher number of patients benefitting from this technology. Although promising, this suggestion needs careful review, first in neuronal modelling studies that build on and improve the model from chapters 7 and 8, and later in prospective clinical trials. In these future studies current and new designs for steering electrodes should be carefully evaluated.

Future perspectives on preoperative and intraoperative imaging

Targeting more lateral, closer to the internal capsule, also means there will be less room for placement inaccuracies. Technological development in CT and MRI applications can help to minimize these inaccuracies, both by optimizing preoperative STN identification and by improving intraoperative verification of the electrode position. Chapter 2 has shown that especially the dorsal and lateral borders of the STN can be hard to identify on T2 MRI. The lateral STN border identified on 7.0 Tesla T2 MRI corresponds better with the MER-based STN borders compared to the lateral border identified with lower field strength T2 MRI. These findings suggest that using high-resolution 7.0 Tesla MRI imaging might be beneficial in minimizing inaccuracies, especially when a more lateral part of the STN is targeted. Ongoing work of our group does indeed show this.[243] Even better would be to advance to real individualized targeting based on the identification of the individual patient's connections between the individual patient's STN and different cortical motor areas[241] using for example 7.0 T MRI tractography. Additionally, intraoperative verification of the electrode position with high-resolution MRI or CT applications in the OR was recently shown by our group to take away more of the remaining placement inaccuracies.[244]

Future perspectives on intraoperative measurements and test stimulation

Intraoperative measurement of neuronal spiking with MER is traditionally used to verify electrode placement within the STN. Especially in DBS surgery where multiple parallel MER trajectories around the planned target are studied, neuronal spiking can be used to select the optimal trajectory. This is generally the trajectory where neuronal spiking typical for the STN can be measured on a large amount of dorsoventral locations. With the MER-based STN model that we have created and used in chapters 2, 3, and 4 we have tried to make most out of the available MER measurements in terms of identifying the STN as a whole and thereby also identifying the dorsolateral target area.

Using a MER-based STN model to determine the electrode position in relation to the STN has the advantage of using real-time intraoperative physiological data from the patient, compared to the indirect preoperative imaging data that MRI uses which can be subject to distortion. Because of this, MER measurements have served as the gold standard for STN location on which many further developments have been based. In our studies, we have analyzed the positions only retrospectively, but with sufficiently fast computing, electrode position relative to the MER-based STN can be assessed directly during surgery. Then, one could intraoperatively assess the mismatch between MER-based STN and MRI-based STN to determine if adjustment of targeting is necessary. This could be done in a safe way. The symptomatic bleeding rate with a MER-driven approach was only 0.8% in our center.

However, with the advancement of preoperative imaging and the availability of accurate intraoperative verification of electrode position with high-resolution CT or MRI, the need for additional verification with multiple MER trajectories is becoming obsolete. The reduction of the amount of parallel MER trajectories makes our STN modelling approach less accurate. Therefore, MER modelling of the STN and its dorsolateral sensorineural part seems to have no place in the future of STN-DBS. Measurement of STN activity in a single trajectory, either intraoperatively, postoperatively, or both, might still provide confirmation of the dorsal and ventral borders of the target nucleus and thereby improve DBS therapy. In addition, local pathological activity can be studied by analyzing neuronal oscillations inside the STN.

One way to gain insight into local STN oscillations is described in chapter 3 where we attempted to optimally analyze the neuronal activity in the STN with only minor changes in the standard surgical procedure. By combining the LFP and the spiking activity measured with MER electrodes, and by analyzing both power and coherence in the beta and gamma frequencies, we were able to distinguish the sensorimotor STN at a group level. However, this method remained vulnerable to inaccuracies and it was not discriminative enough at a patient level. Therefore, it is not a suitable method

for intraoperative identification of the sensorimotor STN. Moreover, with the reduced use of MER, identification of the STN target based only the oscillations in the LFP measured with only macroelectrodes becomes even more important.

With the developments in electrode design, especially steering DBS electrodes now have more and smaller contacts, possibly even facing different directions, together forming an array of macroelectrodes. LFP measurement with these small contacts of the final DBS electrode seems to be the future of intraoperative verification of STN activity. In chapter 6 we confirmed that the 32-contact steering electrode can identify STN activity, i.e., beta band oscillations in the LFP, with enough spatial resolution (0.6 mm) because of the small size of the contacts and the small distance between the contacts. Moreover, the steering contacts measuring oscillations in different directions, could provide insight into the anteroposterior and mediolateral location of the hotspot of pathological activity. Chapter 6 shows that this can be measured intraoperatively, but in the newest generation of steering electrodes, postoperative measurement will also be possible. Conventional DBS electrodes would not be able to identify these oscillations with a similar spatial resolution.

Even if the preferred target could be identified based on only the LFP oscillations measured with the final electrode, it remains important to verify whether steering the stimulation is effective enough at the desired lateral placement. This could possibly be investigated by steering test stimulation with the final electrode, as is described in chapter 5. Although the limitations of test stimulation with regards to the stunning effect remain, it could be used to determine whether steering can increase the threshold for side effects without moving the electrode. However, with the rising application of DBS surgery under general anesthesia, it is questionable if this form of test stimulation remains possible in the future as the side effects could then not be properly evaluated.

Important considerations

Adapting STN-DBS targeting specifically to steering electrodes seems promising, but it needs careful review. More lateral targeting also comes with risks. Targeting closer to the internal capsule leaves less room for error and even with very accurate procedures, steering stimulation might not be able to increase the threshold for side effects of the internal capsule sufficiently for all patients. The risks are higher with DBS surgery under general anesthesia where steering test stimulation cannot be performed. It is possible, with an electrode that is very close to the internal capsule, that side effects are evoked at very low amplitude, even with optimal current steering away from the internal capsule. This means that these patients will have to be stimulated with lower amplitude, possibly leading to less satisfactory motor improvement. In a worst-case scenario, a patient might have to undergo a second surgery to correct electrode placement. When DBS surgery is performed under general anesthesia, although the

risk of needing a second surgery might be higher, the burden of this consequence would be smaller, compared to awake DBS surgery.

The challenge is to carefully study how many patients would benefit from more lateral targeting in combination with steering electrodes, and whether the additional risks would outweigh the expected benefits of targeting this way. A safe first step in studying this would be to use improved versions of the computational models discussed in chapters 7 and 8, with a more detailed segmentation of the sensorimotor projections and a more accurate modelling of the internal capsule fibers. In these models, several varieties of more lateral placement could be studied. If these models would suggest a positive result, this would have to be verified in clinical trials.

This thesis has focused on technological advancements in the DBS procedure and how the application of new techniques could potentially provide a way forward to improve DBS efficacy. We have studied this potential based on motor improvement and side effects. In terms of motor improvement, we have focused only on the motor symptoms that are generally improved by DBS. Axials motor symptoms, which generally do not improve after DBS also require future study. In terms of side effects, we have focused mainly on side effects of the internal capsule, as these are evoked closest to the hotspot for motor improvement. In a chronic setting, steering stimulation could also be used to reduce other side effects, such as cognitive decline or behavioral disturbances, which are not the result of internal capsule stimulation. Although these side effects are more difficult to assess, they have great influence on the burden experienced by PD patients and they also require careful study to improve the quality of life of these patients.

Conclusion

In this thesis, we have studied optimization of the identification of the target for STN-DBS, using MRI imaging of different field strengths, combined with MER and LFP measurements. Additionally, we have investigated the potential of steering DBS electrodes in both the identification and the stimulation of the target with increased accuracy.

We argue that the full potential of the steering DBS electrode might be unleashed when it is combined with deliberately targeting a more lateral part of the STN, closer to the sensorimotor projections and thus the hotspot for motor improvement, but also closer to the side effects inducing corticospinal tract. Whether DBS electrodes are still able to increase the threshold for side effects at this more lateral position seems plausible, but this needs more careful review in future studies. A possible adaptation of STN-DBS targeting especially for steering electrodes should be accompanied with improved implantation accuracy, by preoperative identification of the lateral STN with

high field strength T2 MRI, and by intraoperative verification of the electrode position with high-resolution MRI or CT. Intraoperative and postoperative LFP measurement with the final steering electrode can verify the STN borders and provide insight into the local STN oscillations which could guide one towards the neurophysiological location of the hotspot for motor improvement achieved by DBS.

Reference list

1. Benabid AL, Chabardes S, Mitrofanis J, Pollak P. Deep brain stimulation of the subthalamic nucleus for the treatment of Parkinson's disease. *Lancet Neurol*. 2009;8(1):67-81.
2. Deuschl G, Schade-Brittinger C, Krack P, et al. A Randomized Trial of Deep-Brain Stimulation for Parkinson's Disease. *N Engl J Med*. 2006;355(9):896-908.
3. Krack P, Volkmann J, Tinkhauser G, Deuschl G. Deep Brain Stimulation in Movement Disorders: From Experimental Surgery to Evidence-Based Therapy. *Mov Disord*. 2019;34(12):1795-1810.
4. Limousin P, Krack P, Pollak P, et al. Electrical Stimulation of the Subthalamic Nucleus in Advanced Parkinson's Disease. *N Engl J Med*. 1998;339(16):1105-1111.
5. Anderson VC, Burchiel KJ, Hogarth P, Favre J, Hammerstad JP. Pallidal vs subthalamic nucleus deep brain stimulation in Parkinson disease. *Arch Neurol*. 2005;62(4):554-560.
6. Weaver FM, Follett K, Stern M, et al. Bilateral deep brain stimulation vs best medical therapy for patients with advanced parkinson disease: A randomized controlled trial. *JAMA - J Am Med Assoc*. 2009;301(1):63-73.
7. Odekerken VJJ, Boel JA, Schmand BA, et al. GPi vs STN deep brain stimulation for Parkinson disease. *Neurology*. 2016;86(8):755-761.
8. Holewijn RA, Verbaan D, Van Den Munckhof PM, et al. General Anesthesia vs Local Anesthesia in Microelectrode Recording-Guided Deep-Brain Stimulation for Parkinson Disease: The GALAXY Randomized Clinical Trial. *JAMA Neurol*. 2021;78(10):1212-1219.
9. Kleiner-Fisman G, Herzog J, Fisman DN, et al. Subthalamic nucleus deep brain stimulation: Summary and meta-analysis of outcomes. *Mov Disord*. 2006;21(SUPPL. 14):290-304.
10. Odekerken VJJ, Boel JA, Geurtsen GJ, et al. Neuropsychological outcome after deep brain stimulation for Parkinson disease. *Neurology*. 2015;84(13):1355-1361.
11. Odekerken VJJ, van Laar T, Staal MJ, et al. Subthalamic nucleus versus globus pallidus bilateral deep brain stimulation for advanced Parkinson's disease (NSTAPS study): A randomised controlled trial. *Lancet Neurol*. 2013;12(1):37-44.
12. Williams A, Gill S, Varma T, et al. Deep brain stimulation plus best medical therapy versus best medical therapy alone for advanced Parkinson's disease (PD SURG trial): a randomised, open-label trial. *Lancet Neurol*. 2010;9(6):581-591.
13. Aygun D, Kocabicak E, Yildiz MO, Temel Y. Effect of age and disease duration on the levodopa response in patients with advanced Parkinson's disease for deep brain stimulation of the subthalamic nucleus. *Front Neurol*. 2016;7(JUN):7-11.
14. Bronstein JM, Tagliati M, Alterman RL, et al. Deep brain stimulation for Parkinson disease an expert consensus and review of key issues. *Arch Neurol*. 2011;68(2):165-171.
15. Parent B, Awan N, Berman SB, et al. The relevance of age and disease duration for intervention with subthalamic nucleus deep brain stimulation surgery in Parkinson disease: Clinical article. *J Neurosurg*. 2011;114(4):927-931.
16. Caire F, Ranoux D, Guehl D, Burbaud P, Cuny E. A systematic review of studies on anatomical position of electrode contacts used for chronic subthalamic stimulation in Parkinson's disease. *Acta Neurochir (Wien)*. 2013;155(9):1647-1654.
17. Hamel W, Fietzek U, Morsnowski A, et al. Deep brain stimulation of the subthalamic nucleus in Parkinson's disease: Evaluation of active electrode contacts. *J Neurol Neurosurg Psychiatry*. 2003;74(8):1036-1046.

18. Herzog J, Fietzek U, Hamel W, et al. Most effective stimulation site in subthalamic deep brain stimulation for Parkinson's disease. *Mov Disord*. 2004;19(9):1050-1054.
19. Voges J, Volkmann J, Allert N, et al. Bilateral high-frequency stimulation in the subthalamic nucleus for the treatment of Parkinson disease: Correlation of therapeutic effect with anatomical electrode position. *J Neurosurg*. 2002;96(2):269-279.
20. Wodarg F, Herzog J, Reese R, et al. Stimulation site within the MRI-defined STN predicts postoperative motor outcome. *Mov Disord*. 2012;27(7):874-879.
21. Bot M, Van Den Munckhof P, Bakay R, Sierens D, Stebbins G, Verhagen Metman L. Analysis of Stereotactic Accuracy in Patients Undergoing Deep Brain Stimulation Using Nexframe and the Leksell Frame. *Stereotact Funct Neurosurg*. 2015;93(5):316-325.
22. Buzsáki G, Anastassiou CA, Koch C. The origin of extracellular fields and currents-EEG, ECoG, LFP and spikes. *Nat Rev Neurosci*. 2012;13(6):407-420.
23. Kühn AA, Trottenberg T, Kivi A, Kupsch A, Schneider GH, Brown P. The relationship between local field potential and neuronal discharge in the subthalamic nucleus of patients with Parkinson's disease. *Exp Neurol*. 2005;194(1):212-220.
24. Chen CC, Pogosyan A, Zrinzo LU, et al. Intra-operative recordings of local field potentials can help localize the subthalamic nucleus in Parkinson's disease surgery. *Exp Neurol*. 2006;198(1):214-221.
25. Oswal A, Brown P, Litvak V. Synchronized neural oscillations and the pathophysiology of Parkinson's disease. *Curr Opin Neurol*. 2013;26(6):662-670.
26. Pogosyan A, Yoshida F, Chen CC, et al. Parkinsonian impairment correlates with spatially extensive subthalamic oscillatory synchronization. *Neuroscience*. 2010;171(1):245-257.
27. Neumann WJ, Staub-Bartelt F, Horn A, et al. Long term correlation of subthalamic beta band activity with motor impairment in patients with Parkinson's disease. *Clin Neurophysiol*. 2017;128(11):2286-2291.
28. Martens HCF, Toader E, Decré MMJ, et al. Spatial steering of deep brain stimulation volumes using a novel lead design. *Clin Neurophysiol*. 2011;122(3):558-566.
29. Pollo C, Kaelin-Lang A, Oertel MF, et al. Directional deep brain stimulation: An intraoperative double-blind pilot study. *Brain*. 2014;137(7):2015-2026.
30. Deuschl G, Schade-Brittinger C, Krack P, et al. A Randomized Trial of Deep-Brain Stimulation for Parkinson's Disease. *N Engl J Med*. 2006;355(9):896-908.
31. Rezai AR, Kopell BH, Gross RE, et al. Deep brain stimulation for Parkinson's disease: Surgical issues. *Mov Disord*. 2006;21(SUPPL. 14):S197-218.
32. Fytagoridis A, Åström M, Wårdell K, Blomstedt P. Stimulation-induced side effects in the posterior subthalamic area: Distribution, characteristics and visualization. *Clin Neurol Neurosurg*. 2013;115(1):65-71.
33. Tommasi G, Krack P, Fraix V, et al. Pyramidal tract side effects induced by deep brain stimulation of the subthalamic nucleus. *J Neurol Neurosurg Psychiatry*. 2008;79(7):813-819.
34. Temel Y, Kessels A, Tan S, Topdag A, Boon P, Visser-Vandewalle V. Behavioural changes after bilateral subthalamic stimulation in advanced Parkinson disease: A systematic review. *Park Relat Disord*. 2006;12(5):265-272.
35. Witt K, Daniels C, Reiff J, et al. Neuropsychological and psychiatric changes after deep brain stimulation for Parkinson's disease: a randomised, multicentre study. *Lancet Neurol*. 2008;7(7):605-614.
36. Limousin P, Pollak P, Benazzouz A, et al. Effect on parkinsonian signs and symptoms of bilateral subthalamic nucleus stimulation. *Lancet*. 1995;345(8942):91-95.

37. Daniluk S, G. Davies K, Ellias SA, Novak P, Nazzaro JM. Assessment of the variability in the anatomical position and size of the subthalamic nucleus among patients with advanced Parkinson's disease using magnetic resonance imaging. *Acta Neurochir (Wien)*. 2010;152(2):201-210.
38. Parent A, Hazrati LN. Functional anatomy of the basal ganglia. II. The place of subthalamic nucleus and external pallidium in basal ganglia circuitry. *Brain Res Rev*. 1995;20(1):128-154.
39. Mallet L, Schüpbach M, N'Diaye K, et al. Stimulation of subterritories of the subthalamic nucleus reveals its role in the integration of the emotional and motor aspects of behavior. *Proc Natl Acad Sci U S A*. 2007;104(25):10661-10666.
40. Saint-Cyr JA, Hoque T, Pereira LCM, et al. Localization of clinically effective stimulating electrodes in the human subthalamic nucleus on magnetic resonance imaging. *J Neurosurg*. 2002;97(5):1152-1166.
41. Ulla M, Thobois S, Llorca PM, et al. Contact dependent reproducible hypomania induced by deep brain stimulation in Parkinson's disease: Clinical, anatomical and functional imaging study. *J Neurol Neurosurg Psychiatry*. 2011;82(6):607-614.
42. Yelnik J, Damier P, Demeret S, et al. Localization of stimulating electrodes in patients with Parkinson disease by using a three-dimensional atlas-magnetic resonance imaging coregistration method. *J Neurosurg*. 2003;99(1):89-99.
43. Hamani C, Saint-Cyr JA, Fraser J, Kaplitt M, Lozano AM. The subthalamic nucleus in the context of movement disorders. *Brain*. 2004;127(1):4-20.
44. Temel Y, Blokland A, Steinbusch HWM, Visser-Vandewalle V. The functional role of the subthalamic nucleus in cognitive and limbic circuits. *Prog Neurobiol*. 2005;76(6):393-413.
45. Longhi M, Ricciardi G, Tommasi G, et al. The role of 3T magnetic resonance imaging for targeting the human subthalamic nucleus in deep brain stimulation for Parkinson disease. *J Neurol Surgery, Part A Cent Eur Neurosurg*. 2015;76(3):181-189.
46. Schuurman PR, De Bie RMA, Majoie CBL, Speelman JD, Bosch DA. A prospective comparison between three-dimensional magnetic resonance imaging and ventriculography for target-coordinate determination in frame-based functional stereotactic neurosurgery. *J Neurosurg*. 1999;91(6):911-914.
47. Zonenshayn M, Rezai AR, Mogilner AY, Beric A, Sterio D, Kelly PJ. Comparison of anatomic and neurophysiological methods for subthalamic nucleus targeting. *Neurosurgery*. 2000;47(2):282-294.
48. Lemaire JJ, Coste J, Ouchchane L, et al. Brain mapping in stereotactic surgery: A brief overview from the probabilistic targeting to the patient-based anatomic mapping. *Neuroimage*. 2007;37(SUPPL. 1):S109-S115.
49. Bejjani BP, Dormont D, Pidoux B, et al. Bilateral subthalamic stimulation for Parkinson's disease by using three-dimensional stereotactic magnetic resonance imaging and electrophysiological guidance. *J Neurosurg*. 2000;92(4):615-625.
50. Dormont D, Ricciardi KG, Tandé D, et al. Is the subthalamic nucleus hypointense on T2-weighted images? A correlation study using MR imaging and stereotactic atlas data. *Am J Neuroradiol*. 2004;25(9):1516-1523.
51. Kosta P, Argyropoulou MI, Markoula S, Konitsiotis S. MRI evaluation of the basal ganglia size and iron content in patients with Parkinson's disease. *J Neurol*. 2006;253(1):26-32.
52. Ashkan K, Blomstedt P, Zrinzo L, et al. Variability of the subthalamic nucleus: The case for direct MRI guided targeting. *Br J Neurosurg*. 2007;21(2):197-200.
53. Caire F, Ouchchane L, Coste J, et al. Subthalamic nucleus location: Relationships between stereotactic AC-PC-based diagrams

and MRI anatomy-based contours. *Stereotact Funct Neurosurg*. 2009;87(6):337-347.

54. Hamani C, Richter EO, Andrade-Souza Y, Hutchison W, Saint-Cyr JA, Lozano AM. Correspondence of microelectrode mapping with magnetic resonance imaging for subthalamic nucleus procedures. *Surg Neurol*. 2005;63(3):249-253.
55. Richter EO, Hoque T, Halliday W, Lozano AM, Saint-Cyr JA. Determining the position and size of the subthalamic nucleus based on magnetic resonance imaging results in patients with advanced Parkinson disease. *J Neurosurg*. 2004;100(3):541-546.
56. Polanski WH, Martin KD, Engellandt K, et al. Accuracy of subthalamic nucleus targeting by T2, FLAIR and SWI-3-Tesla MRI confirmed by microelectrode recordings. *Acta Neurochir (Wien)*. 2015;157(3):479-486.
57. Brunenberg EJL, Platel B, Hofman PAM, Ter Haar Romeny BM, Visser-Vandewalle V. Magnetic resonance imaging techniques for visualization of the subthalamic nucleus: A review. *J Neurosurg*. 2011;115(5):970-984.
58. Cho ZH, Min HK, Oh SH, et al. Direct visualization of deep brain stimulation targets in Parkinson disease with the use of 7-tesla magnetic resonance imaging: Clinical article. *J Neurosurg*. 2010;113(3):639-647.
59. Cho ZH, Oh SH, Kim JM, et al. Direct visualization of Parkinson's disease by in vivo human brain imaging using 7.0T magnetic resonance imaging. *Mov Disord*. 2011;26(4):713-718.
60. Starr PA, Christine CW, Theodosopoulos P V., et al. Implantation of deep brain stimulators into the subthalamic nucleus: Technical approach and magnetic resonance imaging-verified lead locations. *J Neurosurg*. 2002;97(2):370-387.
61. Houshmand L, Cummings KS, Chou KL, Patil PG. Evaluating indirect subthalamic nucleus targeting with validated 3-tesla magnetic resonance imaging. *Stereotact Funct Neurosurg*. 2014;92(6):337-345.
62. Guridi J, Rodriguez-Oroz MC, Lozano AM, et al. Targeting the basal ganglia for deep brain stimulation in Parkinson's disease. *Neurology*. 2000;55(12 SUPPL. 6):S21-S28.
63. Bour LJ, Contarino MF, Foncke EMJ, et al. Long-term experience with intraoperative microrecording during DBS neurosurgery in STN and GPi. *Acta Neurochir (Wien)*. 2010;152(12):2069-2077.
64. Schlaier JR, Habermeyer C, Janzen A, et al. The influence of intraoperative microelectrode recordings and clinical testing on the location of final stimulation sites in deep brain stimulation for Parkinson's disease. *Acta Neurochir (Wien)*. 2013;155(2):357-366.
65. Hutchison WD, Lozano AM, Starr PA. Neurophysiological refinement of subthalamic nucleus targeting: Comments. *Neurosurgery*. 2002;50(1):67-69.
66. Gross RE, Krack P, Rodriguez-Oroz MC, Rezai AR, Benabid AL. Electrophysiological mapping for the implantation of deep brain stimulators for Parkinson's disease and tremor. *Mov Disord*. 2006;21(SUPPL. 14):S259-S283.
67. Lanotte MM, Rizzone M, Bergamasco B, Faccani G, Melcarne A, Lopiano L. Deep brain stimulation of the subthalamic nucleus: Anatomical, neurophysiological, and outcome correlations with the effects of stimulation. *J Neurol Neurosurg Psychiatry*. 2002;72(1):53-58.
68. Montgomery EB. Microelectrode targeting of the subthalamic nucleus for deep brain stimulation surgery. *Mov Disord*. 2012;27(11):1387-1391.
69. Toda H, Sawamoto N, Hanakawa T, et al. A novel composite targeting method using high-field magnetic resonance imaging for subthalamic nucleus deep brain stimulation: Clinical article. *J Neurosurg*. 2009;111(4):737-745.
70. Contarino MF, Bot M, Speelman JD, et al. Postoperative displacement of deep brain stimulation electrodes related to lead-anchoring technique. *Neurosurgery*. 2013;73(4):681-688.

71. Moran A, Bar-Gad I. Revealing neuronal functional organization through the relation between multi-scale oscillatory extracellular signals. *J Neurosci Methods*. 2010;186(1):116-129.
72. Cagnan H, Dolan K, He X, et al. Automatic subthalamic nucleus detection from microelectrode recordings based on noise level and neuronal activity. *J Neural Eng*. 2011;8(4):046006.
73. Lourens MAJ, Meijer HGE, Contarino MF, et al. Functional neuronal activity and connectivity within the subthalamic nucleus in Parkinson's disease. *Clin Neurophysiol*. 2013;124(5):967-981.
74. Verhagen R, Zwartjes DGM, Heida T, et al. Advanced target identification in STN-DBS with beta power of combined local field potentials and spiking activity. *J Neurosci Methods*. 2015;253:116-125.
75. Butson CR, Cooper SE, Henderson JM, McIntyre CC. Patient-specific analysis of the volume of tissue activated during deep brain stimulation. *Neuroimage*. 2007;34(2):661-670.
76. Miocinovic S, Noecker AM, Maks CB, Butson CR, McIntyre CC. Cicerone: Stereotactic neurophysiological recording and deep brain stimulation electrode placement software system. Sakas DE, Simpson BA, eds. *Acta Neurochir Suppl*. 2007;97(97 PART 2):561-567.
77. Maciunas RJ, Galloway RL, Latimer JW. The application accuracy of stereotactic frames. *Neurosurgery*. 1994;35(4):682-695.
78. Petersen EA, Holl EM, Martinez-Torres I, et al. Minimizing brain shift in stereotactic functional neurosurgery. *Neurosurgery*. 2010;67(SUPPL. 1):213-221.
79. Slotty PJ, Kamp MA, Wille C, Kinfe TM, Steiger HJ, Vesper J. The impact of brain shift in deep brain stimulation surgery: Observation and obviation. *Acta Neurochir (Wien)*. 2012;154(11):2063-2068.
80. Van Den Munckhof P, Contarino MF, Bour LJ, Speelman JD, De Bie RMA, Schuurman PR. Postoperative curving and upward displacement of deep brain stimulation electrodes caused by brain shift. *Neurosurgery*. 2010;67(1):49-53.
81. McEvoy J, Ughratdar I, Schwarz S, Basu S. Electrophysiological validation of STN-SNr boundary depicted by susceptibility-weighted MRI. *Acta Neurochir (Wien)*. 2015;157(12):2129-2134.
82. Vertinsky AT, Coenen VA, Lang DJ, et al. Localization of the subthalamic nucleus: Optimization with susceptibility-weighted phase MR imaging. *Am J Neuroradiol*. 2009;30(9):1717-1724.
83. Bériault S, Sadikot AF, Alsubaie F, Drouin S, Collins DL, Pike GB. Neuronavigation using susceptibility-weighted venography: Application to deep brain stimulation and comparison with gadolinium contrast: Technical note. *J Neurosurg*. 2014;121(1):131-141.
84. Bot M, Bour L, De Bie RM, Contarino MF, Schuurman PR, Van Den Munckhof P. Can We Rely on Susceptibility-Weighted Imaging for Subthalamic Nucleus Identification in Deep Brain Stimulation Surgery? *Neurosurgery*. 2016;78(3):353-359.
85. Benabid AL, Chabardes S, Mitrofanis J, Pollak P. Deep brain stimulation of the subthalamic nucleus for the treatment of Parkinson's disease. *Lancet Neurol*. 2009;8(1):67-81.
86. Brown P, Eusebio A. Paradoxes of functional neurosurgery: Clues from basal ganglia recordings. *Mov Disord*. 2008;23(1):12-20.
87. Eusebio A, Cagnan H, Brown P. Does suppression of oscillatory synchronisation mediate some of the therapeutic effects of DBS in patients with Parkinson's disease? *Front Integr Neurosci*. 2012;6(JULY 2012):1-9.
88. Amirnovin R, Williams ZM, Cosgrove GR, Eskandar EN. Experience with microelectrode guided subthalamic nucleus deep brain stimulation. *Neurosurgery*. 2006;58(SUPPL. 1):96-102.

89. Bakstein E, Burgess J, Warwick K, Ruiz V, Aziz T, Stein J. Parkinsonian tremor identification with multiple local field potential feature classification. *J Neurosci Methods*. 2012;209(2):320-330.

90. Little S, Pogosyan A, Neal S, et al. Adaptive deep brain stimulation in advanced Parkinson disease. *Ann Neurol*. 2013;74(3):449-457.

91. Priori A, Foffani G, Rossi L, Marceglia S. Adaptive deep brain stimulation (aDBS) controlled by local field potential oscillations. *Exp Neurol*. 2013;245:77-86.

92. Winestone JS, Zaidel A, Bergman H, Israel Z. The use of macroelectrodes in recording cellular spiking activity. *J Neurosci Methods*. 2012;206(1):34-39.

93. Contarino MF, Bour LJ, Bot M, et al. Tremor-specific neuronal oscillation pattern in dorsal subthalamic nucleus of parkinsonian patients. *Brain Stimul*. 2012;5(3):305-314.

94. Trottenberg T, Kupsch A, Schneider GH, Brown P, Kühn AA. Frequency-dependent distribution of local field potential activity within the subthalamic nucleus in Parkinson's disease. *Exp Neurol*. 2007;205(1):287-291.

95. Weinberger M, Mahant N, Hutchison WD, et al. Beta oscillatory activity in the subthalamic nucleus and its relation to dopaminergic response in Parkinson's disease. *J Neurophysiol*. 2006;96(6):3248-3256.

96. Brown P. Oscillatory nature of human basal ganglia activity: Relationship to the pathophysiology of parkinson's disease. *Mov Disord*. 2003;18(4):357-363.

97. Kühn AA, Kupsch A, Schneider GH, Brown P. Reduction in subthalamic 8-35 Hz oscillatory activity correlates with clinical improvement in Parkinson's disease. *Eur J Neurosci*. 2006;23(7):1956-1960.

98. Brown P. Abnormal oscillatory synchronisation in the motor system leads to impaired movement. *Curr Opin Neurobiol*. 2007;17(6):656-664.

99. Jenkinson N, Brown P. New insights into the relationship between dopamine, beta oscillations and motor function. *Trends Neurosci*. 2011;34(12):611-618.

100. Alegre M, Alonso-Frech F, Rodríguez-Oroz MC, et al. Movement-related changes in oscillatory activity in the human subthalamic nucleus: Ipsilateral vs. contralateral movements. *Eur J Neurosci*. 2005;22(9):2315-2324.

101. Androulidakis AG, Kühn AA, Chen CC, et al. Dopaminergic therapy promotes lateralized motor activity in the subthalamic area in Parkinson's disease. *Brain*. 2007;130(2):457-468.

102. Cassidy M, Mazzone P, Oliviero A, et al. Movement-related changes in synchronization in the human basal ganglia. *Brain*. 2002;125(6):1235-1246.

103. Fogelson N, Pogosyan A, Kühn AA, et al. Reciprocal interactions between oscillatory activities of different frequencies in the subthalamic region of patients with Parkinson's disease. *Eur J Neurosci*. 2005;22(1):257-266.

104. Williams D, Tijssen M, Van Bruggen G, et al. Dopamine-dependent changes in the functional connectivity between basal ganglia and cerebral cortex in humans. *Brain*. 2002;125(7):1558-1569.

105. Brown P, Williams D. Basal ganglia local field potential activity: Character and functional significance in the human. *Clin Neurophysiol*. 2005;116(11):2510-2519.

106. Trottenberg T, Fogelson N, Kühn AA, et al. Subthalamic gamma activity in patients with Parkinson's disease. *Exp Neurol*. 2006;200(1):56-65.

107. Weinberger M, Hutchison WD, Lozano AM, Hodaie M, Dostrovsky JO. Increased gamma oscillatory activity in the subthalamic nucleus during tremor in Parkinson's disease patients. *J Neurophysiol*. 2009;101(2):789-802.

108. Juergens E, Guettler A, Eckhorn R. Visual stimulation elicits locked and induced gamma oscillations in monkey intracortical- and EEG-potentials, but not in human EEG. *Exp Brain Res*. 1999;129(2):247-259.

109. Kajikawa Y, Schroeder CE. How local is the local field potential? *Neuron*. 2011;72(5):847-858.

110. Mitzdorf U. Properties of the evoked potential generators: Current source-density analysis of visually evoked potentials in the cat cortex. *Int J Neurosci*. 1987;33(1-2):33-59.

111. Buzsáki G, Anastassiou CA, Koch C. The origin of extracellular fields and currents-EEG, ECoG, LFP and spikes. *Nat Rev Neurosci*. 2012;13(6):407-420.

112. Henze DA, Borhegyi Z, Csicsvari J, Mamiya A, Harris KD, Buzsáki G. Intracellular features predicted by extracellular recordings in the hippocampus in vivo. *J Neurophysiol*. 2000;84(1):390-400.

113. Alavi M, Dostrovsky JO, Hodaie M, Lozano AM, Hutchison WD. Spatial extent of beta oscillatory activity in and between the subthalamic nucleus and substantia nigra pars reticulata of Parkinson's disease patients. *Exp Neurol*. 2013;245:60-71.

114. Luján JL, Noecker AM, Butson CR, et al. Automated 3-dimensional brain atlas fitting to microelectrode recordings from deep brain stimulation surgeries. *Stereotact Funct Neurosurg*. 2009;87(4):229-240.

115. Benarroch EE. Subthalamic nucleus and its connections: Anatomic substrate for the network effects of deep brain stimulation. *Neurology*. 2008;70(21):1991-1995.

116. Dolan K, Martens HCF, Schuurman PR, Bour LJ. Automatic noise-level detection for extra-cellular micro-electrode recordings. *Med Biol Eng Comput*. 2009;47(7):791-800.

117. Grover FS, Buchwald JS. Correlation of cell size with amplitude of background fast activity in specific brain nuclei. *J Neurophysiol*. 1970;33(1):160-171.

118. Halliday DM, Rosenberg JR, Amjad AM, Breeze P, Conway BA, Farmer SF. A framework for the analysis of mixed time series/point process data-Theory and application to the study of physiological tremor, single motor unit discharges and electromyograms. *Prog Biophys Mol Biol*. 1995;64(2-3):237-278.

119. Buzsáki G. Theta oscillations in the hippocampus. *Neuron*. 2002;33(3):325-340.

120. Goto Y, O'Donnell P. Network synchrony in the nucleus accumbens in vivo. *J Neurosci*. 2001;21(12):4498-4504.

121. Logothetis NK. The underpinnings of the BOLD functional magnetic resonance imaging signal. *J Neurosci*. 2003;23(10):3963-3971.

122. Logothetis NK. The neural basis of the blood-oxygen-level-dependent functional magnetic resonance imaging signal. *Philos Trans R Soc B Biol Sci*. 2002;357(1424):1003-1037.

123. Pedemonte M, Barrenechea C, Nuñez A, Gambini JP, García-Austt E. Membrane and circuit properties of lateral septum neurons: Relationships with hippocampal rhythms. *Brain Res*. 1998;800(1):145-153.

124. Lindén H, Pettersen KH, Einevoll GT. Intrinsic dendritic filtering gives low-pass power spectra of local field potentials. *J Comput Neurosci*. 2010;29(3):423-444.

125. Legatt AD, Arezzo J, Vaughan HG. Averaged multiple unit activity as an estimate of phasic changes in local neuronal activity: effects of volume-conducted potentials. *J Neurosci Methods*. 1980;2(2):203-217.

126. Contarino MF, Bour LJ, Verhagen R, et al. Directional steering: A novel approach to deep brain stimulation. *Neurology*. 2014;83(13):1163-1169.

127. Follett KA, Weaver FM, Stern M, et al. Pallidal versus Subthalamic Deep-Brain Stimulation for Parkinson's Disease. *N Engl J Med*. 2010;362(22):2077-2091.

128. Maks CB, Butson CR, Walter BL, Vitek JL, McIntyre CC. Deep brain stimulation

activation volumes and their association with neurophysiological mapping and therapeutic outcomes. *J Neurol Neurosurg Psychiatry*. 2009;80(6):659-666.

129. Plaha P, Ben-Shlomo Y, Patel NK, Gill SS. Stimulation of the caudal zona incerta is superior to stimulation of the subthalamic nucleus in improving contralateral parkinsonism. *Brain*. 2006;129(7):1732-1747.
130. Vergani F, Landi A, Antonini A, et al. Anatomical identification of active contacts in subthalamic deep brain stimulation. *Surg Neurol*. 2007;67(2):140-146.
131. Zonenshayn M, Sterio D, Kelly PJ, Rezai AR, Beric A. Location of the active contact within the subthalamic nucleus (STN) in the treatment of idiopathic Parkinson's disease. *Surg Neurol*. 2004;62(3):216-225.
132. Johnsen EL, Sunde N, Mogensen PH, Østergaard K. MRI verified STN stimulation site - Gait improvement and clinical outcome. *Eur J Neurol*. 2010;17(5):746-753.
133. Nestor KA, Jones JD, Butson CR, et al. Coordinate-based lead location does not predict parkinson's disease deep brain stimulation outcome. *PLoS One*. 2014;9(4):e93524.
134. Sun HP, Jung HH, Lee JY, Kim C, Beom SJ, Dong GK. Electrode position determined by fused images of preoperative and postoperative magnetic resonance imaging and surgical outcome after subthalamic nucleus deep brain stimulation. *Neurosurgery*. 2008;63(5):925-936.
135. McClelland S, Ford B, Senatus PB, et al. Subthalamic stimulation for Parkinson disease: determination of electrode location necessary for clinical efficacy. *Neurosurg Focus*. 2005;19(5):E12.
136. Kasasbeh A, Abulseoud OA, Matsumoto JY, et al. Lack of differential motor outcome with subthalamic nucleus region stimulation in Parkinson's disease. *J Clin Neurosci*. 2013;20(11):1520-1526.
137. Bot M, Schuurman PR, Odekerken VJJ, et al. Deep brain stimulation for Parkinson's disease: defining the optimal location within the subthalamic nucleus. *J Neurol Neurosurg Psychiatry*. 2018;89(5):493-498.
138. Garcia-Garcia D, Guridi J, Toledo JB, Alegre M, Obeso JA, Rodriguez-Oroz MC. Stimulation sites in the subthalamic nucleus and clinical improvement in Parkinson's disease: A new approach for active contact localization. *J Neurosurg*. 2016;125(5):1068-1079.
139. Verhagen R, Schuurman PR, Van Den Munckhof P, Contarino MF, De Bie RMA, Bour LJ. Comparative study of microelectrode recording-based STN location and MRI-based STN location in low to ultra-high field (7.0 T) T2-weighted MRI images. *J Neural Eng*. 2016;13(6):066009.
140. Little S, Pogosyan A, Kuhn AA, Brown P. Beta band stability over time correlates with Parkinsonian rigidity and bradykinesia. *Exp Neurol*. 2012;236(2):383-388.
141. Aviles-Olmos I, Kefalopoulou Z, Tripoliti E, et al. Long-term outcome of subthalamic nucleus deep brain stimulation for Parkinson's disease using an MRI-guided and MRI-verified approach. *J Neurol Neurosurg Psychiatry*. 2014;85(12):1419-1425.
142. Krack P, Hariz MI, Baunez C, Guridi J, Obeso JA. Deep brain stimulation: From neurology to psychiatry? *Trends Neurosci*. 2010;33(10):474-484.
143. Pollak P, Krack P, Fraix V, et al. Intraoperative micro- and macrostimulation of the subthalamic nucleus in Parkinson's disease. *Mov Disord*. 2002;17(SUPPL. 3):S155-S161.
144. Hariz M. Deep brain stimulation: New techniques. *Park Relat Disord*. 2014;20(SUPPL.1):S192-S196.
145. Toader E, Decré MMJ, Martens HCF. Steering deep brain stimulation fields using a high resolution electrode array. In: *2010 Annual International Conference of the IEEE Engineering in Medicine and Biology Society, EMBC'10.* ; 2010:2061-2064.
146. Shannon R V. A Model of Safe Levels for Electrical Stimulation. *IEEE Trans Biomed Eng*. 1992;39(4):424-426.

147. McCreery DB, Agnew WF, Yuen TGH, Bullara L. Charge density and charge per phase as cofactors in neural injury induced by electrical stimulation. *IEEE Trans Biomed Eng*. 1990;37(10):996-1001.

148. Contarino MF, Bour LJ, Bot M, et al. Pallidotomy suppresses beta power in the subthalamic nucleus of Parkinson's disease patients. *Eur J Neurosci*. 2011;33(7):1275-1280.

149. Greenberg BD, Rauch SL, Haber SN. Invasive circuitry-based neurotherapeutics: Stereotactic ablation and deep brain stimulation for OCD. *Neuropsychopharmacology*. 2010;35(1):317-336.

150. Holtbernd F, Eidelberg D. Functional brain networks in movement disorders: Recent advances. *Curr Opin Neurol*. 2012;25(4):392-401.

151. Tass PA, Qin L, Hauptmann C, et al. Coordinated reset has sustained aftereffects in Parkinsonian monkeys. *Ann Neurol*. 2012;72(5):816-820.

152. Benabid AL, Benazzouz A, Hoffmann D, Limousin P, Krack P, Pollak P. Long-term electrical inhibition of deep brain targets in movement disorders. *Mov Disord*. 1998;13(SUPPL. 3):119-125.

153. Benabid AL, Benazzouz A, Limousin P, et al. Dyskinesias and the subthalamic nucleus. *Ann Neurol*. 2000;47(4 Suppl 1):S189-92.

154. Bergman H, Wichmann T, Karmon B, DeLong MR. The primate subthalamic nucleus. II. Neuronal activity in the MPTP model of parkinsonism. *J Neurophysiol*. 1994;72(2):507-520.

155. Bergman H, Wichmann T, DeLong MR. Reversal of experimental parkinsonism by lesions of the subthalamic nucleus. *Science (80-)*. 1990;249(4975):1436-1438.

156. Deuschl G, Agid Y. Subthalamic neurostimulation for Parkinson's disease with early fluctuations: Balancing the risks and benefits. *Lancet Neurol*. 2013;12(10):1025-1034.

157. Pollak P, Benabid AL, Limousin P, Krack P. New surgical treatment strategies. *Eur Neurol*. 1996;36(6):400-404.

158. Wichmann T, Bergman H, DeLong MR. The primate subthalamic nucleus. I. Functional properties in intact animals. *J Neurophysiol*. 1994;72(2):494-506.

159. Silberstein P, Oliviero A, Di Lazzaro V, Insola A, Mazzone P, Brown P. Oscillatory pallidal local field potential activity inversely correlates with limb dyskinesias in Parkinson's disease. *Exp Neurol*. 2005;194(2):523-529.

160. Silberstein P, Kühn AA, Kupsch A, et al. Patterning of globus pallidus local field potentials differs between Parkinson's disease and dystonia. *Brain*. 2003;126(12):2597-2608.

161. Alonso-Frech F, Zamarbide I, Alegre M, et al. Slow oscillatory activity and levodopa-induced dyskinesias in Parkinson's disease. *Brain*. 2006;129(7):1748-1757.

162. Brown P, Oliviero A, Mazzone P, Insola A, Tonali P, Di Lazzaro V. Dopamine dependency of oscillations between subthalamic nucleus and pallidum in Parkinson's disease. *J Neurosci*. 2001;21(3):1033-1038.

163. Priori A, Foffani G, Pesenti A, et al. Rhythm-specific pharmacological modulation of subthalamic activity in Parkinson's disease. *Exp Neurol*. 2004;189(2):369-379.

164. Guo S, Zhuang P, Zheng Z, Zhang Y, Li J, Li Y. Neuronal firing patterns in the subthalamic nucleus in patients with akinetic-rigid-type Parkinson's disease. *J Clin Neurosci*. 2012;19(10):1404-1407.

165. Hammond C, Bergman H, Brown P. Pathological synchronization in Parkinson's disease: networks, models and treatments. *Trends Neurosci*. 2007;30(7):357-364.

166. Moran A, Stein E, Tischler H, Belelovsky K, Bar-Gad I. Dynamic stereotypic responses of basal ganglia neurons to subthalamic nucleus high-frequency stimulation in the parkinsonian primate. *Front Syst Neurosci*. 2011;5(APRIL 2011):21.

167. Buzsáki G. Large-scale recording of neuronal ensembles. *Nat Neurosci*. 2004;7(5):446-451.

168. Priori A, Foffani G, Pesenti A, et al. Movement-related modulation of neural activity in human basal ganglia and its L-DOPA dependency: Recordings from deep brain stimulation electrodes in patients with Parkinson's disease. *Neurol Sci*. 2002;23(SUPPL. 2):S101-S102.

169. Marceglia S, Bianchi AM, Baselli G, et al. Interaction between rhythms in the human basal ganglia: Application of bispectral analysis to local field potentials. *IEEE Trans Neural Syst Rehabil Eng*. 2007;15(4):483-492.

170. Marceglia S, Fiorio M, Foffani G, et al. Modulation of beta oscillations in the subthalamic area during action observation in Parkinson's disease. *Neuroscience*. 2009;161(4):1027-1036.

171. Marceglia S, Foffani G, Bianchi AM, et al. Dopamine-dependent non-linear correlation between subthalamic rhythms in Parkinson's disease. *J Physiol*. 2006;571(3):579-591.

172. Rosa M, Marceglia S, Servello D, et al. Time dependent subthalamic local field potential changes after DBS surgery in Parkinson's disease. *Exp Neurol*. 2010;222(2):184-190.

173. Rossi L, Marceglia S, Foffani G, et al. Subthalamic local field potential oscillations during ongoing deep brain stimulation in Parkinson's disease. *Brain Res Bull*. 2008;76(5):512-521.

174. Foffani G, Bianchi AM, Baselli G, Priori A. Movement-related frequency modulation of beta oscillatory activity in the human subthalamic nucleus. *J Physiol*. 2005;568(2):699-711.

175. Yoshida F, Martinez-Torres I, Pogosyan A, et al. Value of subthalamic nucleus local field potentials recordings in predicting stimulation parameters for deep brain stimulation in Parkinson's disease. *J Neurol Neurosurg Psychiatry*. 2010;81(8):885-889.

176. Stanslaski S, Afshar P, Cong P, et al. Design and validation of a fully implantable, chronic, closed-loop neuromodulation device with concurrent sensing and stimulation. *IEEE Trans Neural Syst Rehabil Eng*. 2012;20(4):410-421.

177. Oostenveld R, Fries P, Maris E, Schoffelen JM. FieldTrip: Open source software for advanced analysis of MEG, EEG, and invasive electrophysiological data. *Comput Intell Neurosci*. 2011;2011.

178. Rodriguez-Oroz MC, Rodriguez M, Guridi J, et al. The subthalamic nucleus in Parkinson's disease: Somatotopic organization and physiological characteristics. *Brain*. 2001;124(9):1777-1790.

179. Hirschmann J, Özkurt TE, Butz M, et al. Distinct oscillatory STN-cortical loops revealed by simultaneous MEG and local field potential recordings in patients with Parkinson's disease. *Neuroimage*. 2011;55(3):1159-1168.

180. Litvak V, Jha A, Eusebio A, et al. Resting oscillatory cortico-subthalamic connectivity in patients with Parkinson's disease. *Brain*. 2011;134(2):359-374.

181. Zaidel A, Spivak A, Grieb B, Bergman H, Israel Z. Subthalamic span of β oscillations predicts deep brain stimulation efficacy for patients with Parkinson's disease. *Brain*. 2010;133(7):2007-2021.

182. Fogelson N, Williams D, Tijssen M, Van Bruggen G, Speelman H, Brown P. Different functional loops between cerebral cortex and the subthalmic area in parkinson's disease. *Cereb Cortex*. 2006;16(1):64-75.

183. Hirschmann J, Özkurt TE, Butz M, et al. Differential modulation of STN-cortical and cortico-muscular coherence by movement and levodopa in Parkinson's disease. *Neuroimage*. 2013;68:203-213.

184. Kühn AA, Kempf F, Brücke C, et al. High-frequency stimulation of the subthalamic nucleus suppresses oscillatory β activity in patients with Parkinson's disease in parallel with improvement in motor performance. *J Neurosci*. 2008;28(24):6165-6173.

185. Lindén H, Tetzlaff T, Potjans TC, et al. Modeling the spatial reach of the LFP. *Neuron*. 2011;72(5):859-872.

186. Anastassiou CA, Montgomery SM, Barahona M, Buzsáki G, Koch C. The effect of spatially inhomogeneous extracellular electric fields on neurons. *J Neurosci*. 2010;30(5):1925-1936.

187. Kajikawa Y, Schroeder CE. How local is the local field potential? *Neuron*. 2011;72(5):847-858.

188. Terman D, Rubin JE, Yew AC, Wilson CJ. Activity Patterns in a Model for the Subthalamopallidal Network of the Basal Ganglia. *J Neurosci*. 2002;22(7):2963-2976.

189. Ammari R, Lopez C, Bioulac B, Garcia L, Hammond C. Subthalamic nucleus evokes similar long lasting glutamatergic excitations in pallidal, entopeduncular and nigral neurons in the basal ganglia slice. *Neuroscience*. 2010;166(3):808-818.

190. Rosenbaum R, Zimnik A, Zheng F, et al. Axonal and synaptic failure suppress the transfer of firing rate oscillations, synchrony and information during high frequency deep brain stimulation. *Neurobiol Dis*. 2014;62:86-99.

191. Zheng F, Lammert K, Nixdorf-Bergweiler BE, Steigerwald F, Volkmann J, Alzheimer C. Axonal failure during high frequency stimulation of rat subthalamic nucleus. *J Physiol*. 2011;589(11):2781-2793.

192. Moran A, Stein E, Tischler H, Bar-Gad I. Decoupling neuronal oscillations during subthalamic nucleus stimulation in the parkinsonian primate. *Neurobiol Dis*. 2012;45(1):583-590.

193. Breit S, Schulz JB, Benabid AL. Deep brain stimulation. *Cell Tissue Res*. 2004;318(1):275-288.

194. Benabid AL. Deep brain stimulation for Parkinson's disease. *Curr Opin Neurobiol*. 2003;13(6):696-706.

195. Machado A, Rezai AR, Kopell BH, Gross RE, Sharan AD, Benabid AL. Deep brain stimulation for Parkinson's disease: Surgical technique and perioperative management. *Mov Disord*. 2006;21(SUPPL. 14):S247-S258.

196. Hamani C, Richter E, Schwalb JM, Lozano AM. Bilateral subthalamic nucleus stimulation for Parkinson's disease: A systematic review of the clinical literature. *Neurosurgery*. 2005;56(6):1313-1321.

197. Krack P, Batir A, Van Blercom N, et al. Five-Year Follow-up of Bilateral Stimulation of the Subthalamic Nucleus in Advanced Parkinson's Disease. *N Engl J Med*. 2003;349(20):1925-1934.

198. Okun MS, Tagliati M, Pourfar M, et al. Management of referred deep brain stimulation failures: A retrospective analysis from 2 Movement Disorders Centers. *Arch Neurol*. 2005;62(8):1250-1255.

199. Fitzpatrick JM, Konrad PE, Nickele C, Cetinkaya E, Kao C. Accuracy of customized miniature stereotactic platforms. *Stereotact Funct Neurosurg*. 2005;83(1):25-31.

200. Zylka W, Sabczynski J, Schmitz G. A Gaussian approach for the calculation of the accuracy of stereotactic frame systems. *Med Phys*. 1999;26(3):381-391.

201. McIntyre CC, Mori S, Sherman DL, Thakor N V., Vitek JL. Electric field and stimulating influence generated by deep brain stimulation of the subthalamic nucleus. *Clin Neurophysiol*. 2004;115(3):589-595.

202. Miocinovic S, Parent M, Butson CR, et al. Computational analysis of subthalamic nucleus and lenticular fasciculus activation during therapeutic deep brain stimulation. *J Neurophysiol*. 2006;96(3):1569-1580.

203. Li S, Arbuthnott GW, Jutras MJ, Goldberg JA, Jaeger D. Resonant antidromic cortical circuit activation as a consequence of high-frequency subthalamic deep-brain stimulation. *J Neurophysiol*. 2007;98(6):3525-3537.

204. Frankemolle AMM, Wu J, Noecker AM, et al. Reversing cognitive-motor impairments in Parkinson's disease patients using a computational modelling approach to

deep brain stimulation programming. *Brain*. 2010;133(3):746-761.

205. Funkiewiez A, Ardouin C, Krack P, et al. Acute psychotropic effects of bilateral subthalamic nucleus stimulation and Levodopa in Parkinson's disease. *Mov Disord*. 2003;18(5):524-530.

206. Krack P, Fraix V, Mendes A, Benabid AL, Pollak P. Postoperative management of subthalamic nucleus stimulation for parkinson's disease. *Mov Disord*. 2002;17(SUPPL. 3):S188-S197.

207. Tamma F, Caputo E, Chiesa V, et al. Anatomo-clinical correlation of intraoperative stimulation-induced side-effects during HF-DBS of the subthalamic nucleus. *Neurol Sci*. 2002;23(SUPPL. 2):S109-S110.

208. Willsie A, Dorval AD. Charge steering in a novel DBS electrode may accommodate surgical targeting errors. *Int IEEE/EMBS Conf Neural Eng NER*. Published online 2013:152-153.

209. Keane M, Deyo S, Abosch A, Bajwa JA, Johnson MD. Improved spatial targeting with directionally segmented deep brain stimulation leads for treating essential tremor. *J Neural Eng*. 2012;9(4).

210. Aström M, Lemaire JJ, Wardell K. Influence of heterogeneous and anisotropic tissue conductivity on electric field distribution in deep brain stimulation. *Med Biol Eng Comput*. 2012;50(1):23-32.

211. Chaturvedi A, Butson CR, Lempka SF, Cooper SE, McIntyre CC. Patient-specific models of deep brain stimulation: Influence of field model complexity on neural activation predictions. *Brain Stimul*. 2010;3(2):65-77.

212. Butson CR, McIntyre CC. Tissue and electrode capacitance reduce neural activation volumes during deep brain stimulation. *Clin Neurophysiol*. 2005;116(10):2490-2500.

213. Butson CR, McIntyre CC. Role of electrode design on the volume of tissue activated during deep brain stimulation. *J Neural Eng*. 2006;3(1):1-8.

214. Chaturvedi A, Foutz TJ, McIntyre CC. Current steering to activate targeted neural pathways during deep brain stimulation of the subthalamic region. *Brain Stimul*. 2012;5(3):369-377.

215. Wakana S, Jiang H, Nagae-Poetscher LM, Van Zijl PCM, Mori S. Fiber Tract-based Atlas of Human White Matter Anatomy. *Radiology*. 2004;230(1):77-87.

216. Tuch DS, Wedeen VJ, Dale AM, George JS, Belliveau JW. Conductivity tensor mapping of the human brain using diffusion tensor MRI. *Proc Natl Acad Sci U S A*. 2001;98(20):11697-11701.

217. Hines ML, Carnevale NT. The NEURON Simulation Environment. *Neural Comput*. 1997;9(6):1179-1209.

218. Sato F, Parent M, Levesque M, Parent A. Axonal branching pattern of neurons of the subthalamic nucleus in primates. *J Comp Neurol*. 2000;424(1):142-152.

219. Parent M, Parent A. The pallidofugal motor fiber system in primates. *Park Relat Disord*. 2004;10(4):203-211.

220. McIntyre CC, Richardson AG, Grill WM. Modeling the excitability of mammalian nerve fibers: Influence of afterpotentials on the recovery cycle. *J Neurophysiol*. 2002;87(2):995-1006.

221. Janssen MLF, Zwartjes DGM, Temel Y, et al. Subthalamic neuronal responses to cortical stimulation. *Mov Disord*. 2012;27(3):435-438.

222. Xu W, Miocinovic S, Zhang J, Baker KB, McIntyre CC, Vitek JL. Dissociation of motor symptoms during deep brain stimulation of the subthalamic nucleus in the region of the internal capsule. *Exp Neurol*. 2011;228(2):294-297.

223. Mathai A, Wichmann T, Smith Y. More than meets the eye-myelinated axons crowd the subthalamic nucleus. *Mov Disord*. 2013;28(13):1811-1815.

224. Rossi PJ, Gunduz A, Judy J, et al. Proceedings of the Third Annual Deep Brain Stimulation Think Tank: A Review of

Emerging Issues and Technologies . *Front Neurosci* . 2016;10:119.

225. Tass PA. A model of desynchronizing deep brain stimulation with a demand-controlled coordinated reset of neural subpopulations. *Biol Cybern*. 2003;89(2):81-88.
226. Rosin B, Slovik M, Mitelman R, et al. Closed-loop deep brain stimulation is superior in ameliorating parkinsonism. *Neuron*. 2011;72(2):370-384.
227. Timmermann L, Jain R, Chen L, et al. Multiple-source current steering in subthalamic nucleus deep brain stimulation for Parkinson's disease (the VANTAGE study): A non-randomised, prospective, multicentre, open-label study. *Lancet Neurol*. 2015;14(7):693-701.
228. Willsie AC, Dorval AD. Computational field shaping for deep brain stimulation with thousands of contacts in a novel electrode geometry. *Neuromodulation*. 2015;18(7):542-550.
229. Steigerwald F, Müller L, Johannes S, Matthies C, Volkmann J. Directional deep brain stimulation of the subthalamic nucleus: A pilot study using a novel neurostimulation device. *Mov Disord*. 2016;31(8):1240-1243.
230. Barbe MT, Maarouf M, Alesch F, Timmermann L. Multiple source current steering - a novel deep brain stimulation concept forcustomized programming in a Parkinson's disease patient. *Park Relat Disord*. 2014;20(4):471-473.
231. Teplitzky BA, Zitella LM, Xiao YZ, Johnson MD. Model-based comparison of deep brain stimulation array functionality with varying number of radial electrodes and machine learning feature sets. *Front Comput Neurosci*. 2016;10(JUN):58.
232. Alonso F, Latorre MA, Göransson N, Zsigmond P, Wårdell K. Investigation into deep brain stimulation lead designs: A patient-specific simulation study. *Brain Sci*. 2016;6(3).
233. Buhlmann J, Hofmann L, Tass PA, Hauptmanna C. Modeling of a segmented electrode for desynchronizing deep brain stimulation. *Front Neuroeng*. 2011;4(NOVEMBER):15.
234. Van Dijk KJ, Verhagen R, Chaturvedi A, et al. A novel lead design enables selective deep brain stimulation of neural populations in the subthalamic region. *J Neural Eng*. 2015;12(4):46003.
235. Butson CR, McIntyre CC. Current steering to control the volume of tissue activated during deep brain stimulation. *Brain Stimul*. 2008;1(1):7-15.
236. Waln O, Jimenez-Shahed J. Rechargeable deep brain stimulation implantable pulse generators in movement disorders: Patient satisfaction and conversion parameters. *Neuromodulation*. 2014;17(5):425-430.
237. Timmermann L, Schüpbach M, Hertel F, et al. A new rechargeable device for deep brain stimulation: A prospective patient satisfaction survey. *Eur Neurol*. 2013;69(4):193-199.
238. Peña E, Zhang S, Deyo S, Xiao Y, Johnson MD. Particle swarm optimization for programming deep brain stimulation arrays. *J Neural Eng*. 2017;14(1):16014.
239. Frequin HL, Bot M, Dilai J, et al. Relative Contribution of Magnetic Resonance Imaging, Microelectrode Recordings, and Awake Test Stimulation in Final Lead Placement during Deep Brain Stimulation Surgery of the Subthalamic Nucleus in Parkinson's Disease. *Stereotact Funct Neurosurg*. 2020;98(2):118-128.
240. Contarino MF, Brinke TRT, Mosch A, et al. How Many Patients would Benefit from Steering Technology for Deep Brain Stimulation? *Brain Stimul*. 2016;9(1):144-145.
241. Akram H, Georgiev D, Mahlknecht P, et al. Subthalamic deep brain stimulation sweet spots and hyperdirect cortical connectivity in Parkinson's disease. *Neuroimage*. 2017;158:332-345.
242. Haynes WIA, Haber SN. The organization of prefrontal-subthalamic inputs in primates

provides an anatomical substrate for both functional specificity and integration: Implications for basal ganglia models and deep brain stimulation. *J Neurosci*. 2013;33(11):4804-4814.

243. Bot M, Verhagen O, Caan M, et al. Defining the Dorsal STN Border Using 7.0-T MRI: A Comparison to Microelectrode Recordings and Lower Field Strength MRI. *Stereotact Funct Neurosurg*. 2019;97(3):153-159.

244. Holewijn RA, Bot M, van den Munckhof P, Richard Schuurman P. Implementation of intraoperative cone-beam computed tomography (O-arm) for stereotactic imaging during deep brain stimulation procedures. *Oper Neurosurg*. 2020;19(3):E224-E229.

Summary

Subthalamic deep brain stimulation for advanced Parkinson's disease

Optimizing localization and stimulation of the target area

Parkinson's disease is a neurodegenerative disorder of the central nervous system, caused by degeneration of dopamine-producing cells in the deep nuclei of the brain. It is characterized mainly by motor symptoms bradykinesia, rigidity, and tremor. In a later stage, disturbances of gait and non-motor symptoms like cognitive decline and autonomic dysfunction also occur. When first-line treatment with dopaminergic medication becomes less effective as the disease progresses, patients often develop medication-induced motor response fluctuations, an on-off pattern, and additional dyskinesias. When changes in medication can no longer sufficiently improve these fluctuations, deep brain stimulation (DBS) is a possible surgical treatment. In DBS, electrodes are permanently implanted in the basal ganglia, the deep nuclei of the brain. These electrodes continuously stimulate a selected target, which can alleviate the motor symptoms of Parkinson's disease.

Chapter 1 provides an introduction of this thesis, where the DBS techniques used in our center and the preferred target for stimulation are described. Although different target areas for stimulation can be chosen, previous research in our center showed that DBS of the subthalamic nucleus (STN) provides superior symptomatic improvement in the off-phase. Therefore, this thesis focuses on stimulation within the STN. It further describes the aims of this thesis, of which the first part focuses on the identification of the STN, before and during DBS surgery with conventionally used surgical techniques. The second part describes how the identification and stimulation of the STN might be further finetuned using a technological development in electrode design, i.e., the steering DBS electrode.

During preoperative planning of the surgical procedure, the STN can be identified using T2-weighted MRI images. Intraoperatively, the nucleus can be identified by the spiking activity of local neurons measured with microelectrode recordings (MER). However, the electrophysiological STN, measured with MER, does not always correspond with the STN seen on MRI images and different MRI field strengths might show the STN differently. In **chapter 2**, we compared the STN borders seen on T2-MRI images of different field strengths with those estimated by MER. For this, we developed a method that automatically generates a detailed estimation of STN shape and size based on multiple-channel MER measurements. We found that the dorsal border of the STN was identified more dorsally on MRI than it was by MER. The lateral border was identified more medial on 1.5 Tesla and 3.0 Tesla MRI compared to MER. In 7.0 Tesla MRI we found

a better correspondence with the MER-based STN at the lateral border. Although 7.0 Tesla MRI does not provide additional benefit compared to 3.0 Tesla MRI in identification of the dorsal STN border, it could improve identification of the lateral border of the STN and thereby improve DBS targeting.

Within the STN, the dorsolateral part is the preferred target because of its sensorimotor connections. In **chapter 3** we investigated how intraoperative measurements can help identify this area. Through simultaneous recordings of local field potentials (LFP) and MER, we studied the temporal relationship between local neuronal spiking and more global beta oscillations (12 – 35 Hz) in the LFP. Due to volume conduction of the LFP, localization of the sensorimotor STN with only LFP recordings is difficult. However, calculating beta power specifically at the frequencies of the LFP spectrum which are coherent with MER, showed to be beneficial in discriminating the sensorimotor part of the STN. This method could be helpful in analyzing the neuronal activity at the preferred target with only minor changes in the standard surgical procedure. However, it remains vulnerable to inaccuracies. Although differences on a group level could be found, the method was not discriminative enough at a patient level, and is therefore not suitable for intraoperative identification of the sensorimotor STN.

Chapter 4 narrows down on the preferred target in a more detailed way. Even within the sensorimotor part of the STN a more specific target may be defined. Therefore, we studied the relation between the location of the active contact and motor improvement one year after surgery. The contact location was identified with CT and expressed relative to the MER-based STN, described in chapter 2. This way, we found a significant relation between active contact location and motor improvement, in which the mediolateral location of the active contact was the greatest predictor of motor improvement. A more laterally placed electrode predicted more motor improvement one year after surgery. From these results, a theoretical hotspot for STN-DBS could be defined at 1.9 mm lateral, 0.9 mm anterior, and 2.6 mm dorsal to the center of the MER-based STN.

In the second part of this thesis, we investigated how identification and stimulation of the target might be further finetuned with the permanent DBS electrode in place. **Chapter 5** describes how a novel steering DBS electrode with 32 multidirectional contacts could modulate the thresholds for beneficial and side effects of stimulation, thereby increasing the therapeutic window with up to 1.5 mA. We found that directional steering of current could increase the threshold for side effects compared to spherical stimulation in almost all cases, potentially improving the effectiveness of DBS. Moreover, measurement of LFP with this novel electrode was found to provide insight into the local oscillatory activity within the STN.

Chapter 6 further explores the potential of multidirectional LFP recordings with this novel steering electrode and investigates the effect of directional stimulation on the LFP oscillations. With simultaneous recordings at different depths, we found that an increase in beta oscillations at the dorsal border of the STN could be measured with the electrode in place. The power of pathological beta oscillations was found to differ when measuring in different directions. The direction with greatest (high) beta (18.5 – 30 Hz) power corresponded with the direction in which stimulation caused greatest motor improvement, where this could be measured. Both beta and gamma LFP oscillations reacted differently to stimulations in different directions. This indicates that multidirectional LFP recordings have the potential to improve the efficiency of DBS by providing confirmation of adequate electrode placement and directional information on physiological and pathological oscillations within the STN.

In chapter 7 and 8, we used a computational modelling approach to compare the effectiveness of cylindrical and steering electrodes. We compared how, with optimized stimulation parameters, they could maximize STN activation without activating fibers of the internal capsule which can potentially cause side effects. We modelled electrodes placed in the center of the STN and in two more lateral positions (1 mm and 2 mm). In **chapter 7**, we studied a steering electrode similar to the one used in chapter 5 and 6, with 40 multidirectional contacts. In all positions, by directional stimulation, this electrode was able to activate more of the STN, compared to the cylindrical electrode. At the more lateral positions, the difference in STN activation between the two electrode types increased in favor of the steering electrode. This indicates that the use of a steering electrode might be favorable compared to the cylindrical electrode, especially in the more lateral positions.

In **chapter 8** the same modeling approach was applied to another steering electrode design, which has less degrees of freedom, i.e., eight contacts of which six are multidirectional, but which is commercially available and can be used in clinical practice. This design has two segmented levels consisting of three separate contacts, enclosed by a cylindrical dorsal and ventral contact. Comparing this electrode with the fully cylindrical electrode, we found similar benefits of directional stimulation in the central and the 1 mm more lateral position. However, the amount of benefit was dependent on the rotation of the steering electrode around its longitudinal axis. In the 2 mm more lateral position, this steering electrode showed no benefit over to the cylindrical electrode. When rotation could be prevented or controlled, this steering electrode type could be beneficial, especially in a 1 mm more lateral position. In a position 2 mm lateral from central, this electrode seems less beneficial than the theoretical 40-contact steering electrode of chapter 7.

Chapter 9 provides a general discussion where the variable topics of this thesis are connected and evaluated. We conclude that a continuous effort should be made to

critically review DBS targeting considering the evolving clinical and technological possibilities. We argue that targeting and steering stimulation are inseparable in optimizing DBS results. When targeting is inaccurate, steering stimulation might compensate for some of the lost potential benefit. However, the current preoperative planning with high field MRI and verification by intraoperative measurements and imaging make the targeting so accurate that it could perhaps be adapted specifically to the steering electrode. This thesis suggests that the full potential of steering electrodes could possibly be unleashed by targeting more specifically aimed at the dorsolateral motor segment of the STN.

Samenvatting

Subthalamische diepe hersenstimulatie voor gevorderde ziekte van Parkinson

Optimalisatie van lokalisatie en stimulatie van het doelgebied

De ziekte van Parkinson is een neurodegeneratieve aandoening van het centrale zenuwstelsel, veroorzaakt door degeneratie van dopamine-producerende cellen in de diepe hersenkernen. Het wordt voornamelijk gekenmerkt door motorische symptomen, bradykinesie, rigiditeit en tremor. In een later stadium treden ook loopstoornissen en niet-motorische symptomen op, zoals cognitieve achteruitgang en autonome disfunctie. Wanneer eerstelijnsbehandeling met dopaminerge medicatie minder effectief wordt naarmate de ziekte vordert, ontwikkelen patiënten vaak door medicatie geïnduceerde motorische responsfluctuaties, een on-off patroon, en bijkomende dyskinesieën. Wanneer veranderingen in medicatie deze fluctuaties niet meer voldoende kunnen verbeteren, is diepe hersenstimulatie (DBS) een mogelijke chirurgische behandeling. Bij DBS worden elektroden permanent geïmplanteerd in de basale ganglia, de diepe hersenkernen. Deze elektroden stimuleren continu een geselecteerd doelwit, wat de motorische symptomen van de ziekte van Parkinson kan verlichten.

Hoofdstuk 1 geeft een inleiding op dit proefschrift, waarin de DBS-technieken die in ons centrum worden gebruikt en het voorkeursdoelwit voor stimulatie worden beschreven. Hoewel verschillende doelgebieden voor stimulatie kunnen worden gekozen, toonde eerder onderzoek in ons centrum aan dat DBS van de subthalamische nucleus (STN) superieure symptomatische verbetering biedt in de off-fase. Daarom richt dit proefschrift zich op stimulatie binnen de STN. Het beschrijft verder de doelstellingen van dit proefschrift, waarvan het eerste deel zich richt op de identificatie van de STN, voor en tijdens DBS-chirurgie met conventioneel gebruikte chirurgische technieken. Het tweede deel beschrijft hoe de identificatie en stimulatie van de STN verder kan worden verfijnd met behulp van een technologische ontwikkeling in elektrodeontwerp, d.w.z. de sturende DBS-elektrode.

Tijdens de preoperatieve planning van de chirurgische ingreep kan de STN worden geïdentificeerd met behulp van T2-gewogen MRI-beelden. Intraoperatief kan de nucleus worden geïdentificeerd door de spiking-activiteit van lokale neuronen gemeten met micro-elektrode opnames (MER). De elektrofysiologische STN, gemeten met MER, komt echter niet altijd overeen met de STN die wordt gezien op MRI-beelden en verschillende MRI-veldsterkten kunnen de STN anders weergeven. In **hoofdstuk 2** vergeleken we de STN-grenzen die te zien zijn op T2-MRI-beelden van verschillende veldsterkten met de grenzen geschat door MER. Hiervoor hebben we een methode

ontwikkeld die automatisch een gedetailleerde schatting van STN-vorm en -grootte genereert op basis van meerkanaals MER-metingen. We ontdekten dat de dorsale grens van de STN meer dorsaal werd geïdentificeerd op MRI dan door MER. De laterale grens werd meer mediaal geïdentificeerd op 1,5 Tesla en 3,0 Tesla MRI in vergelijking met MER. In 7,0 Tesla MRI vonden we een betere overeenkomst met de op MER gebaseerde STN aan de laterale grens. Hoewel MRI van 7,0 Tesla geen extra voordeel biedt in vergelijking met MRI van 3,0 Tesla bij de identificatie van de dorsale STN-grens, zou het de identificatie van de laterale grens van de STN kunnen verbeteren en daardoor de DBS-targeting kunnen verbeteren.

Binnen de STN is het dorsolaterale deel het voorkeursdoelwit vanwege zijn sensomotorische verbindingen. In **hoofdstuk 3** hebben we onderzocht hoe intraoperatieve metingen kunnen helpen bij het identificeren van dit gebied. Door gelijktijdige opnames van lokale veldpotentialen (LFP) en MER, hebben we de temporele relatie tussen lokale neuronale spiking-activiteit en meer globale bèta-oscillaties (12 – 35 Hz) in de LFP bestudeerd. Vanwege volumegeleiding van de LFP is lokalisatie van de sensomotorische STN met alleen LFP-opnames moeilijk. Het berekenen van bèta power specifiek in de frequenties van het LFP-spectrum die coherent zijn met MER, bleek echter behulpzaam te zijn bij het onderscheiden van het sensomotorische deel van de STN. Deze methode kan nuttig zijn bij het analyseren van de neuronale activiteit op het gewenste doelwit met slechts kleine veranderingen in de standaard chirurgische procedure. Het blijft echter kwetsbaar voor onnauwkeurigheden. Hoewel er verschillen op groepsniveau konden worden gevonden, was de methode niet discriminerend genoeg op patiëntniveau en daarom niet geschikt voor intraoperatieve identificatie van de sensomotorische STN.

Hoofdstuk 4 concentreert zich op een meer gedetailleerde manier tot het voorkeursdoelwit. Zelfs binnen het sensomotorische deel van de STN kan een specifieker doelwit worden gedefinieerd. Daarom hebben we de relatie tussen de locatie van het actieve contactpunt en de motorische verbetering een jaar na de operatie onderzocht. De contactpuntlocatie werd geïdentificeerd met CT en uitgedrukt ten opzichte van de op MER gebaseerde STN, beschreven in hoofdstuk 2. Op deze manier vonden we een significante relatie tussen actieve contactpuntlocatie en motorische verbetering, waarbij de mediolaterale locatie van het actieve contactpunt de grootste voorspeller van motorische verbetering was. Een meer lateraal geplaatste elektrode voorspelde meer motorische verbetering een jaar na de operatie. Op basis van deze resultaten kon een theoretische hotspot voor STN-DBS worden gedefinieerd op 1,9 mm lateraal, 0,9 mm anterieur en 2,6 mm dorsaal ten opzichte van het midden van de op MER gebaseerde STN.

In het tweede deel van dit proefschrift hebben we onderzocht hoe identificatie en stimulatie van het doelwit verder kan worden verfijnd met de permanente DBS-

elektrode op zijn plaats. **Hoofdstuk 5** beschrijft hoe een nieuwe sturende DBS-elektrode met 32 multidirectionele contactpunten de drempels voor verbeteringen en bijwerkingen van stimulatie zou kunnen moduleren, waardoor het therapeutische venster met tot 1,5 mA kan worden vergroot. We ontdekten dat directionele sturing van stroom de drempel voor bijwerkingen in bijna alle gevallen zou kunnen verhogen in vergelijking met sferische stimulatie, wat mogelijk de effectiviteit van DBS zou kunnen verbeteren. Bovendien bleek het meten van LFP met deze nieuwe elektrode inzicht te geven in de lokale oscillerende activiteit binnen de STN.

Hoofdstuk 6 kijkt verder naar het potentieel van multidirectionele LFP-opnames met deze nieuwe sturende elektrode en onderzoekt het effect van directionele stimulatie op de LFP-oscillaties. Met gelijktijdige opnames op verschillende diepten, ontdekten we dat een toename van bèta-oscillaties aan de dorsale grens van de STN kon worden gemeten met de elektrode op zijn plaats. De power van pathologische bèta-oscillaties bleek te verschillen bij metingen in verschillende richtingen. De richting met de grootste (hoge) bèta power (18,5 – 30 Hz) kwam overeen met de richting waarin stimulatie de grootste motorische verbetering veroorzaakte, waar dit kon worden gemeten. Zowel bèta- als gamma-LFP-oscillaties reageerden anders op stimulaties in verschillende richtingen. Dit geeft aan dat multidirectionele LFP-opnames de potentie hebben om de efficiëntie van DBS te verbeteren door bevestiging van adequate elektrodeplaatsing en directionele informatie over fysiologische en pathologische oscillaties binnen de STN.

In hoofdstuk 7 en 8 hebben we een computationele modelleringsbenadering gebruikt om de effectiviteit van cilindrische en sturende elektroden te vergelijken. We vergeleken hoe ze, met geoptimaliseerde stimulatieparameters, STN-activering konden maximaliseren zonder vezels van de capsula interna te activeren die mogelijk bijwerkingen kunnen veroorzaken. We hebben elektroden gemodelleerd die in het midden van de STN zijn geplaatst en in twee meer laterale posities (1 mm en 2 mm). In **hoofdstuk 7** hebben we een sturende elektrode bestudeerd, vergelijkbaar met die gebruikt in hoofdstuk 5 en 6, met 40 multidirectionele contactpunten. In alle posities kon deze elektrode door sturende stimulatie meer van de STN activeren in vergelijking met de cilindrische elektrode. Op de meer laterale posities nam het verschil in STN-activering tussen de twee elektrodetypen toe in het voordeel van de sturende elektrode. Dit geeft aan dat het gebruik van een sturende elektrode gunstig kan zijn in vergelijking met de cilindrische elektrode, vooral in de meer laterale posities.

In **Hoofdstuk 8** werd dezelfde modelleringsbenadering toegepast op een ander ontwerp van de sturende elektrode, dat minder vrijheidsgraden heeft, d.w.z. acht contactpunten waarvan zes multidirectioneel, maar die commercieel verkrijgbaar is en in de klinische praktijk kan worden gebruikt. Dit ontwerp heeft twee gesegmenteerde niveaus bestaande uit drie afzonderlijke contactpunten, omsloten door een cilindrisch

dorsaal en ventraal contactpunt. Door deze elektrode te vergelijken met de volledig cilindrische elektrode, vonden we vergelijkbare voordelen van directionele stimulatie in de centrale en de 1 mm meer laterale positie. De hoeveelheid voordeel was echter afhankelijk van de rotatie van de sturende elektrode rond zijn lengteas. In de 2 mm meer laterale positie vertoonde deze sturende elektrode geen voordeel ten opzichte van de cilindrische elektrode. Wanneer rotatie kan worden voorkomen of gecontroleerd, kan dit type sturende elektrode gunstig zijn, vooral in een 1 mm meer laterale positie. In een positie 2 mm lateraal van het midden lijkt deze elektrode minder gunstig dan de theoretische sturende elektrode met 40 contactpunten van hoofdstuk 7.

Hoofdstuk 9 geeft een algemene discussie waarin de variabele onderwerpen van dit proefschrift met elkaar verbonden en geëvalueerd worden. We concluderen dat er een voortdurende inspanning moet worden geleverd om DBS-targeting kritisch te beoordelen, rekening houdend met de evoluerende klinische en technologische mogelijkheden. We stellen dat targeting en sturende stimulatie onlosmakelijk met elkaar verbonden zijn bij het optimaliseren van DBS-resultaten. Wanneer targeting onnauwkeurig is, kan sturende stimulatie een deel van het verloren potentiële voordeel compenseren. De huidige preoperatieve planning met MRI met hoge veldsterkte en verificatie door intraoperatieve metingen en beeldvorming maken de targeting echter zo nauwkeurig dat deze misschien specifiek op de sturende elektrode kan worden aangepast. Dit proefschrift suggereert dat het volledige potentieel van sturende elektroden mogelijk zou kunnen worden ontketend door specifiek meer te targetten op het dorsolaterale motorsegment van de STN.

APPENDICES

Curriculum Vitae

PhD portfolio

List of publications

Dankwoord

Abbreviations

Curriculum Vitae

Rens Verhagen was born on Saturday September 20th, 1986 in Geldrop, Noord-Brabant, the Netherlands. In 2004 he graduated cum laude from secondary school at Scholengemeenschap Augustinianum (VWO + gymnasium) and thereafter started his bachelor's study Technische Geneeskunde at the University of Twente in Enschede. Finishing his bachelor's degree in 2007 with a neuroscientific thesis on mirror neurons, he continued his master's study in Technical Medicine – Medical Signaling at the same university, with an emphasis on the measurement and stimulation of the various signals of the human body. After taking a gap year for travelling in 2008 – 2009 he started his clinical internships and became more and more interested in the field of neuroscience during an internship at the department of Clinical Neurophysiology of the Medisch Spectrum Twente hospital in Enschede. In February 2012, he finished his master's degree with a yearlong clinical internship at the same department and the resulting neuroscientific thesis on event-related desynchronization in acute stroke patients.

In March 2012, Rens assumed a clinical researcher position at the department of Clinical Neurophysiology of the Academic Medical Center in Amsterdam, in the field of deep brain stimulation for Parkinson's disease, under the supervision of dr. ir. L.J. Bour, dr. M.F. Contarino. He was captivated by the patient population, the clinical considerations, and the technological possibilities of the implantable medical devices used. His interest in the implantable technology further increased during a close cooperation with Sapiens Steering Brain Stimulation in Eindhoven.

Soon after, he started his PhD project at the departments of Neurology, Clinical Neurophysiology and Neurosurgery of the Academic Medical Center in Amsterdam on the same subject under the supervision of dr. ir. L.J. Bour, prof. dr. I.N. van Schaik, and prof. dr. P.R. Schuurman. The project was a collaboration with the Biomedical Signals and Systems research group from the MIRA institute for Biomedical Engineering and Technical Medicine at the University of Twente, working closely together with fellow PhD student Kees van Dijk, supervised by dr. ir. T. Heida and prof. dr. ir. P.H. Veltink. In 2013, Rens travelled to Cleveland, Ohio, for a course on DBS computer models at the department of Biomedical Engineering of Case Western Reserve University, under the supervision of prof. C.C. McIntyre.

Since March 2017, Rens works for MED-EL Medical Electronics, a global innovation leader in medical device industry, where he further explores the field of implantable medical technology for hearing loss and other applications. Starting as a clinical engineer, he is now clinical technical manager of the Netherlands and heads a small team overseeing the Dutch branch of this global company. He works together with all seven university hospitals, and other clinics, in the Netherlands to enable both the day-to-day clinical application of these devices as well as the collaborations to perform scientific research on these devices.

PhD portfolio

Name PhD student:	Rens Verhagen
PhD period:	March 2012 – April 2022
Promotores:	prof. dr. P.R. Schuurman and prof. dr. I.N. van Schaik
Copromotores:	dr. ir. L.J. Bour and dr. ir. T. Heida

1. PhD training

	Year	ECTS
General courses		
The AMC World of Science – Graduate School, UvA, Amsterdam	2013	0.7
Clinical Epidemiology – Graduate School, UvA, Amsterdam	2013	0.7
Practical Biostatistics – Graduate School, UvA, Amsterdam	2013	1.1
Systematic Reviews – Graduate School, UvA, Amsterdam	2013	0.7
BROK Legislation and Organization for Clinical Researchers – NFU/ UvA, Amsterdam	2013	1.5
Scientific Writing in English for Publication – Graduate School, UvA, Amsterdam	2014	1.5
Advanced Topics in Biostatistics – Graduate School, UvA, Amsterdam	2014	2.1
Oral Presentation in English – Graduate School, UvA, Amsterdam	2015	0.8
Specific courses		
DBS computer modelling: Three-dimensional finite element electric field models and multicompartment cable models of neural populations – Department of Biomedical Engineering, Case Western Reserve University, Cleveland, OH, USA	2013	2.0
Seminars, workshops, and master classes		
Seminar 'Speeding up Matlab and handling large data sets' – The Mathworks Inc., Zoetermeer	2012	0.1
Seminar on Clinical Neurophysiology Technology – Department of Clinical Neurophysiology, UMCG, Groningen	2013	0.1
Seminar on new developments in the field of DBS – Department of Applied Mathematics, University of Twente, Enschede	2013	0.1

PhD workshop on "Who wrote my paper" by dr. Drummond Rennie – Graduate School, UvA, Amsterdam	2013	0.1
The Symposium for the Retirement of dr. ir. L.J. Bour	2014	0.3
Weekly clinical seminars – Department of Neurology, AMC, Amsterdam	2012-2016	1.5

Presentations		
Poster presentation at The Movement Disorder Society's 16th International Congress of Parkinson's Disease and Movement Disorders	2012	0.5
Poster presentation at The Movement Disorder Society's 17th International Congress of Parkinson's Disease and Movement Disorders	2013	0.5
Oral presentation "Quantified objective assessment of deep brain stimulation for Parkinson's Disease" at The Symposium for the Retirement of dr. ir. L.J. Bour	2014	0.5
Poster presentation at the German Society for Clinical Neurophysiology and Functional Imaging's 30th International Congress of Clinical Neurophysiology	2014	0.5
Poster presentation at The Movement Disorder Society's 18th International Congress of Parkinson's Disease and Movement Disorders	2014	0.5
Poster presentation at The Movement Disorder Society's 19th International Congress of Parkinson's Disease and Movement Disorders	2015	0.5
Poster presentation at The European Society for Stereotactic and Functional Neurosurgery's 22nd Congress of the European Society for Stereotactic and Functional Neurosurgery	2016	0.5

(Inter)national conferences		
The Movement Disorder Society's 16th International Congress of Parkinson's Disease and Movement Disorders, Dublin, Ireland	2012	1.3
The Movement Disorder Society's 17th International Congress of Parkinson's Disease and Movement Disorders, Sydney, Australia	2013	1.3
Nederlandse Vereniging voor Technische Geneeskunde, 4th National Scientific Congress, Utrecht	2013	0.3

German Society for Clinical Neurophysiology and Functional Imaging's 30th International Congress of Clinical Neurophysiology, Berlin, Germany	2014	1.0
Nederlandse Vereniging voor Technische Geneeskunde, 5th National Scientific Congress, Utrecht	2014	0.3
The Movement Disorder Society's 18th International Congress of Parkinson's Disease and Movement Disorders, Stockholm, Sweden	2014	1.3
The Movement Disorder Society's 19th International Congress of Parkinson's Disease and Movement Disorders, San Diego, CA, USA	2015	1.3
The European Society for Stereotactic and Functional Neurosurgery's 22nd Congress of the European Society for Stereotactic and Functional Neurosurgery, Madrid, Spain	2016	1.0

Other		
Weekly video sessions – Department of Movement Disorders, AMC, Amsterdam	2012-2016	1.0
Journal club – Department of Movement Disorders, AMC, Amsterdam	2012-2016	1.0

2. Teaching

	Year	**ECTS**
Tutoring, Mentoring		
Clinical tutoring of bachelor's degree student Electrical Engineering	2014	1.0
Clinical tutoring of master's degree student Electrical Engineering	2014-2015	2.0
Supervising		
Assessment of thesis and colloquium of bachelor's degree student Electrical Engineering	2014	0.5
Assessment of thesis and colloquium of master's degree student Electrical Engineering	2015	0.5

3. Parameters of Esteem

	Year
Grants	
German Society for Clinical Neurophysiology and Functional Imaging – travel grant	2014

List of publications

Publications in this thesis and author contributions

Verhagen R, Schuurman PR, van den Munckhof P, Contarino MF, de Bie RM, Bour LJ. Comparative study of microelectrode recording-based STN location and MRI-based STN location in low to ultra-high field (7.0 T) T2-weighted MRI images. J Neural Eng. 2016 Dec;13(6):066009.

Conceptualization, R.V., L.B., P.v.d.M., and P.S.; Formal analysis, R.V.; Investigation, R.V., L.B., M.C., P.v.d.M., P.S., and R.d.B.; Methodology, R.V., P.v.d.M., P.S., and L.B.; Supervision, L.B., P.S., and R.d.B.; Visualization, R.V.; Writing—original draft, R.V.; Writing—review & editing, R.V., L.B., M.C, P.v.d.M., P.S., and R.d.B.

Verhagen R, Zwartjes DG, Heida T, Wiegers EC, Contarino MF, de Bie RM, van den Munckhof P, Schuurman PR, Veltink PH, Bour LJ. Advanced target identification in STN-DBS with beta power of combined local field potentials and spiking activity. J Neurosci Methods. 2015 Sep 30;253:116-25.

Conceptualization, L.B., T.H., D.Z., R.V., P.v.d.M., R.d.B., and P.S.; Formal analysis, R.V., D.Z. and E.W.; Investigation, R.V., D.Z., L.B., M.C., P.v.d.M., R.d.B., and P.S.; Methodology, L.B., T.H., D.Z., R.V., and E.W.; Supervision, L.B., P.S., P.V., and R.d.B.; Visualization, R.V.; Writing—original draft, R.V.; Writing—review & editing, R.V., D.Z., E.V., L.B., T.H., P.V., M.C., P.v.d.M., R.d.B., and P.S.

Verhagen R, Bour LJ, Odekerken VJJ, van den Munckhof P, Schuurman PR, de Bie RMA. Electrode Location in a Microelectrode Recording-Based Model of the Subthalamic Nucleus Can Predict Motor Improvement After Deep Brain Stimulation for Parkinson's Disease. Brain Sci. 2019 Mar 1;9(3):51.

Conceptualization, R.V., L.B., P.v.d.M., and P.S.; Formal analysis, R.V.; Investigation, R.V., L.B., V.O., P.v.d.M., P.S., and R.d.B.; Methodology, R.V. and L.B.; Supervision, L.B., P.S., and R.d.B.; Visualization, R.V.; Writing—original draft, R.V.; Writing—review & editing, R.V., L.B., V.O., P.v.d.M., P.S., and R.d.B.

Contarino MF, Bour LJ, **Verhagen R**, Lourens MA, de Bie RM, van den Munckhof P, Schuurman PR. Directional steering: A novel approach to deep brain stimulation. Neurology. 2014 Sep 23;83(13):1163-9.

Conceptualization, M.C., L.B., R.V., P.v.d.M., R.d.B., and P.S.; Formal analysis, M.C., L.B., M.L., and R.V.; Investigation, M.C., L.B., R.V., P.v.d.M., R.d.B., and P.S.; Methodology, L.B., M.C., R.V., P.v.d.M., R.d.B., and P.S.; Supervision, R.d.B. and P.S.; Visualization, M.C., R.V., and M.L.; Writing—original draft, M.C.; Writing—review & editing, M.C., L.B., R.V., M.L., P.v.d.M., R.d.B., and P.S.

Bour LJ, Lourens MA, **Verhagen R**, de Bie RM, van den Munckhof P, Schuurman PR, Contarino MF. Directional Recording of Subthalamic Spectral Power Densities in Parkinson's Disease and the Effect of Steering Deep Brain Stimulation. Brain Stimul. 2015 Jul-Aug;8(4):730-41.

Conceptualization, L.B., M.C., R.V., M.L., P.v.d.M., R.d.B., and P.S.; Formal analysis, L.B., M.L., and R.V.; Investigation, L.B., M.C., R.V., P.v.d.M., R.d.B., and P.S.; Methodology, L.B., M.L, M.C., and R.V.; Supervision, M.C., R.d.B., and P.S.; Visualization, L.B. and M.L.; Writing—original draft, L.B.; Writing—review & editing, L.B., M.L., R.V., M.C., P.v.d.M., R.d.B., and P.S.

van Dijk KJ, **Verhagen R**, Chaturvedi A, McIntyre CC, Bour LJ, Heida C, Veltink PH. A novel lead design enables selective deep brain stimulation of neural populations in the subthalamic region. J Neural Eng. 2015 Aug;12(4):046003.

Conceptualization, K.v.D., R.V., A.C., C.M., L.B., and C.H.; Formal analysis, K.v.D. and R.V.; Investigation, K.v.D. and R.V.; Methodology, K.v.D., R.V., A.C., C.M., L.B., and C.H.; Supervision, C.C., L.B., C.H., and P.V.; Visualization, K.v.D.; Writing—original draft, K.v.D.; Writing—review & editing, K.v.D., R.V., A.C., C.M., L.B., C.H., and P.V.

van Dijk KJ, **Verhagen R**, Bour LJ, Heida C, Veltink PH. Avoiding Internal Capsule Stimulation With a New Eight-Channel Steering Deep Brain Stimulation Lead. Neuromodulation. 2018 Aug;21(6):553-561.

Conceptualization, K.v.D., R.V., L.B., and C.H.; Formal analysis, K.v.D. and R.V.; Investigation, K.v.D. and R.V.; Methodology, K.v.D., R.V., L.B., and C.H.; Supervision, L.B., C.H., and P.V.; Visualization, K.v.D.; Writing—original draft, K.v.D.; Writing—review & editing, K.v.D., R.V., L.B., C.H., and P.V.

Other publications

Bot M, Schuurman PR, Odekerken VJJ, **Verhagen R**, Contarino FM, De Bie RMA, van den Munckhof P. Deep brain stimulation for Parkinson's disease: defining the optimal location within the subthalamic nucleus. J Neurol Neurosurg Psychiatry. 2018 May;89(5):493-498.

Nijmeijer SWR, de Bruijn E, **Verhagen R**, Forbes PA, Kamphuis DJ, Happee R, Tijssen MAJ, Koelman JHTM. Spectral EMG Changes in Cervical Dystonia Patients and the Influence of Botulinum Toxin Treatment. Toxins (Basel). 2017 Aug 23;9(9):256.

van den Noort JC, **Verhagen R**, van Dijk KJ, Veltink PH, Vos MCPM, de Bie RMA, Bour LJ, Heida CT. Quantification of Hand Motor Symptoms in Parkinson's Disease: A Proof-of-Principle Study Using Inertial and Force Sensors. Ann Biomed Eng. 2017 Oct;45(10):2423-2436.

Sharifi S, Luft F, **Verhagen R**, Heida T, Speelman JD, Bour LJ, van Rootselaar AF. Intermittent cortical involvement in the preservation of tremor in essential tremor. J Neurophysiol. 2017 Nov 1;118(5):2628-2635.

Tangwiriyasakul C, **Verhagen R**, Rutten WL, van Putten MJ. Temporal evolution of event-related desynchronization in acute stroke: a pilot study. Clin Neurophysiol. 2014 Jun;125(6):1112-20.

Tangwiriyasakul C, **Verhagen R**, van Putten MJ, Rutten WL. Importance of baseline in event-related desynchronization during a combination task of motor imagery and motor observation. J Neural Eng. 2013 Apr;10(2):026009.

Dankwoord

Dit proefschrift had niet tot stand kunnen komen zonder de bijdrage van veel verschillende mensen. Hier wil ik graag iedereen die heeft bijgedragen, in welke vorm dan ook, bedanken voor hun steun en samenwerking. In het bijzonder wil ik stilstaan bij de volgende mensen.

Allereerst gaat mijn dankbaarheid uit naar alle patiënten die vrijwillig mee hebben gedaan aan de onderzoeken die in dit proefschrift beschreven worden. Tijdens deze promotie heb ik gemerkt dat de Parkinsonpatiënt in dit opzicht werkelijk een uitzonderlijke patiënt is. Keer op keer werd mij duidelijk hoe welwillend de Parkinsonpatiënt is om mee te werken aan wetenschappelijk onderzoek, zelfs wanneer hiervoor geen kleine offers gevraagd werden, zoals het (langer) stoppen van medicatiegebruik en het (langer) wakker zijn tijdens de operatie. Dit moet een niet te onderschatten weerslag hebben op de patiënt. Toch zijn zij vrijwel allemaal zeer gemotiveerd om een bijdrage te leveren aan de wetenschap, ondanks dat zij weten dat ze het niet voor henzelf doen, maar voor hun toekomstige lotgenoten. Daar heb ik bijzonder veel respect voor en ik ben hen zeer dankbaar.

Daarnaast wil ik mijn promotores bedanken, prof. dr. Rick Schuurman en prof. dr. Ivo van Schaik.

Ivo, van een afstandje hield je mijn planning in de gaten en deelde je jouw kritische blik waar nodig. Hoewel ik me niet altijd netjes aan die planning hield, heb ik je inbreng en je pragmatische begeleiding wel zeer gewaardeerd.

Rick, tegen de tijd dat jij echt mijn promotor en begeleider werd, was ik al bijna weg uit het AMC. Dat heeft het vast niet gemakkelijk gemaakt om mijn begeleider te zijn, zeker op de momenten dat ik druk was met mijn dagelijkse werk. Toch vind ik dat onze samenwerking heel goed is geweest. Bedankt dat je altijd geduldig was en het begreep als mijn prioriteiten soms even elders lagen. Daarmee maakte je de laatste lootjes net iets minder zwaar. Toch wist je op de juiste momenten subtiele druk op me uit te oefenen waardoor het proefschrift nu wel af is. Zonder jou was dat (nog) niet gelukt. Pas het laatste jaar merkte ik echt goed hoe vaak we hetzelfde over dingen denken. Ik zou willen dat ik al eerder tijdens mijn promotie in deze intensieve mate met je had samengewerkt.

Ook wil ik mijn copromotores bedanken, dr. ir. Lo Bour en dr. ir. Ciska Heida. Ook prof. dr. ir. Peter Veltink mag hierbij niet ontbreken.

Ciska en Peter, ik wil jullie beide hartelijk bedanken voor de samenwerking met jullie vakgroep aan de Universiteit Twente. Het was bijzonder fijn en leerzaam om tijdens dit project echt op het grensvlak van de medische praktijk en de techniekontwikkeling te werken en bovendien mooi dat mijn eigen link met de Universiteit Twente hierdoor behouden kon blijven. Ook ben ik dankbaar voor jullie kritische blik op de manuscripten en jullie bijzonder goede contacten met de stichting TWIN en buitenlandse vakgroepen zoals die van professor McIntyre aan Case Western Reserve University in Cleveland. Deze samenwerking heeft een mooie extra dimensie aan het project gegeven.

Lo, jou wil ik in het bijzonder bedanken. Jij was tenslotte tot je welverdiende pensioen (en daarna ook nog) mijn dagelijkse begeleider. Ik ben blij dat je ondanks je pensionering bij deze promotie in de functie van copromotor betrokken kan zijn. De eerste jaren heb je me geïnspireerd met je ongetemperde enthousiasme en je visie voor de toekomst van DBS. Daarnaast wil ik je bedanken voor je contacten met de Universiteit Twente en met de technologische bedrijven zoals Sapiens Steering Brain Stimulation, die deze promotie vormgegeven hebben. Maar met name wil ik je bedanken voor jouw opstelling ten opzichte van mij (en de andere promovendi die je begeleidde). Bedankt dat jij op de juiste momenten de 'bad cop' wilde zijn, zodat ik de 'good cop' kon zijn. Die instelling heeft veel indruk op me gemaakt en de dag dat je dat zo letterlijk tegen me zei, zal ik niet snel vergeten. Ik heb er bijzonder veel respect voor dat jij je op een dergelijke manier in dienst kon stellen van je promovendi.

Mijn dank gaat ook uit naar de stichting TWIN voor het mogelijk maken van deze promotie. Zonder adequate financiering is er geen wetenschappelijk onderzoek. Ik wil graag de bestuursleden van de stichting TWIN bedanken voor de werving en het beheer van de financiën en daarnaast wil ik alle mensen bedanken die via deze stichting de door hen verworven middelen belangeloos inzetten om wetenschappelijk onderzoek mogelijk te maken.

Dit onderzoek heeft met name zijn vorm gekregen door het uitwisselen van ideeën en ervaringen met de verschillende betrokken clinici. Naast de mensen die al genoemd zijn, wil ik vooral mijn dank uitspreken naar Fiorella Contarino, Pepijn van den Munckhof, Rob de Bie, Vincent Odekerken, Maarten Bot, Miranda Postma, Marije Scholten en alle anderen bij wie ik voor vragen of inspiratie terecht kon.

Ook de technische bedrijven, met name Sapiens Steering Brain Stimulation, ben ik dankbaar voor de samenwerking en het brainstormen over de ontwikkeling en toepassing van nieuwe DBS technologie. Mijn dank gaat daarbij vooral uit naar Hubert Martens, Gijs van Elswijk, Wim Pollet en Rutger Nijlunsing.

Kees van Dijk, mijn 'mede-promovendus' aan de kant van de Universiteit Twente wil ik hartelijk bedanken voor de mooie samenwerking, met name het delen van kennis

over de soms zo verschillende onderwerpen. Ik denk dat we elkaar op een hele goede manier aanvulden, zowel in ons project als tijdens de tripjes die we samen maakten naar Cleveland en San Diego.

Ik ben er erg gelukkig mee dat de afdeling Klinische Neurofysiologie (KNF) mijn uitvalbasis was tijdens deze promotie. Ik wil dan ook de 'KNF-familie' (o.a. Fleur, Camiel, José, Edwin, Stéfanie, Hannah, Marijke, Rosanne, Thijs, Wouter en Dwar) bedanken voor de geweldige sfeer op deze afdeling. Met name dank aan KNF-familieleden Hans Koelman, Janny Ree en Erik Mans voor het creëren van een dergelijk werkklimaat. Door jullie manier van leiding geven was de KNF werkelijk een veilige haven binnen het soms roerige AMC.

Dan dat ene kamertje op de KNF waar alles gebeurde, D2-136, en de mensen waarmee ik daar elke dag zat. Bas, Joost, Sarvi, Yasmine en Arthur, kamergenoten, collega's en vrienden, zonder jullie was deze promotie waarschijnlijk al jaren geleden klaar geweest, maar ik had het toch voor geen goud willen missen. Het was soms behoorlijk lastig om geconcentreerd te werken, maar we hebben wel echt heel veel gelachen. Vaak was dat op ons kamertje, maar ook op borrels, feestjes, congressen en bijbehorende tripjes naar allerlei plekken in de wereld, of gewoon op vrijdag in Het Oude Gasthuis of De Twee Zwaantjes in Amsterdam.

Bas, op de KNF konden we het al snel goed met elkaar vinden, maar ook daarbuiten zijn we goede vrienden geworden. In de kroeg, in ons hockeyteam, tijdens reisjes, maar ook als het persoonlijk even wat minder goed gaat, kunnen we bij elkaar terecht. Bedankt dat je me een beetje wegwijs hebt gemaakt in Amsterdam en bedankt dat je accepteert dat ik toch altijd een Brabander zal blijven. Ik ben blij dat je mijn paranimf wilt zijn en ik weet zeker dat jouw weloverwegen analyserend en geruststellend vermogen me op de dag van de verdediging zal helpen.

Joost, jij en ik waren altijd de niet-dokters van onze groep en juist daarom misschien wat nuchterder ingesteld dan de anderen. Het klikte direct goed tussen ons en ook buiten het ziekenhuis kan ik je nuchtere en toch avontuurlijke instelling nog steeds heel erg waarderen. Laten we snel samen weer gaan surfen, een zeiltochtje maken, of iets anders geks doen. Ik ben blij dat je mijn paranimf wilt zijn, en weet zeker dat jouw uitgesproken no-nonsense mentaliteit me op de dag van de verdediging zal helpen.

Sarvi, we kenden elkaar natuurlijk al uit Twente, dus ik was heel blij jouw bekende gezicht te zien op mijn eerste dag in het AMC. Meteen konden we het goed vinden en dat is alleen maar beter geworden over de jaren. We dachten direct over zo veel dingen hetzelfde, onder andere over hoe leuk Matlab is, wat echt een verademing was. Ondanks dat jouw humor soms echt niet te volgen is, hebben we toch heel veel gelachen samen en ik hoop dat we dat in de toekomst ook nog heel veel zullen doen.

Yasmine, het was misschien wel even wennen toen we elkaar net leerden kennen. Ik denk dat we op veel punten tegenpolen zijn, maar juist daarom ben ik je heel snel gaan waarderen en is dat over de jaren heen alleen maar meer geworden. Ik ben blij dat we elkaar buiten het AMC nog steeds zien en je nog altijd probeert de Amsterdammer in me naar boven te halen. Misschien lukt dat ooit nog. Laten we in elk geval doorgaan met onze tripjes en samen biertjes drinken in De Twee Zwaantjes, zodat je het kunt blijven proberen.

Arthur, ik ken niemand die zo ambitieus, gedreven en ondernemend kan zijn als jij en tegelijkertijd zo van de hak op de tak en altijd in voor een geintje. Ik heb veel respect voor hoe jij je volledig ergens op kunt storten en toch heel relaxt kunt blijven. Dat heeft me geïnspireerd in onze tijd op de KNF, en ik hoop dat we elkaar ook na deze promotietijd kunnen blijven zien.

Uiteraard wil ik ook mijn familie bedanken voor alle steun en vertrouwen die zij mij gegeven hebben tijdens deze promotie en op de weg die daaraan voorafging.

Tim, Anita, Hannah en Daan, onze band is vaak onuitgesproken maar daarom zeker niet minder sterk. Ik weet dat ik altijd op jullie kan rekenen en jullie op mij. Ik ben heel dankbaar om jullie in mijn familie en in mijn leven te hebben.

Papa en Mama, jullie voortdurende steun heeft me gemaakt tot wie ik nu ben. Wetende dat ik altijd op jullie kan rekenen en als het nodig is op jullie terug kan vallen, heeft me in staat gesteld om me te ontwikkelen zoals ik gewild heb en om nu vol zelfvertrouwen vrij zorgeloos in het leven te kunnen staan. Ik weet dat dit voor jullie vanzelfsprekend is, maar wat voor jullie vanzelfsprekend mag zijn, is mij zo veel waard en ik ben jullie er levenslang dankbaar voor.

Lieve Aniek, als laatst wil ik jou bedanken voor al je steun en geduld in de afgelopen twee jaar. Bedankt dat je me de tijd gaf om in de weekenden aan deze promotie te werken en dat je me af en toe subtiel onder druk zette wanneer ik moeite had om mezelf ertoe te zetten. Zonder jou was dit proefschrift zeker nog niet af geweest. Ik zal heel blij zijn als we de weekenden weer voor onszelf hebben en ik kijk ernaar uit de wereld verder met jou te ontdekken.

Abbreviations

3D	Three-dimensional
AC – PC	Anterior commissure – posterior commissure
AD	Analog-to-digital
AMC	Academisch Medisch Centrum
ANOVA	Analysis of variance
BROK	Basiscursus regelgeving en organisatie voor klinisch onderzoekers
CC-lead	Cylindrical contact lead
CI	Confidence interval
CMRR	Common mode rejection ratio
CSF	Cerebrospinal fluid
CT	Computed tomography
DBS	Deep brain stimulation
DC	Direct current
DICOM	Digital imaging and communications in medicine
DTI	Diffusion tensor imaging
FDA	Food and drug administration
FEM	Finite element method
GPi	Globus pallidus interna
HD-lead	High density lead
IC	Internal capsule
IPG	Implanted pulse generator
ISO	International Organization for Standardisation
LFP	Local field potential
M	Mean
MCP	Midcommissural point
MDS	Movement Disorder Society
MER	Microelectrode recording
MRI	Magnetic resonance imaging
MU-ST	Multiple unit spike train
NFU	Nederlandse Federatie van Universitair Medische Centra
NSTAPS	Netherlands subthalamic and pallidal stimulation
PD	Parkinson's disease
PSD	Power spectral density
RMS	Root mean square
SD	Standard deviation
SMPI	Sensorimotor powerindex
STN	Subthalamic nucleus
TE	Echo time
TR	Repetition time
TSE	Turbo spin-echo
UMCG	Universitair Medisch Centrum Groningen
UPDRS	Unified Parkinson's disease rating scale
UvA	Universiteit van Amsterdam
VTA	Volume of tissue activated
WMO	Wet medisch-wetenschappelijk onderzoek met mensen